



UNIVERSITAT ROVIRA I VIRGILI

## TAILOR-MADE CHEMICAL SENSING PLATFORMS FOR DECENTRALIZED HEALTHCARE AND WELLBEING

Rocío Cánovas Martínez

**ADVERTIMENT.** L'accés als continguts d'aquesta tesi doctoral i la seva utilització ha de respectar els drets de la persona autora. Pot ser utilitzada per a consulta o estudi personal, així com en activitats o materials d'investigació i docència en els termes establerts a l'art. 32 del Text Refós de la Llei de Propietat Intel·lectual (RDL 1/1996). Per altres utilitzacions es requereix l'autorització prèvia i expressa de la persona autora. En qualsevol cas, en la utilització dels seus continguts caldrà indicar de forma clara el nom i cognoms de la persona autora i el títol de la tesi doctoral. No s'autoritza la seva reproducció o altres formes d'explotació efectuades amb finalitats de lucre ni la seva comunicació pública des d'un lloc aliè al servei TDX. Tampoc s'autoritza la presentació del seu contingut en una finestra o marc aliè a TDX (framing). Aquesta reserva de drets afecta tant als continguts de la tesi com als seus resums i índexs.

**ADVERTENCIA.** El acceso a los contenidos de esta tesis doctoral y su utilización debe respetar los derechos de la persona autora. Puede ser utilizada para consulta o estudio personal, así como en actividades o materiales de investigación y docencia en los términos establecidos en el art. 32 del Texto Refundido de la Ley de Propiedad Intelectual (RDL 1/1996). Para otros usos se requiere la autorización previa y expresa de la persona autora. En cualquier caso, en la utilización de sus contenidos se deberá indicar de forma clara el nombre y apellidos de la persona autora y el título de la tesis doctoral. No se autoriza su reproducción u otras formas de explotación efectuadas con fines lucrativos ni su comunicación pública desde un sitio ajeno al servicio TDR. Tampoco se autoriza la presentación de su contenido en una ventana o marco ajeno a TDR (framing). Esta reserva de derechos afecta tanto al contenido de la tesis como a sus resúmenes e índices.

**WARNING.** Access to the contents of this doctoral thesis and its use must respect the rights of the author. It can be used for reference or private study, as well as research and learning activities or materials in the terms established by the 32nd article of the Spanish Consolidated Copyright Act (RDL 1/1996). Express and previous authorization of the author is required for any other uses. In any case, when using its content, full name of the author and title of the thesis must be clearly indicated. Reproduction or other forms of for profit use or public communication from outside TDX service is not allowed. Presentation of its content in a window or frame external to TDX (framing) is not authorized either. These rights affect both the content of the thesis and its abstracts and indexes.



UNIVERSITAT  
ROVIRA i VIRGILI

# Tailor-made chemical sensing platforms for decentralized healthcare and wellbeing

Doctoral Thesis

Rocío Cánovas Martínez



UNIVERSITAT ROVIRA I VIRGILI

TAILOR-MADE CHEMICAL SENSING PLATFORMS FOR DECENTRALIZED HEALTHCARE AND WELLBEING

Rocío Cánovas Martínez

Rocío Cánovas Martínez

**Tailor-made chemical sensing platforms  
for decentralized healthcare and  
wellbeing**

Doctoral Thesis

*supervised by*

Dr. Francisco J. Andrade



**UNIVERSITAT  
ROVIRA i VIRGILI**

Department of Analytical and Organic Chemistry

Tarragona, 2018

UNIVERSITAT ROVIRA I VIRGILI

TAILOR-MADE CHEMICAL SENSING PLATFORMS FOR DECENTRALIZED HEALTHCARE AND WELLBEING

Rocío Cánovas Martínez

Rocío Cánovas Martínez

# Tailor-made chemical sensing platforms for decentralized healthcare and wellbeing

***Tribunal members:***

Prof. Francesc Xavier Rius Ferrús – Universitat Rovira i Virgili

Prof. Jose Manuel Costa – Universidad de Oviedo

Dr. Devin Daems – Katholieke Universiteit Leuven

***External examiners:***

Prof. Mabel Beatriz Tudino – University of Buenos Aires

Prof. Joseph Wang – University of California San Diego



UNIVERSITAT  
ROVIRA i VIRGILI

Department of Analytical and Organic Chemistry

Tarragona, 2018

UNIVERSITAT ROVIRA I VIRGILI

TAILOR-MADE CHEMICAL SENSING PLATFORMS FOR DECENTRALIZED HEALTHCARE AND WELLBEING

Rocío Cánovas Martínez

**DEPARTAMENT DE QUÍMICA ANALÍTICA I  
QUÍMICA ORGÀNICA**

Campus Sescelades, Marcel·lí Domingo, 1, 43007,  
Tarragona

Tel.: +34 977 55 95 62

E-mail: *franciscojavier.andrade@urv.cat*

*Francisco J. Andrade*, associate professor at the Department of Analytical and Organic Chemistry at the University Rovira i Virgili (URV).

---

I STATE that the present study, entitled “**Tailor-made chemical sensing platforms for decentralized healthcare and wellbeing**”, presented by *Rocío Cánovas Martínez* for the award of the degree of Doctor, has been carried out under my supervision at the Department of Analytical and Organic Chemistry of this university.

---

Tarragona, January 11<sup>th</sup> 2018

Doctoral Thesis Supervisor

**Dr. Francisco Javier Andrade**



UNIVERSITAT ROVIRA I VIRGILI

TAILOR-MADE CHEMICAL SENSING PLATFORMS FOR DECENTRALIZED HEALTHCARE AND WELLBEING

Rocío Cánovas Martínez

## ACKNOWLEDGEMENTS

First of all, I would like to deeply thank *Prof. Xavier Rius* and my supervisor *Dr. Francisco Andrade* for giving me the opportunity to join the Nanosensors group and doing my PhD. Their respect, teaching and guidance have accompanied me throughout these three and a half years. All the training about innovation received in the Innovation Hub, complementary courses at the Universitat Rovira I Virgili, PhD stay in San Diego (USA) and attendance to international conferences have made me grow as a researcher in the field.

Second, I would like to thank all my family members for believing in me and encouraging me during all my life in every possible way. I could not name all and each one of them, because we are a very large family; but specially my mum and dad - *Rosalía* and *Pepe*-, whose unconditional love and energy accompanies me wherever I go; my Russian sister *Taty*; my godson, nephews and nieces, cousins, aunts and uncles from Sevilla, Murcia and Barcelona; and grandparents (*Lina, Juan, Lola y Jose Antonio*) that, wherever they are I am sure that they are guiding and protecting me.

Third, I would like to thank:

All the colleagues from the Nanosensors group, from *Xavier Rius* -recently retired- till the master and ungraduated students. I will remember all the fun moments making *castanyadas, calçotadas*, and Argentinean barbecues, among others. Specially, I would like to thank *Pascal Blondeau* for all the help and guidance provided in the last year of my doctorate, *Santiago Macho* because all the informatics support and *Marta Borràs* one of the most generous person than I have known, for all the friendly support inside and outside the lab as well as for the good moments shared in the international conferences.

*Professor Joseph Wang*, for allowing me to do my PhD stay in his group at the University of California, San Diego (UCSD). All the period was really profitable and productive, learning a lot about wearable electrochemical sensors and sharing the lab and free time out of the lab with wonderful people such as *Dr. Jorge Delezuk, Dr. Adriana Pavinatto* and *Dr. Berta Fernandez*; you guys made the stay a great experience to remember.

## ACKNOWLEDGEMENTS

All my friends from many years, whom I love because they demonstrate me that no matter how far you are, they will be always there: *Isa, Inma, Laura, Jose, Aldara, María, Chano, Mar, Claudia, Irene, Helena, Anichi*, etc. And all my lovely friends/family from here: *Francesc, Lara, Rocío, Santi, Carlota, Jaume, Mireia, Joan, Gemma, Jesus, Marta, Montxo*, etc. And of course, my family “in-laws” who have welcomed me here as if I were their own daughter, niece or granddaughter.

Finally, I do not have enough words to thank my friend, partner, lab mate and fiancé *Marc Parrilla*, who has helped, taught, supported and guided me inside and outside the lab during all these years. Thank you for being the way you are, a generous, honest, brave and strong person that believes in my abilities even when I doubt it and that shares with me all his enthusiasm. Working side by side with you has been a privilege that hopefully we will repeat.

## TABLE OF CONTENTS

<b>1. INTRODUCTION.....</b>	<b>9</b>
1.1. REVOLUTION OF SOCIAL CONNECTIVITY .....	12
1.1.1. mHealth: auto-management of health as a social need .....	15
1.2. POINT OF CARE TECHNOLOGIES: towards a decentralized healthcare .....	18
1.3. APPROACHES TO DEVELOP DECENTRALIZED CHEMICAL SENSORS: key aspects to consider .....	22
1.3.1. The “ <i>Holy Trinity</i> ” of decentralized sensors.....	22
1.3.2. From an analytical device to a viable product .....	27
1.4. OBJECTIVES.....	29
1.5. REFERENCES .....	31
<b>2. FOUNDATIONAL ASPECTS OF THE DETECTION.....</b>	<b>35</b>
2.1. ELECTROCHEMICAL TECHNIQUES .....	37
2.1.1. Potentiometry.....	37
2.1.2. Voltammetry and Amperometry .....	40
2.2. ELECTROCHEMICAL POTENTIALS .....	41
2.2.1. Redox potential.....	41
2.2.2. Donnan potential.....	42
2.2.3. Mixed potential.....	42
2.3. ELECTROCHEMICAL SENSORS .....	43
2.3.1. Potentiometric systems.....	45
2.3.2. Voltammetric systems.....	55
2.3.3. Reference systems .....	59
2.4. ANALYTICAL PERFORMANCE PARAMETERS.....	61
2.5. REFERENCES .....	64
<b>3. EXPERIMENTAL .....</b>	<b>67</b>
3.1. MATERIALS.....	69
3.1.1. Conductive inks.....	69
3.1.2. Carbon nanotubes .....	69
3.1.3. Membranes components for ISEs and RE .....	69
3.1.4. Elastomers .....	70
3.1.5. Other reagents .....	70
3.2. PROCEDURES.....	71
3.2.1. Preparation of conductive substrates.....	71
3.2.2. Membrane cocktails .....	72

## TABLE OF CONTENTS

3.2.3. Approaches for membrane deposition .....	73
3.2.4. Conditioning step .....	74
3.3. CHARACTERIZATION .....	74
3.3.1. Mechanical characterization .....	74
3.3.2. Microscopic characterization.....	74
3.3.3. Electrochemical characterization .....	75
3.3.4. Optical characterization .....	77
3.4. REFERENCES .....	77
<b>4. A TEXTILE-BASED STRETCHABLE MULTI-ION POTENTIOMETRIC SENSOR .....</b>	<b>79</b>
4.1. INTRODUCTION .....	81
4.2. EXPERIMENTAL .....	82
4.2.1. Materials preparation .....	82
4.2.2. Electrochemical measurements.....	83
4.2.3. Fabrication of the textile sensor .....	83
4.3. RESULTS AND DISCUSSION .....	85
4.3.1. Stretchable sensor facing mechanical stress.....	85
4.3.2. Wireless integration .....	91
4.4. CONCLUSIONS .....	92
4.5. REFERENCES .....	92
<b>5. A BALLOON-EMBEDDED SENSOR WITHSTANDING EXTREME MULTIAXIAL STRETCHING AND GLOBAL BENDING MECHANICAL STRESS: TOWARDS ENVIRONMENTAL AND SECURITY MONITORING.....</b>	<b>95</b>
5.1. INTRODUCTION .....	97
5.2. EXPERIMENTAL .....	99
5.2.1. Reagents and materials .....	99
5.2.2. Electrochemical measurements.....	99
5.2.3. Solid-state electrolytes.....	100
5.2.4. Mechanical deformation studies .....	100
5.2.5. Fabrication of the expandable sensor on the balloon surface.....	100
5.3. RESULTS AND DISCUSSIONS .....	101
5.3.1. Practical fabrication considerations and materials selection.....	101
5.3.2. Modelling .....	104
5.3.3. Mechanical deformation studies .....	107
5.3.4. Design considerations .....	110
5.3.5. Liquid-phase sensing.....	112

## TABLE OF CONTENTS

5.3.6. Vapor-phase sensing .....	114
5.4. CONCLUSIONS.....	116
5.5. REFERENCES .....	116
<b>6. ENHANCED POTENTIOMETRIC DETECTION OF HYDROGEN PEROXIDE USING A PLATINUM ELECTRODE COATED WITH NAFION .....</b>	<b>119</b>
6.1. INTRODUCTION .....	121
6.2. EXPERIMENTAL .....	123
6.2.1. Reagents and Solutions.....	123
6.2.2. Materials .....	123
6.2.3. Electrochemical Measurements.....	124
6.3. RESULTS AND DISCUSSION.....	124
6.3.1. Potentiometric detection enhancement.....	124
6.3.2. Nafion as a permselective membrane.....	132
6.4. CONCLUSIONS.....	135
6.5. REFERENCES .....	136
<b>7. PAPER-BASED ENZYMATIC ELECTRODE WITH ENHANCED POTENTIOMETRIC RESPONSE FOR MONITORING GLUCOSE IN BIOLOGICAL FLUIDS.....</b>	<b>139</b>
7.1. INTRODUCTION .....	141
7.2. EXPERIMENTAL .....	144
7.2.1. Materials and methods.....	144
7.2.2. Electrochemical measurements.....	144
7.2.3. Fabrication of glucose biosensor .....	144
7.2.4. Analysis of real samples .....	145
7.3. RESULTS AND DISCUSSION.....	145
7.3.1. Characterization of the platinized paper-based electrodes .....	145
7.3.2. Electrode response and principle of detection .....	146
7.3.3. Optimization of the detection of glucose .....	150
7.3.4. Analytical performance .....	151
7.3.5. Membrane characterization .....	153
7.3.6. Analysis of real samples .....	156
7.4. CONCLUSIONS.....	159
7.5. REFERENCES .....	159
<b>8. A NOVEL WIRELESS PAPER-BASED POTENTIOMETRIC PLATFORM FOR MONITORING GLUCOSE IN BLOOD.....</b>	<b>163</b>
8.1. INTRODUCTION .....	165

## TABLE OF CONTENTS

8.2. EXPERIMENTAL .....	167
8.2.1. Instrumentation and measurements .....	167
8.2.2. Analysis of real samples .....	168
8.2.3. Fabrication of the enzymatic paper-based potentiometric cell .....	168
8.3. RESULTS AND DISCUSSION .....	170
8.3.1. Optimization of the potentiometric sensor.....	170
8.3.2. Analytical performance of the integrated devices (ID) .....	175
8.3.3. Prediction of glucose in real samples .....	177
8.3.4. Instrumental advantages and future prospects .....	178
8.4. CONCLUSIONS .....	180
8.5. REFERENCES .....	180
<b>9. NEW ADVANCEMENTS IN THE DEVELOPMENT OF POTENTIOMETRIC BIOSENSORS .....</b>	<b>183</b>
9.1. INTRODUCTION .....	185
9.2. PART 1: Exploring alternatives redox-sensitive substrates.....	187
9.2.1. Experimental.....	187
9.2.2. Results and Discussion .....	188
9.3. PART 2: Searching an alternative polyelectrolyte matrix .....	194
9.3.1. Experimental.....	194
9.3.1. Results and Discussion .....	195
9.4. CONCLUSIONS .....	203
9.5. REFERENCES .....	204
<b>10. CONCLUSIONS.....</b>	<b>207</b>
10. CONCLUSIONS .....	209
10.1. REFERENCES .....	212
<b>APPENDICES.....</b>	<b>215</b>
APPENDIX 1. ABBREVIATIONS.....	217
APPENDIX 2. FIGURE INDEX .....	222
APPENDIX 3. TABLE INDEX .....	228
APPENDIX 4. LIST OF PUBLICATIONS.....	229
Journal Publications:.....	229
Poster Presentations: .....	229

## SUMMARY AND CHAPTER OVERVIEW

The main motivation of this doctoral thesis is the development of affordable and user-friendly tools for the digitalization of the chemical analysis in different scenarios, with the main goal of improving the quality of life of people by facilitating the decision-making process.

The digital revolution together with many other technological advances, have boosted the development of sensors with ability to monitor several physical parameters in our daily life. This type of sensors have been implemented in cars, homes, hospitals, in the form of embedded or wearable devices, etc. offering the ability to generate a plethora of information in order to make real-time decisions. However, nowadays there is still a technology gap in the digitalization of the chemical information required to address pressing social needs in healthcare, wellbeing, environmental monitoring and threat assessments, among many others. Although the advances in these fields are also progressing quickly, its implementation in real scenarios has been very slow mostly because of the complexity and scalability of these systems. Hence, huge efforts in the scientific community have fostered the progress of analytical devices, particularly in the development and application of portable and low-cost tools for the decentralization of the chemical analysis. This technological revolution will result in an improvement of our wellbeing, an optimization of the healthcare costs, control of pollution and improved security and surveillance, which are some of the main current issues that concern society.

In order to address these challenges, the overall goal of this thesis is the exploration and development of novel, intuitive and affordable (bio)chemical sensors that can pave the way to the construction of affordable, robust, scalable, user-friendly and simple platforms for decentralized settings. The main added value of this thesis is the introduction of new electrochemical sensors integrated in different types of affordable and tailor-made platforms, which can be used for several applications from personalized healthcare as well as the monitoring of chemical compounds in the environment. In addition, this thesis remarks the necessity of the development of chemical sensors as an instrument for helping society and improving the healthcare system and wellbeing at all levels.

The work has been focussed in two main issues. In the first part of this thesis, wearable and embedded electrochemical sensors based on resistant materials that address the problems related to the user interface are described. In the second part, a new detection strategy for the fabrication of enzymatic sensors with potentiometric detection showing an excellent example of the whole analytical process -from fundamental to applications- is presented.

The thesis has been structured in 10 different chapters, each one containing the following information:



## SUMMARY AND CHAPTER OVERVIEW

**Chapter 1** provides a general overview of current social needs and challenges in healthcare and wellbeing. The chapter explains how the technological advances could help and improve the current system. It makes emphasis in the joint development of mobile health and point of care technologies as a solution to these challenges.

**Chapter 2** describes the foundational aspects of the different electrochemical techniques used in this thesis. Moreover, general definitions and conventions about the main components and working principles of the electrochemical sensors developed during the thesis are detailed. Definitions about analytical parameters used for the characterization are also discussed.

**Chapter 3** corresponds to the experimental section, where the main materials, procedures and instrumentation common throughout all the work are described.

**Chapter 4** describes the development of a wearable multi-ion potentiometric sensor in a commodity material such as textile. The analytical performance of this sensor under different types of mechanical stress is discussed. The integration of this sensor with common textiles opens new opportunities for using wearable chemical sensing in different fields such as: diagnostics, healthcare and sport.

**Chapter 5** presents the integration of an electrochemical sensor in a user-friendly platform such as rubber balloons. The sensor based on resilient nanocomposited inks is able to monitor explosive compounds. This is a clear example of decentralization of the environmental analysis beyond the most common topic of decentralization of healthcare.

**Chapter 6** this chapter together with the following two explore a novel approach to develop potentiometric biosensors with enhanced sensitivity. This chapter is focussed on the understanding of the mechanism involved in the detection of hydrogen peroxide by a platinum electrode coated with a Nafion membrane.

**Chapter 7** describes the development of a paper-based enzymatic electrode for determination of glucose in biological samples. It is presented as an interesting alternative for the development of simple and affordable devices for decentralized settings.

**Chapter 8** responds to the goal pursued during the last two chapters presenting a novel low-cost, compact and sensitive paper-based platform for the accurate monitoring of glucose in biological fluids. This low-cost analytical device opens up new prospects for rapid diagnostic results in non-laboratory settings.

**Chapter 9** provides some alternative modifications in order to improve the outcomes of potentiometric biosensors. In first place, challenging the affordability of the device by

## SUMMARY AND CHAPTER OVERVIEW

developing alternative redox substrates; and in second place, using a different polyelectrolyte coating that confers more interesting features to the biosensor.

**Chapter 10** outlines the main conclusions derived from experimental work as well as details on next steps in order to continue with the improvement of these devices in the field.

Finally, some appendices have been added with additional information:

- Appendix 1 corresponds with the list of abbreviations.
- Appendix 2 shows the figure index.
- Appendix 3 displays the table index.
- Appendix 4 provides the list of publications resulting from this thesis.

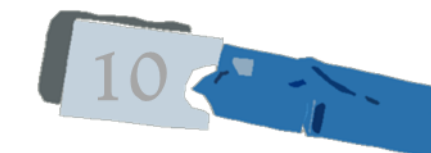
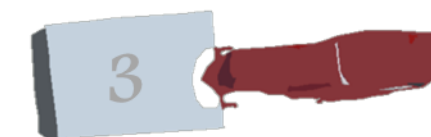
UNIVERSITAT ROVIRA I VIRGILI

TAILOR-MADE CHEMICAL SENSING PLATFORMS FOR DECENTRALIZED HEALTHCARE AND WELLBEING

Rocío Cánovas Martínez

# INTRODUCTION

---



UNIVERSITAT ROVIRA I VIRGILI

TAILOR-MADE CHEMICAL SENSING PLATFORMS FOR DECENTRALIZED HEALTHCARE AND WELLBEING

Rocío Cánovas Martínez

This chapter provides a general overview on some current and most pressing social needs, such as healthcare and wellbeing, for an increasingly growing and ageing population. Along this chapter, these needs will be described as challenges that will have to be faced in the coming years using technological advances that could help to improve the quality of life of people. Additionally, some of the requirements to improve the healthcare system together with the state of the art and some of the current progress in this field will be briefly described.

Every society needs to evolve and adapt to the conditions of a changing environment. While sometimes adaptations require incremental changes, there are moments in which paradigm-shifting challenges require the implementation of revolutionary approaches to the way the things are done. These revolutions are needed when the existing systems become obsolete, i.e., they cannot fulfil anymore the needs for which they were originally conceived. This is the case, for example, of the healthcare systems, where the centralized approaches that were introduced many centuries ago do not allow anymore to address current social needs. The increasing number of people and ageing of the population are becoming a growing global concern for governments, as the problems of healthcare cost and management are leaving large fractions of the people out of the system. Therefore, the challenges on the economical sustainability of the current system are promoting the generation of new ideas on how to leverage technological advances in order to provide better and affordable healthcare.

Current healthcare models lack of approaches in areas such as decentralized monitoring of chemical parameters, thus failing to provide remote diagnostics. For example, the current standard protocol to perform a generic blood test may take up to 10 days from the moment in which the blood is extracted from the patient until the result of the analysis is obtained. In addition to the cost, another factor to take into account is the uncertainty that users experience while waiting for these results. Clearly, there is a need to solve these issues (sometimes critical) when starting a treatment or making decisions in real time is crucial. The development of decentralized chemical sensors and platforms will greatly improve both costs and decision-making processes when facing any medical condition, particularly while monitoring chronic diseases.

For many years, physical sensors (i.e., those that measures physical parameters) have been used for the monitoring of critical parameters around people and processes. These sensors have been successfully adopted in the present market and are being broadly used. The reason of their success relies on key features of this type of sensors such as high stability, lack of calibration step, etc. Hence, physical sensors have been integrated in our cars, houses, electrical appliances, etc. In contrast, it is the lack of integration and currently limited features of

chemical sensors that has to be improved in order to provide truly needed and useful tools for society. The challenge thus is the design of novel chemical sensors that perform similarly to physical sensors but measuring chemical parameters. This challenge is hard as new issues and complex systems must be faced along the way. In this direction, this thesis shows in the following chapters advances that address the present issues, and accordingly, will lead to the development of decentralized chemical sensors.

One of the most promising solutions within this global trend of decentralization is the use of existing technological platforms (e.g. smartphones, computers, internet connectivity, cloud computing, etc.) to improve the healthcare system. These commodity technologies might work in connecting diagnostic tools, minimizing the unnecessary visits to doctors or hospitals. Thus, people will receive a better care without leaving their homes, while decreasing the overall public healthcare expenditure. Novel systems such as portable devices must be then created in order to successfully address these new and emerging issues. These new systems can be conceptually revolutionary, but for these ideas to come up to life, new tools and techniques are required. This is the goal of this thesis work, to provide new platforms and procedures to address the needs of a new world, with new and complex social challenges that must be urgently addressed.

## **1.1. REVOLUTION OF SOCIAL CONNECTIVITY**

The digital revolution that began during the second half of the 20<sup>th</sup> century provoked a massive shift from the traditional mechanical and analogue systems to the new digital electronic technology. This trend of adoption and proliferation of digital computers and digital record keeping grew exponentially and still continues to grow till present days. If the first wave of digitalization was the emergence of computing and increasing storing power, a second and even more powerful wave started during the 1970's through the widespread connectivity of these digital devices, a trend that will give rise, a few decades later, to the emergence of the internet. For this reason, during the last decades, the digital revolution was followed and empowered by the expansion and increasing availability of the internet and mobile devices, which can be now reached by the vast majority of the world population. Furthermore, the possibility of accessing Internet through these devices is another of the great landmarks of the last years. Last, but not least, cloud computing has recently emerged as global platform that minimizes the hardware requirements and facilitates the sharing of information. All in all, in only a few decades, the digital revolution has provided a widespread technological platform with the ability to acquire, process, store, transmit and access to the information at any time, in any point of the planet, at almost zero cost. Because of its deep scientific, technological and -above

all- social impact, this revolution can be considered as one of the greatest technological breakthrough in human history so far, with a potential to improve social systems globally.

The social change promoted by the advent of smartphones and the extended use of similar devices affects many aspects of our daily lives.<sup>[1]</sup> In recent years, mobile devices have experienced a deep expansion with almost total adoption in our society. This market penetration can be clearly seen in the use of these devices by sectors of the population that have traditionally remained distant from the progress in the information and communications technologies (ICT), such as the population over 65 years old. In addition, as a user-friendly technology, anyone without training can make use of it in a simple and almost intuitive way. Data from Pew Research Center reveal that in the age range over 65, the use of mobile phones is around 76%. Undoubtedly, these data corroborate that the traditional boundaries in the digital domain are blurred. For instance, in the United States, more than 75% of adults under 49 years old own a smartphone and an estimated 73% of teenagers own or have access to a smartphone.<sup>[2,3]</sup> Moreover, on an average day, teenagers spend more than 2.5 hours using a smartphone, 4 with their device always in close proximity. The success of mobile terminals seems to be linked to many reasons such as the exceptional penetration in the market, rapid acceptance by most of the society and widespread use.

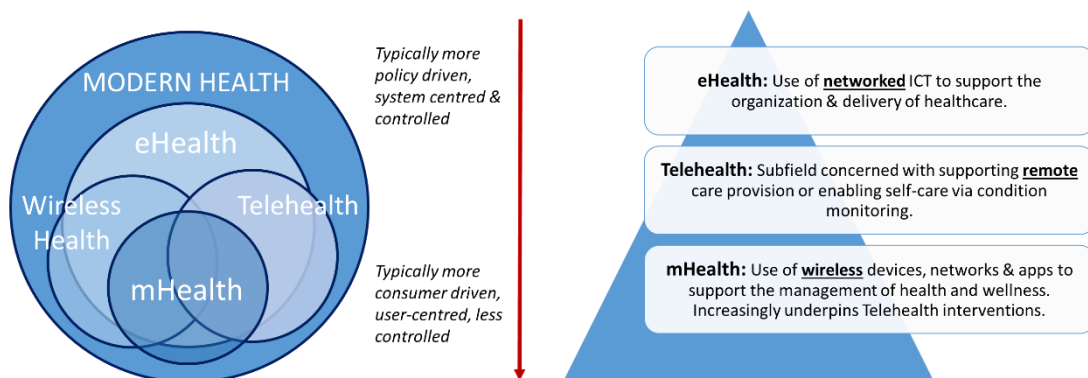


**Figure 1.1.** Left: diagram summarizing how the concepts inside modern health are interwoven with each other. Right: definitions for eHealth, telehealth and mHealth.<sup>[12]</sup>

Nowadays, decentralization is a major trend in most organizations, and as this phenomenon progress at fast pace, new management approaches are needed. In the knowledge society, information is an invaluable resource that allows taking effective and more efficient actions. In some way, the information society has introduced a process of continuous social transformation and the search for the constant reduction of inequalities and sustainable



development. Decentralization has emerged as one of the key strategies to promote equal human development. In particular, technological decentralization generally responds to the need to make information technology (IT) services more effective and efficient to address specific issues that require the immediate implementation of a system to achieve fast results.

This technological decentralization has been very useful in sanitary terms. Society has made great progress in this regard since, thanks to the implementation of decentralized units and portable devices, monitoring of health conditions and communication with patients can be done in a much more fluid and simple way for everyone. It is important to introduce at this point the concepts of eHealth, telehealth and mobileHealth (also refer to as mHealth). eHealth is a relatively recent term for healthcare backed by electronic processes and communication; it is based on the use of networked ICT to support the organization and delivery of healthcare. eHealth dates back to at least two decades ago, and involves a general domain that includes - among others- many other flourishing areas such as telehealth, personal health, mHealth, ubiquitous health, health 2.0 and connected health, which are frequently overlapped and used as synonyms in the literature.<sup>[4]</sup> The diagrams shown in Figure 1.1 are an attempt to summarize how the concepts are interwoven with each other. eHealth encapsulates a wide range of remote healthcare services and applications using ICTs for home care, long-term care, prevention, health promotion, self-care and support for the integration of social and healthcare services.<sup>[5]</sup> Furthermore, eHealth systems normally offer functionalities to help the patients follow and understand this information so that they can be better informed as to the state and evolution of their condition.<sup>[6]</sup> These new tools can be also used by the healthcare practitioners for monitoring the health of the population, for real-time early detection and rapid intervention.<sup>[7,8]</sup> Moreover, within the sanitary framework, the ICTs offer a great potential for improving patient safety when facilitating the acquisition, communication and analysis of information, which improves the decision-making and its implementation process.<sup>[9-11]</sup>

As the quality of the services needs major improvements through approaches that guarantee the sustainability of the social and healthcare systems, telehealth is currently one of the fields of greatest growth. The implementation of new models for attention of chronic patients is may be one of the most attractive areas.<sup>[13]</sup> A large number of telehealth pilot projects and demonstrations have been launched since the end of the 20<sup>th</sup> century. To facilitate the adoptions, the development of wearable and biomedical devices and mobile broadband communications systems help to turn the individuals into connection nodes within telehealth networks. Smartphones and tablet terminals act then as invaluable support platforms for applications within a smart environment.<sup>[4]</sup> In parallel, the introduction of the mHealth through the use of wireless devices to support the management of health and wellness is leading a

revolution in healthcare, which is expected to be integrated under the four "Ps" model, namely: personalized, predictive, participatory and preventive. The communication between patients and professionals through telehealth is growing towards new forms well beyond text messages -such as video calls-, among others. The constant increase of applications offers new tools to communicate with the professionals, providing channels for fast consultations or for improving clinical records. Moreover, it is important to stress that through this revolution, patients are becoming more engaged in their own healthcare process, so that they can gain some expertise in their pathology and can carry out the monitoring of signs or symptoms through mHealth devices (e.g. diagnostics devices such as a connected glucometer), which are followed and transmitted electronically to the doctor. In this way, it is the own patient who can be empowered in the decision-making process involving its medical condition. This framework requires doctors that not only prescribe drugs but also indicate the use of personalized applications that allow the patient to be guided towards a more direct participation in the care of their own health.

### **1.1.1. mHealth: auto-management of health as a social need**

One of the reasons of the mHealth proliferation is the ubiquitous nature of mobile platforms, which has kept a fast pace of growth with a continuous wave of technological advances. In this sense, mobile devices are targeted for the promotion of healthcare and disease management.<sup>[8,14]</sup> In recent years, we have witnessed a growing adoption of eHealth tools in the healthcare sector, mostly focused on the improvement of the quality and efficiency of the care of chronic patients and the elderly, as well as for the protection and promotion of the general health of the population. The development of these categories in the healthcare model was propelled by the growing technological capacity in mobile broadband communications, wearable sensors, internet, social networks, biomedical devices, big data, cloud computing, automation of processes, and many other hard and soft technologies incorporated into the components and subsystems used (Figure 1.2). This requires taking into consideration new situations in many technological and human aspects in relation to other ICT applications for mHealth, where patient safety and security are critical aspects.<sup>[13]</sup> Addressing all these needs is a crucial step to guarantee a broader and deeper adoption of mHealth at all levels.



**Figure 1.2.** Interconnectivity of components in a digital health ecosystem.<sup>[15]</sup>

The sharp growth of mHealth interventions can be linked to several factors. For example, the use of mobile platforms ranges from prevention and diagnostics to treatment of several types of conditions. Mobile tools can be used as communication devices either between peers or between doctors and patients and even for connection of patients with other patients, providers, family, friends, and community organizations, in order to improve health status, and share information and vital experiences. Furthermore, mHealth devices can collect dynamic health-related data and deliver the content to patients in their homes, far from a clinical environment. In addition, this kind of high-throughput data that is available from sensors and smartphones, increases the ability of researchers to tailor interventions in participants in real time and to enhance patient engagement with positive health behaviours. Last but not least, the app marketplace has quickly become filled with a wide range of mHealth-related platforms because businesses have recognized the value of the wealth of data that these apps can provide.<sup>[14]</sup> According to PricewaterhouseCoopers (PwC), mHealth is becoming one of the basic pillars of healthcare because it facilitates an improvement in the quality of care, greater efficiency and a significant saving in healthcare costs (which is expected to be around 100,000

million euros in the European Union by 2017). Therefore, the market is evolving rapidly, so there are a number of new mobile technologies potentially available for the healthcare system. Indeed, mobile health-related applications have the potential to reach the general public, address specific needs, and complement other technological developments. It is believed that this will generate a change in the healthcare model. It will minimize costs, diagnostic errors, and probably be able to break the communication barrier that is established on many occasions between the hospital and the patient throughout the care process.

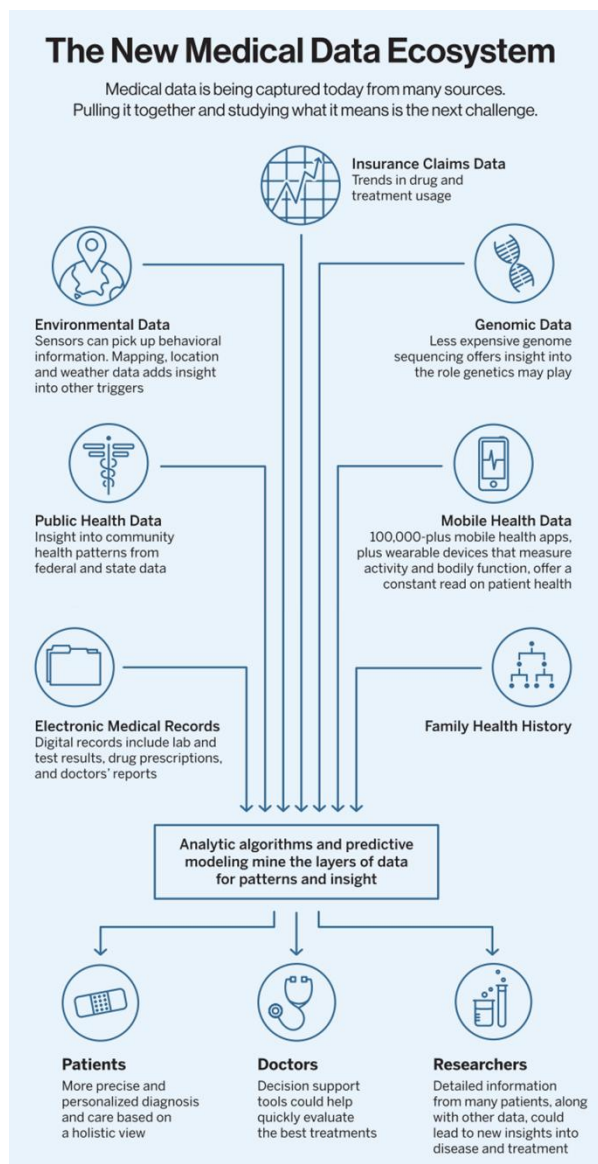


**Figure 1.3.** The new model of the sanitary ecosystem in which the different sources where the information is obtained converge towards the three main pillars where this information is used.<sup>[16]</sup>

mHealth technology can be currently used to monitor sleep patterns, heart rate, activity levels, and even more advanced key metrics such as blood oxygen, glucose levels, and stress. This kind of information may be useful and interesting for anyone, but it can become essential for the millions living with chronic conditions like depression, heart disease, and diabetes.<sup>[16]</sup> However, the treatment and understanding of the information by the user is a crucial issue in order to improve the medical status of the patients. Overall, the innovation gap existing between the self-care and the conventional healthcare system is being filled with this type of tools based on mHealth.

This new ecosystem of medical data allowed medicine to enter into the information age. Mobile technologies, genome sequencing, sensors and advances in analytical software (see Figure 1.3) are some of the mayor enablers of this change. Hence, it is possible to capture large amounts of information about almost everything around us from individual to environmental variables. The sum of this information could transform medicine, turning a field aimed at treating the average patient into a truly personalized care that is customized to each individual's need. Moreover, more control and responsibility are shifted from doctors to patients.<sup>[16]</sup> Personal biomedical devices and wearable sensors in mHealth and telehealth applications may be used for tele-monitoring the state of the patients while, at the same time, increasing their commitment to their treatment.<sup>[17]</sup> Hence, the use of mHealth plus the consequent generation of information is changing the role of patients, offering them a chance to play a more central part in their own healing process.

The general scheme of the ecosystem promotes the interconnection of different areas from the research and diagnostic point of view until the development of sensors and its integration in a device. In this way, the patients are able to transmit information about their own condition, quality of life and vital signs to the healthcare provider, who can then analyze the data generated (Figure 1.4). A market oriented at healthcare consumers has recently emerged based on smartphones and tablets using email, SMS messaging and mobile Internet. Indeed, there are a growing number of Apps that can be directly downloaded for their use by the patients and carers<sup>[6]</sup> making the management of the own health easier.

## **1.2. POINT OF CARE TECHNOLOGIES: towards a decentralized healthcare**

Point-of-care (POC) testing can be defined as the “provision of a test at or near the point of care of the patient, with the result that will be used to make a decision and to take appropriate action, which will lead to an improved health outcome”.<sup>[5]</sup> In this case, the main feature of these devices is the user-friendliness involved in the decision-making process. On the other hand, some definitions give more importance to time required, i.e., whether the results will be

available instantly or in a very short timeframe with immediate diagnosis or clinical intervention. However, there is a plethora of definitions of POC technologies and no accepted universal definition has yet been proposed.<sup>[19]</sup>

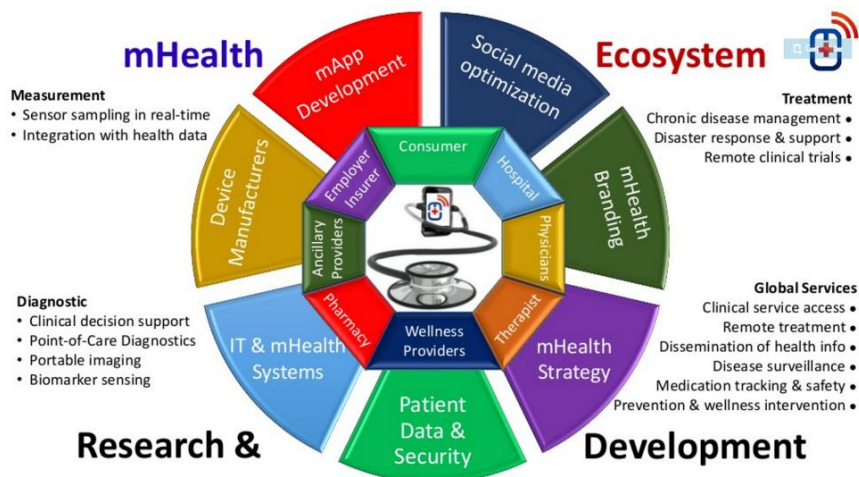


**Figure 1.4.** Subgroups involved and problems in the existing ecosystem of healthcare and the possible solutions arising with the implementation of mHealth.<sup>[18]</sup>

The parallel development of mHealth and POC technologies can be elucidated like a pair of convergent paths toward a potential solution. On the one hand, mHealth supports the management of the health and wellness by using mobile wireless communication. These networks and devices can obtain relevant information from health status of people involving physical and physiological sensing, and transmit it globally over the web. On the other hand, POC diagnostics such as urinalysis dipsticks, lateral flow immunoassays or handheld glucometers provide examples of simple and inexpensive devices that enable minimally qualified users to perform chemical testing. Recently, many devices are exploring that attempt to connect mHealth with POC testing.<sup>[20–26]</sup> In that sense, the connection between mHealth and POC devices could be the best option to decentralize the way in which the information and monitoring of Health are approached.

In order to build a full network of decentralized sensors, the current technology needs to be reviewed. The ability to understand and diagnose diseases has dramatically progressed due to advances in quantitative measurements of molecular biomarkers over the last several decades. Techniques such as flow cytometry, mass spectrometry, genetic sequencing, or nuclear magnetic resonance have enabled sophisticated and highly sensitive measurements of biological material. Technological niches are becoming a reality thanks to the improvement in

early diagnosis as well as the monitoring of diseases. Hence, it is possible to understand better the causes and mechanisms related to diseases. However, patient care may be limited by the cost needed to support the infrastructures of this technology.<sup>[27]</sup> It is for that reason that the field of POC testing is growing by trying to solve these limitations of affordability, simplicity and miniaturization among others.

POC approaches are nowadays seen as a very important way for democratizing the access to mHealth, since they can be implemented either by a healthcare practitioner or by the patient itself without the need for a clinical lab, thus greatly improving access to medical diagnostics. Simple POC diagnostics tools such as glucose monitors for diabetic patients and home pregnancy tests have been available for many years and have provided tremendous benefits for the people. Motivated by the success of these simple devices, there has been a strong push to develop more complex tools that can automate and miniaturize advanced diagnostics currently performed only in laboratories. These proposed “lab-on-a-chip” devices combine advances in electronics, photonics, micro-electromechanical systems (MEMS), and microfluidics to build small and low-cost chips that can perform extremely complex tasks.<sup>[28,29]</sup> Much research has gone towards the development of these lab-on-a-chip systems, but only recently this technology has begun to reach the level of maturity for practical use.<sup>[27]</sup>

POC and personalized medicine are highly valuable for the improvement of healthcare worldwide. POC platforms which can diagnose diseases and track their development through the detection of several bioanalytes represent one of the newest and most exciting advancements towards mass-screening applications. POC diagnostics is commonly based on portable, inexpensive, and user-friendly platforms that allow sensitive, robust, and real-time detection of biotargets. Two aspects that strengthen the value of POC diagnostics are the possibility to detect multiple bioanalytes in a single device and the integration of POC biosensors with mobile platforms technology. Hence, these chemical sensors should have a proper design to be user-friendly and affordable while providing the analytically relevant information. POC devices require an integration of chemistry, fluidics, software and hardware. Originally, POC areas were focus in chemistry and microfluidics, but rapid progress is taking place in other technological and non-technological components which need to be considered<sup>[30]</sup> (Figure 1.5). Besides, the accuracy and reliability of disease diagnostic protocols can be improved by analyzing multiple biomarkers and using multiplexed assays. Multiplexing is a decisive technological breakthrough since it allows the multivariate analysis of large numbers of samples from different patients or multivariate analysis of a large numbers of targets from the same sample. During the last years, the diagnostic potential of multiplexed point-of-care biosensing systems has generated a strong interest in the scientific community. For example,

the inexpensive, portable, and rapid POC diagnostics for detecting multiple biomarkers related to infectious diseases and microorganisms is currently feasible.<sup>[31]</sup> Today's smartphone is a multifaceted device which can be used as a camera, sensor for health status, activity tracker, and social networking client which provides the perfect platform for developing point-of-care devices. Hence, when POC testing is combined with smartphone technology, it becomes a powerful, user-friendly, and versatile tool, especially for those in remote and poor regions of the planet. With this emerging trend, smart and fully integrated multiplexed biosensors will surely revolutionize the medical and smartphone industries alike.<sup>[32]</sup>

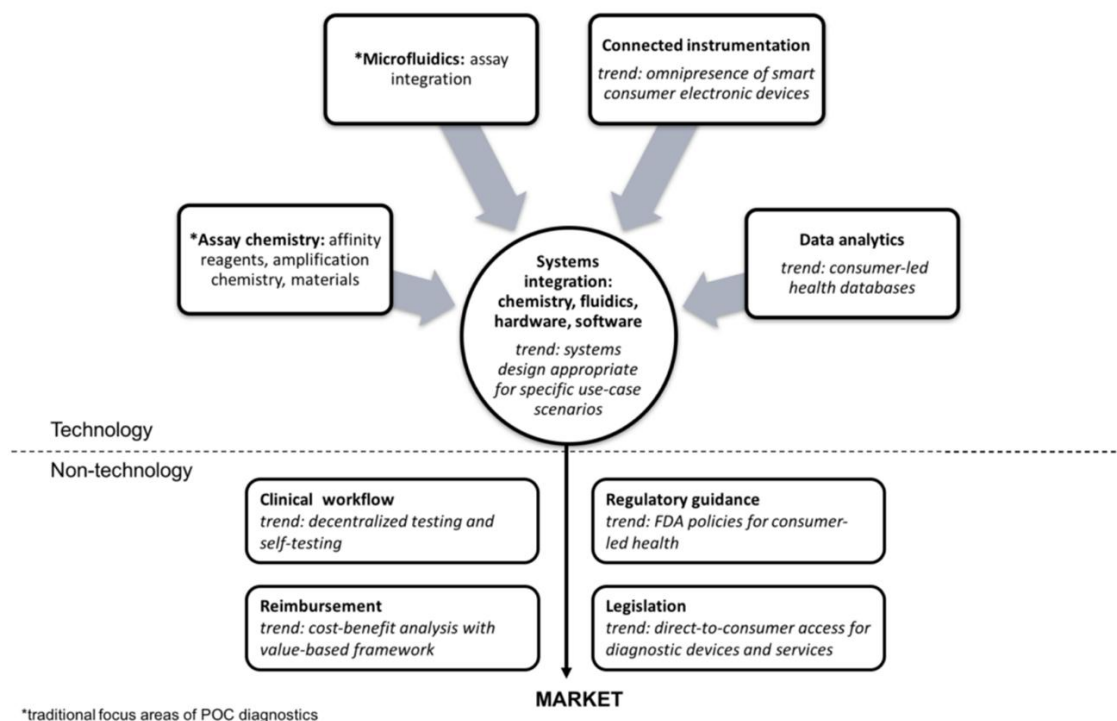


**Figure 1.5.** Schematic representation of the integration of different fields required for POC devices.<sup>[30]</sup>

Despite all the advantages that mHealth technology is providing, there are also several growing concerns, such as data analytics and security. Indeed, this technology is expected to generate unprecedented volumes of information originating from a wide variety of heterogeneous sources, such as different physical and chemical sensors. Moreover, the information that POC devices collect and report to their patient/physician/caregiver is confidential. For this reason, security issues are attracting huge attention. As more consumers rely on POC devices, they expose themselves to potential security breaches. As a result, data



protection protocols have thus become one of the most crucial factors for the operation of mobile and POC devices.<sup>[33]</sup> For example, these health records must comply with measures of protective digital privacy, required to prevent unauthorized access to computers, databases and websites as well as to protect personal data from corruption. Providing secured and relevant analytical information in an easy-to-understand way is thus essential for widespread adoption of mHealth technology.

In conclusion, mHealth devices based on POC technologies might provide a wide range of advantages to society as decentralized tools. Actually, these devices will bring the opportunity to improve the quality of life of the patients. At the same time, the adoption of these tools along the healthcare network should produce a decrease in the cost of medical expenditure. For example, the use of a faster diagnostic device will reduce the use of medication, thus decreasing the final cost in the care process. Also, a decrease in the analytical time will decrease the indirect cost of healthcare. Moreover, the use of decentralized platforms can provide health services in rural areas or low-income regions favouring the democratization of health, which is the actual challenge today. All in all, an optimization of these health services through the use of decentralized sensors will result in an overall improvement of the healthcare system.

### **1.3. APPROACHES TO DEVELOP DECENTRALIZED CHEMICAL SENSORS: key aspects to consider**

The growing demand for tools to generate (bio)chemical information in decentralized settings is creating a vast range of opportunities for chemical sensors. However, selectivity, easy manipulation during the detection process, calibration issues, stability of the sensors and affordability are among the current problems that hinder the wider dissemination of chemical sensors in the market. Hence, the detection of chemical substances is a complex process that requires highly advanced technology in order to selectively discriminate the analyte of interest. Indeed, crucial features are key in the progress of a full decentralization of the chemical analysis. By addressing the combination of robustness, simplicity of operation and cost, chemical sensors could hardly be rivalled by any other sensing system.

#### **1.3.1. The “Holy Trinity” of decentralized sensors**

Advanced and versatile devices based on electronic systems wirelessly connected through the cloud could bring a plethora of advantages. These devices could make possible to monitor millions of physical and chemical interactions that continuously occur between our body and the surrounding environment (from the weather conditions to the presence of an infection or disease). Controlling these parameters produces a sense of peace of mind in the society and

helps to make real-time decisions. To develop a technology with ability to provide this level of assurance, this technology should accomplish the “holy trinity” of any mass market product:

- i. **Robustness:** the sensor should be able to measure the target while being insensitive to the external conditions of the environment (physical stress, humidity, temperature, light, etc.). In some cases when the sensor could be embedded in substrates like a textile, thus requiring high tolerance to mechanical stress such as bending, stretching or crumpling.
- ii. **Affordability:** inexpensive sensors that everybody can get from medical centre or hospital till individual user or practitioners.
- iii. **Simplicity of operation:** a non-expert can handle and use the sensor in an intuitive way.

Point-of-care diagnostic tools should aim to address all these three requirements simultaneously (Figure 1.6).

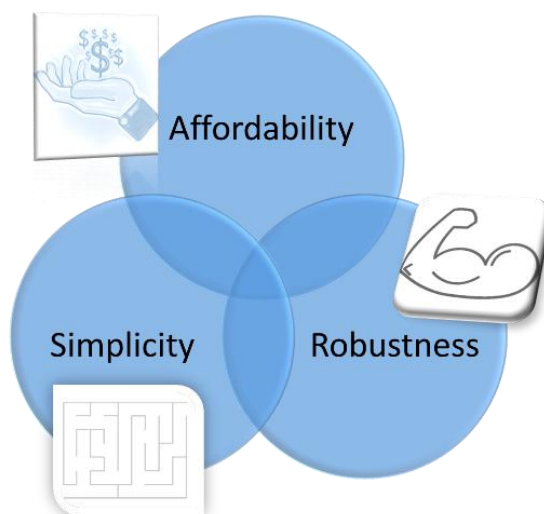


**Figure 1.6.** Summary of the three main characteristics included in the *Holy Trinity* concept.

#### 1.3.1.1. The use of paper as an affordable substrate to build analytical tools

Paper is a good example of substrate that encompasses the three main characteristics of the *Holy Trinity*. Paper is a term used to refer to thin bulk-manufactured fibrous porous materials of many different types, mainly made of cellulose. As a modern analytical substrate dates back to the 1940s and 1950s, when it was used for chromatography<sup>[34]</sup> and

electrophoresis.<sup>[35]</sup> In the 1980s, the use of nitrocellulose membrane emerged as the platform for the home pregnancy test based on paper substrates,<sup>[36]</sup> and has remained a gold standard for lateral flow assays -simple devices based on different types of paper substrates intended to detect the presence (or absence) of a target analyte in a sample (matrix) without the need for specialized and costly equipment- and commercial diagnostics more generally. In fact, the broad use of paper in the present market remains in forms of lateral-flows assays, the widespread pH strips as well as other bioactive papers (common term used for sensors based on functionalized papers with biomolecules and/or chemical compounds) for food, healthcare and environmental analysis.<sup>[37,38]</sup> The success of paper-based sensors is because paper is widely available, versatile and inexpensive. Besides, its cellulose fiber is easy to modify and compatible with biological samples. However, a good fraction of the paper-based sensors available in the market still rely mostly in optical readout.

Paper-based devices have been recently taken to a next level once they have been proposed as a two-dimensional microfluidic diagnostic platform by Whitesides's group in 2007, with the introduction of the microfluidic paper-based analytical device ( $\mu$ PAD).<sup>[39]</sup> Since their pioneer work, there has been an exponential increase in paper-based diagnostics research. Several factors motivate this surge: (i) paper is inexpensive and ubiquitous, (ii) is biocompatible, (iii) wicks fluids via capillary action and does not require external pumping sources, (iv) can be easily modified (i.e., chemically treated, cut, folded, stacked and bendable), (v) can be safely disposed by incineration, and (vi) is scalable (i.e., amenable to printing and roll-to-roll manufacturing).<sup>[40]</sup> Recent reviews of paper-based microfluidics cover different features such as fluid transport, fabrication methods, detection and readout strategies, and diagnostic applications.<sup>[41-44]</sup> In particular, paper is an ideal platform for global health diagnostics owing to its low cost and, ultimately, its inherent ability to wick fluids. Fluid transport by wicking eliminates the need for expensive peripheral pumping instrumentation, which aligns well with the "simple and low-cost" mantra for paper-based diagnostics. All this explains the significant progress of this field during the last decade. There is now a formidable toolbox of advanced strategies for fluid and analyte manipulation in paper-based assays. Moreover, smartphone technology is expanding the analytical power of paper-based assays, as well as their accessibility in the developing world. As paper-based technologies continue to mature, collective efforts should address the key remaining challenges of translation and commercialization.<sup>[45]</sup> In fact, it is not just the sensors that must be affordable and deliverable to end-users, but it is the whole analytical platform that should be built as a fully decentralized and affordable tool. Overall, paper-based diagnostic technologies are affordable, user-friendly,

rapid, robust, and scalable for manufacturing, thus holding great potential to deliver point-of-care diagnostics to resource-limited settings.

### 1.3.1.2. Robustness: Electrochemical biosensors

Electrochemical biosensors have played an important role in the development of point-of-care diagnostic devices. Existing diagnostic tests (e.g., ELISA) are sometimes not rapid enough and the experimental assays are performed when the detected proteins are at levels corresponding to advanced stages of the disease. Therefore, smaller, faster, and cheaper (one-step) devices are highly desired for replacing time-consuming laboratory-analyses. Due to their affordability, specificity, speed, user-friendly, rapid and robust, equipment-free and portable, and deliverable to end-users (ASSURED),<sup>[46]</sup> electrochemical biosensors offer exciting opportunities for numerous decentralized clinical applications, ranging from 'alternative-site' testing (e.g., physician's office) emergency-room screening, bedside monitoring, or home self-testing.<sup>[47]</sup>

For this reason, this field of decentralized sensors using electrochemical detection has been experiencing a fast growth during the last decades. For instance, a rapid affordable, user-friendly and accurate kit to diagnose malaria could become a lifesaver for hundreds of millions of people. Compared with standard laboratory testing, novel approaches towards electrochemical sensing are rapid, simple and inexpensive, and thus have great accessibility to resource-limited settings.<sup>[48]</sup> Moreover, the use of nanomaterials and its combination with electrochemical sensors is becoming essential in POC diagnostics to initiate and scale up on-site medical care for the prevention and control of diseases.<sup>[49,50]</sup> These novel nanomaterials enable electrochemical sensors with enhanced analytical parameters that currently fit the necessities of actual diagnostics thus amplifying the spectrum of valuable applications for real scenarios. Therefore, the integration of electrochemical sensors, nanomaterials and paper-based microfluidics holds great potential to deliver outstanding POC diagnostics to end-users. Indeed, this type of devices have been widely researched in the last decade and are starting to successfully reach the market with some POC devices due to their easy manufacturing that fulfils the mass-market requirements.<sup>[51]</sup>

The use of enzymes to build biosensors is applied as common strategy because of their unique specificity when acting as catalysts. From a qualitative point of view, enzymes are highly selective to a particular analyte of interest and represent a key point in the general scheme to build biosensors. Additionally, catalytic reactions can be used to amplify the signal obtained. From a quantitative perspective, the use of the enzymes to quantify the amount of product generated from the reaction is also widely used. Enzymes immobilized on the surface

of a substrate -such as paper-, have been widely used as diagnostic kits.<sup>[52]</sup> One of the biggest challenges to consider is the immobilization method which can significantly affect the shelf-life of enzyme-based  $\mu$ PADs, especially in applications where the sensors could be exposed to high temperatures during storage and transport. Moreover, some works reported that the immobilization via covalent linkage has been needed to prevent the enzymes being washed out during analysis.<sup>[53,54]</sup> However, these immobilization methods may give considerably lower enzyme activities, likely due to enzyme deactivation by chemical residues from conjugation reactions and disruption to the catalytic pockets of the enzymes. On the other hand, layer-by-layer entrapment methods (where enzymes were mixed with bilayer ionic polymer covered on the surface of the paper) yielded higher enzymatic activity than the other strategies that were investigated.<sup>[52]</sup> Therefore, immobilizing enzymes into the cellulose network of paper adjacent to electrodes or use of polyelectrolyte polymers might become an attractive alternative.

Beyond the enzyme immobilization, electrochemical sensors also require systems, such as a conductive element, which can transduce the output signal. Noble metals such as gold, silver or platinum are excellent electrode materials due to their good electron transfer capabilities. Thin film deposition is among the most common methods for creating metallic electrodes on paper-based substrates in a non-expensive way and can be achieved by evaporation, spraying metals on paper through a mask, or sputtering (as it will be shown along this thesis).

A very good example of applicability of electrochemical biosensors is the blood glucometer, a device that has served as an invaluable tool for screening, diagnosis, and long-term management of diabetes. Even though glucometers are readily purchased by consumers and patients, it still remains a challenge to achieve rapid, accurate, continuous, affordable, reliable, and sensitive glucose measurements, particularly for the developing world.<sup>[55]</sup>

### 1.3.1.3. Simplicity: a feature of progress

The simplicity of the system encompasses the use of an intuitive (ideally fully automated) device that can produce information from the environment in an easy manner. Several points can be stressed: (i) the device should act as an interface ready to analyse the sample and transduce the signal for a valuable interpretation; (ii) it should integrate the suitable sample capture and treatment; (iii) the sensor must be also connected for data transmission to the end-user. Furthermore, it should be designed as a user-friendly, familiar and simple to operate device. Hence, patients can use it because the tool makes the whole process as amenable and intuitive as possible. For this reason, the use of common platforms or materials to create attractive interfaces with electrochemical sensors has become a trend.<sup>[56,57]</sup> For example, conventional substrates such rubber have been used to turn it into sensing platforms,<sup>[58]</sup> and

also, electrochemical sensors have been embedded onto textile and other materials for monitoring applications.<sup>[59]</sup> As a consequence, a vast opportunity for analytical chemistry to move closer to the end-user has emerged.

### 1.3.2. From an analytical device to a viable product

To achieve the distribution of health-monitoring and POC devices in a worldwide market, many obstacles must be overcome to economically produce the sensing components onto a substrate using macroscale fabrication processes. In particular, health-monitoring sensors and advanced manufacturing technologies need to be integrated.<sup>[60]</sup> While few new classes of POC diagnostic devices have been introduced into the market, there has been significant progress in POC technologies. The continued progress in microfluidics, combined with dramatic advances in connected devices, is bringing the prospects of fulfilling the lofty promises of POC diagnostics closer than ever to reality.<sup>[61,62]</sup> In today's connected age, this progress is being made within the context of a broader and more diverse POC ecosystem than before.<sup>[30]</sup> This means the emergence of new profiles of new products in the field of POC (Figure 1.7).

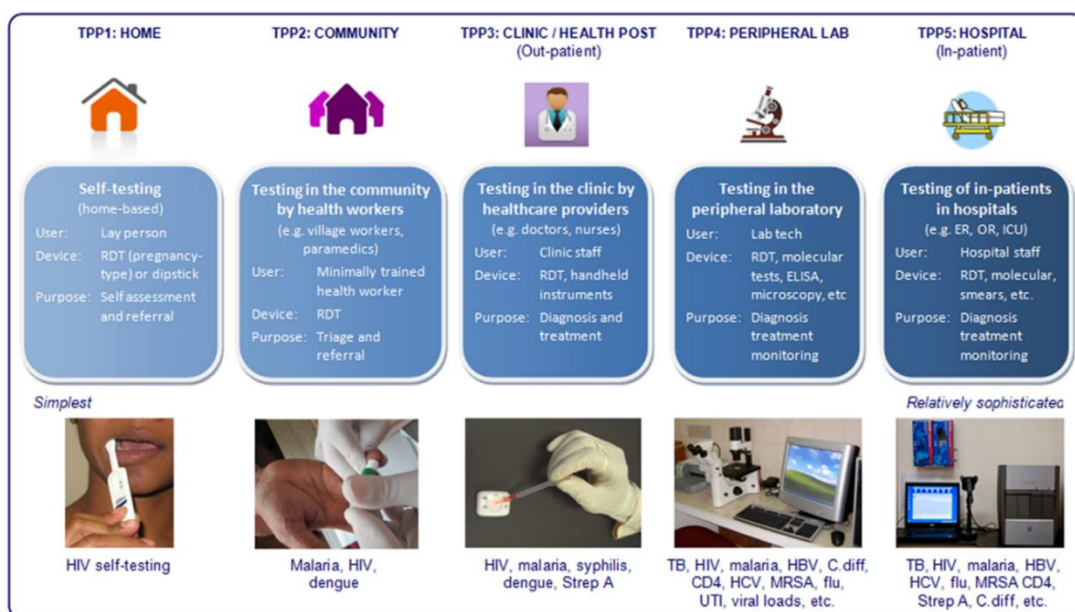


**Figure 1.7.** Examples of the diversity of target product profiles, users, and settings within the spectrum of POC testing.<sup>[19]</sup>

A clear advantage of analytical devices for POC applications is the ability to operate with simple equipment. Application of  $\mu$ PADs is particularly favoured in point-of-need settings that

require rapid analysis with low cost and simple operation.<sup>[63]</sup> These advantages have driven growth of the field toward applications of the portable analytical devices for clinical diagnostics, environmental monitoring, and food safety assurance. In addition, fabrication methods often target the scalability of the device thus lowering the cost per device by increasing production volume, or adding assay functionality among other strategies.<sup>[43]</sup>

The novelty of  $\mu$ PADs comes from the low-cost relative to conventional analytical methods where these sensors can also be designed to provide interpretable analysis results without any external equipment or reader. Being equipped with both a light source and a detector, smartphones can perform rapid measurements on paper devices for point-of-care applications. The trend is advantageous for the growth of telemedicine and integrated global environmental screening. Accordingly, the integration of smartphone and paper-based sensors have been demonstrated for monitoring air and water pollution,<sup>[64,65]</sup> disease outbreaks,<sup>[66]</sup> presence of hazardous metal<sup>[67]</sup> and glucose levels in biological samples.<sup>[68]</sup>

These innovations have been possible by new microfabrication techniques, surface modifications, and a variety of new materials with improved properties and novel applications. In fact, the number of useful and smart sensors for applications in different fields such as healthcare, security, fitness, or environmental is increasing due to the incorporation of new materials.<sup>[69-71]</sup> For instance, highly stretchable materials are being used as interfaces for analytical purposes to provide valuable insights into the decentralization of the chemical analysis.<sup>[72]</sup> These advanced materials will bring enhanced properties over the materials that are commonly used that will suit common lifestyle situations. All in all, moving a laboratory technology to the point-of-need can be complicated; however, the utilization in these conditions is the ultimate goal for developing many novel technological platforms. In the meantime, the World Health Organization, the Environmental Protection Agency, and other similar organizations have actively updated public health and environmental concerns all around the world, which are informative in guiding the development of new devices for innovative applications.<sup>[43]</sup>

In conclusion, the combination of the digital revolution and the progress in analytical devices has led to the development and application of portable tools that can be used for wellbeing, healthcare and improved safety. This technological revolution will result in an improvement of our wellbeing, an optimization of the healthcare system, an enhancement of the quality of life of many people, a more pleasant ageing, and specially, a facilitator in the decision-making processes among many daily situations.

In this thesis two main issues with their corresponding contribution to the field are shown separately. On the one hand, the first part addresses the problem related to the user interface by designing tools such as electrochemical sensors that can be directly integrated on different user-friendly surfaces. On the other hand, this thesis provides an excellent example of the whole analytical process from fundamental to applied science: (i) a novel detection strategy using potentiometric enzymatic sensors, (ii) the understanding of their mechanism of response, (iii) the use of affordable platforms to apply the novel approach, and, (iv) the applicability of the sensor to develop a whole device able to challenge the actual POC paradigm.

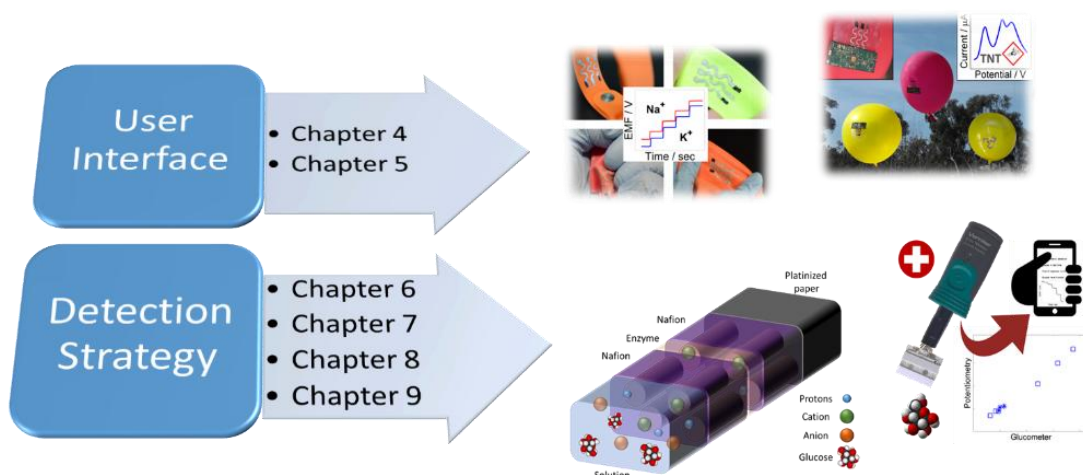


**Figure 1.8.** Basic scheme of the main topics addressed -classified into different chapters- within this thesis.

## 1.4. OBJECTIVES

The overall goal of this thesis is the exploration and development of novel, intuitive and affordable sensors that can pave the way to the construction of robust, simple and cost-effective platforms for decentralized chemical and biochemical analysis. It is expected that these platforms can be successfully implemented to address social needs in healthcare and wellbeing, environmental monitoring, threat assessment, etc.

This general objective can be divided in the following specific objectives:

1. Development of wearable electrochemical sensors using commodity materials to monitor body or environmental functions by screen-printing techniques.
2. Evaluation of the analytical performance of electrochemical sensors under high mechanical stress.



3. Integration of embedded sensors with wireless systems for the use in decentralized settings.
4. Fabrication of paper-based potentiometric biosensors based on enzymatic reactions to monitor physiologically relevant targets.
5. Validation of the paper-based device with human samples (blood and serum) compared to standard methodologies.
6. Integration of paper-based potentiometric biosensors with wireless electronic devices for the monitoring at real-time like a mHealth tool for a rapid disease management.
7. Explore new directions and strategies to develop alternative platforms able to extremely simplify the detection as well as decrease the cost of POC devices.

Overall, the main added value of this thesis is the introduction of new electrochemical sensors integrated in different types of affordable and tailor-made platforms, which can be used for several applications from personalized healthcare as well as the monitoring of chemical compounds in the environment (Figure 1.8). In addition, this thesis remarks the necessity of the development of sensors as an instrument for helping society and improving the healthcare system and wellbeing at all levels (Figure 1.9).

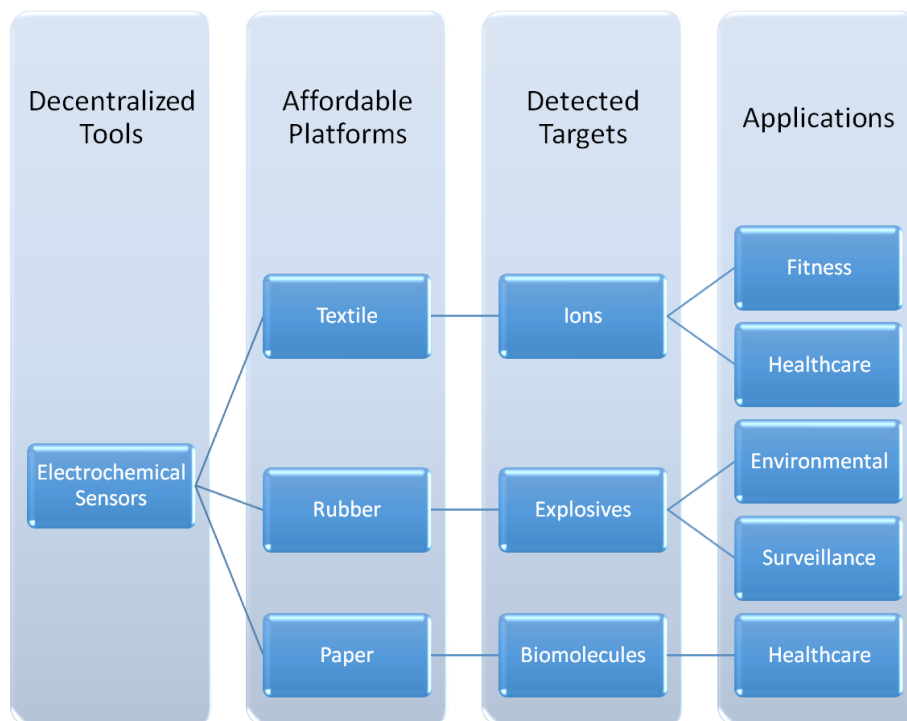


**Figure 1.9.** Diagram of the different parts of the research performed during this thesis.

## 1.5. REFERENCES

- [1] T. L. Webb, J. Joseph, L. Yardley, S. Michie, *J. Med. Internet Res.* **2010**, 12, 1.
- [2] A. Lenhart, *Teens, Social Media and Technology Overview 2015: Smartphones Facilitate Shifts in Communication Landscape for Teens*, **2015**.
- [3] H. Anglada, G. Riu, M. Martin, M. Rovira, J. M. Sotoca, C. Codina, *Int. J. Clin. Pract.* **2015**, 69, 9.
- [4] C. Koop, R. Mosher, L. Kun, J. I. M. Geiling, E. Grigg, S. Long, C. Macedonia, R. C. Merrell, R. M. Satava, J. Rosen, *IEEE Eng. Med. Biol. Mag.* **2008**, 29.
- [5] J. Kahn, J. Yang, J. Kahn, *Health Aff.* **2010**, 2, 252.
- [6] R. Junker, H. Schlebusch, P. B. Luppá, *Dtsch. Arztebl. Int.* **2010**, 107, 561.
- [7] A. A. Kumar, J. W. Hennek, B. S. Smith, S. Kumar, P. Beattie, S. Jain, J. P. Rolland, T. P. Stossel, C. Chunda-Liyoka, G. M. Whitesides, *Angew. Chemie Int. Ed.* **2015**, 54, 5836.
- [8] C. H. Salvador, A. Ruiz-Sanchez, M. A. González de Mingo, M. Carmona Rodríguez, M. P. Carrasco, P. G. Sagredo, J. A. Fragua, F. Caballero-Martinez, F. García-López, J. N. Márquez-Montes, J. L. Monteagudo, *IEEE Trans. Inf. Technol. Biomed.* **2008**, 12, 696.
- [9] J. L. Monteagudo Peña, O. Moreno Gil, *E-Health for Patient Empowerment in Europe*, **2007**.
- [10] R. Parasuraman, T. B. Sheridan, C. D. Wickens, *IEEE Trans. Syst. Man, Cybern. - Part A Syst. Humans* **2000**, 30, 286.
- [11] L. G. Kun, *Comput. Methods Programs Biomed.* **2001**, 64, 155.
- [12] C. Pagliari, "mHealth, telehealth and the digital society: Where does the 'value' lie?" **2012**, <https://es.slideshare.net/HINZ/pagliari-m-health-telehealth-and-digital-society-15205160>.
- [13] M. Swan, *Int. J. Environ. Res. Public Health* **2009**, 6, 492.
- [14] D. A. Fedele, C. C. Cushing, A. Fritz, C. M. Amaro, A. Ortega, M. K, *JAMA Pediatr.* **2017**, 41, 835.
- [15] INTRAPRISE. Healthcare. **2017**. <http://intraprise.com/Healthcare/>
- [16] MIT Technology Review, **2014**, 117, 1.
- [17] M. Boulos, S. Wheeler, C. Tavares, R. Jones, *Biomed. Eng. Online* **2011**, 10, 24.
- [18] G. Jones, "mHealthHub" **2012**. <https://es.slideshare.net/elcid84/mhealth-hub>.
- [19] N. P. Pai, C. Vadnais, C. Denkinge, N. Engel, M. Pai, *PLOS Med.* **2012**, 9, 1.
- [20] D. Estrin, I. Sim, *Science.* **2010**, 330, 759.
- [21] D. S. Lee, B. G. Jeon, C. Ihm, J.-K. Park, M. Y. Jung, *Lab Chip* **2011**, 11, 120.
- [22] L. Liu, J. Liu, *Front. Mech. Eng.* **2011**, 6, 160.
- [23] O. Mudanyali, S. Dimitrov, U. Sikora, S. Pasmanabhan, I. Navruz, A. Ozcan, *Lab Chip* **2012**, 12, 2678.
- [24] P. B. Lillehoj, M.-C. Huang, N. Truong, C.-M. Ho, *Lab Chip* **2013**, 13, 2950.
- [25] J. L. Delaney, E. H. Doeven, A. J. Harsant, C. F. Hogan, *Anal. Chim. Acta* **2013**, 803, 123.

- [26] A. Nemiroski, D. C. Christodouleas, J. W. Hennek, A. a Kumar, E. J. Maxwell, M. T. Fernández-abadul, G. M. Whitesides, *Proc. Natl. Acad. Sci.* **2014**, *111*, 1.
- [27] C. D. Chin, S. Y. Chin, T. Laksanasopin, S. K. Sia, Eds.: D. Issadore, R.M. Westervelt, Ed. Springer, Point of care diagnostic on a chip, **2013**, ISBN 978-3-642-29267-5.
- [28] J. P. Esquivel, J. Colomer-Farrarons, M. Castellarnau, M. Salleras, F. J. del Campo, J. Samitier, P. Miribel-Català, N. Sabaté, *Lab Chip* **2012**, *12*, 4232.
- [29] C. Renault, M. J. Anderson, R. M. Crooks, *J. Am. Chem. Soc.* **2014**, 4616.
- [30] S. Nayak, N. R. Blumenfeld, T. Laksanasopin, S. K. Sia, *Anal. Chem.* **2016**, *89*, 102.
- [31] R. W. Peeling, D. Mabey, *Clin. Microbiol. Infect.* **2010**, *16*, 1062.
- [32] A. Romeo, T. S. Leung, S. Sánchez, W. Su, X. Gao, *et al.*, *J. Electrochem. Soc.* **2016**, *145*, 406.
- [33] A. J. Bhandarkar, I. Jeerapan, J. Wang, *ACS Sensors* **2016**, *1*, 464.
- [34] A. J. P. Martin, R. L. M. Synge, *Biochem. J.* **1941**, *35*, 1358.
- [35] H. G. Kunkel, A. Tiselius, *J. Gen. Physiol.* **1951**, *35*, 89.
- [36] T. Chard, *Hum. Reprod.* **1992**, *7*, 701.
- [37] R. Pelton, *TrAC - Trends Anal. Chem.* **2009**, *28*, 925.
- [38] F. Kong, Y. F. Hu, *Anal. Bioanal. Chem.* **2012**, *403*, 7.
- [39] A. W. Martinez, S. T. Phillips, M. J. Butte, G. M. Whitesides, *Angew. Chem. Int. Ed. Engl.* **2007**, *46*, 1318.
- [40] J. P. Rolland, D. A. Mourey, *MRS Bull.* **2013**, *38*, 299.
- [41] D. M. Cate, J. A. Adkins, J. Mettakoonpitak, C. S. Henry, *Anal. Chem.* **2015**, *87*, 19.
- [42] A. M. López\_Marzo, A. Merkoçi, *Lab. Chip* **2016**, *0*, 1.
- [43] Y. Yang, E. Noviana, M. P. Nguyen, B. J. Geiss, D. S. Dandy, C. S. Henry, *Anal. Chem.* **2016**, *89*, 71.
- [44] K. Mahato, A. Srivastava, P. Chandra, *Biosens. Bioelectron.* **2017**, *96*, 246.
- [45] M. M. Gong, D. Sinton, *Chem.Rev.* **2017**, *117*, 8447.
- [46] D. Lee, T. Cui, *Biosens. Bioelectron.* **2010**, *25*, 2259.
- [47] J. Wang, *Biosens. Bioelectron.* **2006**, *21*, 1887.
- [48] R. Hart, M. Mauk, C. Liu, X. Qiu, J. Thompson, D. Chen, D. Malamud, W. Abrams, H. Bau, *Oral Dis.* **2011**, *17*, 745.
- [49] T. S. Hauck, S. Giri, Y. Gao, W. C. W. Chan, *Adv. Drug Deliv. Rev.* **2010**, *62*, 438.
- [50] M. C. Chuang, J. R. Windmiller, P. Santhosh, G. V. Ramírez, M. Galik, T. Y. Chou, J. Wang, *Electroanalysis* **2010**, *22*, 2511.
- [51] J. Hu, S. Wang, L. Wang, F. Li, B. Pinguang-Murphy, T. J. Lu, F. Xu, *Biosens. Bioelectron.* **2014**, *54*, 585.
- [52] E. W. Nery, L. T. Kubota, *J. Pharm. Biomed. Anal.* **2016**, *117*, 551.
- [53] A. A. Dias, T. M. G. Cardoso, R. M. Cardoso, L. C. Duarte, R. A. A. Muñoz, E. M. Richter, W. K. T. Coltro,

- Sensors Actuators, B Chem.* **2016**, 226, 196.
- [54] R. Cao, L. Guan, M. Li, J. Tian, W. Shen, *Sens. Bio-Sensing Res.* **2015**, 6, 13.
- [55] E. H. Yoo, S.-Y. Lee, *Sensors* **2010**, 10, 4558.
- [56] J. R. Windmiller, J. Wang, *Electroanalysis* **2013**, 25, 29.
- [57] A. J. Bandodkar, J. Wang, *Trends Biotechnol.* **2014**, 32, 363.
- [58] A. J. Bandodkar, A. M. O'Mahony, J. Ramírez, I. A. Samek, S. M. Anderson, J. R. Windmiller, J. Wang, *Analyst* **2013**, 138, 5288.
- [59] S. Coyle, V. F. Curto, F. Benito-Lopez, L. Florea, D. Diamond, *Wearable Sensors Fundam. Implement. Appl.* **2014**, 65.
- [60] K. Takei, W. Honda, S. Harada, T. Arie, S. Akita, *Adv. Healthc. Mater.* **2015**, 4, 487.
- [61] S. K. Sia, L. J. Kricka, *Lab Chip* **2008**, 8, 1982.
- [62] C. D. Chin, V. Linder, S. K. Sia, *Lab Chip* **2012**, 12, 2118.
- [63] O. D. Renedo, M. a. Alonso-Lomillo, M. J. A. Martínez, *Talanta* **2007**, 73, 202.
- [64] A. Ismail, M. O. Araújo, C. L. S. Chagas, S. Griveau, F. D'Orlyé, A. Varenne, F. Bedioui, W. K. T. Coltro, *Analyst* **2016**, 141, 6314.
- [65] C. Sicard, C. Glen, B. Aubie, D. Wallace, S. Jahanshahi-Anbuhi, K. Pennings, G. T. Daigger, R. Pelton, J. D. Brennan, C. D. M. Filipe, *Water Res.* **2015**, 70, 360.
- [66] S. Jain, R. Rajasingham, F. Noubary, E. Coonahan, R. Schoeplein, R. Baden, M. Curry, N. Afdhal, S. Kumar, N. R. Pollock, *PLoS One* **2015**, 10, 1.
- [67] S. M. Kang, S. C. Jang, Y. S. Huh, C. S. Lee, C. Roh, *Chemosphere* **2016**, 152, 39.
- [68] W. Gao, S. Emaminejad, H. Y. Y. Nyein, S. Challa, K. Chen, A. Peck, H. M. Fahad, H. Ota, H. Shiraki, D. Kiriya, D.-H. Lien, G. A. Brooks, R. W. Davis, A. Javey, *Nature* **2016**, 529, 509.
- [69] D. J. Lipomi, Z. Bao, *Energy Environ. Sci.* **2011**, 4, 3314.
- [70] F. Dal Dosso, E. Pérez-Ruiz, D. Daems, H. Agten, O. Al-Ghezi, O. Bollen, J. Breukers, F. De Rop, M. Katsafadou, J. Lepoudre, L. Lyu, P. Piron, R. Saesen, S. Sels, R. Soenen, E. Staljanssens, J. Taraporewalla, T. Kokalj, D. Spasic, J. Lammertyn, *Anal. Chim. Acta* **2017**, 1.
- [71] D. J. Lipomi, M. Vosgueritchian, B. C.-K. Tee, S. L. Hellstrom, J. a Lee, C. H. Fox, Z. Bao, *Nat. Nanotechnol.* **2011**, 6, 788.
- [72] A. J. Bandodkar, I. Jeerapan, J. M. You, R. Nuñez-Flores, J. Wang, *Nano Lett.* **2016**, 16, 721.

UNIVERSITAT ROVIRA I VIRGILI

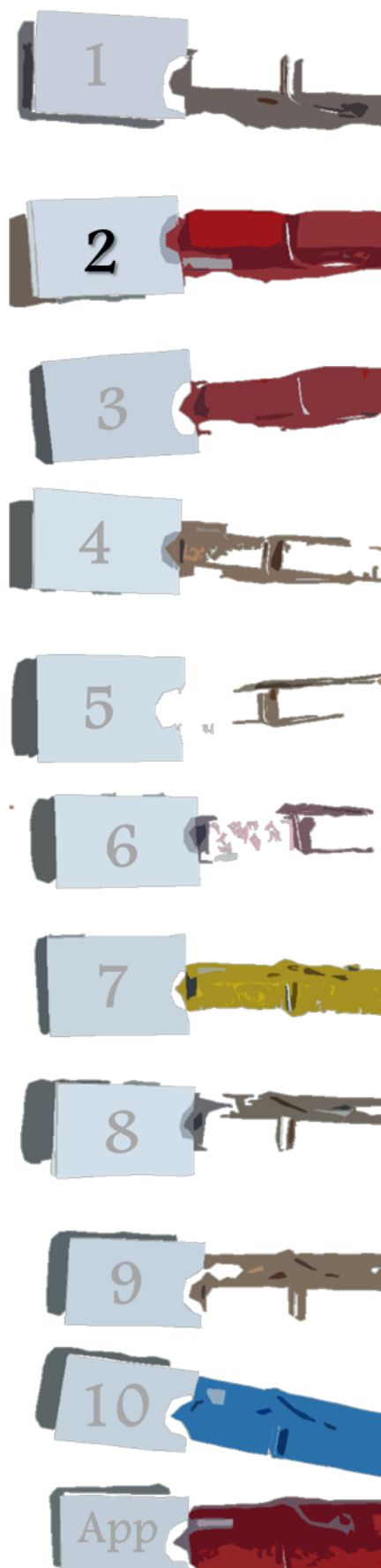
TAILOR-MADE CHEMICAL SENSING PLATFORMS FOR DECENTRALIZED HEALTHCARE AND WELLBEING

Rocío Cánovas Martínez

# FOUNDATIONAL ASPECTS OF THE DETECTION

---

---



UNIVERSITAT ROVIRA I VIRGILI

TAILOR-MADE CHEMICAL SENSING PLATFORMS FOR DECENTRALIZED HEALTHCARE AND WELLBEING

Rocío Cánovas Martínez

Many of the challenges of the decentralization of chemical analysis can be addressed using electrochemical sensors. Since these tools present several advantages, such as versatility, affordability, robustness, and last but not least, they have been studied for decades, so their use and foundations are well established. Therefore, despite of the high number of devices that have been already developed, there are still many needs that electrochemical sensors can fulfil. Electrochemistry encompasses several techniques that have evolved during the years to address different necessities depending of the final application. This chapter provides an overview of the foundational aspects of different electrochemical techniques used in this thesis. Moreover, general definitions and conventions about the main components of the electrochemical sensors developed during the thesis will be provided. Finally, the working principles of electrochemical sensors will be briefly mentioned trying to elucidate the generation of the response obtained in each case.

## **2.1. ELECTROCHEMICAL TECHNIQUES**

Electrochemical techniques are based on the measurement of potential (volts), charge (coulombs), electrical resistance (conductimetry or impedance measurements) (ohms) or current (amperes) to determine the presence and concentration of an analyte or to characterize the chemical reactivity of this analyte in an electrochemical cell. The electrochemical cell can be built by different electrodes that allow the successful completion of the electrical circuit. Depending on which aspects of the cell are controlled and which are measured there are several categories (see Figure 2.1), some of them will be explained in the following sections.

### **2.1.1. Potentiometry**

Potentiometry is a well-established analytical method that was consolidated as an attractive electrochemical technique in analytical chemistry at the beginning of the twentieth century and that has experienced a massive progress ever since. In this technique the potential of an electrochemical cell under well stirred conditions is measured. Since no current, (to be fair only a negligible current), flows through the electrochemical cell, the solution composition remains unchanged, making potentiometry an ideal non-destructive quantitative method. The first quantitative potentiometric applications appeared soon after the formulation of the Nernst equation (see Equation 2.1), which relates an electrochemical cell's potential to the activity (relation of the concentration of the analyte in the matrix) of electroactive species in the cell.

The difference of potential between a working and a reference electrode, is measured using a high-impedance voltmeter (a potentiometer). The main role of the reference electrode (RE) is to maintain a constant potential, while the working electrode (WE) must change its potential following a change on the activity of the analyte of interest in the problem solution. Hence, the



difference of potential can be easily related with the concentration of our target and this potential is referred in terms of electromotive force (EMF).

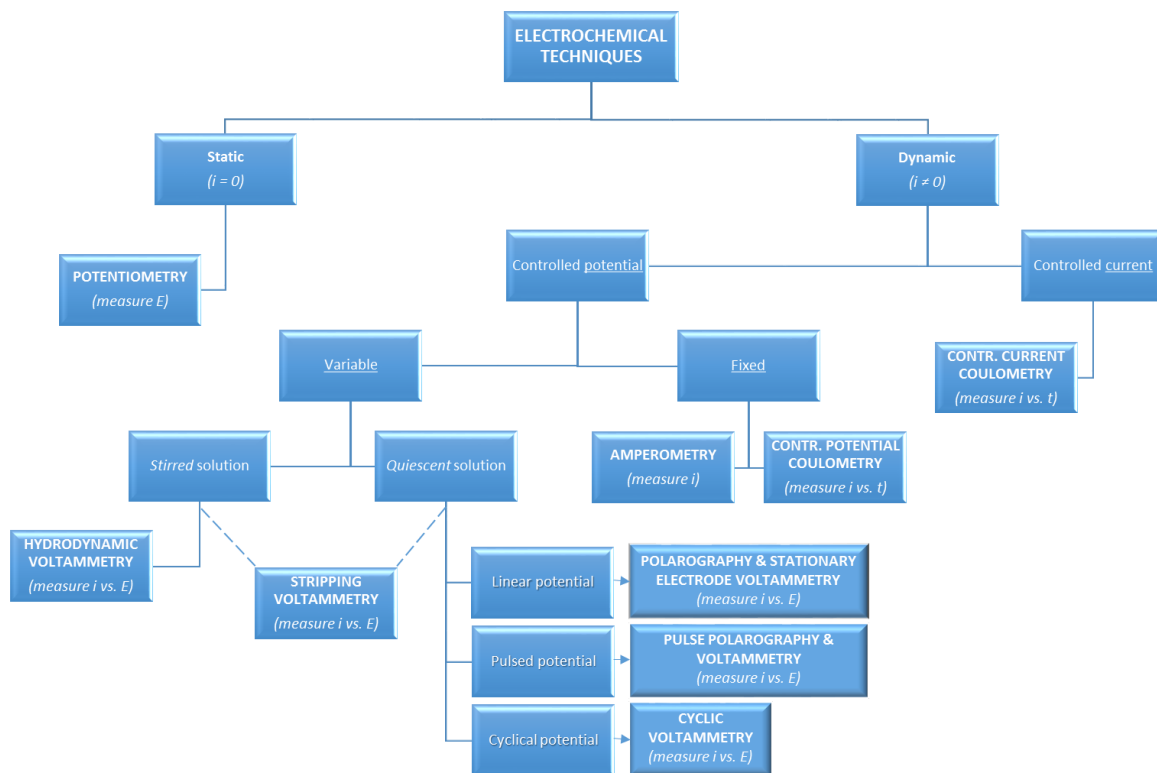


**Figure 2.1.** Classification of the electrochemical techniques according to the parameters that can be controlled and measured.

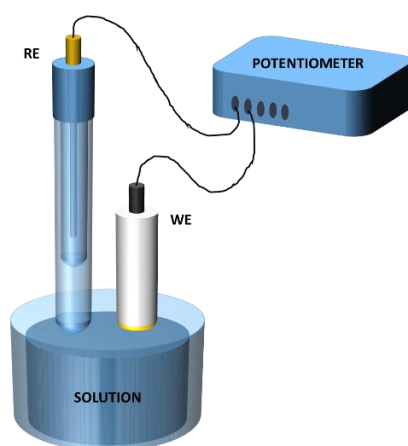


**Figure 2.2.** Schematic representation of a potentiometric cell with the reference (RE) and working electrodes (WE) plus the device needed to transduce the analytical signal, a potentiometer.

In the most basic form, the potentiometric response is represented by the Nernst equation (Equation 2.1), which describes the expected difference of potential between the working and reference electrodes according to:

$$E = E^0 + \frac{RT}{nF} \log a_{i(aq)} \quad (\text{Equation 2.1})$$

where  $E$  is the difference of electrical potential measured in the electrochemical cell,  $E^0$  is the standard electrochemical potential of the cell,  $n$  is the number of electrons involved in the reaction or the charge of the ion,  $R$  is the universal gas constant ( $8.314 \text{ J}\cdot(\text{K}\cdot\text{mol})^{-1}$ ),  $T$  the absolute temperature in Kelvin,  $F$  the Faraday constant ( $96485 \text{ C}\cdot\text{mol}^{-1}$ ) and  $a_{i(aq)}$  is the activity of the uncomplexed primary ion in the aqueous phase.

Activities determine the “effective concentration” of species as well as the real chemical potential. The activity can be estimated with the concentration ( $c$ ) and the activity coefficient ( $\gamma$ ), this coefficient is 1 for ideal conditions (Equation 2.2).

$$a_I = \gamma_I \cdot c_I \quad (\text{Equation 2.2})$$

Activities can be calculated using, for example, the Debye-Hückel approximation<sup>[1]</sup> for diluted solutions. Here the ionic strength term is introduced (Equation 2.3).

$$\ln(\gamma_I) = -Az_I^2\sqrt{I} \quad (\text{Equation 2.3})$$

where  $A$  is a constant that depends on the temperature,  $z_I$  is charge and  $I$  is the ionic strength. This ionic strength is used to express the effect of the charge of the ions that are in the media (Equation 2.4).

$$I = 0.5 \sum c_I z_I^2 \quad (\text{Equation 2.4})$$

where  $z_I$  is the charge of each one of the species in solution.

Potentiometry has several advantages over other electrochemical techniques, particularly when field-based methodologies are considered. One of the main advantages is its unrivalled simplicity of operation and instrumentation, roughness, fast response, wide linear dynamic range, and low instrumental cost. Regarding the limitations, it is important to remark the limited selectivity, the relatively poorer limits of detection (compared with other electrochemical methods) and the need for calibration of the electrodes (something that is common to almost all the techniques).<sup>[2-4]</sup> Despite of all limitations, potentiometry presents many advantages to be a truly candidate for the development of decentralized chemical devices over other electrochemical techniques as it is demonstrated along this thesis.

## 2.1.2. Voltammetry and Amperometry

In both methods, voltammetry and amperometry, the current resulting from the application of a voltage to the system is directly correlated to the bulk concentration of electroactive species or their production-consumption rate within the contiguous catalytic layer. Unlike potentiometry, the voltammetric and amperometric techniques make use of three electrodes. Besides the working and reference electrodes (WE and RE), a third electrode called counter electrode (CE) or auxiliary is required. The current passes between the working and counter electrode and it is recorded as a function of its potential measured against a reference electrode. To carry out these electrochemical techniques a special electronic device called potentiostat is needed (Figure 2.3). On this way it is possible a carefully control of the voltage or current that the system receives (see Figure 2.1).

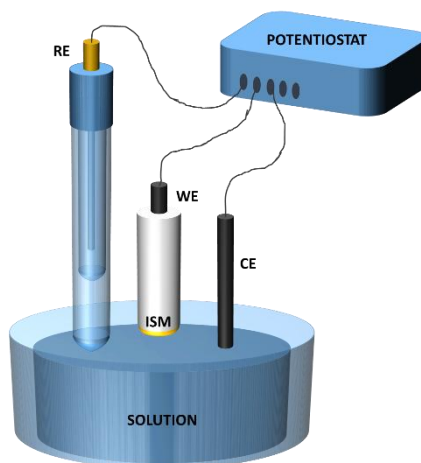


**Figure 2.3.** Illustration of an electrochemical cell where three electrodes working, counter and reference (WE, CE and RE) are measuring current by using a potentiostat.

Voltammetry is not a single technique, but it refers to a number of techniques in which an applied potential causes an electrochemical oxidation or reduction of electroactive species (redox reaction) that produces a measurable current, i.e., an electrolysis of the species. There are different types of voltammetric methods depending on the way how the applied potential is changing over the system to obtain a current. One of these most used methods is the cyclic voltammetry (CV), which is performed by cycling the potential of a working electrode. In the linear sweep voltammetry the potential is swept linearly in time. In each case, current is measured and represented as a function of the applied voltage.

Amperometry is one of the most widely used electrochemical techniques in analytical chemistry. It is based on measuring a current generated while maintaining a constant applied

potential (where the electrochemical reaction happens) at a metallic (platinum, gold or carbon) based working electrode or on array of electrodes (counter electrode where an electrical current is expected to flow) with respect to a reference electrode. The resulting current is directly correlated to the bulk concentration of the electroactive species or its production or consumption rate within the adjacent biocatalytic layer. As biocatalytic reaction rates are often chosen to be first order dependent on the bulk analyte concentration, such steady-state currents are usually proportional to the concentration of the analyte in the bulk.<sup>[5]</sup> In the following sections it will be explained in detail the working principles of this type of measurements.

## 2.2. ELECTROCHEMICAL POTENTIALS

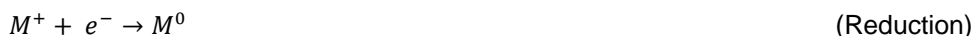
Electrochemical potential is a thermodynamic magnitude that results from the combination of electrical and chemical potentials. Electric potential, at a given point, is the work per unit of charge required to bring a charge from infinity to that point in the electric field and the chemical potential of a substance in a mixture of substances is directly related to the Gibbs free energy (G) of the mixture. By definition of the IUPAC, the electrochemical potential of a substance in a specified phase is the partial molar Gibbs free energy of the substance at the specified electric potential. Accordingly, all the charged chemical species have an electrochemical potential ( $\text{J}\cdot\text{mol}^{-1}$ ) at a given point in space that is generated by the influenced of the electrical field of the system as well as the chemical gradient of the species.

### 2.2.1. Redox potential

Oxidation-reduction (redox) reactions involve the energy transfer of an electron from a donor to an acceptor species. Since the difference of redox potential is measured under conditions of zero flux of current (the "reversible" conditions of classical thermodynamics, or the open circuit potential -OCP-), it is a direct measure of the free energy change of the reaction of the electrochemical cell. The tendency of these electrons is measured by the standard reduction potential of the chemical species, when the tendency is to acquire electrons (therefore be reduced), or release electrons (therefore be oxidized) (Equation 2.5). As any redox reaction can be divided into two half reactions, one in which a chemical species undergoes oxidation and one in which another chemical species undergoes reduction, if a half-reaction is written as a reduction, the driving force is the reduction potential. If the half-reaction is written as oxidation, the driving force is the oxidation potential related to the reduction potential by a sign change. So the redox potential is the reduction/oxidation potential of a compound measured under standards conditions against a standard reference half-cell that follows the Nernst equation (Equation 2.6) as it was mentioned previously.



Two half-reactions:



$$E = E^0 - \frac{RT}{nF} \ln \frac{[Red]}{[Ox]} \quad \text{(Equation 2.6)}$$

### 2.2.2. Donnan potential

Donnan equilibrium consists in the behaviour of charged particles under an unequal distribution due to differential mobility near a semi-permeable membrane or impermeable boundary for one of the ionic species. The usual cause is the presence of a different charged substance that is unable to pass through the membrane and thus creates an uneven electrical charge distribution, such as those occurring in blood plasma with large anionic proteins that are not permeable to capillary walls. In general, when there is a difference in mobility of the negative and positive charges, and one of them is fixed, there will be a Donnan potential associated. Lots of studies show that the establishment of Donnan equilibrium is a complex process and can be affected by various interactions such as pH.<sup>[6]</sup> The Donnan membrane principle is widely used in many fields, allowing -for example- many engineered processes and materials to achieve better sustainability.<sup>[7]</sup>

### 2.2.3. Mixed potential

The concept of mixed potential was introduced by Wagner and Traud several decades ago.<sup>[8,9]</sup> The mixed potential system was commonly used in corrosion field and other areas such as reaction kinetics<sup>[10]</sup> and catalysis.<sup>[11,12]</sup> The main idea behind this concept is that the resting potential of an electrode can be defined either by the open circuit potential (OCP) -i.e., is the equilibrium potential where the zero total current flows in the electrode-, or a mixed potential under kinetically controlled, non-equilibrium conditions. The resting potential of an electrode where the solution contains no reversible redox couple to establish the electrode potential, other half reactions may combine to produce a zero net current. On that way, the potential of the electrode can be set to the so-called mixed potential of the system<sup>[13]</sup> where two (or more) simultaneous reactions occur in parallel giving way to a series of potentials whose combination will give the resting potential of the system.

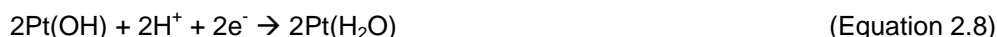
Through the concept of the mixed potential it is possible to explain why during the oxygen reduction reaction (ORR) in a weakly adsorbing electrolyte on polycrystalline platinum (Pt), the hydrogen peroxide (even if it is form as an intermediate) cannot be detected in the bulk

solution. This concept also reveals that reactions of the hydrogen peroxide will critically depend on the Pt surface state, which is also affected by the electrode potential. For instance, when the hydrogen peroxide interacts with reduce sites it decomposes producing adsorbed OH species, meanwhile when it interacts with oxidized Pt sites the hydrogen peroxide is oxidized to O<sub>2</sub> by reducing the surface. At the end, the ratio of oxidation/reduction of hydrogen peroxide can be used to establish the surface oxidation state.<sup>[14]</sup>

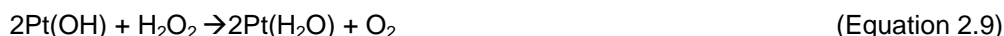
Following the approach proposed by Katsounaros *et al.*, on an OH-free Pt surface at sufficiently low potentials, first hydrogen peroxide dissociates on at least two oxide-free platinum sites to OH<sub>ads</sub> in a non-electrochemical step:



The dissociative adsorption of H<sub>2</sub>O<sub>2</sub> to form adsorbed OH species has been also suggested by many computational studies.<sup>[15,16]</sup> Since adsorbed OH on Pt is not stable at these low potentials, the surface sites are rapidly regenerated in an electrochemical reduction step, so that the free Pt sites become again available to dissociate other hydrogen peroxide molecules:



In contrast, at sufficiently positive potentials, where oxygenated species are adsorbed on platinum sites, first hydrogen peroxide is oxidized on two OH-covered platinum sites to O<sub>2</sub> in a non-electrochemical step:



The oxide-free Pt surface is however not stable at such positive potentials, so that in an electrochemical step the reduced surface sites are re-oxidized and become available again to oxidize H<sub>2</sub>O<sub>2</sub>:



This mechanism, which is based on the generation of an inhomogeneous surface of Pt coated by oxide islands is a complex kinetic process where part of the same electrode will trigger anode(oxidation)-type reactions, while the other will assume a cathode(reduction)-nature. From the balance of these two reactions (whose currents, similar and opposite, cancel each other) the resting potential of the electrode will finally emerge.

### 2.3. ELECTROCHEMICAL SENSORS

Sensors are devices used to detect properties of the surrounding environment. Physical sensors usually involve interactions with energy sources (light, temperature, sound, etc). A large number of this type of sensors is nowadays at the mass market level. A wide range of

physical parameters -such as vibration, light or motion- can be monitored. Chemical sensors are also an important field of research, where parameters from a single ion to proteins or even microorganisms can be detected. In the case of chemical sensors, however, direct interactions between the target species and a sensing surface are usually required. Chemical sensors, which have been applied in a plethora of fields,<sup>[17]</sup> can be roughly split into electrochemical and optical sensors. Both types of devices have an interface that interacts to generate a signal as manageable parameter. The focus of this thesis is centred on the transformation of chemical parameter into electrical signals by the use of suitable devices. A transducer element is usually required in the sensors in order to translate the signal from the chemical to the electrical domain. In summary, chemical and electrochemical sensors normally have two main components, a recognition element (that provides the sensor with high selectivity towards the target) and a physico-chemical transducer (that transforms the chemical information into an analytically useful signal) -see Figure 2.4-

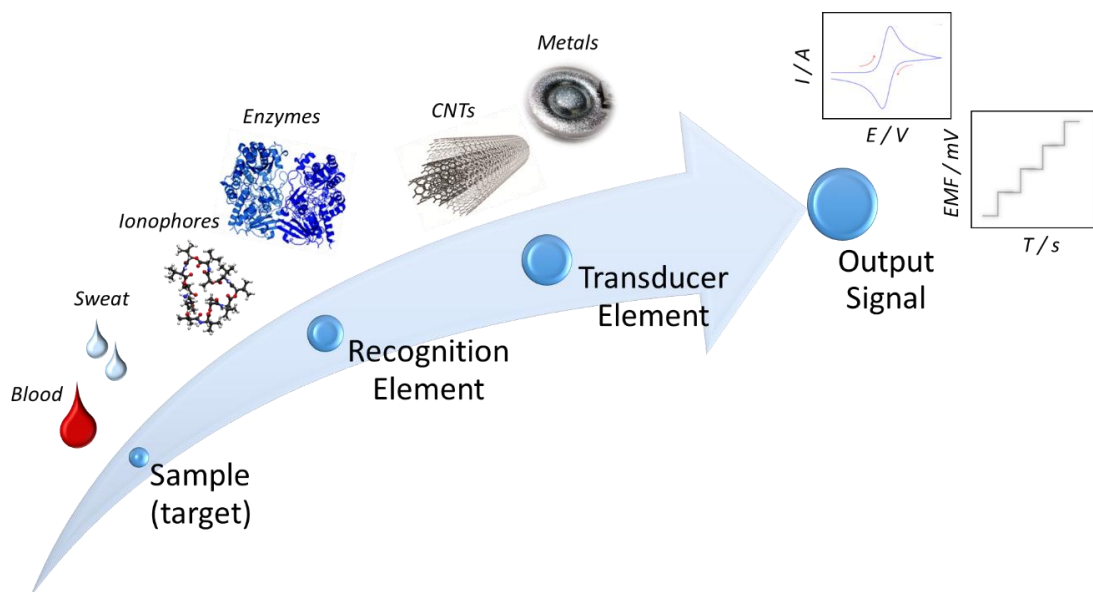


**Figure 2.4.** General overview of the measuring process in an electrochemical sensor.

The activity in the field of electrochemical sensors has undergone a massive development over the last decades,<sup>[18]</sup> with devices that range from ion selective electrodes to enzymatic sensors to monitor either biological or non-biological analytes.<sup>[5]</sup> More recently, the development of chemical sensors for decentralized tools has become one of the areas where electrochemical sensors have made a major influence, representing a massive opportunity to build platforms with the ability to collect and record data in remote settings. The growth of

electrochemical tools has facilitated the shift from the lab-based measurements into the point of need testing (e.g., the glucometer).<sup>[19]</sup> Advances in easiness of use, portability, specificity, and affordability of sensors and biosensors are offering new and exciting opportunities for numerous decentralized applications, ranging from 'alternative-site' testing (e.g., physician's office emergency-room screening, bedside monitoring, or home self-testing)<sup>[20]</sup> to a completely established intelligent data acquisition system, such as those required in smart cities.

The main components as well as the working principle of the electrochemical sensors developed during this thesis will be displayed with more detail in the following sections. Although there are several ways to manufacture a sensor, the key elements of differentiation are the recognition and transducer components. Hence, the discussion will be structured mostly around these two elements and not in the construction processes itself. The components involved in the fabrication of different types of sensors will be discussed and different working principles will be described in order to understand how the sensors developed during this thesis selectively detect the analyte of interest. The type of response will depend on the type of electrochemical sensor used for a specific application.

### **2.3.1. Potentiometric systems**

#### Components of solid-contact ion selective electrode

Ion-selective electrodes (ISEs) are an important subgroup of electrochemical sensors characterized by their small size, portability, low-energy consumption and low cost.<sup>[21]</sup> The history of ISEs goes back all the way to 1906, when Max Cremer developed the pH-sensitive glasses,<sup>[22]</sup> which led to the first commercial pH glass electrodes in the 1930s.<sup>[23,24]</sup> This type of potentiometric sensors produces an electrical potential upon variations in the activity of one specific ion in solution. ISEs based on polymeric membranes containing neutral or charged carriers called ionophores are available since many years ago for the determination of a large number of targets.<sup>[25,26]</sup> Depending on the membrane (which is designed according to the ion of interest) the ISE is able to sense the target more selectively than other ions present in the solution. In this thesis, a type of ISE called solid-contact ion selective electrode (SC-ISE) is used instead of the internal solution ion selective electrode (IS-ISE). The most important part of an ISE probably is the ion selective membrane (ISM). This key component has all the sensing elements needed for the recognition of the analyte: selective receptor or ionophore, lipophilic ion-exchanger and a polymeric matrix dissolved in a plasticizer (see Figure 2.5).



### Ionophore

The ionophore is a molecule that acts as receptor of the target species and that plays an important role, since it defines the selectivity of the sensors by binding the primary ion. Therefore, ionophores are specifically designed and synthesized according to the nature of each analyte in terms of charge, size and shape. In general, ionophores are based on the ability to form supramolecular (host-guest) assemblies by hydrogen bonds, metal coordination and hydrophobic/lipophilic forces. In order to obtain a successful ionophore, is important to take into account other factors such as the equilibrium and formation constant related with the interaction between ionophore and analyte and the stoichiometry of the reaction involved.<sup>[27]</sup> The affinity constant of the ionophore determines the sensitivity and linear range of the sensor among others, thus affecting the analytical performance.

### Lipophilic ion-exchanger

This is normally a salt composed by a large organic molecule that can have both, positively or negatively charge, and a small cation or anion that acts like a counterion. This element guarantees the permselectivity of the membrane (Donnan exclusion), which means that the ion-exchanger avoids co-extraction of ions with different charges from the sample into the membrane phase. Typical salts normally used are Sodium tetrphenylborate (NaTPB), Potassium tetrakis[p-chlorophenylborate] (KTPCIPB) and Potassium tetrakis[3,5-bis(trifluoromethyl)phenyl]borate (KTFPB).

### Polymeric matrix

This element provides a mechanical support and stability to the ISM. Usually, a very high molecular weight vinyl chloride homopolymer such as polyvinyl chloride is employed. The polymers are inert and insoluble in water, promoting a distribution of ions in two different phases, namely: lipophilic (membrane) and aqueous media. Typical polymers used include: poly(vinyl-chloride) (PVC), polyurethane (PU) and other types of membranes based in n-butyl acrylate (n-BA), methyl (MMA) and decyl methacrylate (DMA) have been emerged.<sup>[28-30]</sup>

### Plasticizer

The main role of this component is to make the membranes softer, flexible and more homogeneous and resilient to mechanical stress such as bending or stretching. The advantage of use a plasticizer is to facilitate the movement of the polymer macromolecules and thus influencing the partitioning of ions, because the diffusion coefficients (and so the mobility of the ions). Some of the commonest used plasticizers are: Bis(2-ethylhexyl sebacate) (DOS with apolar properties) or o-nitrophenyl octyl ether (o-NPOE with polar properties).

## Transducer

This element converts the change on a given (physical or chemical) property into a measurable electrical signal. In potentiometry, transducers are responsible for ion-to-electron signal conversion. The first transducers used in potentiometry were liquids (i.e., inner solution electrodes). However, due to the revolution of the solid-contact sensors new materials appeared, such as conducting polymers and nanostructured materials.<sup>[31]</sup> In this thesis carbon nanotubes (CNTs) have been used as transducers.

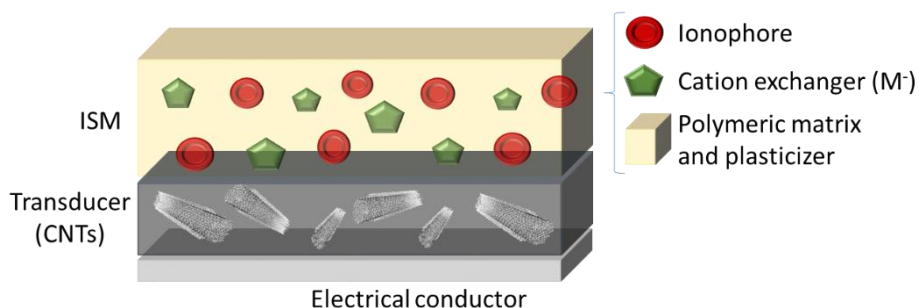


**Figure 2.5.** Schematic representation of a solid-state ion-selective electrode (SC-ISE). The magnification shows the elements of an ion-selective membrane (ISM).

## Working principle of solid contact ion-selective electrode

Solid contact ion-selective electrodes (SC-ISE) are one type of potentiometric sensor that can selectively determine the activity of their primary ion in a solution in the presence of other ions, depending on a membrane composition. SC-ISEs are a technological evolution of the conventional ISEs, which are usually based on the use of an inner solution. The first type of these electrodes was the glass electrode, reported back in 1909.<sup>[32]</sup> This type of sensor is still widely used for measuring pH and it is established in almost every laboratory in the world for its robustness and usefulness. The potential generated is measured against the reference electrode, and it is proportional to the logarithm activity of the primary ion according to Nernst equation (see section 2.1.1).

The difference of potential or electromotive force (EMF) measured between the RE and the ISE is the sum of potential of both electrodes plus additional potentials that can appear across the circuit (see Figure 2.6). These calculations are the same either IS-ISEs or SC-ISEs. The main contributions to the EMF read by the instrument can be summarised as:

$$EMF = E_M + E_{D,Ref} + E_{Const} \quad (\text{Equation 2.11})$$

Where:

$E_M$  = EMF considered as the sum of the sample-membrane boundary potentials.

$E_{D,Ref}$  = liquid junction potential at the interface with the reference electrode (double junction)

$E_{Const}$  = constant potential generated at the internal interfaces from membrane-transducer and transducer-conductor.

The actual potentiometric measurement determines the EMF as the difference in the electrical potentials between the connecting wire of the ISE and the connecting wire of a reference electrode.<sup>[24]</sup> Accordingly, the EMF in a potentiometric measurement equals the sum of all phase boundary potentials.

To describe the membrane potential different models (based on similar considerations) have been proposed. One of the most popular models to explain the generation of the electrochemical potential in ISEs is the phase-boundary potential,<sup>[33]</sup> which was originally conceived for the inner solution electrodes. It has been also extrapolated to SC-ISEs, and thereby, the  $E_M$  is divided into three potentials:  $E_{PB}$ , the phase boundary potential between the inner solid contact (transducer) and the membrane;  $E_D$ , the diffusion potential inside the membrane; and,  $E_{PB}$ , the phase boundary potential between the membrane and sample solution (Equation 2.12).

$$E_M = E_{PB} + E_D + E_{PB} \quad (\text{Equation 2.12})$$

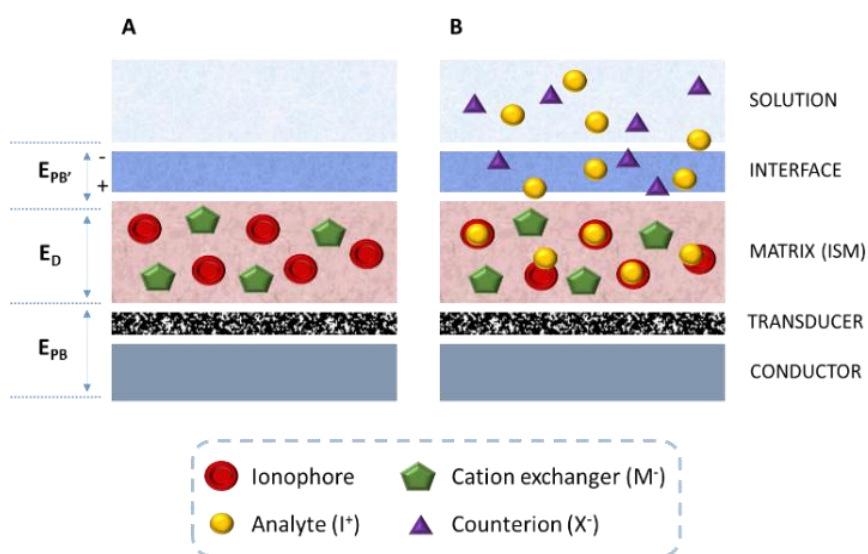


**Figure 2.6.** Diagram of the mechanism of the phase boundary potential. (A) SC-ISE in an aqueous solution without ions (B) membrane placed in contact with an aqueous solution that contains the primary ion and counterion ( $I^+$  and  $X^-$ ) reaching the electrochemical equilibrium.

To simplify the calculation of the membrane potential and the border effects that are always difficult to model, some assumptions might be applied. First of all, the contribution of the diffusion potential ( $E_D$ ) is ignored, assuming thus the electroneutrality in the bulk of the membrane. Secondly, the internal phase boundary potential  $E_{PB}$  is considered constant. As a matter of fact, the control of this potential is what made possible the emergence of solid state technology. Indeed, an attempt to develop SC-ISEs was the coated-wire electrode, reported back in the '70s.<sup>[34]</sup> It was a primitive form of the SC-ISE that did not use ion-to-electron transducer. Therefore, it had a highly variable  $E_{PB}$  that made impossible any practical application. Thanks to the use of other transducers such as conductive polymers and nanomaterials, this inner potential was stabilized and hold constant during the measurements. As a result, membrane potential depends only on the phase boundary potential in contact with the sample ( $E_M = E_{PB}$ ). Moreover, the electrochemical equilibrium is assumed at the sample (aqueous phase) and membrane (organic phase) (Equation 2.13).

$$E_M = E_{PB} = \frac{\mu_{i(aq)}^0 - \mu_{i(org)}^0}{n_i F} + \frac{RT}{n_i F} \ln \frac{a_{i(aq)}}{a_{i(org)}} \quad (\text{Equation 2.13})$$

where  $\mu_{i(aq)}^0$  is the standard chemical potential in the aqueous phase,  $\mu_{i(org)}^0$  is the standard chemical potential in the organic phase,  $n_i$  is the charge of the primary ion,  $R$  is the universal gas constant ( $8.314 \text{ J} \cdot (\text{K} \cdot \text{mol})^{-1}$ );  $T$  the absolute temperature,  $F$  the Faraday constant ( $96485 \text{ C} \cdot \text{mol}^{-1}$ ),  $a_{i(aq)}$  the activity of the uncomplexed primary ion in the aqueous sample and  $a_{i(org)}$  the activity of the primary ion in contact with the organic phase.

The following mathematical expression explains the generation of the potential at the interface being  $\Delta G_{tr}^{0,w \rightarrow m}$  the free standard energy of the distribution process of ion  $i$  between two phases and  $k_i$  correspond to the "single ion distribution coefficient" (Equation 2.14). Indeed,  $k_i$  is function of the relative free energies of solvation in both the sample and the membrane phase.

$$\mu_{i(aq)}^0 - \mu_{i(org)}^0 = \Delta G_{tr}^{0,w \rightarrow m} = RT \ln k_i \quad (\text{Equation 2.14})$$

In the classical potentiometric arrangement, electrochemical potential arises from the chemical work (Equation 2.15):

$$W_{Chem} = (\mu - \mu_0) = RT \ln \frac{a_{i(aq)}}{a_{i(org)}} \quad (\text{Equation 2.15})$$

as a consequence of the generation of a chemical gradient (charge separations due to partition of cations and anions between the organic membrane and aqueous sample) and the electrical work (Equation 2.16) performed with the electrical field generated by the charges.

$$W_{El} = QV = n_i FV \quad (\text{Equation 2.16})$$

Then, obtaining Equation 2.17 for the calculation of the membrane potential and consequently Equation 2.18.

$$n_i FV = RT \ln \frac{a_{i(aq)}}{a_{i(org)}} \quad (\text{Equation 2.17})$$

$$(V - V_0) = \frac{RT}{n_i F} \ln \frac{a_{i(aq)}}{a_{i(org)}} \quad (\text{Equation 2.18})$$

Considering that the standard potential ( $V_0$ ) is ideally constant (includes factors affecting the solvation of the ion in the membrane and solution phases) and the activity coefficients are constant in the organic phase (then included into the constant part of the equation), a simple mathematical representation can be obtained in the well-known form of the Nernst equation (Equation 2.1).

The charge separations between cations and anions at the interface membrane-aqueous solution are generated due to the difference in the free Gibbs energies in each phase (thus hydration energies and ionophore affinity play a very important role in this phenomenon). Accordingly, the cation or anion ( $I^{+/-}$ ) (depending on the membrane composition) has a greater tendency to pass into the membrane phase than the counterion ( $X^{+/-}$ ) (due to the ion exchanger molecule and ionophore properties), generating an electrical double layer at the interface (charge separation) thus raising a difference of electrochemical potential. Under ideal conditions, the arrangement of the gradient of charges will lead to a magnitude of the electrical

potential that is proportional to the logarithm of the concentration of the ions, as described by Equation 2.1.

### Components of enzymatic electrodes

Biosensors can be made with a plethora of different approaches and materials.<sup>[35]</sup> In this thesis, sensors that use an enzyme as recognition element will be described. The main elements of these type of sensors are shown in Figure 2.7.

#### Conductor

Sensors need a surface that can carry the electrical signal from the interface to the measurement device. In the case of some biosensors, such as the enzymatic sensors used in this work, the conductive component can act also as a transducer. Some of the metallic conductors used for the development of enzymatic sensors are: platinum and carbon-based inks decorated with platinum nanoparticles.

Both cases share the same principle, the platinum transducer (either coating or nanoparticles electrodeposited) is capable of sensing the hydrogen peroxide produced by the enzymatic reaction. Since platinum is a noble metal with a positive standard potential (+1.7 against hydrogen standard electrode) it has high tendency to be reduced. In some studies, it has been reported that platinum strongly catalyzes the decomposition of hydrogen peroxide into water and oxygen and, for example, it can be used in fuel cells as a catalyst for the reduction of oxygen.<sup>[36]</sup>

#### Polymeric matrix

The polymers used in this work have as a main role the entrapment of the enzyme and create the suitable environment where the enzymatic reaction should occur. In addition to build the mechanical support, polymers can also offer a wide range of advantages such as separation of the electrode from the rest of the solution, which also helps to avoid the effect of some important interferences such as ascorbic acid in physiological samples. Polymers employed during this work consist in polyelectrolytes such as Nafion, Aquivion, Chitosan, etc.

- Chitosan is a linear polysaccharide composed of randomly distributed  $\beta$ -(1 $\rightarrow$ 4)-linked D-glucosamine (deacetylated unit) and N-acetyl-D-glucosamine (acetylated unit).
- Nafion and Aquivion are sulfonated tetrafluoroethylene based fluoropolymer-copolymer with proton exchange capabilities. Pores allow movement of cations but the membranes do not conduct anions or electrons. The main difference between

them is the length of the chain and because of that, Aquivion has more density of sulfonated groups.

### Enzymatic layer

The enzymatic layer (recognition element) acts as natural receptor that specifically interact with the analyte, catalysing a reaction in a selective way. In other words, this layer proves high selectivity to the sensor.

Although several oxidases enzymes have been tested (such as cholesterol, galactose or uric acid oxidases) the leading enzyme utilized in the vast majority of the works during this thesis was glucose oxidase (GOx). Other types of enzymes (also tested) need a cofactor in order to facilitate the enzymatic reaction of interests (such as glucose dehydrogenase). Besides, depending on the electroanalytical technique used along the process, a mediator might be used in order to facilitate the current transduction, thus decreasing the potential applied.

It is important to remark that not all the enzymes have the same characteristics. For instance, some parameters like the activity or the optimal working pH are specific of each enzyme. Hence, it is crucial to understand the chemical behaviour of each one of them in order to maximize the electrochemical performance of each biosensor and to know the limitations of each enzymatic reaction.

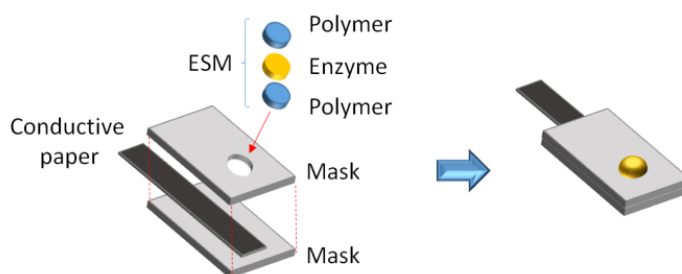


**Figure 2.7.** Schematic representation of a paper-based enzymatic electrode. The enzymatic selective membrane (ESM) is also outlined in three main components.

### Working principle of enzymatic sensors

Enzymatic sensors (biosensors) are commonly known and used in the field of amperometry but not so much in potentiometry.<sup>[35]</sup> However, a good part of this thesis is devoted to the development of potentiometric paper-based enzymatic biosensors. In this type of biosensors the enzyme is incorporated in the recognition layer to selectively interact with one specific

target. These interactions between the enzyme and the analyte promote a chemical reaction where the enzymatic products produce a difference of potential. The first potentiometric enzyme-based electrode was a urea biosensor that consisted on a urease immobilized over a glass ammonium electrode.<sup>[37]</sup> This working principle is still the most used in potentiometric enzyme electrodes.<sup>[38]</sup>

Figure 2.8 summarizes in a very basic way how the potentiometric biosensor works. First, the target (for instance glucose) can interact with the enzyme that normally will be entrapped or immobilized in between a polymeric matrix (all this matrix is the enzymatic selective membrane -ESM-). Then, the enzyme acts as a catalyst of a chemical reaction. Finally, the product or by-product (such as hydrogen peroxide in our case or ammonium ion in the urea biosensor) can be detected by the rest of the electrode (normally the conductive element).

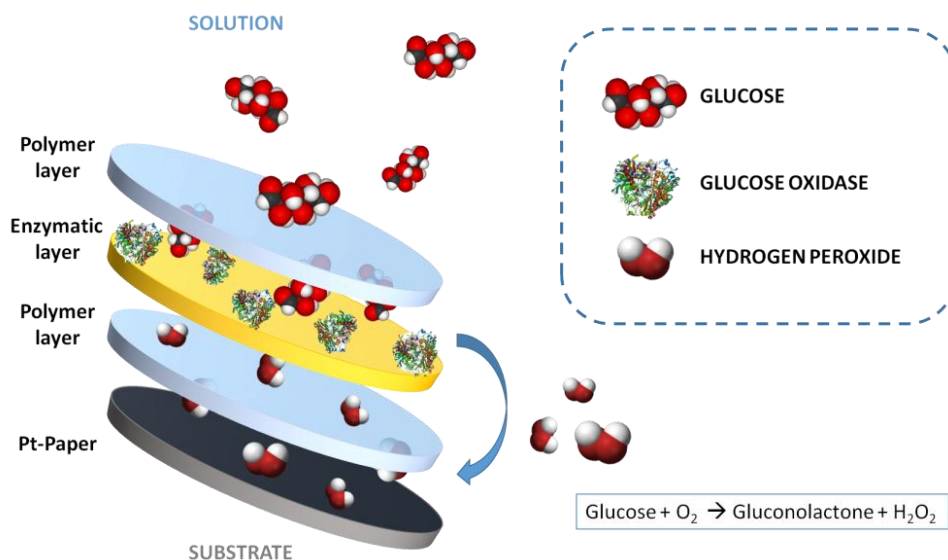


**Figure 2.8.** Layers (plus substrate) involved in the ESM of a paper-based enzymatic electrode and the detection of the analyte of interest due to the enzymatic reaction that happens in between of these layers.

Malcon Dixon and Edwin Webb proposed in 1958 one classification of enzymes that is formed by six different groups: oxidoreductases, transferases, hydrolases, lyases, isomerases and ligases. The classification is based in the specificity of the enzymatic reactions that enzymes catalyze as well as the specificity of the substrates and co-substrates or co-enzymes of the reaction. For example, the first group “oxidoreductases” encompasses all the enzymes that catalyze the redox reactions (oxidation or reduction). Generally, they are called as



dehydrogenases because the oxidized substrate is a donor of hydrogen. The term “reductases” can be also used. Only when the oxygen is the acceptor of the electrons they are called oxidases.<sup>[39]</sup>

In the reaction catalyzed by an enzyme, the formation of the intermediate enzyme-substrate complex (ES) must be taken into account. This ES complex turns into a transition state or activated ES\* complex. If a model elemental reaction, Substrate  $\leftrightarrow$  Product, catalyzed by an enzyme (E), composed of a single substrate (S) and a single product (P) is assumed, we can consider the following steps:

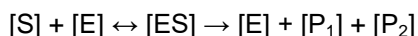


Following this sequence of reactions a series of Gibbs free energies can be defined (Equation 2.19).

$$AG_S = AG_S^0 + RT \ln \frac{[ES]}{[E][S]} \quad (\text{Equation 2.19})$$

where  $[ES]$ ,  $[E]$  and  $[S]$  represent the current concentrations of free enzyme, enzyme-substrate complex and substrate respectively.

According to the Michaelis and Menten studies, the enzyme can rapidly form a complex with the substrate in an unstable way that decomposes in the free enzyme and two products ( $P_1$ ) and ( $P_2$ ):



The dissociation constant of the enzyme-substrate complex is:

$$K_S = \frac{[E][S_0]}{[ES]} \quad (\text{Equation 2.20})$$

where  $[S_0]$  is the initial concentration of substrate,  $[E]$  enzyme free concentration and  $[ES]$  is the concentration of the enzyme-substrate complex.

At the same time, the rate at which the reaction occurs can be measured as the disappearance of substrate with respect to time or as the appearance of product with respect to time. The Michaelis-Menten equation indicates the velocity behavior with respect to the substrate concentration (Equation 2.21).

$$v_0 = V_{max} \frac{[S_0]}{K_s + [S_0]} \quad (\text{Equation 2.21})$$

During this thesis enzyme oxidases have been widely employed such as glucose oxidase (GOx). Thanks to its catalytic activity, in presence of glucose and oxygen, the enzyme is able to produce gluconolactone and hydrogen peroxide, which is the byproduct directly measured by our sensors.

### 2.3.2. Voltammetric systems

#### Components of voltammetric electrodes

There are countless types of voltammetric sensors that can be manufactured with different components. The most distinctive electrode in voltammetric sensors is the working electrode. Working electrodes can be made by different conducting materials. The most used materials are metallic elements such as platinum, gold, silver, mercury, and carbon that might be applied for the detection at different potentials. Except for the carbon paste electrode, a solid electrode is fashioned into a disk and sealed into the end of an inert support with a conducting wire. The carbon paste electrode is usually made by filling the cavity at the end of the inert support with a paste consisting of carbon particles and viscous oil. Solid electrodes are not without problems, the most important of which is the ease with which the electrode's surface is altered by the adsorption of a solution species or by the formation of an oxide layer. For this reason, a solid electrode needs frequent reconditioning, either by applying an appropriate potential or by polishing.

Depending on the voltammetric technique applied, a specially designed working electrode will be developed taking into consideration the materials used to fulfil the range of the working potential. Moreover, each working electrode will be fashioned with the corresponding elements in order to selectively produce a current signal. For example, enzymes, cofactors and mediators are used in amperometric sensors in order to detect a particular analyte.

Overall, a plethora of working electrodes can be designed to perform electrochemical analysis of a wide range of targets. In this thesis, the fabrication and assembly of the different layers (see Figure 2.9) are crucial steps during the electrode manufacturing.

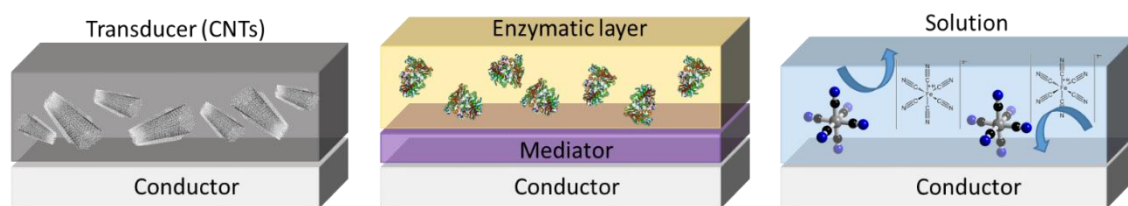


**Figure 2.9.** Schematic representation of all the elements involved in the development of different types of voltammetric electrodes depending on the voltammetric technique applied (such as stripping voltammetry, amperometry or cyclic voltammetry).

Figure 2.9 shows three different examples of voltammetric electrodes. From left to right direction, the first scheme displays an electrical conductor with a layer of transducer formed by carbon nanotubes. This electrode could measure the analyte of interest applying stripping voltammetric as technique. In the middle of the figure it is possible to see another system composed by the same electrical conductor layer, a mediator that favours the reaction that produces the signal and on top of it an enzymatic layer where the reaction occurs. This enzymatic system with mediator could be used with amperometric techniques. The last configuration (right part of the figure) consists in a simple scheme where an electrical conductor is immersed in a solution that contains redox species such as ferrocyanide. The application of techniques such as cyclic voltammetry can be very useful with this type of systems.

### Working principles of voltammetric sensors

Cyclic voltammetry is generally used to study the electrochemical properties of an analyte in solution.<sup>[40,41]</sup> It is often used to study a variety of redox processes, to determine the stability of reaction products, the presence of intermediates in redox reactions,<sup>[42]</sup> electron transfer kinetics,<sup>[43]</sup> and the reversibility of a reaction.<sup>[44]</sup> CV can also be used to determine the electron stoichiometry of a system, the diffusion coefficient of an analyte, and the formal redox potential of an analyte, which can be used as an identification tool. In addition, because concentration is proportional to current in a reversible, Nernstian system, the concentration of an unknown solution can be determined by generating a calibration curve of current vs. concentration.<sup>[45]</sup> Thus, a calibration curve can be obtained measuring the peak currents that increase proportionally with the target concentration (see Figure 2.10).

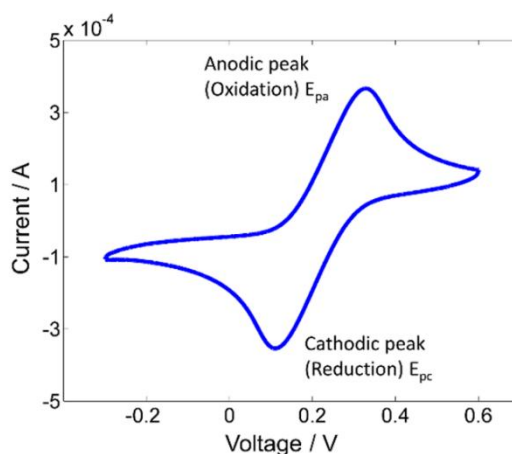


**Figure 2.10.** Typical CV spectra of a redox couple species.  $E_{pa}$  and  $E_{pc}$  are the potential corresponding to the anodic and cathodic peaks respectively.

CV is one of the most versatile electroanalytical techniques for the study of electroactive species. The potential scan is programmed to begin at an initial potential where no electrolysis occurs. The scan continues at the desired linear scan rate to the switching potential, then reverses direction and returns to the initial potential. The scan rate can be chosen over a wide range, typically from 0.001 to 200 or more  $V \cdot s^{-1}$ . The output of cyclic voltammetry is a plot of the current flowing in the electrochemical cell during the cyclic potential scan. Considering a solution containing electroactive species ( $O$ ) in the cell with a metal working electrode, which also contains a large concentration (e.g. 0.01 to 1 M) of inert electrolyte to lower the cell resistance and minimize electrical migration. Assuming that  $O$  is reversibly and rapidly reduced. Then equation 2.22 occurs, where  $n$  is the number of electrons transferred from the electrode to  $O$ .



This reaction is under diffusion control, i.e., the cell current is governed by the rate of diffusion of  $O$  to the electrode surface. In contrast, kinetic control may be active if the rate of the electrode reaction is slow with respect to the rate of potential scan.<sup>[46]</sup>

One way to test the efficacy of an electrochemical sensor using cyclic voltagrams is measuring the electroactive surface area. According to the Randles–Sevcik, the electroactive surface area can be calculated as the following equation shows (Equation 2.23):

$$A = \frac{I_p}{2.69 \times 10^{-5} D^{1/2} n^{3/2} \nu^{1/2} C} \quad (\text{Equation 2.23})$$

where  $A$  is the surface area ( $\text{cm}^2$ ),  $D$  is diffusion coefficient of the molecule in solution ( $\text{cm}^2 \cdot \text{s}^{-1}$ ),  $i_p$  is the peak current value,  $n$  is the number of electrons involved in the reaction,  $C$  is the concentration of the probe molecule in the solution ( $\text{mol} \cdot \text{cm}^{-3}$ ) and  $\gamma$  is the potential scan rate ( $\text{V} \cdot \text{s}^{-1}$ ).

Another way to check how the electrochemical sensor is stable in the presence of different types of manipulations is measuring the redox peak separation ( $\Delta E_p$ ) as well as the oxidation peak current ( $i_p$ ) using a ferricyanide probe.

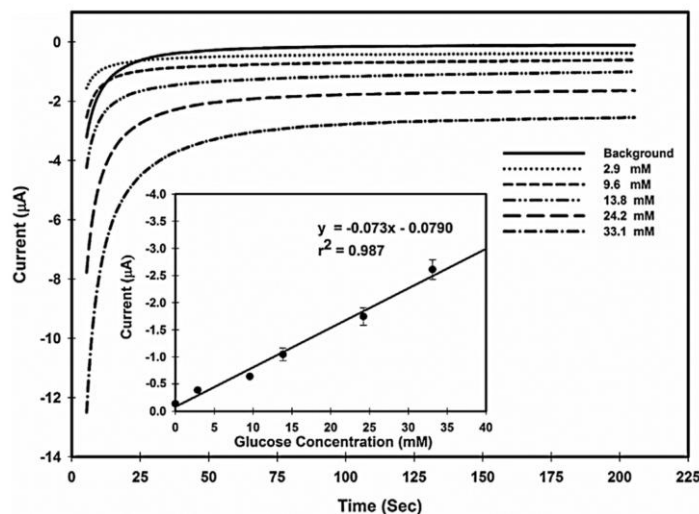


**Figure 2.11.** Typical chronoamperogram spectra by chronoamperometric technique from increasing concentrations of glucose.<sup>[47]</sup>

Voltammetric as well as chronoamperometric measurements are also carried out in order to test the performance of the sensors. Chronoamperometry is an electrochemical technique in which the potential of the working electrode is stepped at the same potential and the resulting current from faradaic processes occurring at the electrode (caused by the potential step) is monitored as a function of time. The current generated is established by the equilibrium in the diffusion of the analyte through the matrix onto the electroactive surface that undergoes reduction or oxidation of its species (depending on the applied potential). Therefore, the analyte concentration will be proportional to the equilibrium and the current produced, and accordingly, a calibration curve could be obtained (see Figure 2.11). Most commonly investigated sensors use a three electrode system, although some commercial sensors use two electrode configurations, where the counter and reference electrode work as the same electrode. Since the current is integrated over relatively longer time intervals, chronoamperometry can give a better signal to noise ratio in comparison to other voltammetric techniques.

Adsorptive stripping voltammetry (AdSV) is an electrochemical technique where the analyte of interest is first adsorbed onto the working electrode before being removed or 'stripped'. During removal the cell current is measured as a function of time and as a function of the potential between the working and reference electrodes. The intensity of the current generated is proportional to the concentration of analyte deposited on the surface. Besides, this technique allows the measurement of certain species taking advantage of some of the properties between the materials of the working electrode and the target analyte. For instance, it is well-known that nitroaromatic compounds are adsorbed by carbon nanomaterials thus allowing the detection of this type of compounds (see Figure 2.12). The specific patterns of each compound (according to the redox processes occurred during the potential scan) permit a selective recognition of the target analyte and a discrimination between other interferences.

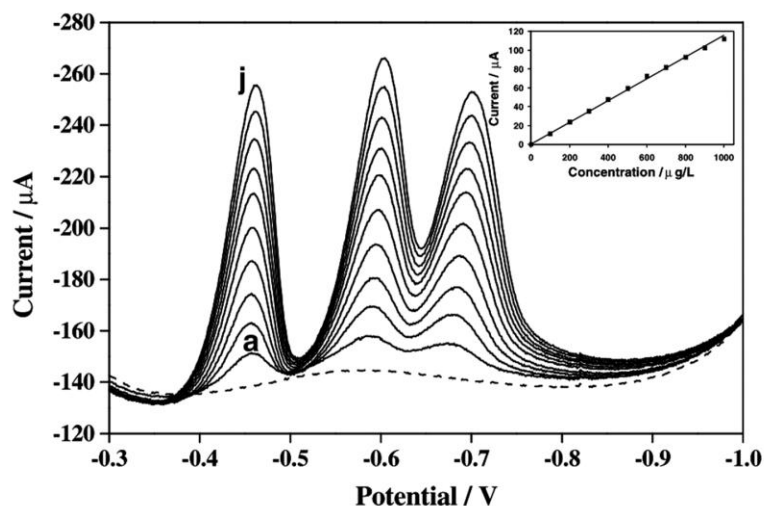


**Figure 2.12.** Typical reduction peaks obtained by adsorptive stripping voltammetry from increasing concentrations of organic molecules such as 2, 4, 6-trinitrotoluene (TNT).<sup>[48]</sup>

### 2.3.3. Reference systems

#### Components of reference electrodes

The most typical reference electrodes (RE) are composed by three main parts: the internal reference element, which is normally a Ag wire coated with solid silver chloride (Ag/AgCl), a solution compartment, where a highly concentrated salt solution (usually 3 M or even saturated KCl) and a liquid junction through which the electrical contact between the inner solution and the testing solution occurs. An outflow of the internal reference solution is generated which helps to stabilize the liquid-junction potential. In order to minimize the problem of

contaminations, double-junction reference electrodes have been developed. The double junction RE have two different compartments, the internal filled of a solution of potassium chloride 3 M is called inner filling, and the external one, outer filling that usually contains lithium acetate 1 M. This salt minimizes all the problems that arise from a liquid junction. All this combination is aimed to maintain a constant electrical potential. The fact that the reference electrode keeps a constant potential is essential to guarantee a change in EMF that only depends on the working electrode.

This type of RE has some limitations such as the miniaturization, the fixed working position and the need of periodical maintenance. To overcome all these limitations, solid contact reference electrodes have been developed. A polyvinyl butyral (PVB) solid-state reference electrode was built using a membrane based on the redox system  $\text{Ag}|\text{AgCl}|\text{NaCl}$ . In this specific case, the PVB saturated of sodium chloride acts as a hydrophilic polymer that creates a controlled diffusion (minimizing the leaching of species) between the membrane and the solution while maintaining the electrical potential of the  $\text{Ag}/\text{AgCl}$  and the conductivity over the circuit.

Next Figure 2.13 shows the main components of the REs mentioned in this section.

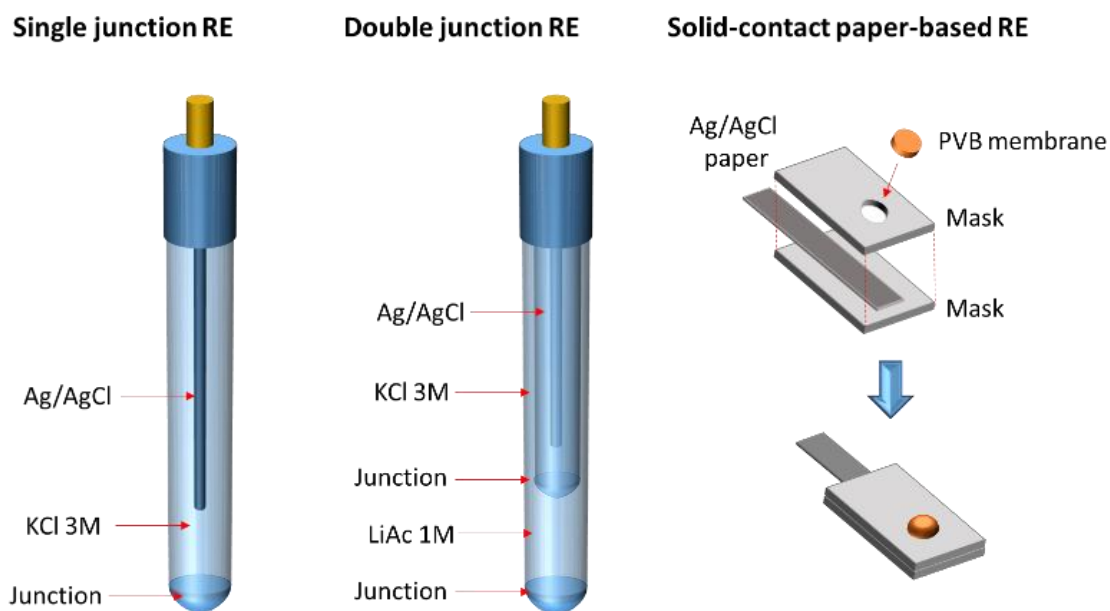


**Figure 2.13.** Schematic representation of the three different types of RE explained in this section: single junction, double junction and solid contact paper-based reference electrodes.

## Working principles of reference electrode

The reference electrode (RE) is a system whose response is insensitive to the change of composition of the solution. It shows a stable, reversible and reproducible potential when the composition of the sample changes. In case of signal fluctuation, it must return rapidly to its equilibrium value. There are many versions of reference electrodes such as standard hydrogen electrode, saturated calomel electrode, silver-silver chloride electrode, etc. Most of them are based on a redox system with a high concentration of a salt that allows controlling the potential when the current is flowing through the system. Most commonly used in potentiometry and during this thesis is the redox system based on silver-silver chloride electrode. Equation 2.24 shows that equilibrium:



where the solid silver chloride ( $AgCl$ ) is in contact with a silver wire, the ( $Ag$ ) is the metallic silver and the ( $Cl$ ) is the chloride ion.

In order to maintain a constant potential upon changes of concentration, an internal reference electrolyte with high concentration of  $Cl^-$  is used. This equilibrium can be expressed from Nernst equation as:

$$E_{AgCl/Ag} = E_{AgCl/Ag}^0 - \frac{RT}{F} \log a_{Cl^-} \quad (\text{Equation 2.25})$$

where  $E_{AgCl/Ag}^0$  includes the constant of solubility of  $AgCl$  ( $K_{ps}$ ).

When two different solutions are in contact (for example between inner liquid of reference electrode and the matrix), a liquid-junction or diffusion potential is created. The more concentrated solution will have a tendency to diffuse into the less concentrated one. As anions and cations have a different rate of diffusion depending on the electric field and the speed, its diffusion through time will result in an electrical double layer of positive and negative charges at the junction of the two solutions. This liquid-junction potential cannot be measured but can be estimated following the Henderson equation.<sup>[49]</sup> The use of KCl solution minimize the rise of junction potentials because both cation and anion have approximately equal mobility.

## **2.4. ANALYTICAL PERFORMANCE PARAMETERS**

In order to determine quantitatively the analytical performance of the sensor, different parameters have been extensively described. The most used parameters to fully validate the outstanding performance of electrochemical sensors (in particular potentiometric electrodes) are described in the following paragraphs.



## Sensitivity

The sensitivity is calculated from the slope of the calibration curve within the linear range. In potentiometry with ISEs, the slope is well established by the Nernst equation and it depends on the number of charges. The theoretical sensitivity is defined by  $RT/n_iF$  ( $59.2/n_i$  [mV·decade<sup>-1</sup>] at 25°C) ideally. Therefore, sensitivity gives information about the proper functioning of the working electrode. Nevertheless, it is important to remark that super and sub Nernstian sensitivity can be obtained in some cases.

## Linear range

The linear range is defined as the range of concentrations or ion activity where the calibration curve presents Nernstian linearity. This range determines the region where a sample of interest could be quantitatively measured. When developing sensors, this parameter is very important because if the measurements are not within the relevant linear range it will be difficult to obtain reliable results working in a real scenario.

## Limit of detection

The limit of detection (LOD) can be divided into lower and upper limit of detection. IUPAC defines the limits by the cross section of two extrapolated linear segments of the calibration curve.<sup>[50]</sup> The upper LOD is reached when the permselectivity is lost. On the other hand, lower LOD is of great interests for the applications of ISEs. It is calculated as the activity/concentration of the analyte at the intersection point between the linear segments of linear range and the low concentration level segment of the calibration curve. One of the main issues that may affect the lower LOD is the presence of interfering species in the sample solution. The lower LOD will be utilized to determine this analytical parameter along this thesis.

## Stability

In order to characterize the stability of the electrodes (WE or RE) an evaluation of the signal along short, medium and long periods is a very relevant parameter. Normally this kind of experiments are commonly used with potentiometric sensors (although it can be performed also in other types of electrodes) and the value of stability is expressed as a drift in mV·h<sup>-1</sup>. Interestingly, high stability is crucial for long real-time measurements and on-site applications, situations where a calibrated electrode is previously needed.

## Response time

The response time is the time required for a sensor to change from its previous potential to a final stable potential upon the addition of your target analyte, which is established according

to the experimental conditions. Usually, the response time is measured as the time lapse between the electrodes reaches the new concentration until gets 90% of the final value.

### Selectivity

Selectivity is one of the most important parameter because displays the ability of a sensor to detect a particular analyte in a complex mixture without interference from other components in that solution. The selectivity of the sensor has to be quantified individually for each particular interference and in potentiometry is expressed in terms of selectivity coefficients ( $K_{ij}^{pot}$ ). Theory and the experimental determination of the selectivity have been discussed for a long time.<sup>[51]</sup>

There are two main widely used methods to determine the selectivity coefficient in ISEs.<sup>[52]</sup> In the separate solution method (SSM), calibration curves with the interfering ions ( $j$ ) are performed, followed by a calibration curve of the primary analyte ( $i$ ) (Equation 2.26). Standard potential of each interfering ion ( $E_j^0$ ) and the primary analyte ( $E_i^0$ ) are extrapolated from the obtained calibration curves. Equitable selectivity coefficients are obtained only if the standard potential has been calculated with ISE exhibiting a Nernstian response for both ions.

$$K_{ij}^{pot} = e^{\frac{n_i F}{RT}(E_j^0 - E_i^0)} \quad (\text{Equation 2.26})$$

where  $n_i$  is the charge of the primary ion,  $R$  is the universal gas constant ( $8.314 \text{ J} \cdot (\text{K} \cdot \text{mol})^{-1}$ );  $T$  the absolute temperature and  $F$  the Faraday constant ( $96485 \text{ C} \cdot \text{mol}^{-1}$ ).

Fix interference method (FIM) is another widespread methodology to calculate the selectivity coefficient. In this case, the concentration of the primary analyte is gradually increased in a solution with a fixed concentration of the interfering species. The activity of the primary analyte at the LOD,  $a_i(DL)$ , is calculated from the calibration curve obtained, and according to the activity of the interfering ion in the background solution,  $a_j(BG)$ , the coefficient can be determined as follows the Equation 2.27:

$$\log K_{ij}^{pot} = \log \frac{a_i(DL)}{a_j(BG)^{n_i/n_j}} \quad (\text{Equation 2.27})$$

where  $n_i$  and  $n_j$  are the charge of the primary ion and interference, respectively.

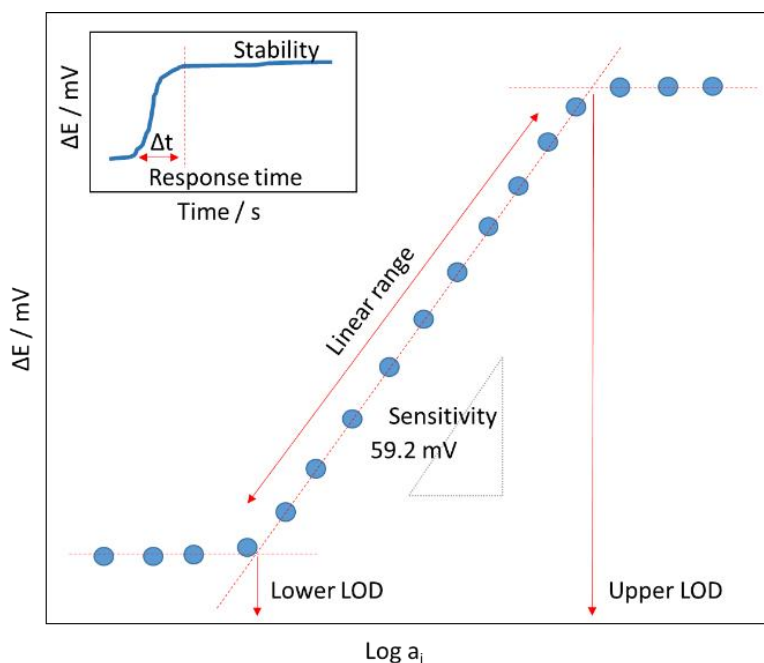


Figure 2.14. Graphical representation of some analytical parameters.

## 2.5. REFERENCES

- [1] P. C. Meier, *Anal. Chim. Acta* **1982**, 136, 363.
- [2] S. Yajima, K. Tohda, P. Bühlmann, Y. Umezawa, *Anal. Chem.* **1997**, 69, 1919.
- [3] E. Bakker, M. Nägele, U. Schaller, E. Pretsch, *Electroanalysis* **1995**, 7, 817.
- [4] E. Bakker, E. Pretsch, P. Bühlmann, *Anal. Chem.* **2000**, 72, 1127.
- [5] D. Thevenot, K. Toth, R. Durst, G. Wilson, D. Thevenot, K. Toth, R. Durst, G. Wilson, *Biosens. Bioelectron.* **2001**, 16, 121.
- [6] J. Zhang, Y. Zhao, C. G. Yuan, L. N. Ji, X. D. Yu, F. Bin Wang, K. Wang, X. H. Xia, *Langmuir* **2014**, 30, 10127.
- [7] S. Sarkar, A. K. Sengupta, P. Prakash, *Environ. Sci. Technol.* **2010**, 44, 1161.
- [8] C. W. Wagner, W. Z. Traud, *Elektrochem.* **1938**, 44, 391.
- [9] C. W. Wagner, W. Z. Traud, *Corrosion.* **2006**, 62, 843.
- [10] T. N. Andersen, H. J. Eyring, *Phys. Chem.* **1963**, 67,92.
- [11] M. Spiro, *J. Chem. Soc., Faraday Trans. 1* **1979**, 75, 1507.
- [12] J. A. S. Roberts, R. M. Bullock, *Inorg. Chem.* **2013**, 52, 3823.
- [13] S. J. Percival, A. J. Bard, *Anal. Chem.* **2017**, 89, 9843.

- [14] I. Katsounaros, W. B. Schneider, J. C. Meier, U. Benedikt, P. U. Biedermann, A. a. Auer, K. J. J. Mayrhofer, *Phys. Chem. Chem. Phys.* **2012**, *14*, 7384.
- [15] A. Panchenko, M. T. M. Koper, T. E. Shubina, S. J. Mitchell, E. Roduner, *J. Electrochem. Soc.* **2004**, *151*, A2016.
- [16] X. Li, D. Heryadi, A. A. Gewirth, *Langmuir* **2005**, *21*, 9251.
- [17] E. F. Coyle, *J. Sports Sci.* **2004**, *22*, 39.
- [18] A. J. Bandodkar, I. Jeerapan, J. Wang, *ACS Sensors* **2016**, *1*, 464.
- [19] J. Hu, S. Wang, L. Wang, F. Li, B. Pingguan-Murphy, T. J. Lu, F. Xu, *Biosens. Bioelectron.* **2014**, *54*, 585.
- [20] J. Wang, *Biosens. Bioelectron.* **2006**, *21*, 1887.
- [21] J. Bobacka, A. Ivaska, A. Lewenstam, *Chem. Rev.* **2008**, *108*, 329.
- [22] M. Dole, *J. Chem. Educ.* **1940**, 134.
- [23] W. G. Hines, R. De Levie, *J. Chem. Educ.* **2010**, *87*, 1143.
- [24] P. Bühlmann, L. D. Chen, Eds: P. A. Gale, J. W. Steed, Ed. Wiley Onlyne Library, Supramolecular Chemistry: From Molecules to Nanomaterials, Ion-Selective Electrodes With Ionophore-Doped Sensing Membranes, **2012**, Online ISBN: 9780470661345.
- [25] E. Bakker, P. Bühlmann, E. Pretsch, *Chem. Rev.* **1997**, *97*, 3083.
- [26] P. Bühlmann, E. Pretsch, E. Bakker, *Chem. Rev.* **1998**, *98*, 1593.
- [27] E. Bakker, M. Willer, M. Lerchi, K. Seiler, E. Pretsch, *Anal. Chem.* **1994**, *66*, 516.
- [28] G.J., Moody, R.B., Oke, J.D.R., Thomas, *Analyst.* **1970**, *95*, 910.
- [29] L.Y., Heng, E.A.H., Hall, *Anal. Chim. Acta.* **1996**, *324*, 47.
- [30] L.Y., heng, E.A.H. Hall, *Anal. Chim. Acta.* **2000**, *403*, 77.
- [31] S. A. Ansari, Q. Husain, *Biotechnol. Adv.* **2012**, *30*, 512.
- [32] F. Haber, E. Z. Klemensiewicz, *Phys. Chem.* **1909**, *67*, 385.
- [33] E. Bakker, P. Bühlmann, E. Pretsch, *Talanta* **2004**, *63*, 3.
- [34] R. W. Cattrall, H. Freiser, R. W. Cattrall, *Anal. Chem.* **1971**, *43*, 1905.
- [35] M. Pohanka, C. Republic, *Methods* **2008**, *6*, 57.
- [36] C. Wang, H. Daimon, T. Onodera, T. Koda, S. Sun, *Angew. Chemie - Int. Ed.* **2008**, *47*, 3588.
- [37] G. G. Guilbault, J. G. Montalvo, *J. Am. Chem. Soc.* **1969**, *91*, 2164.
- [38] X. L. Luo, J. J. Xu, Y. Du, H. Y. Chen, *Anal. Biochem.* **2004**, *334*, 284.
- [39] I. Nuñez de Castro, Ed. Pirámide S. A., *Enzimología*, **2001**, ISBN: 8436814681.
- [40] R. S. Nicholson, I. Shain, *Anal. Chem.* **1964**, *36*, 706.
- [41] N. Elgrishi, K. Hammon, B. McCarthy, T. Eisenhart, J. Dempsey, *J. Chem. Educ.* **2017**, 123.

- [42] R. S. Nicholson, *Anal. Chem.* **1965**, 37, 1351.
- [43] S. H. DuVall, R. L. McCreery, *Anal. Chem.* **1999**, 71, 4594.
- [44] A. M. Bond, S. W. Feldberg, *J. Phys. Chem. B* **1998**, 102, 9966.
- [45] G. A. Carriedo, *J. Chem. Educ.* **1988**, 65, 1020.
- [46] G. A. Mabbott, *J. Chem. Educ.* **1983**, 60, 697.
- [47] J. Noiphung, T. Songjaroen, W. Dungchai, C. S. Henry, O. Chailapakul, W. Laiwattana, *Sens. Actuators B* **2013**, 188, 39.
- [48] J. Wang, S. B. Hocevar, B. Ogorevc, *Electrochem. commun.* **2004**, 6, 176.
- [49] T. Sokalski, P. Lingelfelter, A. Lewenstam, *J. Phys. Chem. B* **2003**, 107, 2443.
- [50] G. Guibault, *Pure Appl. Chem.* **1989**, 53, 1907.
- [51] E. Bakker, *J. Electrochem. Soc.* **1996**, 143, L83.
- [52] E. Bakker, E. Pretsch, P. Bühlmann, *Anal. Chem.* **2000**, 72, 1127.

# EXPERIMENTAL

---

---



UNIVERSITAT ROVIRA I VIRGILI

TAILOR-MADE CHEMICAL SENSING PLATFORMS FOR DECENTRALIZED HEALTHCARE AND WELLBEING

Rocío Cánovas Martínez

This chapter summarizes relevant information regarding common materials, procedures and characterization (including instrumentation) of materials and sensors broadly used throughout this thesis.

### **3.1. MATERIALS**

The choice of materials is a really critical step for the fabrication of robust and sensitive electrochemical sensors. This election might involve several crucial decisions for the sensing strategy: (i) tune either the selectivity of the sensor towards the analyte of interest or the adhesion of the selective elements; (ii) materials are the building blocks of the sensors and will account for the final cost of the device thus the affordability from the end-user point of view and; (iii) extra features can be added to the sensor by using resilient, flexible or biodegradable materials.

#### **3.1.1. Conductive inks**

Ag/AgCl ink (113-09) as well as screen-printable electrically conductive carbon ink were obtained from Creative Materials, Inc., Ayer, MA, USA. Also, Ag/AgCl ink screen-printable (E2414) was obtained from Ercon Inc., Wareham, USA. These inks are medical grade, electrically conductive ink and coating suitable for application by screen printing and dip coating.

#### **3.1.2. Carbon nanotubes**

Single-wall carbon nanotubes (SWCNTs) of 95 % purity (1–2 nm outer diameter, 5–30  $\mu\text{m}$  length) were purchased from Chengdu Organic Chemicals Co. (Chengdu, Sichuan, China). Multi-wall carbon nanotubes (MWCNTs) of 95 % purity (30–50 nm outer diameter,  $\sim 15 \mu\text{m}$  length) were also purchased from Chengdu Organic Chemicals Co. (Chengdu, Sichuan, China). Carboxylic acid functionalized multi-walled carbon nanotubes (MWCNTs) purity >95%, diameter = 10-20 nm, length = 10-30  $\mu\text{m}$  were purchased from US Research Nanomaterial, Inc. Both SWCNTs and MWCNTs were used without further purification.

#### **3.1.3. Membranes components for ISEs and RE**

##### 3.1.3.1. Ion selective membrane

##### Ionophores

Valinomycin (potassium ionophore I), sodium ionophore X, tridodecylamine (hydrogen ionophore) were obtained in Sigma-Aldrich.<sup>[1]</sup>



### Ion-exchangers

Potassium tetrakis (4-chlorophenyl)borate (KTCIPB) with >98% purity and sodium tetrakis[3,5-bis-(trifluoromethyl)phenyl]borate (NaTFPB)<sup>[2]</sup> were purchased from Sigma-Aldrich.

### Polymeric Matrix

As a polymer for Ion-Selective Membrane, polyvinyl chloride (PVC) of high molecular weight and polyurethane (PU) (Tecoflex SG-80A) was obtained from Lubrizol, USA were used.

Nafion® 117 solution (ca. 5% in a mixture of lower aliphatic alcohols and water), Nafion® perfluorinated resin solution (5 wt% in a mixture of lower aliphatic alcohols and water, 45% water) and Aquivion® D98-25BS consisting in a liquid dispersion, 25% in water, PFSA eq. wt. 980 g/mole SO<sub>3</sub>H with CF<sub>3</sub> polymer and chain ends as stabilizer were obtained in Sigma-Aldrich.

### Plasticizers

Bis(2-ethylhexyl)sebacate (DOS) with >97% purity and 2-nitrophenyl-octyl ether (o-NPOE) with >99% purity also acquired from Sigma-Aldrich.

#### 3.1.3.2. Reference membrane

Polyvinyl butyral (PVB) B-98 was obtained from Quimidroga S.A., Spain, sodium chloride and methanol. Everything was purchased from Sigma-Aldrich.

#### **3.1.4. Elastomers**

Polyurethane (PU) (Tecoflex SG-80A) was obtained from Lubrizol, USA. Also, platinum-catalyzed silicone elastomer, Ecoflex 0030 was obtained from Smooth-On, Inc., USA.

#### **3.1.5. Other reagents**

Whatman® qualitative filter paper, Grade 5, sodium dodecylbenzenesulfonate (SDBS), poly(ethylene-co-acrylic acid) (PEAA) with 15 wt % of acrylic acid, glucose oxidase with 228.253 U/g (GOx) as well as uricase 5 U/mg, galactose 3.000 U/g (GalOx) and cholesterol ≥ 50 U/mg (ChOx) oxidases, 30% (w/w) hydrogen peroxide (H<sub>2</sub>O<sub>2</sub>) standard solution, Triton X 100, Chloroplatinic acid hexahydrate ≥ 37.5 %, methanol, tetrahydrofuran (THF), mineral oil, potassium ferricyanide (III) with ≥ 99.99 % purity and potassium ferrocyanide (II) hydrate with ≥ 99.99 % purity were acquired from Sigma-Aldrich.

Analytical-grade chloride salts of ammonium, calcium, magnesium, potassium, and sodium were purchased from Sigma-Aldrich. Sodium hydrogen carbonate, sodium-L-ascorbate,

potassium hydrogen phosphate, glucose, cholesterol, galactose, uric acid and urea were also purchased from Sigma-Aldrich.

Phosphate buffered saline (PBS) 0.1 M was prepared with 79 mM  $\text{Na}_2\text{HPO}_4$ , 21 mM  $\text{KH}_2\text{PO}_4$ , 138 mM NaCl and 2.7 mM KCl. All solutions were prepared using deionized water ( $18.2 \text{ M}\Omega \cdot \text{cm}^{-1}$  specific resistivity) obtained from MilliQ PLUS (Millipore Corporation, Bedford, MA, USA).

## 3.2. PROCEDURES

This section presents the preparation of the conductive substrate for the transduction of the electrochemical signal as well as the detailed fabrication of the selective membrane. It is essential to build a substrate that keeps the electrical conductivity during the sensing process, specially when the sensing is performed under high mechanical stress or deformation such as in wearable applications. Moreover, in the case of ion-selective electrodes, the right formulation of a selective membrane should confer the ability to accurately discriminate in a complex sample the analyte of interest from other interfering species.

### 3.2.1. Preparation of conductive substrates

There are multiple techniques for the development of conductive platforms. In this section, some suitable techniques that fit the scenario of the proposed sensing applications, as well as the mechanism of response, will be displayed.

#### Platinum Sputtering

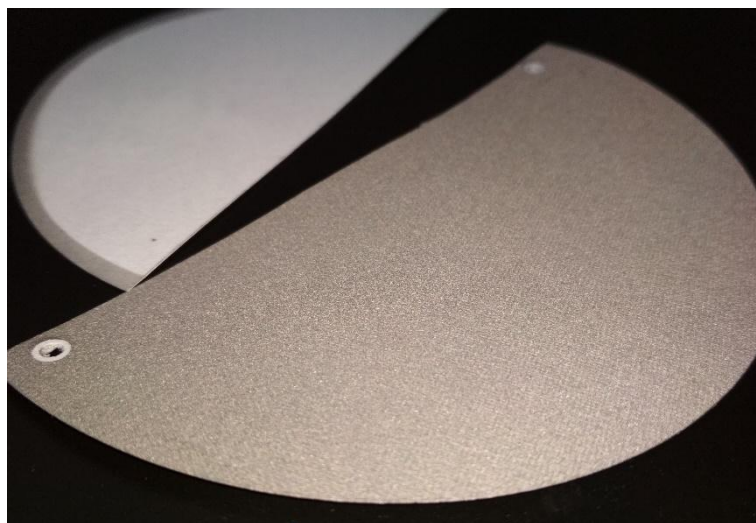


**Figure 3.1.** Image showing the platinumized paper.

Sputtering of platinum was performed using an ATC Orion 8-HV (AJA International, Inc. MA, U.S.A.) at 200 W, 3 mTorr and magnetron DC sputtering onto a Whatman N° 5 filter paper. Platinum targets have a purity of 99.99 %. The thickness of the platinum layer is 100 nm and its conductivity achieved is 15  $\Omega$  approximately. The metallic layer avoids the entrance of the water into the paper's fiber which is very useful to preserve the electrochemical signal during the analytical measurements. Figure 3.1 shows the platinized paper widely used along this thesis.

### Carbon ink decorated with platinum nanoparticles (Pt-NPs)

Electrodeposition of Pt-NPs was performed in a solution composed by chloroplatinic acid hexahydrate ( $\text{H}_2\text{PtCl}_6 \cdot 6\text{H}_2\text{O}$ )  $\geq 37.5$  % 1.3 mM and sulfuric acid ( $\text{H}_2\text{SO}_4$ ) 0.5 M using chronoamperometry. The electrode was immersed in the solution applying a constant potential of -0.25 V during 5 minutes under gentle stirring condition.<sup>[3]</sup> The substrate of this electrode consist on filter paper covered with carbon ink.

### Stretchable CNT ink

Stretchable CNT ink was prepared by mixing CNTs with mineral oil (MO), proportion (1 mg CNT: 0.7 mg MO). MWCNT were previously heated and ground to remove moisture. This composition (190 mg MWCNTs and 133 mg MO) was mixed in THF (2 mL) and placed for 1 h in the shaker. Thereafter, the ink was homogenized using ultrasonic bath for 30 minutes. The mixture was kept in the shaker overnight. Then, 40% of polyurethane (PU) was added (previous mixture = 60%) and the resulting mixture was shaken overnight. A solid-to-solvent ratio (1 mg: 9  $\mu\text{L}$ ) was maintained for printing purposes.

### Stretchable Ag/AgCl Ink

The stretchable Ag/AgCl ink was prepared by thoroughly mixing 90% of Ag/AgCl ink (E2414, Ercon Inc., Wareham, MA) with 10% of biodegradable plastic Ecoflex (A+B).

## **3.2.2. Membrane cocktails**

The membrane is an essential element in the ion-selective electrodes as it confers the selectivity to the sensor. Importantly, membrane cocktails have become the centrepiece of the work performed during the fabrication of the electrochemical sensors as they have the potential to be deposited over the electroactive area of the electrode in an easy and convenient manner. Overall, the cocktails used in this thesis are in liquid phase as it facilitates the spreading of a homogenous layer over the surface of the electrode.

### Reference membrane

The reference membrane contains 50 mg of sodium chloride, and 78 mg of polyvinyl butyral (PVB). The membrane is prepared by dissolving the solid mixture in 1 mL of methanol. First, the mixture is vigorously shaken in a vortex and then placed in an ultrasonic bath for 20 minutes until a completely homogenous solution is obtained.

### Ion-selective membrane

The ion-selective membrane used for potentiometric electrode was prepared as follows:

- a) Ionophore: between 15-30 mmol·kg<sup>-1</sup> (membrane) depending on the stoichiometric ratio between the ionophore and the primary analyte.
- b) Lipophilic anion or cation exchanger: 20-40% ratio of ionophore
- c) Polymeric matrix and plasticizer: in a ratio 1:2 wt., respectively.

These membranes are usually prepared for a final weight ranging between 100-200 mg. Subsequently, the components are dissolved in tetrahydrofuran (THF) anhydrous 99.99% and the mixture is vigorously shaken in a vortex and then placed in an ultrasonic bath for 20 minutes until a completely homogenous solution is obtained.

### Enzymatic membranes

Enzymatic membranes can be considered along this thesis like two different schemes:

- a) First, the entrapment of the enzymatic layer consisted on enzyme dissolved in MilliQ water or phosphate buffer (PBS) sandwiched by two polymer layers.
- b) Enzyme powder diluted in a mixture of chitosan (CHI) and polyvinyl alcohol (PVAL).

### **3.2.3. Approaches for membrane deposition**

#### Drop casting

The method of drop casting consists in the deposition by pipette of a certain amount of the membrane or cocktail. This aliquot of cocktail is directly drop cast onto the active area of the electrode. Just as there are several types of electrodes, the way in which we deposit the membrane can vary in quantity or layers deposited. Normally, these parameters are optimized to achieve the suitable thickness and thus obtain the right analytical performance.

#### Dip coating

The process that requires dip coating is simple, involves immersing the electroactive area of the electrode inside the cocktail or solution as many times (allowing it to dry in between) as

necessary to obtain a suitable thickness. As with the previous method, the thickness must be optimized to improve the sensor response.

### Electropolymerization

Electropolymerization of the enzymatic membrane (composed by the enzyme GOx + CHI + PVAL) was performed immersing the electrode into the cocktail and using a multi current step method that apply 25  $\mu$ A during 1000 seconds on top of platinized paper.

#### **3.2.4. Conditioning step**

In order to reach a suitable performance of these ISEs, two basic steps were performed:

- a) First, the electrode after the deposition and drying of the membrane is placed in a relatively concentrated solution ( $10^{-2}$  M) of the primary ion for 24 h.
- b) Second, after the first step of conditioning, the electrodes have to be washed with DIW and placed in a diluted solution of the primary analyte ( $10^{-4}$  M) for 24 h.

### **3.3. CHARACTERIZATION**

After the fabrication of the electrodes, it is crucial to understand their analytical performance either to improve it or to study their inherent behaviour. Hence, the characterization of different properties of the sensor is mandatory. Depending on the application of each type of sensor, some techniques might vary, although electroanalytical characterization is always performed.

#### **3.3.1. Mechanical characterization**

The analytical performance and stability of the wearable and expandable sensors were characterized by carrying out several mechanical stress test. This is a key point to keep in mind as these sensors must withstand different types of stretching, bending, wrinkling, or even cleaning (in the case of being integrated into textiles). On one hand, bending, stretching and crumpling test were carried out by exerting force manually. The cycles were repeated several times in order to check the influence of the stress before, during and after the physical deformation. At the same level, degrees of inflation were applied using an air supply system for the expandable tests. On the other hand, the cleaning simulation was performed in a beaker and water applying a rotating force.

#### **3.3.2. Microscopic characterization**

Microscopy is considered a key tool in characterizing materials and surfaces. The ability to observe the distribution of nanomaterials and microstructures helps to understand how they are organized at the electrodes. Besides, this visualization helps to elucidate how the electrodes

work and how are they going to behave as well as the understanding to a better extent how the used membranes are deposited and adhered. Overall, it can also contribute in explaining some questions with respect to the mechanism involved in the detection of our target.

### Environmental Scanning Electron Microscopy (ESEM)

Environmental scanning electron microscopy (ESEM, FEI Quanta 600, USA) was used for the surface characterization of the platinum sputtering, Pt-NPs electrodeposited and Nafion membranes deposited on electrodes by drop-casting method. The electrodes were attached to the support inside the ESEM chamber by a carbon-based sticker. To obtain the maximum resolution of the images parameters such as potential, pressure and working distance were characterized in each case. In some cases, a gold sputtered is needed in low-conductive substrates such as Nafion membranes in order to allow the electron transfer and thus obtain high magnification images. The foundational aspects of the ESEM as well as all the information regarding instrumentation and operation is included elsewhere.<sup>[4]</sup>

### **3.3.3. Electrochemical characterization**

Electrochemical characterization is crucial to obtain insights on the electrode analytical performance as well as understand the mechanism involved in a complex system. Different techniques were used in this thesis to characterize the developed sensors. The foundational aspects of the electrochemical techniques commented here have been already discussed in Chapter 2.

### Potentiometry

During the experiments (always using electrodes by triplicate) electromotive force (EMF) was measured with a high input impedance ( $10^{15} \Omega$ ) EMF16 multichannel data acquisition device (Lawson Laboratories, Inc. Malvern) and a Keithley high-input impedance ( $10^{15} \Omega$ ) electrometric workstation (Keithley Instruments, Inc., Ohio) at room temperature (22 °C) in a well stirred cell with distilled water without any ionic strength adjuster. A double junction Ag/AgCl/KCl 3 M reference electrode (type 6.0726.100, Metrohm AG) containing a 1 M LiAc electrode bridge was used. The substrate of the working electrode was a glassy carbon rod, platinum bare electrode, carbon ink or platinized paper-based electrode, depending on the application.<sup>[5]</sup> The EMF values were corrected using the Henderson equation for the liquid-junction potential and the activity coefficients calculated by the Debye–Hückel approximation (already explained in Chapter 2).

### Cyclic Voltammetry (CV)

CV is considered one the most versatile electroanalytical technique for the study of electroactive species.<sup>[6]</sup> In this thesis this technique is mainly used to provide information about the electrode surface and the electron-transfer process. CV measurements were performed using a potentiostat/galvanostat Autolab PGSTAT128N with a frequency response analyzer electrochemical impedance module (FRA2) (AUTOLAB, Eco Chemie, B.V., Utrecht, The Netherlands) fitted with a three electrode electrochemical cell and NOVA software (v.1.11, The Netherlands) as a measuring interface. The electrode (Pt bare, paper-based, etc) was used as the working electrode, a glassy carbon rod with a diameter of 3 mm as the counter electrode, and a Ag/AgCl/KCl 3 M (type 6.0733.100, Metrohm AG) single junction electrode as the reference electrode. The scan rate can be chosen over a wide range, typically from 0.001 to 200 or more V·s<sup>-1</sup>. The measurements were taken in a solution of 0.1 M KCl or ferrocyanate at room temperature (25°C).

### Adsorptive Stripping Voltammetry (ASV)

The studies were executed using an AUTOLAB Type II (EcoChemie, B. V., Utrecht, The Netherlands) and NOVA software (v.1.11, The Netherlands) as a measuring interface. For electrochemical measurements, a three-electrode configuration was employed, consisting of two screen-printed MWCNTs-composite, serving as a working and counter electrodes, while a screen-printed Ag/AgCl served as a pseudo-reference electrode.<sup>[7]</sup>

### Chronoamperometry

Chronoamperometric studies<sup>[8]</sup> were executed using an AUTOLAB Type II (EcoChemie, B. V., Utrecht, The Netherlands) and NOVA software (v.1.11, The Netherlands) as a measuring interface, at room temperature (22 °C) in PBS (0.1 M at pH 7.4). Current was sampled 60 s at potential -0.9 V for monitoring the reduction of hydrogen peroxide at liquid and gas-phase assays.

### Electrochemical Impedance Spectroscopy (EIS)

EIS measurements were performed using a potentiostat/galvanostat Autolab PGSTAT128N with a frequency response analyzer electrochemical impedance module (FRA2) (AUTOLAB, Eco Chemie, B.V., Utrecht, The Netherlands) fitted with a three electrode electrochemical cell and NOVA software (v.1.11, The Netherlands) as a measuring interface. The electrode used in each case<sup>[9]</sup> was used as the working electrode, a glassy carbon rod with a diameter of 3 mm as the counter electrode, and a Ag/AgCl/KCl 3 M (type 6.0733.100, Metrohm AG) single junction electrode as the reference electrode. The impedance spectra were recorded within the

frequency range 100 kHz to 10 MHz by using a sinusoidal excitation signal that was superimposed on a constant direct current potential, ( $E_{dc}=0.2$  V). The electrodes were studied using an excitation amplitude of 10 mV. The measurements were taken in a solution of 0.1 M KCl at room temperature (25°C).

### 3.3.4. Optical characterization

In parallel, some optical techniques were employed in order to deepen in the status of some of the reactions involved in the process of the sensor development.

#### Fourier-Transform Infrared (FT-IR) spectroscopy

FT-IR spectrophotometer from JASCO Analítica (Madrid, Spain) with a single reflection diamond (ATR Specac Golden Gate) provided structural data about the enzymatic membrane before and after calibration curves experiments. The scan was performed between 900 and 4000  $\text{cm}^{-1}$ . All the principles and instrumentation required for this technique are widely explained elsewhere.<sup>[10]</sup> The previous potentiometric measurements before the FTIR analysis were performed in PBS pH 7.4 at 25°C.

#### Ultraviolet-Visible (UV-Vis) spectroscopy

Absorbance measurements were performed in an 8453 UV-Vis spectrophotometer from Agilent Technologies (Barcelona, Spain) with and OS High Precision Cell optical glass cuvette fo 10 mm light path (Hellma Analytics, Germany). The UV-Vis spectroscopy gave information about the homogeneity of the cholesterol solution. All the principles and information of this technique can be found elsewhere.<sup>[11]</sup>

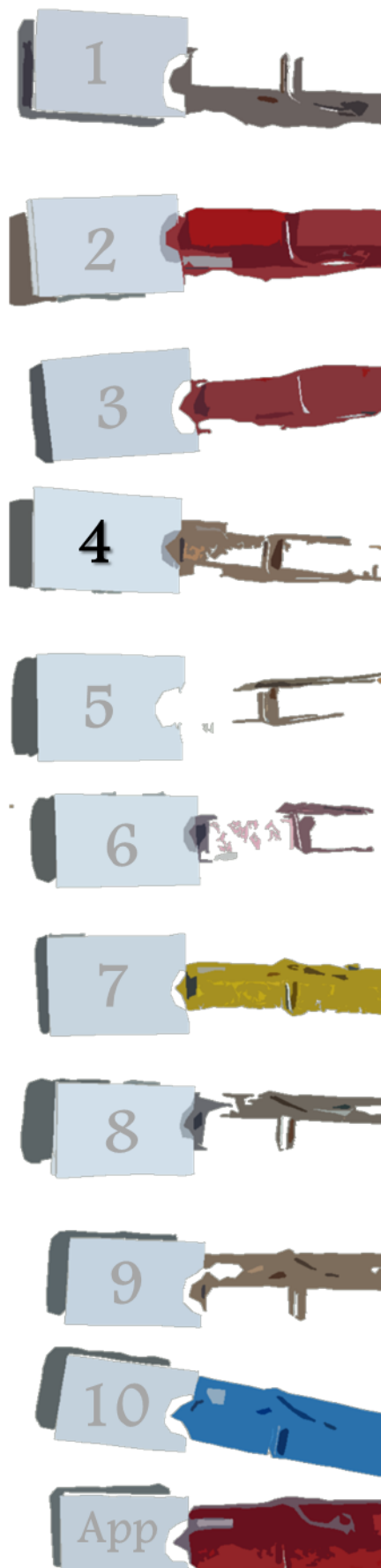
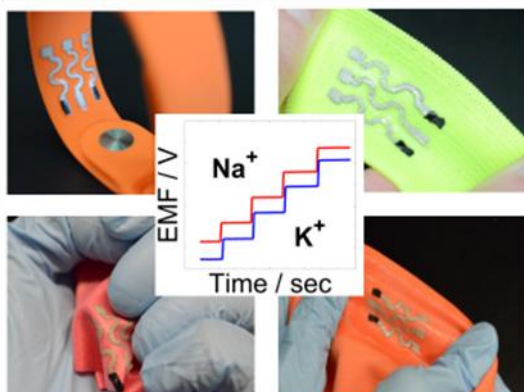
## 3.4. REFERENCES

- [1] W. Gao, S. Emaminejad, H. Y. Y. Nyein, S. Challa, K. Chen, A. Peck, H. M. Fahad, H. Ota, H. Shiraki, D. Kiriya, D.-H. Lien, G. A. Brooks, R. W. Davis, A. Javey, *Nature* **2016**, 529, 509.
- [2] E. Bakker, E. Pretsch, *Angew. Chemie - Int. Ed.* **2007**, 46, 5660.
- [3] X. Chu, D. Duan, G. Shen, R. Yu, *Talanta* **2007**, 71, 2040.
- [4] G. D. Danilatos, *Advances in Electronics and Electron Physics*, **1988**, 71, 110.
- [5] E. Bakker, E. Pretsch, *Angew. Chemie - Int. Ed.* **2007**, 46, 5660.
- [6] P. T. Kissinger, W. R. Heineman, *J. Chem. Educ.* **1983**, 60, 702.
- [7] J. Wang, S. B. Hocevar, B. Ogorevc, *Electrochem. commun.* **2004**, 6, 176.
- [8] J. G. Limon-Petersen, J. T. Han, N. V. Rees, E. J. F. Dickinson, I. Streeter, R. G. Compton, *J. Phys. Chem. C* **2010**, 114, 2227.
- [9] J. Schröder, S. Doerner, T. Schneider, P. Hauptmann *Meas. Sci. Technol.* **2004**, 15, 1271.



- [10] P. R. Griffiths, J. A. De Haseth, Eds: J. D. Winefordner, 2<sup>nd</sup> Ed. Wiley, Fourier Transform Infrared Spectrometry, **2007**, ISBN-10: 0471194042.
- [11] A. Lobnik, Eds. F. Baldini, A.N. Chester, J. Homola, S. Martellucci, Ed. Springer, Optical Chemical Sensors, **2004**, ISBN-10 1-4020-4610-3 (PB).

# A TEXTILE-BASED STRETCHABLE MULTI- ION POTENTIOMETRIC SENSOR



UNIVERSITAT ROVIRA I VIRGILI

TAILOR-MADE CHEMICAL SENSING PLATFORMS FOR DECENTRALIZED HEALTHCARE AND WELLBEING

Rocío Cánovas Martínez

As it was mentioned in the introduction, the first part of this work (chapter 4 and 5) addresses the problems of the user interface by designing electrochemical sensors that can be directly integrated onto different user-friendly surfaces. This chapter describes a textile-based wearable multi-ion potentiometric sensor array. The printed flexible sensors operate favorably under extreme mechanical stress (that might be employed during daily activity) while offering attractive real-time and non-invasive monitoring of electrolytes such as sodium and potassium ions in sweat.

## 4.1. INTRODUCTION

The progression in the eHealth field is promoting the research and development of technologies for individualized therapies and diagnostics. Indeed, recent trends in personalized healthcare have led to growing demands for real-time monitoring of the physiological status of human subjects. Major efforts have been put forward in order to design portable and connected devices such as mHealth tools that could contribute with the analysis of accurate personal data.

The detection of disorders involved in the imbalance of electrolyte levels, such as hyperkalemia, hypernatremia, hypokalemia or hyponatremia is a really relevant and critical challenge.<sup>[1,2]</sup> Indeed, electrolyte imbalance represents a potential risk of fatal abnormal heart rhythms.<sup>[3,4]</sup> For example, electrolyte loss is a major concern in disorders such as Cystic Fibrosis<sup>[5]</sup> and hyperhidrosis.<sup>[6]</sup> Besides, monitoring key electrolytes may also alert to latent cardiac problems<sup>[7]</sup> and diagnose apparent life-threatening events.<sup>[8,9]</sup> Overall, real-time measurements of electrolyte concentrations could indicate the patient, doctor, coach or athlete to potential electrolyte loss,<sup>[10]</sup> dehydration status<sup>[11]</sup> and the associated need for electrolytes replenishment.<sup>[12]</sup> In contrast, cumbersome methods to measure the sodium and potassium imbalance, such as electrocardiogram and sweat patch, have been reported.<sup>[13,14]</sup> Fortunately, recent activity have led to wearable electrochemical (potentiometric) devices for non-invasive electrolyte monitoring.<sup>[15,16]</sup> However, the success of wearable sensing devices for health monitoring requires proper attention to key challenges concerning their mechanical resilience and large-scale manufacturing. Recent efforts to address these issues have relied on stretchable printable electrochemical devices.<sup>[17]</sup>

This chapter reports for the first time on a highly stretchable and printable textile-based potentiometric sensor array for simultaneous multi-ion sweat determination using a variety of fabric materials towards diverse healthcare and fitness applications. Screen-printing has been applied recently for fabricating amperometric sensors<sup>[18]</sup> and biofuel cells<sup>[19]</sup> on common textiles, but not in connection to potentiometric sensors or stretchable textile devices.<sup>[20]</sup>

Textiles are attractive components of wearable sensing devices and offer rich elastomeric properties towards achieving conformal contact between the sensor and the body. Integrating chemical sensors directly into fabrics offer major advantages for future healthcare monitoring systems. Yet, a key issue involving textile-based sensing devices is the ability to operate under extreme mechanical tensions (that reflect daily activity) without compromising their analytical performance. In this work, highly stretchable textile-based potentiometric sensors have been realized by combining polyurethane (PU)-based ion-selective membranes and inks with a serpentine sensor pattern and recently developed stretch-enduring printed electrodes.<sup>[21]</sup> The compositions of the selective potentiometric membrane and of the printed inks have thus been tailored for ensuring selectivity, electrical conductivity, reproducible printing, and strong adherence to conventional textiles.

## 4.2. EXPERIMENTAL

Common reagents and materials are described in Chapter 3.

### 4.2.1. Materials preparation

Tetrahydrofuran (THF) with HPLC grade and dimethylformamide (DMF) was purchased from Fisher Chemical (Fair Lawn, NJ). All other chemicals were of analytical grade and were used without further purification. Artificial sweat matrix containing 6 mM KCl, 80 mM NaCl, 0.08 mM MgCl<sub>2</sub>, and 5 mM NH<sub>4</sub>Cl was prepared.<sup>[22]</sup>

Ecoflex® 00-30 was prepared in-house by mixing equal volumes of pre-polymer A with pre-polymer B provided by the supplier. A polyester textile laminated with polyurethane, polyester nylon reinforced reflective band, silicone watch straps and polyester-based underwear were used as a fabric to build the sensors.

#### CNT and Ag/AgCl ink preparation

Stretchable CNT ink was prepared by mixing CNTs with mineral oil (MO), THF and PU such as is detailed in Chapter 3 as well as the stretchable Ag/AgCl ink using Ecoflex®.

#### Ion-selective membranes and reference membrane

PU polymer was used to build the ion-selective membrane (ISM) instead of the typical polyvinyl chloride (PVC) membranes. Hence, the use of PU for the ISM made possible to build flexible and stretchable membranes.

Sodium-selective membrane (Na<sup>+</sup>SM). The Na<sup>+</sup>SM contained 0.7 wt% of Sodium ionophore X, 0.25 wt% of potassium tetrakis (4-chlorophenyl) borate, 66.05 wt% of 2-nitrophenyl octyl ether (o-NPOE) and 33 wt% of PU.

Potassium-selective membrane ( $K^+SM$ ). The  $K^+SM$  contained 2 wt% Valinomycin (Potassium ionophore I), 0.5 wt% of potassium tetrakis (4-chlorophenyl) borate, 64.7 wt% of bis (2-ethylhexyl) sebacate (DOS) and 32.8 wt% of PU.

Both membranes compositions were obtained as described elsewhere.<sup>[23]</sup> The membranes were prepared by dissolving each mixture (100 mg) in THF (1mL). The cocktails were vigorously shaken for 1 hour. Once membranes were deposited, cocktails were kept in the fridge at 4 °C, and remained stable for 2 weeks.

A solid-state reference membrane was prepared as described elsewhere.<sup>[24]</sup> Briefly, the cocktail was made by dissolving PVB (78 mg) and NaCl (50 mg) in methanol (1 mL). The mixture was vigorously shaken for 30 minutes. Once used, the cocktail is kept in the fridge and remains stable for 1 week.

#### 4.2.2. Electrochemical measurements

Electromotive force (EMF) was recorded using a high-input impedance data acquisition device (AUTOLAB Type II – EcoChemie, B. V., Utrecht, The Netherlands) and NOVA software (v.1.11, The Netherlands) as a measuring interface, at room temperature (22 °C) without any ionic strength adjuster. EMF wireless measurements were recorded using Go Wireless® Electrode Amplifier (Vernier Software & Technology, Beaverton, USA).

#### 4.2.3. Fabrication of the textile sensor

##### Fabrication of the electrodes

The process employed an MPM-SPM semi-automatic screen printer (Speedline Technologies, Franklin, MA). Sensor patterns were designed in AutoCAD (Autodesk, San Rafael, CA) and outsourced for fabrication on stainless steel through-hole 12" x 12" framed stencils of 125  $\mu m$  thickness (Metal Etch Services, San Marcos, CA). For the analytical performance studies of the textile sensor, a common stretchable textile was used based on polyester fabric laminated with polyurethane. A sequence of stretchable Ag/AgCl ink, stretchable CNT ink and Ecoflex layer was printed to realize the complete electrochemical device array. The printed stretchable Ag/AgCl and CNT patterns were cured (90°C for 10 min and 85°C for 10 min) in a convection oven, respectively. The final Ecoflex layer, used to define the electrode area and contact pads, was cured at room temperature for 2h (Figure 4.1A). The device array was subsequently modified with specific reagents for achieving ion-selective sensors (Figure 4.1B).

For the other different substrates (such as bands and underwear) a previous treatment was necessary to develop a smooth layer where the ink could be well-attached. The printing

process comprised of first screen printing a thick layer (100  $\mu\text{m}$ ) of Ecoflex on each supporting substrate. Precaution was taken to avoid entrapment of air bubbles while placing the Ecoflex layer onto the supporting surface. Subsequently, a thick layer (75  $\mu\text{m}$ ) of a 15 wt % PU in DMF solution was deposited onto each supporting surface and was cured (50°C for 10 minutes). After that, the substrates were ready for printing the electrodes as discussed earlier (Figure 4.1C).

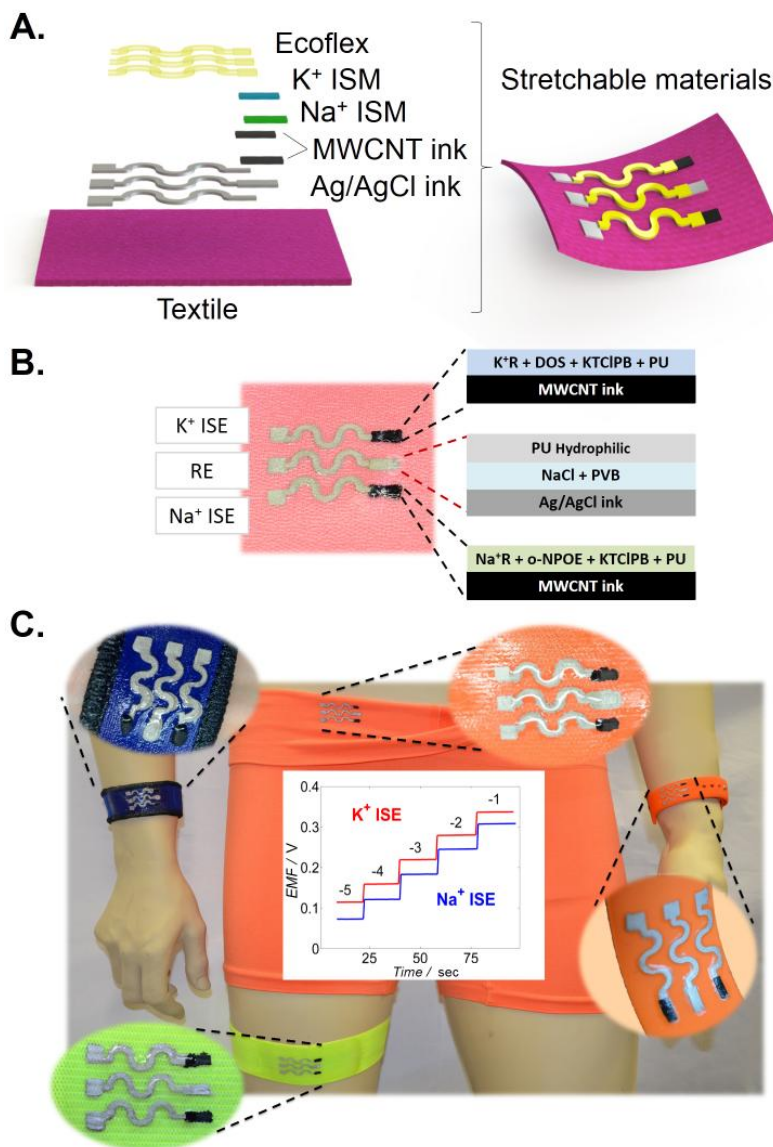


**Figure 4.1.** (A) Schematic representation of the tailor-made stretchable materials and manufacturing process. (B) Image depicting the wearable sensor based on textile and ion-selective membranes (ISM) composition. (C) Image of the stretchable printed sensors on different common textiles and typical time trace plots for potassium and sodium.

## Fabrication of stretchable sodium and potassium ion-selective sensors

To fabricate the stretchable potentiometric ion-selective sensor, the reference membrane cocktail (2  $\mu\text{L}$ ) was drop-casted twice onto the Ag/AgCl reference electrode (10 minutes drying time between drops), and the sodium and potassium working electrodes were modified by dropping of the sodium-selective membrane (2  $\mu\text{L}$ ) and potassium-selective membrane cocktail (2  $\mu\text{L}$ ) 7 times (3 min drying time between drops) onto CNT working electrode, respectively. Membrane deposition was optimized in order to get a stable and reproducible performance by drop-casting different amounts of the ion-selective membrane cocktail. It is important to note that low amount of cocktail drop-casted was needed to avoid dissolving the CNT ink. Then, the sensor was allowed to dry overnight before use; an important step for the reference electrode.<sup>[25]</sup> Subsequently, a hydrophilic polyurethane aqueous solution (1  $\mu\text{L}$ ) was dropped onto the reference membrane and let it dry for 3h. Finally, an overnight conditioning step was applied. The step consisted on drop cast 0.1 M NaCl solution onto sodium-selective electrode, 0.01 M KCl solution onto potassium-selective electrode and 3 M KCl solution onto the reference membrane. The sensor was kept at room temperature until use (Figure 4.1B).

### **4.3. RESULTS AND DISCUSSION**

#### **4.3.1. Stretchable sensor facing mechanical stress**

To provide the necessary biocompatibility and further resistance to mechanical stress polyurethane was used as replacement to the common PVC matrix of ion-selective sensing membranes as well as the binder of the printed CNT trace. Polyurethanes have attractive mechanical and biocompatibility properties that make them suitable for many wearable devices. These materials are known to minimize unwanted inflammation, fouling and other adverse physiological effects,<sup>[26]</sup> while providing exceptional analytical performance using potentiometric technique.<sup>[27]</sup> As illustrated in Figures 4.1A and 4.1B, such PU-based membrane and CNT ink have been coupled to an Ecoflex-containing Ag/AgCl ink and combined with a solid-contact reference electrode, leading to highly stretchable textile-based potentiometric sensors that transduce their potential response under extreme mechanical stress.

The resilience and analytical performance of the novel dual-electrolyte textile-based printable wearable potentiometric sensor was examined using open-circuit potential measurements (Figure 4.1C). A calibration curve was executed by recording the electromotive force (EMF) versus the time and changing the concentration of NaCl and KCl. Sensor array in Figure 4.1C exhibited a Nernstian response of 59.4 mV/log  $[\text{Na}^+]$ , linear range from  $10^{-4}$  M up to  $10^{-1}$  M and limit of detection (LOD) of  $10^{-4.9}$  M for its sodium selective electrode ( $\text{Na}^+$  ISE) and a Nernstian response of 56.5 mV/log  $[\text{K}^+]$  from  $10^{-4}$  M up to  $10^{-1}$  M and a LOD of  $10^{-4.9}$  M for the



potassium selective electrode ( $K^+$  ISE). Both results are comparable to the values reported previously using similar ion-selective membranes.<sup>[28]</sup> These dynamic ranges cover the physiological sodium and potassium levels in sweat before, during and after prolonged exercise.<sup>[29]</sup> Electrolyte concentrations progressively increase during such exercise activity to provide a useful indicator of the dehydration status.<sup>[30]</sup> Moreover, understanding the amount of ionic species loss during exercise could facilitate recovery of the ionic balance during and after exercise.<sup>[31]</sup>

Stretchability tests were performed initially employing different strain conditions (Figure 4.2A). The textile was anchored and moved away at a speed of  $1 \text{ mm}\cdot\text{s}^{-1}$ . This process was repeated 10 times at 0%, 25%, 50%, 75% and 100% strains. Subsequently, the stretchability was tested by using a fixed 75% linear strain during 60 minutes, emulating a prolonged strain force during exercise. A calibration curve of each electrode was recorded every 15 minutes (Figure 4.2B). Both tests indicated a robust analytical performance under the different strains. Larger (>100%) strains of the textile led to some damage in the reference membrane and hence to an inferior performance.

Bending represents another common mechanical stress expected during daily wear. Bending of the textile sensor was tested by twisting it back and forth for  $0^\circ$ ,  $45^\circ$ ,  $90^\circ$  and  $180^\circ$  10 times in each angle. The subsequently recorded calibration curve indicates no apparent change in the sensitivity (Figure 4.2C). A crumpling test was also performed, consisting of wrinkling the textile with the hand for multiple times (Figure 4.2D). A calibration curve was recorded after 0, 5, 15 and 30 such wrinkling. No apparent variation in the performance was observed under these repeated textile manipulations.

Finally, as shown in Figure 4.2E, a simulation of a conventional washing procedure was performed. This test consisted on immersing the sensor in a beaker full of water under a vigorous agitation for periods of 10 and 40 minutes. A calibration plot of each electrode was recorded after complete drying of the sensor, leading to favorable analytical results. Such attractive behavior indicates strong surface adherence of the organic polymeric membranes with no apparent leaching of the membrane components. In addition, placing the hydrophilic polyurethane membrane on top of the reference membrane prevents leaching of NaCl from the porous PVB membrane and maintains the baseline potential even after a prolonged mechanical agitation. Table 4.1 summarizes the analytical performance of the sensor under different mechanical deformations shown in Figure 4.2.

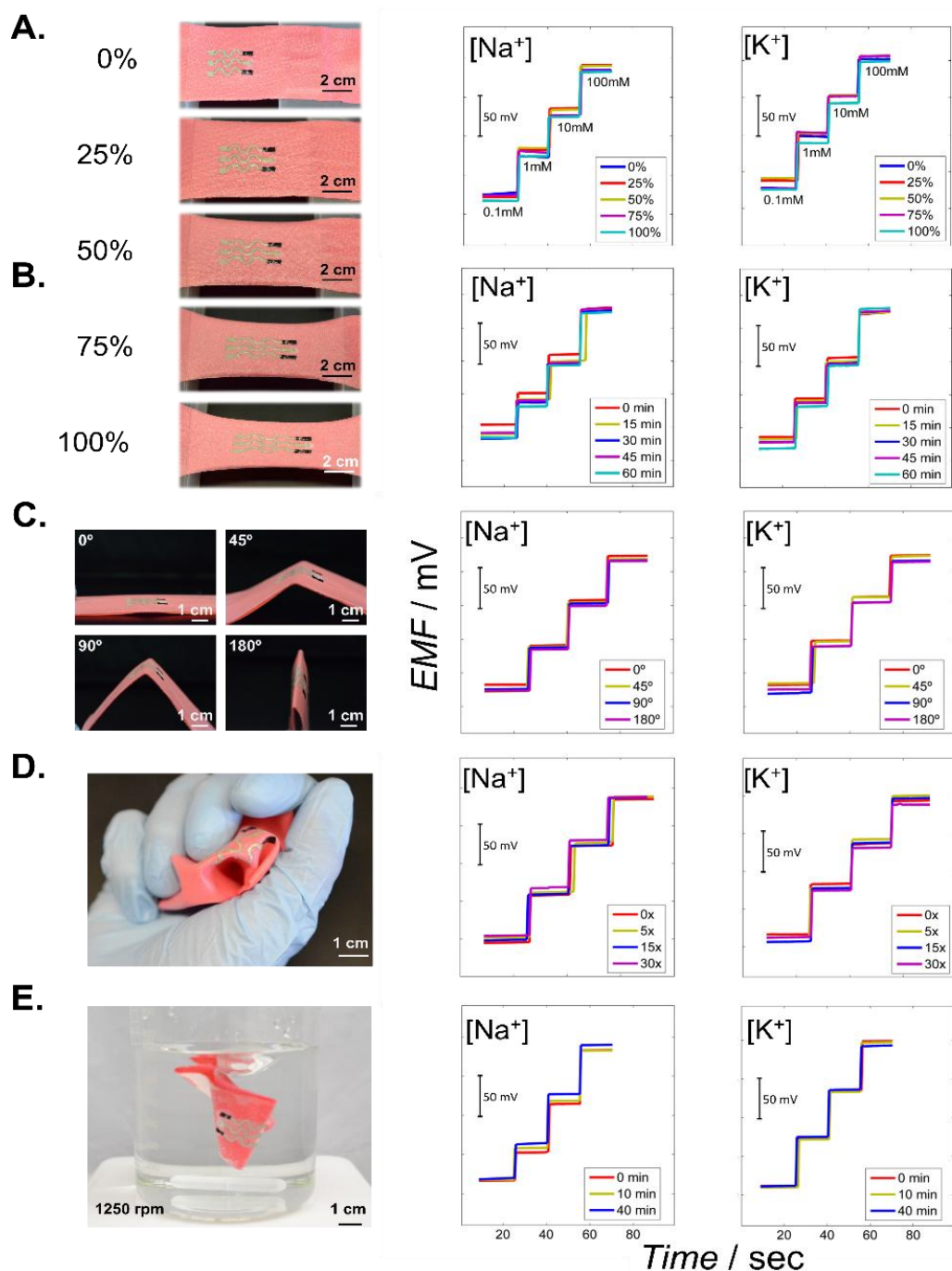


**Figure 4.2.** Images illustrating resilience studies involving exposing the printable textile potentiometric sensor to increasing levels of strain (left) along with the corresponding time trace calibration plots (right). (A) Linear stretchability test up to a total of 100% strain, 10 repetitions in each strain step. (B) Stretchability test, using a 75% linear strain for a total of 60 min (time trace recorded after every 15 min). (C) Bending assessment, up to a total of 180°, 10 repetitions in each angle. (D) Crumpling evaluation, up to 30 times wrinklings. (E) Washing step simulations (without soap) using short and long (10 and 40 minutes) periods.

**Table 4.1.** Average sensitivity values and intercept values obtained during several mechanical deformations of the textile ISE system.

<b>Na<sup>+</sup> selective electrode</b>				
<b>Test</b>	<b>Sensitivity [mV/log [Na<sup>+</sup>]]</b>	<b>%RSD</b>	<b>Intercept [mV]</b>	<b>%RSD</b>
<b>Stretching</b>	54.1 ± 1.5	2,7	239.5 ± 6.3	2,6
<b>Hold stretched</b>	61.3 ± 1.9	3,1	179.8 ± 2.3	1,3
<b>Bending</b>	64.4 ± 0.7	1,0	282.6 ± 3.5	1,2
<b>Crumpling</b>	62.6 ± 0.9	1,5	250.3 ± 1	0,4
<b>Washing</b>	56.2 ± 0.9	1,7	186 ± 6.4	3,5
<b>K<sup>+</sup> selective electrode</b>				
<b>Test</b>	<b>Sensitivity [mV/log [K<sup>+</sup>]]</b>	<b>%RSD</b>	<b>Intercept [mV]</b>	<b>%RSD</b>
<b>Stretching</b>	56.9±1.6	2,9	313.3±4.2	1,3
<b>Hold stretched</b>	64.9±2.8	4,3	235.4±4.1	1,7
<b>Bending</b>	64.1±1.1	1,7	335±4.4	1,3
<b>Crumpling</b>	60.6±2.6	4,2	307.5±8	2,6
<b>Washing</b>	61.8±1.1	1,8	258.3±2.8	1,1

Overall, the wearable textile potentiometric array displays an attractive analytical performance before and after exposures to severe mechanical stress. Such resilience can be explained by considering the behavior of the printed materials at the microscopic level. When an external force is applied to the stretchable sensor, the stress is absorbed mostly by the stretchable Ecoflex component in the Ag/AgCl ink and by the PU as a stretchable binder in the CNT ink. When the printed Ag/AgCl trace undergo high strain, its Ecoflex polymeric component stretches while maintaining the physical contact between randomly oriented multilayers of its conductive particles. Similarly, when the printed CNT trace is subject to extreme stress, its PU binder stretches while maintaining the electrical contact of the randomly distributed CNT. This ability to operate under high strain conditions meets the demands of using these printed textile potentiometric sensors in real-life scenarios involving extreme and repeated movements of the wearer.

Repeatability represents another important feature of wearable biomedical sensors. It is crucial to obtain highly reproducible results for prolonged monitoring of fluctuating ions concentrations. Hence, the repeatability was evaluated through a carry-over test before, during and after the exposure to middle-high strain (50% stretched) (Figure 4.3A). The results from  $10^{-4}$  M to  $10^{-1}$  M showed a slope of  $61.2 \pm 0.7$  mV/log [Na<sup>+</sup>] and an intercept of  $243.7 \pm 4$  mV before mechanical stress, a slope of  $59.2 \pm 1.4$  mV/log [Na<sup>+</sup>] and an intercept of  $247.6 \pm 4.4$  mV during 50% strain and a slope of  $61.5 \pm 0.9$  mV/log [Na<sup>+</sup>] and an intercept of  $247.1 \pm 2$  mV after

the resilience test. These carry-over tests demonstrate the ability to follow rapidly fluctuating ions levels. Finally, a carry-over test was performed in artificial sweat over the narrow physiological range of the target electrolytes (Figure 4.3B), using 10-110 mM NaCl (with 5 mM KCl) and the potassium sensor from 1-8 mM KCl (with 80 mM NaCl). The response of the array yielded a slope of  $64.3 \pm 1.2$  mV/log  $[\text{Na}^+]$  with an intercept of  $343.3 \pm 1.5$  mV from  $10^{-2}$  M to  $10^{-0.96}$  M and a slope of  $57.4 \pm 1.6$  mV/log  $[\text{K}^+]$  with an intercept of  $383.4 \pm 3.8$  mV from  $10^{-3}$  M to  $10^{-2.09}$  M. These data showed favorable reproducibility, stability and repeatability while varying the sodium and potassium concentrations within the physiological range, demonstrating the promise of the new potentiometric textile sensors in different real-life scenarios.

A slope value of  $60.3 \pm 4$  mV/log  $[\text{Na}^+]$  (6.6 %RSD, N=5) and an intercept of  $263.3 \pm 67.6$  mV (25.7 %RSD, N=5) from  $10^{-4}$  M to  $10^{-1}$  M for  $\text{Na}^+$  ISE and a slope value of  $60.6 \pm 3.9$  mV/log  $[\text{K}^+]$  (6.4 %RSD, N=5) and an intercept of  $316.6 \pm 56.3$  mV (17.8 %RSD, N=5) from  $10^{-4}$  M to  $10^{-1}$  M for  $\text{K}^+$  ISE were obtained. High %RSD values in the intercept values could be attributed to the use of sensors produced in different batches. Moreover, some of the electrodes were previously exposed to mechanical stress to test their variability. In contrast, constant values in the slope were obtained giving highly reproducible sensors. In this way, the variability in the intercept remains an issue for the wearable potentiometric sensors that needs to be addressed by calibrating each electrode before or after the potentiometric measurement. The results showed that the textile sensor offered a relatively fast change of EMF upon changing the ion concentration for both ions, reaching the steady-state response in about 10 seconds.

Another important parameter to assess is the selectivity of the working electrodes. This critical evaluation is needed to corroborate the feasibility of the sodium and potassium monitoring within physiological range. Sweat, rich in sodium and potassium, can act as interference for the working electrodes. For this reason, selectivity coefficient values were calculated by separate solution method (SSM) for each of the working electrode against the interfering ion. The results can be seen in Table 4.2. Slightly differences were obtained in the selectivity coefficient values. Regularly, ion-selective membranes are prepared with PVC instead of PU used in this work.<sup>[32]</sup> Different impurities found in the polymers can cause this change in the values. Typical values of  $\text{K}^+$  in sweat fall within the 0.2 to 8 mM range<sup>[33]</sup> and for  $\text{Na}^+$  from 20 to 110 mM.<sup>[34]</sup> Selectivity coefficients obtained in this work indicate that interferences should not affect the potentiometric measurements.

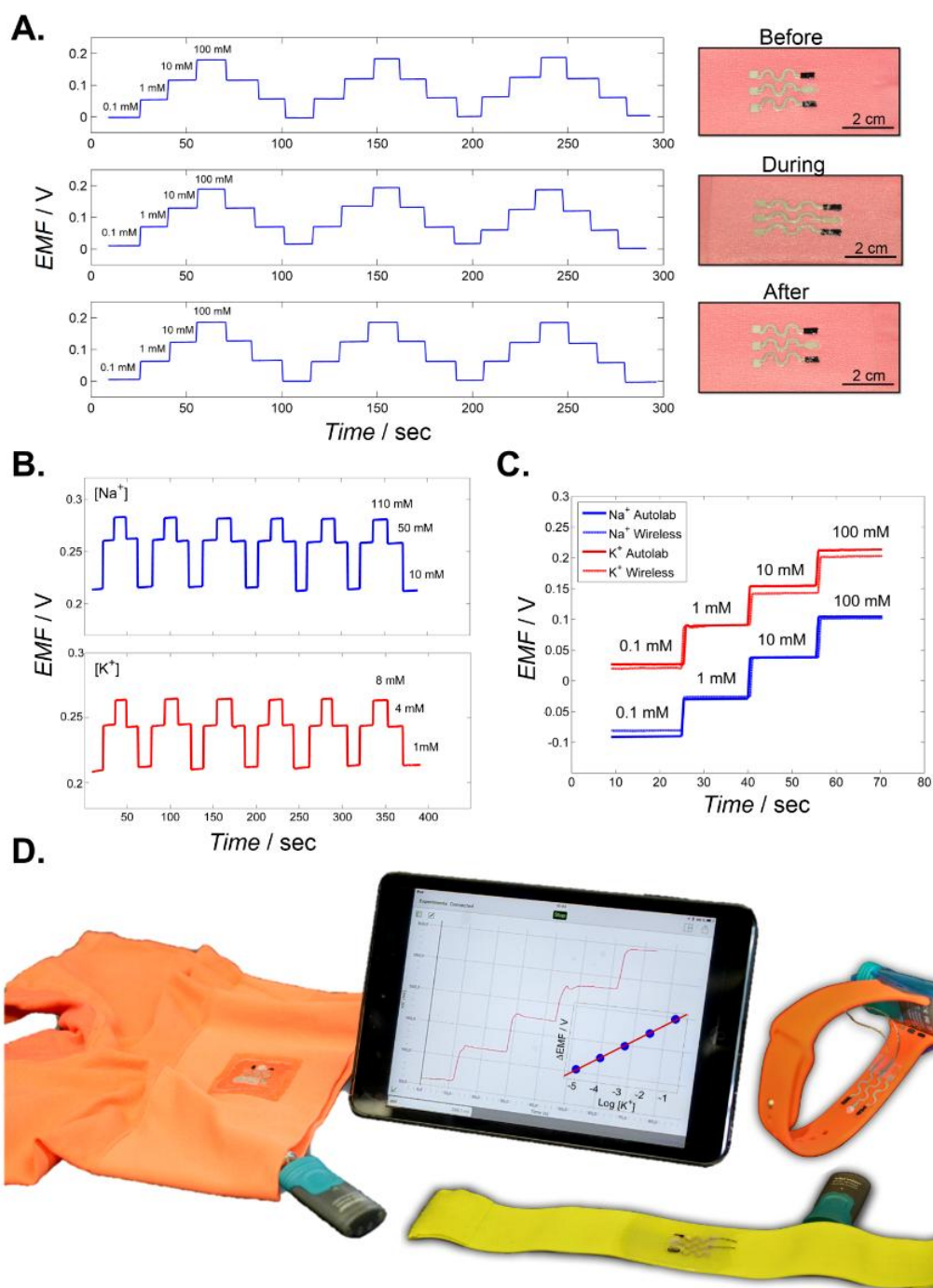


**Figure 4.3.** (A) Carry-over test of a textile-based sensor before, during (50% strain) and after such mechanical deformation. (B) Carry-over testing using artificial sweat test within the physiological range. (C) Correlation of calibration experiments carried out using a compact wireless high-input voltmeter and a conventional potentiostat. (D) Images depicting the versatility of the printable and stretchable sensor array on different common wearable substrates. The tablet displays a real-time trace of increasing potassium levels obtained wirelessly by the underwear printed sensor.

**Table 4.2.** Selectivity values obtained experimentally and in literature for the sodium and potassium-based polymeric membrane.

Analyte	Log K <sub>KY</sub> <sup>a</sup>	Log K <sub>NaY</sub> <sup>a</sup>	Log K <sub>KY</sub> <sup>b</sup>	Log K <sub>NaY</sub> <sup>b</sup>
Na <sup>+</sup>	-3.34	-	-4.1	-
K <sup>+</sup>	-	-1.93	-	-1.9

<sup>a</sup> Results obtained in this work.

<sup>b</sup> Results found in literature.<sup>[35,36]</sup>

### 4.3.2. Wireless integration

Following the detailed characterization of the textile sensors, it was necessary to meet further the practical demands of their real-life wearable operation. Particular important is the integration of the textile sensors with wearable supporting electronics and wireless transmission devices. Hence, we addressed the miniaturization of the reader device and a real-time wireless data transmission to another portable device (e.g., cell phone or a tablet). Complete integration and miniaturization of the textile sensor system was accomplished using a wireless high-input impedance voltmeter, with the potentiometric data being recorded with an iOS® application on an Ipad® tablet. Figure 4.3C compares calibration curves using the textile sensor array obtained with the compact wireless high-input voltmeter and with a benchtop Autolab potentiostat. The excellent agreement between the plots obtained using the two instruments support the integration of the wireless device with the textile-based potentiometric sensor. The response of the array from 10<sup>-4</sup> M to 10<sup>-1</sup> M yielded a slope of 63.1 ± 2.7 mV/log [Na<sup>+</sup>] with an intercept of 164.8 ± 5.3 mV and a slope of 61.1 ± 1.8 mV/log [K<sup>+</sup>] with an intercept of 270.1 ± 9.5 mV.

Wearable devices have large versatility in terms of the diverse types of substrate materials used. It is thus important to take advantage of existing commercial platforms to print the wearable electrolyte sensors. Accordingly, new potentiometric sensors were printed onto conventional textiles such as underwear, watch straps and elastic band (Figure 4.3D). Coupling screen printing technology with commodity textiles could offer large-scale low-cost production of variety of electrochemical sensors and flexible electronics systems.<sup>[37]</sup> Nevertheless, in some cases, such as elastic band or underwear, the rough material surface might become a problem when external tensile load is applied, requiring pretreatment by printing of the stretchable ink. Firstly, an Ecoflex layer was deposited on top of the sensor zone, creating a smooth thin layer. Subsequently, a PU layer was deposited on top of the Ecoflex layer prior to printing the CNT and Ag/AgCl inks. This step was essential to maintain strong adherence of the potentiometric sensor onto the substrate, and hence a remarkable sensor stretchability and durability.

The performance of the potentiometric sensor array printed in this way on different substrates was tested. The watch-straps based sensors yielded a sensitivity of 51.6 mV/log [K<sup>+</sup>] and 51.8 mV/log [Na<sup>+</sup>], compared to 50 mV/log [K<sup>+</sup>] and 52.6 mV/log [Na<sup>+</sup>] for the elastic-band sensors and 56.6 mV/log [K<sup>+</sup>] and 52.5 mV/log [Na<sup>+</sup>] using the underwear sensors. All the sensors performed favorably within a 10<sup>-3</sup> M to 10<sup>-1</sup> M linear range, yielding a near-Nernstian sensor response. Figure 4.3D illustrates the time-trace plot obtained with the underwear textile sensor for increasing potassium levels, as recorded wirelessly with the Bluetooth application. This resulted in a favorable Nernstian response with a slope of 59.9 mV/log [K<sup>+</sup>] over the 10<sup>-5</sup> M to 10<sup>-1</sup> M range.

#### 4.4. CONCLUSIONS

A stretchable textile-based potentiometric sensor that exhibits a Nernstian behavior under extreme conditions has been demonstrated for the first time. Combining stretchable components as the PU, Ecoflex and stretch-enduring inks, along with a serpentine design, this printed textile sensor array can withstands high tensile stress without provoking major cracking common to previous electrochemical devices. Mechanical deformation studies revealed that stretching up to 100%, along with repeated bending, crumpling or prolonged washing have negligible effects on the potentiometric response. Moreover, the screen printing process offers large-scale mass production of low-cost reproducible textile sensors. Further functionalization of the stretchable electrodes with other materials could enable a large arsenal of wearable textile sensors. Such integration of flexible chemical sensors with common textiles will lead to next-generation platform for personalized medicine, and will bring new opportunities for using wearable chemical sensing in the diagnostics, healthcare and sport fields.

#### 4.5. REFERENCES

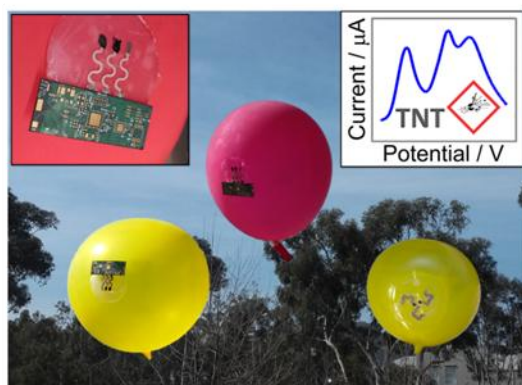
- [1] M. H. Rosner, J. Kirven, *Clin. J. Am. Soc. Nephrol.* **2006**, 2, 151.
- [2] A. Lehnhardt, M. J. Kemper, *Pediatr. Nephrol.* **2011**, 26, 377.
- [3] C. V Leier, L. Dei Cas, M. Metra, *Am. Heart J.* **1994**, 128, 564.
- [4] S. P. von Duvillard, W. A. Braun, M. Markofski, R. Beneke, R. Leithäuser, *Nutrition* **2004**, 20, 651.
- [5] E. Scurati-Manzoni, E. F. Fossali, C. Agostoni, E. Riva, G. D. Simonetti, M. Zanolari-Calderari, M. G. Bianchetti, S. a G. Lava, *Pediatr. Nephrol.* **2014**, 29, 1015.
- [6] E. Moraites, O. A. Vaughn, S. Hill, *Dermatol. Clin.* **2014**, 32, 457.
- [7] A. Bielecka-Dabrowa, D. P. Mikhailidis, L. Jones, J. Rysz, W. S. Aronow, M. Banach, *Int. J. Cardiol.* **2012**, 158, 12.
- [8] E. Tirosh, F. Haddad, A. Lanir, Y. Tal, A. Cohen, *Acta Paediatr.* **1994**, 83, 1268.

- [9] C. S. D. Almond, A. Y. Shin, E. B. Fortescue, R. C. Mannix, D. Wypij, B. A. Binstadt, C. N. Duncan, D. P. Olson, A. E. Salerno, J. W. Newburger, D. S. Greenes, *N. Engl. J. Med.* **2005**, *352*, 1550.
- [10] R. J. Maughan, S. M. Shirreffs, *J. Sports Sci.* **1997**, *15*, 297.
- [11] L. E. Armstrong, *J. Am. Coll. Nutr.* **2007**, *26*, 575S.
- [12] R. J. Maughan, S. M. Shirreffs, *Int. J. Sport Nutr. Exerc. Metab.* **2008**, *18*, 457.
- [13] C. E. Dziedzic, M. L. Ross, G. J. Slater, L. M. Burke, *Int. J. Sport Physiol. Perform.* **2014**, *9*, 832.
- [14] D. B. Diercks, G. M. Shumaik, R. A. Harrigan, W. J. Brady, T. C. Chan, *J. Emerg. Med.* **2004**, *27*, 153.
- [15] L. Florea, D. Diamond, *Sensors Actuators B Chem.* **2015**, *211*, 403.
- [16] A. J. Bandodkar, D. Molinnus, O. Mirza, T. Guinovart, J. R. Windmiller, G. Valdés-Ramírez, F. J. Andrade, M. J. Schöning, J. Wang, *Biosens. Bioelectron.* **2014**, *54*, 603.
- [17] A. J. Bandodkar, R. Nuñez-Flores, W. Jia, J. Wang, *Adv. Mater.* **2015**, *27*, 3060.
- [18] M. C. Chuang, J. R. Windmiller, P. Santhosh, G. V. Ramírez, M. Galik, T. Y. Chou, J. Wang, *Electroanalysis* **2010**, *22*, 2511.
- [19] W. Jia, X. Wang, S. Imani, A. J. Bandodkar, J. Ramírez, P. P. Mercier, J. Wang, *J. Mater. Chem. A* **2014**, *2*, 18184.
- [20] J. R. Windmiller, J. Wang, *Electroanalysis* **2013**, *25*, 29.
- [21] A. J. Bandodkar, I. Jeerapan, J.-M. You, R. Nuñez-Flores, J. Wang, *Nano Lett.* **2015**, *16*, 721.
- [22] C. Callewaert, B. Buyschaert, E. Vossen, V. Fievez, T. Van de Wiele, N. Boon, *J. Microbiol. Methods* **2014**, *103*, 6.
- [23] S. Y. Yun, Y. K. Hong, B. K. Oh, G. S. Cha, H. Nam, S. B. Lee, J. I. Jin, *Anal. Chem.* **1997**, *69*, 868.
- [24] T. Guinovart, A. J. Bandodkar, J. R. Windmiller, F. J. Andrade, J. Wang, *Analyst* **2013**, *138*, 7031.
- [25] T. Guinovart, G. a. Crespo, F. X. Rius, F. J. Andrade, *Anal. Chim. Acta* **2014**, *821*, 72.
- [26] S. Y. Yun, Y. K. Hong, B. K. Oh, G. S. Cha, H. Nam, S. B. Lee, J. I. Jin, *Anal. Chem.* **1997**, *69*, 868.
- [27] V. V Cosofret, M. Erdosy, J. S. Raleigh, T. a Johnson, M. R. Neuman, R. P. Buck, *Talanta* **1996**, *43*, 143.
- [28] T. Guinovart, M. Parrilla, G. a Crespo, F. X. Rius, F. J. Andrade, *Analyst* **2013**, *138*, 5208.
- [29] L. B. Baker, J. R. Stofan, A. a Hamilton, C. a Horswill, *J. Appl. Physiol.* **2009**, *107*, 887.
- [30] M. J. Buono, K. D. Ball, F. W. Kolkhorst, *J. Appl. Physiol.* **2007**, *103*, 990.
- [31] E. F. Coyle, *J. Sports Sci.* **2004**, *22*, 39.
- [32] V. V Cosofret, M. Erdosy, J. S. Raleigh, T. a Johnson, M. R. Neuman, R. P. Buck, *Talanta* **1996**, *43*, 143.
- [33] M. J. Patterson, S. D. Galloway, M. a Nimmo, *Exp. Physiol.* **2000**, *85*, 869.
- [34] C. E. Dziedzic, M. L. Ross, G. J. Slater, L. M. Burke, *Int. J. Sport Physiol. Perform.* **2014**, *9*, 832.
- [35] A. M. Cadogan, D. Diamond, M. R. Smyth, M. Deasy, M. A. Mckerverey, S. J. Harris, *Analyst* **1989**, *114*, 1551.
- [36] E. Bakker, *J. Electrochem. Soc.* **1996**, *143*, L83.



- [37] J. P. Metters, R. O. Kadara, C. E. Banks, *Analyst* **2011**, 136, 1067.

# A BALLOON-EMBEDDED SENSOR WITHSTANDING EXTREME MULTIAXIAL STRETCHING AND GLOBAL BENDING MECHANICAL STRESS: TOWARDS ENVIRONMENTAL AND SECURITY MONITORING



UNIVERSITAT ROVIRA I VIRGILI

TAILOR-MADE CHEMICAL SENSING PLATFORMS FOR DECENTRALIZED HEALTHCARE AND WELLBEING

Rocío Cánovas Martínez

Following a user-friendly approach, this chapter presents the integration of electrochemical sensors on a commodity substrate (a commercial rubber balloon) in order to build an expandable balloon-embedded sensor. Tailor-made stretchable inks have been tested to develop expandable and flexible sensors over a curvilinear surface. This new sensor has been characterized under multidimensional strains and tested towards security surveillance and environmental missions. High mechanical compliance and negligible electrochemical variations were observed during the detection of explosive following dramatic (400%) increases of the balloon area. In this case, the integration of this electrochemical sensor in a user-friendly platform is a clear example of decentralization of the environmental analysis, beyond the central topic of decentralization of healthcare.

## 5.1. INTRODUCTION

Wearable sensors have received considerable attention due to their ability to continuously record valuable data regarding medical conditions, fitness level and air quality.<sup>[1]</sup> Most early applications of such devices have been devoted for on-body monitoring of the wearer physiological status,<sup>[2]</sup> and focused on monitoring of physical parameters and movement.<sup>[3,4]</sup> Indeed, recent efforts have led to the introduction of wearable chemical sensors and biosensors for biomedical and fitness applications in a wristband.<sup>[5]</sup> However, wearable devices should not be limited to on-body measurements.<sup>[6]</sup> Indeed, these sensors hold considerable promise for diverse environmental and security monitoring applications when mounted on other surfaces, ranging from building walls to moving vehicles.

This chapter describes the development of balloon-embedded sensors that withstand a simultaneous extreme multiaxial and global bending mechanical deformation, as well as demonstrates their potential to environmental and security monitoring (Figure 5.1). The integration of flexible and expandable conductive components based on hybrid nanocomposites on a conventional rubber balloon is of considerable significance for two important reasons. First, it examines the fundamental role of the simultaneous multiaxial stretching and global bending motion upon the electrochemical behavior during repeated inflation and deflation cycles. Second, it offers considerable prospects for developing balloon-embedded sensors for in-situ security surveillance and environmental monitoring, as it will be illustrated below for the detection of different explosive compounds.

Conductive materials that can withstand high levels of mechanical deformation have been widely investigated.<sup>[7,8]</sup> Early studies of flexible printable electrodes examined the effect of their bending<sup>[9]</sup> or linear stretching deformations,<sup>[10]</sup> and led to stretchable electrochemical devices for potential wearable applications.<sup>[11–13]</sup> Nevertheless, materials that offer only flexibility or

stretchability have limited potential for applications requiring bonding to or wrapping around non-planar substrates. Thus, there are considerable needs for enhancing the elastomeric properties of such materials to address new demanding applications.<sup>[14]</sup> Conformable and elastic electrochemical devices have the potential for seamless integration with variety of surfaces.<sup>[15,16]</sup> These devices are compliant with complex and dynamic surfaces while retaining their electrochemical properties. Such technology was used to develop a multifunctional balloon catheter with an expandable array of sensors for ablation therapy.<sup>[17]</sup> Other applications in which an expandable platform is needed are found in the wearable sensors field. Compressive garments, such as gloves, athletics suit and sport socks, might require to withstand extreme mechanical deformations and adapt to the muscle activity during rapid body movements. Accordingly, it is of considerable interest to study the mechanical stress produced by multiaxial stretchable spherical surfaces, as will be investigated here using electrochemical sensors embedded in conventional elasto-rubber curved balloon.

Inflatable technology has applicability in numerous fields, including mechanical and biomedical applications.<sup>[18–20]</sup> Over the past five decades several groups have worked on the static and dynamic inflation analysis and related deformation of different geometries and platforms.<sup>[21–23]</sup> Recent work has been focused on understanding the mechanics of inflation and applying it for the modelling of biomedical stents.<sup>[24,25]</sup> The present study represents the first example of modelling and testing such mechanical deformation using electrochemical devices on inflated platforms toward environmental and security monitoring.

Continuous terrorist threats greatly underscore the urgent needs for improved national security measures, in general, and vapor explosive detection, in particular.<sup>[26]</sup> Hence, there are growing demands for reliable decentralized methods for detecting common explosives such as nitroaromatic and peroxide-based compounds. The inherent redox activity of these explosives makes them ideal candidates for electrochemical (voltammetric) monitoring.<sup>[27]</sup> The advantages of electrochemical sensors for field measurements of explosives include remarkable sensitivity and selectivity, a wide linear range, portability, minimal power requirements, and low-cost instrumentation.<sup>[28]</sup> The development of wearable electrochemical explosive-detection platforms thus represents a logical extension of recent activities in the areas of explosive detection and wearable sensors.

Flying balloon platforms are particularly attractive for security surveillance applications aimed at detecting chemical threats in common scenarios. The successful realization of the new sensor-embedded balloon requires understanding of the effect of extreme mechanical deformations upon the structure and performance of the corresponding printed hybrid

nanocomposite electrodes. The printed carbon and silver inks, described here, have been tailored made with elastomers (Ecoflex and polyurethane) and dispersing agent (mineral oil) to withstand high degrees of mechanical stress associated with the inflation of the balloon substrate without compromising their electrochemical properties. Multiple inflation and deflation cycles, involving over 400% increase of the balloon surface area, thus result in negligible changes in the electrochemical behavior. The functionality of the new balloon-based printed sensor system is demonstrated using electrochemical detection of nitro-explosives and amperometric measurements of hydrogen peroxide in the liquid and vapor phases. While the new concept of balloon-embedded sensors is presented here toward explosive detection, such flying platform could serve in a variety of defense and environmental monitoring missions.

## 5.2. EXPERIMENTAL

### 5.2.1. Reagents and materials

Polyurethane (PU) (Tecoflex SG-80A), platinum-catalyzed silicone elastomer Ecoflex® 0030 (Smooth-On, Inc., USA), permanent fabric adhesive (Aleene's, Inc., USA), Ag/AgCl ink (E2414, Ercon Inc., Wareham, MA). Analytical grade salts, 30% (w/w) H<sub>2</sub>O<sub>2</sub> standard solution, mineral oil, agarose type I-A (low EEO), gelatin from porcine skin (type A) and 1-ethyl-3-methylimidazolium tetrafluoroborate ([EMIm][BF<sub>4</sub>]) were purchased from Sigma Aldrich (St. Louis, MO). Tetrahydrofuran (THF) with HPLC grade and dimethylformamide (DMF) was purchased from Fisher Chemical (Fair Lawn, NJ). Ecoflex® 00-30 was prepared in-house by mixing equal volumes of pre-polymer A with pre-polymer B provided by the supplier. Natural rubber latex balloons were employed to build the expandable sensors, purchased in a local store. Stretchable CNT and Ag/AgCl inks were prepared such as is described in Chapter 3.

### 5.2.2. Electrochemical measurements

Cyclic voltammetry (CV) studies were performed using an AUTOLAB Type II (EcoChemie, B. V., Utrecht, The Netherlands) and NOVA software (v.1.11, The Netherlands) as a measuring interface, at room temperature (22 °C). The electrolyte redox probe consisted of ferricyanide (10 mM) in (0.1 M) phosphate buffer (PBS) (pH 7.4). Doubly deionized water (18.1 MΩ·cm<sup>-1</sup>) was employed in all the experiments. CV plots were recorded in the -0.2 V to 0.6 V potential range with a scan rate of 0.1 V·s<sup>-1</sup>.

Resistivity studies were carried out using an Agilent 34411A digital multimeter (Agilent Technologies Inc., USA) and Keysight BenchVue software (Keysight Technologies Inc., USA) as a measuring interface, at room temperature (22°C).

Chronoamperometric studies were executed as experimental section describes in Chapter 3.

Adsorptive stripping voltammetry (AdSV) measurements of nitro explosives were carried out in a PBS solution (0.1 M). Following a 200 seconds accumulation step (at -0.4 V potential for DNT and at -0.1 V for TNT) and after a 15 seconds equilibration, the potential was scanned linearly at  $0.1 \text{ V}\cdot\text{s}^{-1}$ , usually from -0.4 V to -1.3 V for DNT and -0.1 V to -1.0 V for TNT. A cleaning step was not required between successive runs. Measurements employed a background subtraction protocol involving storing the response for the blank solution and subtracting it from the analytical signal.

### 5.2.3. Solid-state electrolytes

Two types of solid-state electrolytes were explored towards the vapor explosive detection. Firstly, the agarose hydrogel (2% w/v) was prepared with NaCl (0.5 M) as a supporting electrolyte. A drop (150  $\mu\text{L}$ ) was cast over the sensing part and was quickly deployed. After 1h drying period, the sensor was ready to use. Secondly, a room temperature ionic liquid in the form of ionogel was used.<sup>[29]</sup> A gelator agent (gelatin from porcine skin) (40  $\text{mg}\cdot\text{mL}^{-1}$  solution) was mixed with RTIL 1-ethyl-3-methyl imidazolium tetrafluoroborate ([EMIm][BF<sub>4</sub>]) at ratio (3:7) respectively. A thin layer (25  $\mu\text{L}$ ) was drop cast along the sensing area and let it dry overnight.

### 5.2.4. Mechanical deformation studies

The ability to sustain high levels of expandability was evaluated by measuring the resistance between each electrode of the serpentine. Firstly, increasing inflation levels (by air blowing) at constant speed (ca.  $3 \text{ mm}^2\cdot\text{s}^{-1}$ ) followed by holding it at each level state for 5 seconds was performed. Besides, the multiaxial stretching study consisted of inflating and deflating the electrochemical device until more than 400% its initial area at constant speed (ca.  $3 \text{ mm}^2\cdot\text{s}^{-1}$ ). Subsequently, the study was aimed at assessing the electrochemical properties of the device while under continuous expandability load, comprised of multiaxial stretching the device during each of the inflation levels for a total of 5 levels at constant speed (ca.  $3 \text{ mm}^2\cdot\text{s}^{-1}$ ). Finally, CV plots were recorded before and after application of 4 inflation-deflation stress cycles for a total of 8 iterations.

### 5.2.5. Fabrication of the expandable sensor on the balloon surface

The process employed an MPM-SPM semi-automatic screen printer (Speedline Technologies, Franklin, MA). Sensor patterns were designed in AutoCAD (Autodesk, San Rafael, CA) and outsourced for fabrication on stainless steel through-hole 12" x 12" framed stencils (125  $\mu\text{m}$  thickness) (Metal Etch Services, San Marcos, CA). Previously, the balloon

was inflated and was kept stretched (30 minutes). Subsequently, the balloon was spread into a planar surface and ready for the printing. Firstly, the planar surface was treated by applying and Ecoflex solidified thick layer (1 mm). Precaution was taken to avoid entrapment of air bubbles while placing the Ecoflex layer onto the supporting surface. Then, a thin layer (ca. 75  $\mu\text{m}$ ) of PU (15 wt%) in DMF solution was deposited on top of the balloon surface and was cured (50°C for 20 minutes). The PU layer fixed the Ecoflex layer onto the balloon surface and served as a smooth material to stick the printed electrodes. Subsequently, the Ag/AgCl – Ecoflex (86 %wt – 14 %wt) ink was printed on the treated balloon surface, followed by curing (10 min at 95°C). After printing this trace, the CNTs ink was used to print the working and counter electrodes (10 min curing at 85°C). Finally, a layer of a permanent stretchable adhesive was used to isolate the sensor print by deploying a thin layer on top. Overnight drying step left the expandable sensor ready to use.

### 5.3. RESULTS AND DISCUSSIONS

#### 5.3.1. Practical fabrication considerations and materials selection

Rapid inflation and deflation cycles of the sensor-embedded balloon platform result in extreme mechanical stress of the printed electrodes (Figure 5.1B). An elastomeric hybrid nanocomposite, tailored with multi-walled carbon nanotubes (MWCNTs) and materials with high viscoelasticity, is used to comply with the extreme multiaxial and global bending mechanical stress associated with the balloon inflation (Figure 5.2A). The nanocomposite electrode addresses current limitations in stretchable electronics by taking advantage of the high elastic properties of the elastomeric materials (polyurethane and Ecoflex silicone rubber) to withstand extreme mechanical deformations without affecting the electronic properties and electrochemical activity of the MWCNTs. Elastomeric polymers provide remarkably complex and nonlinear macroscopic motions, due to their viscoelastic features, enabling large geometrical changes without compromising their physical properties.<sup>[30]</sup> A conductive backbone, the randomly aligned MWCNTs, is entrapped within the polyurethane matrix maintaining their outstanding electron transport properties during the mechanical deformation associated with the balloon inflation. Similar behavior is observed for the printed contacts and reference electrode with the silver/silver chloride and Ecoflex ink, where the long elastomeric chain is surrounded by Ag/AgCl particles and shows ability to reconfigure itself in order to distribute the applied deformation.

Successful sensor operation should be realized by addressing the stretchability of the materials tightly attached to the surface. After observing experimentally the expandable behavior of the balloon, an elastomeric layer (Ecoflex) was placed below the printed sensor to



absorb the tangential strain energy yielded associated with the inflation deformation and avoid potential fractures from the electrochemical device. The large Si-O-Si bond angles and bond lengths of the Ecoflex backbone confers high flexibility and stretchability to the polymer.

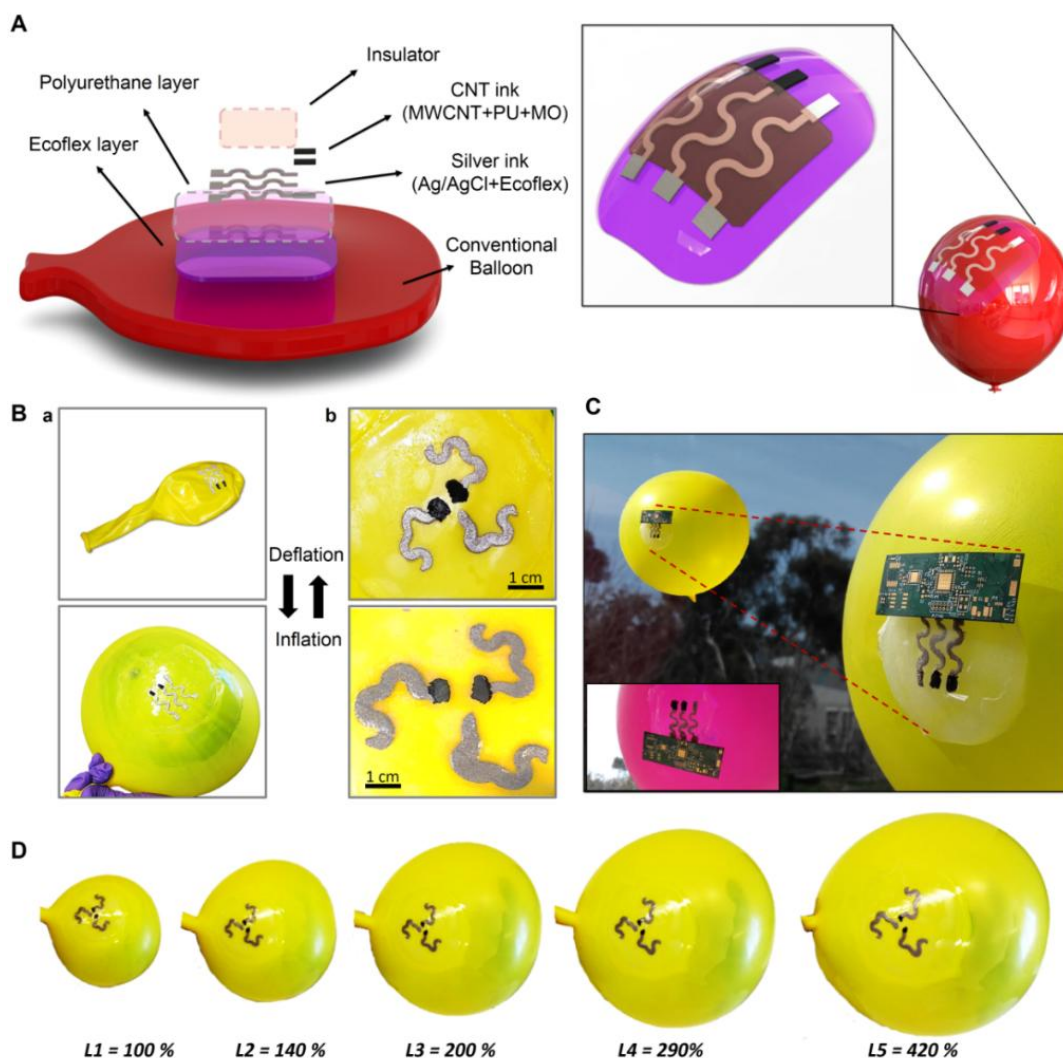


**Figure 5.1.** Expandable electrochemical device. (A) Schematic representation of the layers composition for the expandable balloon device and the representation of its adaptability to curvilinear surfaces. Multiple layers consist of Ecoflex layer (inner), polyurethane (intermediate), printable sensor (Ag/AgCl with Ecoflex composite), the CNT hybrid nanocomposite layer (PU, MO and MWCNTs) and flexible insulator layer (upper). (B) Inflation and deflation status for both designs ((a) linear serpentine and (b) clover designs). (C) Integration of a flexible electronic/wireless circuitry with the expandable balloon device. (D) Different inflation levels (IL) used during the mechanical deformation study and the explosives monitoring.

Crucial steps in the fabrication and assembly of the different layers are applied in the sensor manufacturing. These procedures add functionality to the balloon significantly enhancing their mechanical properties or the levels of expansion that they can accommodate. The printed conductive sensor traces can tolerate linear tensile strains of up to 500% without cracking through optimal composition and patterns guided by mechanics modelling. The strain distributions obtained through analytical modelling capture, quantitatively, the nature of these deformations.<sup>[31]</sup> After multiple repeated inflation and deflation cycles, involving over 400% increase of the balloon area, all devices and interconnects experienced negligible change in their performance.

To address the aforementioned requirements, two strategies were exploited in mechanics.<sup>[32]</sup> First the use of design patterns that stretch to accommodate the stress (Figure 5.1B and 5.1D). Second the use of materials that stretch, the intrinsic stretchability of the printed hybrid materials nanocomposite, imparted by combining CNT with elastomeric polyurethane. PU is acting as the stretchable binder due to its ability to form hydrogen bonds with the carboxyl groups of the CNTs, thus leading to improved dispersion of CNTs within the PU binder.<sup>[33]</sup> Mineral oil further assists the CNT dispersion to create randomly distributed CNTs branches along the stretchable polymer and providing multiscale electron path even during highly mechanical stress, thus retaining the electronic properties of the conductive material.

The printed device conforms four different layers of elastic materials (Figure 5.1A). An inner silicone elastomer layer (Ecoflex) yields uniform distribution of the multiaxial deformation through the convex surface during the inflation and deflation cycle. Subsequently, an intermediate PU layer is printed on top of the inner layer before printing the sensor trace. Improved adhesion between balloon and a stretchable ink by the use of a PU and Ecoflex layer increase the effective stretchability of the sensor by distributing strain uniformly. In a poorly adhered film, global tensile strains localize to delaminated regions and thus form cracks at much smaller strains than for systems with better adhesion.<sup>[15]</sup> Then, the sensor is printed using previously selected stretchable materials based on an analytical procedure. Ag/AgCl particles with the elastomeric Ecoflex material permit electrodes to sustain high degree of expandability as well as PU and CNT to stretch over the surface. Finally, an outer layer made by stretchable insulator is deposited on top of the sensor pattern leaving just the sensing area and the connector part.

Figure 5.1Ba displays the deflated and inflated balloons, the sensor pattern is expanded through the hemispherical surface producing bending and multiaxial stretching mechanical

deformation. Materials start to accommodate mechanical stress energy during inflation until the point where the sensor starts its visual deformation is reached. The effect of device design and stretchable inks provides the printed sensor with high tolerance toward inflation and deflation cycles. The images underscore the ability of the printed sensor to endure extreme and complex multidimensional strains with minimal effect on its structural integrity. Besides, different design patterns are tested in order to increase the sensor expandability (Figure 5.1Bb). Improvement in the curvatures of the sensor patterns (via a clover design) distributes the strain energy more equally during the inflation process, thus decreasing the deformation and fracture of the electrodes. The clover design displays higher compliance toward multidimensional mechanical deformation.

Finally, for the on-site explosives detection, wireless system integration is needed. Figure 5.1C shows a small flexible wireless circuit board able to record voltammetric signals upon an open area. The flexible electronic module can be coupled to the printed electrodes via magnetic connectors to enable real-time measurements and wireless data transmission. This flexible electronic board is compatible with the non-planarity of the balloon and offers resistance to mechanical stress. Automated systems are needed for the detection, and consequently warn of potential threats in public areas. The miniaturization and the ability of the wireless reader to withstand hard atmospheric conditions are key issues needed to validate the system in real scenarios. Hence, further improvements on these features will be necessary to test in the field.

### 5.3.2. Modelling

Before studying experimentally the mechanical deformation ability of the highly stretchable and flexible hybrid nanocomposite-based ink, a careful view to the inflation and deflation mechanism is needed to understand the expandability of the printed device. Figure 5.1D displays the inflation levels of the electrochemical device through the conventional balloon inflation. Hence, the geometric area could be calculated by having a look at the inflation technique as it will be carefully explained later.<sup>[34]</sup>

The novel expandability approach is studied by examining the rheological properties of the tailored printed ink on the curvature surface resulted from the balloon inflation and leads to multiaxial symmetric deformation. Several forms of the strain-energy function have been developed to describe these deformations of “rubber-like” materials. Hence, some mathematical expressions describing this deformation are documented in the literature.<sup>[21,22,35]</sup>

Figure 5.1D shows the evolution in the configuration of a multiaxial stretchable hemispherical surface associated with the use of a conventional elasto-rubber material such as

a conventional curved balloon. The inflation and deflation cycles result in high strain levels (involving both multiaxial stretching with global bending motion, Figure 5.2) over the sensor design, imparting expandability to the field of electrochemical sensors. Such curvatures produce the next level of mechanical deformation, resulting in an ideally equivalent multiaxial tensile strain, which many materials used in electrochemical devices cannot accommodate without crack or fracture. The mechanical properties of the new tailored ink allow the expandable sensor to maintain its electrochemical sensing behavior. Besides, the selected materials were required to stretch a planar layer over a hemispherical surface without generating wrinkles during the inflation and deflation cycles. The clearest application of expandable sensors is perhaps integration with components that deform regularly as part of their operation, or those that deform at randomly in response to their environment, such as the balloon in atmospheric conditions.

In the inflation technique test, the balloon is deposited with the circumference nozzle held in a clamp. Then, it is inflated to as spherical balloon shape using pressurised air. This method has long been used by many researchers for the characterization of synthetic polymers, especially rubbers and polymer melts.<sup>[18,19,23]</sup> Several attempts have been performed to simplify the study of the strain produced by the inflation test. An analysis that strives the non-uniformity in thickness of the studied element propose an analytical procedure for calculating the stress and strain at the top of the balloon from the experimental data.<sup>[34]</sup> The analysis is based on the following assumptions: 1) the rubber is incompressible, 2) the balloon is spherical and 3) each rubber particle is shifted normally to itself during inflation. As the balloon inflates, the wall thickness reduces. However, due to the non-uniform deformation along the surface of the balloon, the thickness at the top is smaller than the thickness at the base of the balloon (close to the clamp) thus a thickness distribution arises. Therefore, an approach to calculate the thickness  $t$ , stress  $\sigma$ , planar strain  $\varepsilon$ , radius of curvature  $R$  and volume  $V$  at the top of the balloon can be executed with the following equations:

$$t = t_0 \left[ \frac{a^4 + s^2 h^2}{a^2 (a^2 + h^2)} \right]^2 \quad (\text{Equation 5.1})$$

$$\sigma = \frac{PR}{2t_t} \quad (\text{Equation 5.2})$$

$$\varepsilon = \ln \left( 1 + \frac{h^2}{a^2} \right) \quad (\text{Equation 5.3})$$

$$R = \frac{a^2 + h^2}{2h} \quad (\text{Equation 5.4})$$

$$V = \frac{\pi}{6}h(3a^2 + h^2) \quad \text{(Equation 5.5)}$$

where  $t_0$  is the original sample thickness,  $t_i$  the thickness at the balloon top,  $a$  the original sample radius,  $h$  the height,  $P$  the pressure inside the balloon and  $s$  the distance from the centre of the sample. Figure 5.2B illustrates the schematic representation related with the represented parameters in the equations.

On the other hand, the uniform balloon thickness could be assumed. On this way, the thickness  $t$  and balloon surface area  $S$  could be calculated by the next equation:

$$t = \frac{\pi a^2 t_0}{S} \quad \text{(Equation 5.6)}$$

$$S = 2\pi R^2 \pm 2\pi R\sqrt{R^2 - a^2} \quad \text{(Equation 5.7)}$$

Finally, with this simplified approach, the expansion percentage could be calculated according to the surface area (Equation 5.7) of each inflation level from each radius of extension (Equation 5.4). Figure 5.1D displays the balloon inflation levels using the clover pattern with each calculated inflation percentage. Considerations during the printing are taken into account after the thickness assumptions regarding the position of the sensor in the balloon. To increase the inflation level, sensor should be printed in the lower part of the balloon (as close to the nozzle as possible) to avoid high stretching stress from the material thickness.

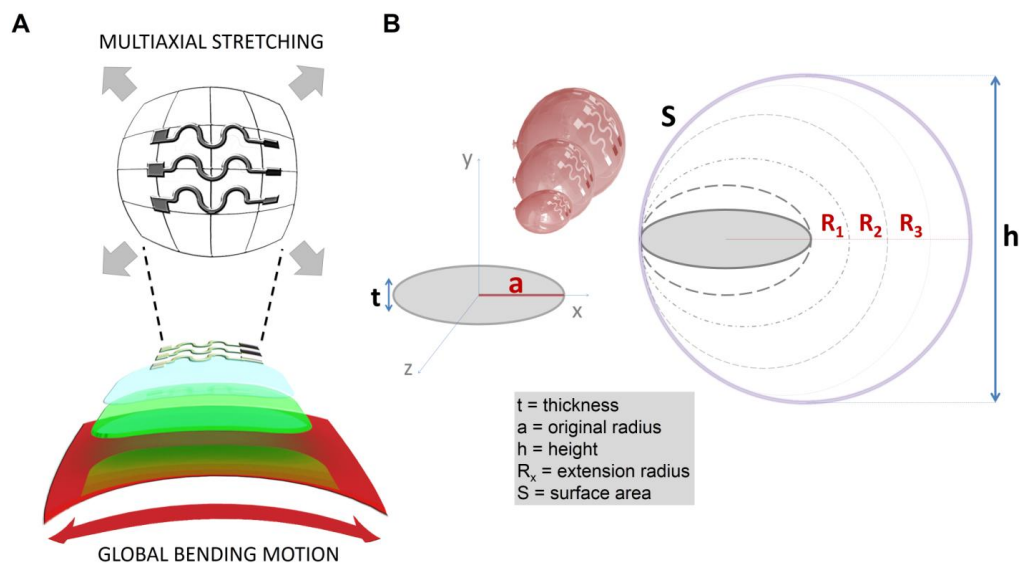


**Figure 5.2.** (A) Multi-axial stretching with bending motion schematics and (B) schematic representation related with the parameters in the equations.

A realistic modelling of the expandability mechanism is critical because the inflation pressure, transmitted through the elastic material, is locally uniform but its direction follows the deformed balloon. A careful examination of the inflation procedure shows that, except at the ends, the structure is almost uniformly dilated and finally evenly expanded. Thus, it seems justifiable to model expansion by considering a finite enlargement under uniform radial internal pressure. Such assumption can be represented by different approaches. The simplest model can be represented as a uniaxial stretching of a rubber band (2D model). The band should be situated over the perimeter of the balloon surface, while inflation, the band is stretched and bended.

### 5.3.3. Mechanical deformation studies

In order to test the inflation challenge and the corresponding mechanical stress that occurs to the printed sensor, some mechanical tests were applied to the expandable device. The remarkable expandability and attractive performance of the new printable electrochemical sensor have been examined using conductivity measurements and cyclic voltammetry (CV) probing of changes in the electrochemical properties and in the electrode-electrolyte interface. Therefore, the expandable behavior of the sensor was assessed under static resistance measurements in each electrode during levels of inflation (Figure 5.3A). All the electrodes display low resistance values ( $< 80 \Omega$ ) under these inflation-induced mechanical stress, with a slight resistance increase (from around  $10 \Omega$ ) upon increasing the inflation level. Microscopic cracks on the conductive track and increased resistance have been observed after the 5<sup>th</sup> inflation level. While these still allowed electrochemical measurements, the stability and reproducibility are compromised. Further inflation of the balloon led to macroscopic fractures that did not allow sensing work.

The outstanding resiliency against mechanical deformation of the printed composite conductive traces can be explained by delving at the microscopic level of the printed traces (Figure 5.3B). When an external expansion load is applied to the sensor, the stress generated within the printed pattern is absorbed by the stretchable elastomeric component that is able to deform and rebound to its original geometrical area without any distortion. For the Ag/AgCl ink under tensile stress, the interpenetrating Ecoflex long chains undergo stretching while maintaining the physical contact between the randomly printed conductive particles. Similarly, when the printed composite MWCNT working and counter electrodes are subject to extreme stress, their PU binder stretches while maintaining the electrical contact of the randomly distributed CNT. This hybrid nanocomposite is made by mixing functionalized MWCNTs with the PU elastomer to enhance the mechanical properties. The homogenous dispersion of the

MWCNT reflects the hydrogen bonds between C=O groups and NCO groups of the PU chains with the COOH of the MWCNT-COOH.<sup>[36]</sup> Moreover, the hybrid nanocomposite improves the tensile strength and modulus in comparison with bare PU.<sup>[37]</sup> The elastomer cross-linkages ensure also that the polymer returns to its original position during deflation without affecting the electrical properties of the nanocomposite.

Interestingly, the electroactive area of the hybrid nanocomposited electrode is not changed during the balloon inflation and corresponding sensor stretching. As illustrated in Figure 5.3B, no alterations in the conducting carbon area take place upon inflating the balloon and expanding the printed nanocomposited MWCNT-PU electrodes. Although the geometrical area of the electrode increases dramatically due to the elastomeric behavior of polyurethane molecules, the same electrochemical active surface area (in direct contact with the solution) is maintained. This reflects the finite amount of the embedded MWCNTs. Therefore, the elongation of the chains from the elastomeric binder (PU) component is performed while maintaining the electrical connections of the composite electrode associated with the randomly aligned MWCNTs. Figure 5.3B illustrates the expansion of the elastomeric molecular chains while maintaining the same amount of MWCNTs, thus retaining the same electroactive area of the sensor. According to the Randles-Sevcik equation (Equation 5.8), the electroactive surface area maintained during the inflation over the electrode is ca. 0.19 cm<sup>2</sup>.

$$A = \frac{I_p}{2.69 \times 10^{-5} D^{1/2} n^{3/2} \gamma^{1/2} C} \quad (\text{Equation 5.8})$$

where  $A$  is the surface area in cm<sup>2</sup>,  $D$  is diffusion coefficient of the molecule in solution (cm<sup>2</sup>·s<sup>-1</sup>),  $I_p$  is the peak current value,  $n$  is the number of electrons involved in the reaction,  $C$  is the concentration of the probe molecule in the solution and  $\gamma$  is the potential scan rate (V·s<sup>-1</sup>).

The assumption of unchanged electroactive area is supported further from the reproducible cyclic voltammograms of Figure 5.3Da, recorded for balloons inflated from level 1 to level 5. This is indicated from the reproducibility of the charging background current. Note also the similarity of the peak potentials that indicate that the small resistance changes have minimal effect on the electrochemical behavior. In addition, no resistance changes are observed for the clover pattern for repeated balloon inflation/deflation cycles (Figure 5.3Cd). Similarly, the cyclic voltammograms of Figure 5.3Db show no apparent change in the electrochemical performance during such repeated cycles.

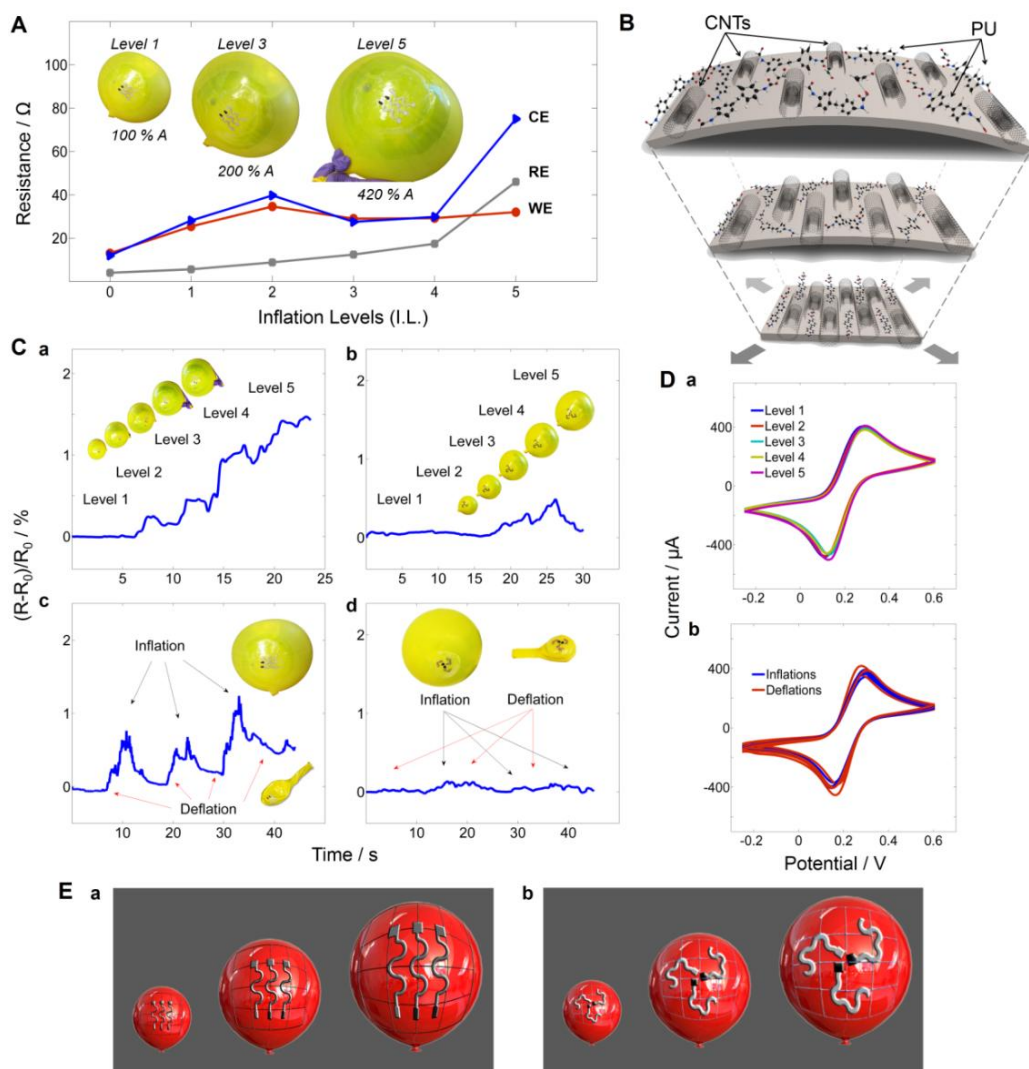


**Figure 5.3.** Mechanical deformation study and modelling of the expandable device. (A) Static resistance study during increasing inflation levels with the linear serpentine pattern for working, reference and counter electrodes. (B) Schematic representation of the expandable hybrid nanocomposite model of the carbon nanotubes (CNTs) and elastomeric stretchable polyurethane from deflation until inflation status. (C) Dynamic resistance study and comparison between different designs. (D) Cyclic voltammetry study for mechanical compliance assessment (Da) over all the inflation levels and (Db) during inflation and deflation cycles. (E) Schematics of the models between device patterns during the balloon inflation levels.

After understanding the behavior of the expanding sensor at the molecular level, a careful dynamic study for the resistance change was carried out during the balloon inflation status and upon repeated inflation/deflation cycles. Figure 5.3C illustrates the comparison between the linear serpentine and clover sensor designs by monitoring resistance change during different



mechanical expansion tests. Figures 5.3Ca (linear pattern) and 5.3Cb (clover design) show the different behavior of the two designs upon the increasing inflation levels. Figure 5.3Cc (linear pattern) and 5.3Cd (clover design) show the resistance changes during inflation and deflation cycles. As indicated from Figure 5.3C (reference electrodes) and Figure 5.4 (working electrodes), the resistance study for both designs illustrates a higher signal stability using the clover design. Hence, more favorable outcomes are obtained for the clover pattern that offers a more uniform absorption of the tensile strain energy along the sensor trace.

A slight increase in the sensor resistance is observed during the balloon inflation. Such resistance change does not affect the explosive detection (described below). However, after certain inflation level, the resistance of the Ag/AgCl electrodes increases reflecting the limited density of Ag/AgCl particles (during the expansion of the Ecoflex material). Experimentally seen, the crack density is greatest at the non-curvilinear parts of the sensor pattern.

As shown in Figure 5.3D, the redox peak separation ( $\Delta E_p$ ) as well as the oxidation peak current ( $i_p$ ) of the ferricyanide probe remain nearly identical even when the sensor undergoes high level of mechanical stress during inflation (RSD for  $i_p = 3\%$ ). Even during extreme stress cycles (continuous inflation and deflation cycles), the sensor displays an excellent peak heights stability (RSD for  $i_p = 5.9\%$ ). These data indicate that the sensor can withstand high degree of multiaxial mechanical fatigue with minimal effect on the electrochemical properties.

#### 5.3.4. Design considerations

Following the detailed inflation model, the sensor pattern will be discussed. Figure 5.3E illustrates the conceptual explanation of the balloon expandability containing the different sensor designs ((a) linear and (b) clover). These schematics and resistance tests suggest that the clover pattern should offer improved expandability of the sensor by alleviating the stress applied during inflation (Figure 5.3Eb). Such clover design helps in the expandability and functionality of the sensor, instead of the linear one (Figure 5.3Ea) used earlier to sustain high amount of linear stretchability.<sup>[10]</sup> This assumption is supported by the resistance evaluation during different inflation levels shown in Figure 5.3C for the reference electrode and in Figure 5.4 for the working electrode. Figure 5.3C, Figure 5.4A and Figure 5.4B display resistance measurements using the balloon-embedded linear and clover serpentine patterns, respectively.

The resistance increases gradually upon increasing the inflation level for the linear serpentine design (Figure 5.3Ca). In contrast, as shown in Figure 5.3Cb, the clover design is more resilient to resistance changes, with no apparent change up to the 3<sup>rd</sup> level. Similar advantages of the clover pattern are observed upon repeated inflation and deflation cycles (Figure 5.3Cd). Under this stress the linear design displays rapid increase of the resistance

during the inflation step (Figure 5.3Cc), unlike the clover pattern that tends to accommodate more uniformly the energy stress associated with the inflation mechanical deformation. Interestingly, Figure 5.4Ab and 5.4Ac as well as Figure 5.4Bb and 5.4Bc show that the working electrodes underscore less increment of resistance to allow a more stable signal. Such behaviour reflects the difference in the binder characteristics. PU adhered to the CNT ink can absorb the energy coming from the mechanical stress more easily than Ecoflex found in Ag/AgCl ink. This ability to operate under extreme mechanical stress conditions meets the demands of using these balloon-embedded printed sensors for real-time atmospheric monitoring.

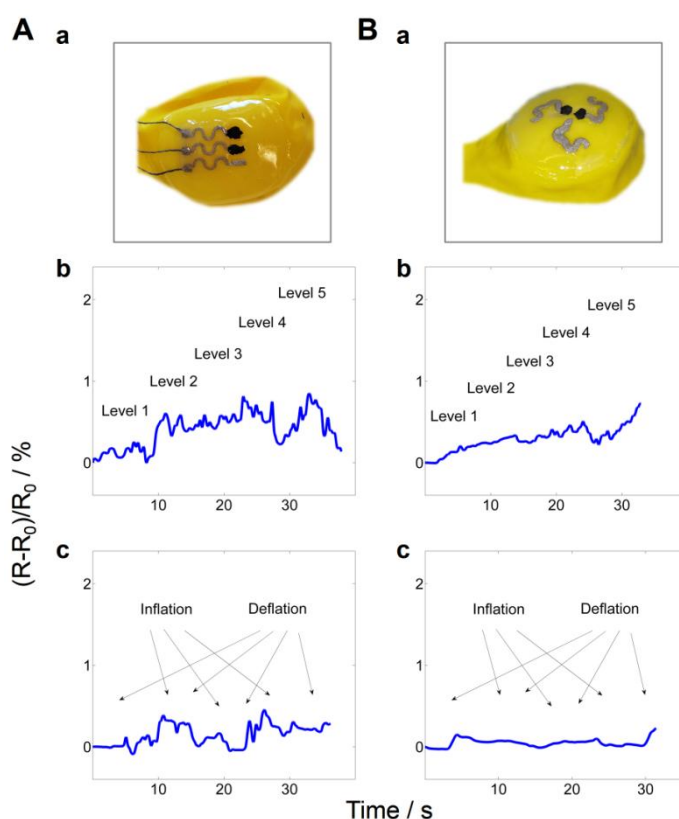


**Figure 5.4.** Dynamic resistance study and comparison between different designs: (A) linear serpentine pattern and (B) clover pattern, shown in (a). Figure (b) and (c) displays the change of resistance upon different mechanical expansion tests: increasing the inflation levels and inflation-deflation cycles, respectively, for working electrodes.

Overall, the clover sensor pattern offers several advantages. Firstly, the elevated thickness is capable of sustaining more strain energy, leading to a higher level of inflation. As discussed previously in the modelling, the balloon thickness decrease upon increasing the inflation level

and high tensile strength is produced over the surface area of the sensor. Hence, high thickness in the sensor trace facilitates better distribution of the strain. Secondly, the curvilinear shape of the clover serpentine accommodates more mechanical stress than the linear one. Finally, a decrease of the geometrical sensing area is produced due to a circular shape instead of the linear shape allowing to a homogenous deposition of the solid-state electrolyte. The clover design thus leads to higher multiaxial stretchability without compromising the integrity of the sensor. Previous work yielded to an inferior electrical resistance of linear serpentine pattern with higher angle, between the extremities of the circular shape, compared to lower angle toward external strain.<sup>[31,38]</sup> Therefore, decreasing the connecting angle as well as increasing the thickness of the clover serpentine leads to considerably higher resiliency and conductivity to strains associated with the balloon inflation.

### 5.3.5. Liquid-phase sensing

Electrochemical devices are advantageous for addressing the urgent needs for on-site detection of nitroaromatic explosives, such as 2,4,6-trinitrotoluene (TNT)<sup>[39]</sup> or 2,4-dinitrotoluene (DNT)<sup>[40]</sup> and of peroxide-based homemade explosives and their hydrogen peroxide (H<sub>2</sub>O<sub>2</sub>) precursor.<sup>[41]</sup> The ability of the balloon-embedded sensors to detect explosives has been evaluated first in the liquid-phase using variety of relevant mechanical strains associated with the balloon inflation. The strong accumulation of nitroaromatic compounds onto CNT can be used for effective pre-concentration step towards achieving highly sensitive explosive detection.<sup>[42]</sup> Figure 5.5A displays voltammetric signals for different TNT concentrations using highly sensitive adsorptive stripping measurements. The resulting stripping voltammograms reveal three well-defined redox processes, at -0.43V, -0.65V, and -0.78V (vs. the Ag/AgCl reference), characteristics of the stepwise TNT reduction to the corresponding hydroxylamine and amine.<sup>[42]</sup> The first signal (at -0.43V), exhibiting the most favorable characteristics, was selected for subsequent analytical work. Figure 5.5Aa and 5.5Ab demonstrates the analytical performance of the sensor in the 1<sup>st</sup> and 4<sup>th</sup> levels of the balloon inflation, along with the corresponding calibration curve (inset). The peak currents increase proportionally with the TNT concentration from 20 to 100  $\mu\text{g}\cdot\text{mL}^{-1}$  to yield a highly linear calibration plot, with a slope of 1.82  $\mu\text{A}\cdot\text{mL}\cdot\mu\text{g}^{-1}$  for the 1<sup>st</sup> level of inflation. Besides, the analytical performance of the 4<sup>th</sup> level of inflation sensor yields a slope of 2.09  $\mu\text{A}\cdot\text{mL}\cdot\mu\text{g}^{-1}$ . To understand if the sensor can withstand different levels of inflation, the voltammetric signal using 60  $\mu\text{g}\cdot\text{mL}^{-1}$  TNT was recorded at different levels of inflation (Figure 5.5Ac). Such investigation discloses its attractive performance even when subjected to increasing inflation levels (RSD for  $i_p$  = 7.7 %). Figure 5.5Ba and 5.5Bb display the sensor response for DNT (a TNT precursor) recorded during the 1<sup>st</sup> and 4<sup>th</sup> levels of inflation, respectively. The calibration plot (inset) yields a 3.31  $\mu\text{A}\cdot\text{mL}\cdot\mu\text{g}^{-1}$

and  $3.72 \mu\text{A}\cdot\text{mL}\cdot\mu\text{g}^{-1}$  for the 1<sup>st</sup> and 4<sup>th</sup> level of inflation (using  $-1.1 \text{ V}$  DNT reduction peak) respectively. Figure 5.5Bc examines the sensor performance during different levels of deformation (L1-L5). These voltammetric data illustrate that the response for  $60 \mu\text{g}\cdot\text{mL}^{-1}$  DNT is nearly independent of the inflation level of the balloon (RSD for  $i_p = 6.4 \%$ ).

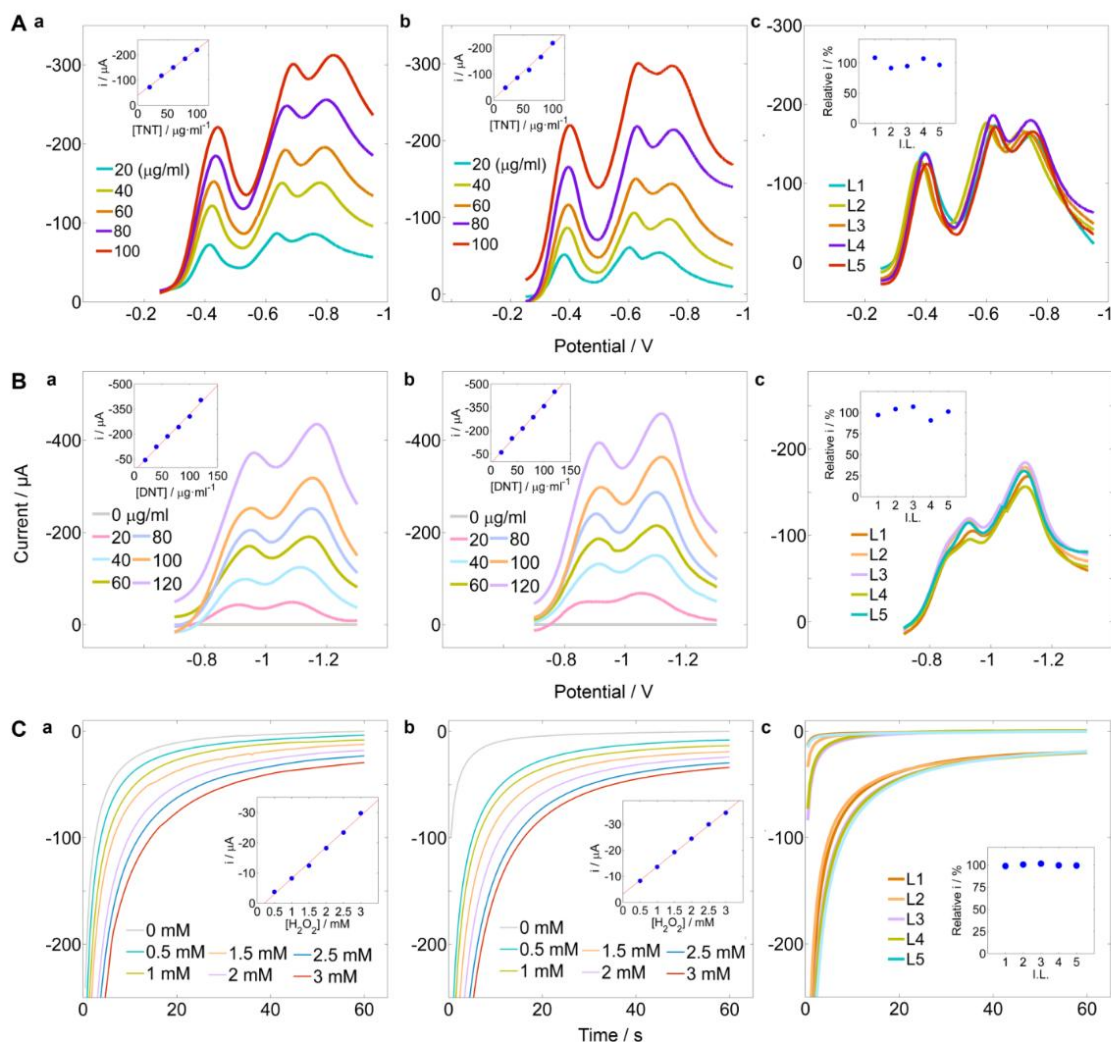


**Figure 5.5.** Explosive detection liquid-phase TNT, DNT and H<sub>2</sub>O<sub>2</sub> using the balloon-embedded sensor. (A) TNT calibration curve in (Aa) the 1<sup>st</sup>, (Ab) the 4<sup>th</sup> level of inflation for the expandable device and (Ac) voltammetric signals during increasing inflation levels. (B) DNT calibration curve in (Ba) the 1<sup>st</sup>, (Bb) the 4<sup>th</sup> level of inflation for the expandable device and (Bc) voltammetric signals during increasing inflation levels. (C) H<sub>2</sub>O<sub>2</sub> calibration curve in (Ca) the 1<sup>st</sup>, (Cb) the 4<sup>th</sup> level of inflation for the expandable device and (Cc) amperometric signals during increasing inflation levels.

Before applying the vapor-phase test, factors affecting the chronoamperometric detection of diluted peroxide aqueous solutions at the smart balloon were optimized. The signal increases slowly upon changing the potential from -0.6V to -0.9V where the reduction of the peroxide occurs. Hence, the analytical performance was examined by recording the current during 60 seconds at -0.9 V while varying the peroxide concentration from 0.5 mM to 3 mM. Figure 5.5Ca (1<sup>st</sup> level of inflation) and 5.5Cb (4<sup>th</sup> level of inflation), and corresponding calibration plots (insets), illustrate that the current increases linearly with the peroxide concentration. These plots lead to similar sensitivity (slope) between these 1<sup>st</sup> and 4<sup>th</sup> inflation levels (10.34  $\mu\text{A}\cdot\text{mM}^{-1}$  and 10.54  $\mu\text{A}\cdot\text{mM}^{-1}$ , respectively). Finally, Figure 5.5Cc shows a mechanical stress study recording chronoamperometric signals for 1.5 mM hydrogen peroxide (lower lines) during different levels of inflation (RSD for  $i = 1.1\%$ ). Figure 5.5Cc also displays the corresponding background currents under these inflations (upper lines). Interestingly, only a negligible change in the current response is observed upon increasing the mechanical stress.

The results obtained from the voltammetric analysis of explosives compounds, TNT, DNT and hydrogen peroxide greatly support the ability of the expandable sensor to monitor these compounds under extreme degree of mechanical strain. The system can thus be utilized for real-time security screening in real-scenarios.

### 5.3.6. Vapor-phase sensing

Following the successful liquid-phase explosive detection, the balloon-embedded sensor system was tested for its ability to detect explosive vapor, in view of future security surveillance applications. Essential considerations for the electrochemical gas sensing of such explosive compounds must be taken in order to perform an accurate measurement. Firstly, a solid-state electrolyte with suitable transport properties is needed. Secondly, sensors must survive rapid atmospheric changes such as temperature and pressure. Preliminary gas-phase explosive sensing was carried out using the systems shown in the images of Figure 5.6, using vapors of DNT (A) and hydrogen peroxide (B). Such gas-phase DNT measurements have been facilitated by coating the printed electrodes with a thin layer of a solid-state electrolyte such as hydrogel (using agarose).<sup>[40]</sup> Figure 5.6Aa demonstrates the vapor-phase detection of DNT using the smart balloon. Plot exhibits the voltammetric DNT detection through different exposure times while blowing air to the sample (100 mg DNT powder) to accelerate the vapor diffusion through hydrogel layer. As expected, the DNT response increases upon using longer exposure times. Figure 5.6Ab displays the linearity of the voltammetric signal upon increasing the amount of DNT from 100 to 500 mg after 4 minutes air blowing. Hence, a linear relationship of 0.3  $\mu\text{A}\cdot\text{mg}^{-1}$  slope was obtained. Figure 5.6Ac shows the configuration of the system.

Room temperature ionic liquids (RTILs) are gaining growing interests for gas sensing due to their outstanding electrochemical stability.<sup>[43]</sup> The curvilinear shape of the balloon makes the viscosity and surface tension of the RTIL not sufficient for maintaining a thin layer onto the sensing area. For this reason, an ionogel approach, involving mixing the RTIL with gelatin, has been developed for its easy shaping to curvilinear surfaces while maintaining the RTIL properties.<sup>[44]</sup> Figure 5.6Ba shows the influence of the equilibration time upon chronoamperometric vapor peroxide measurements using 1 mL of 1% w/w H<sub>2</sub>O<sub>2</sub> in a 35 mL beaker. Figure 5.6Bb displays current–time chronoamperometric recordings for H<sub>2</sub>O<sub>2</sub> vapor generated during a 15 min equilibration with 1 mL droplets containing increasing levels of hydrogen peroxide in 2% increments. The system was evaluated from 2% to 8% following the configuration of Figure 5.6Bc. The current (sampled after 60 seconds) is proportional to the peroxide concentration. The resulting calibration plot (inset) yields a slope of 2.45  $\mu\text{A} [\% \text{ w/w H}_2\text{O}_2]^{-1}$ .

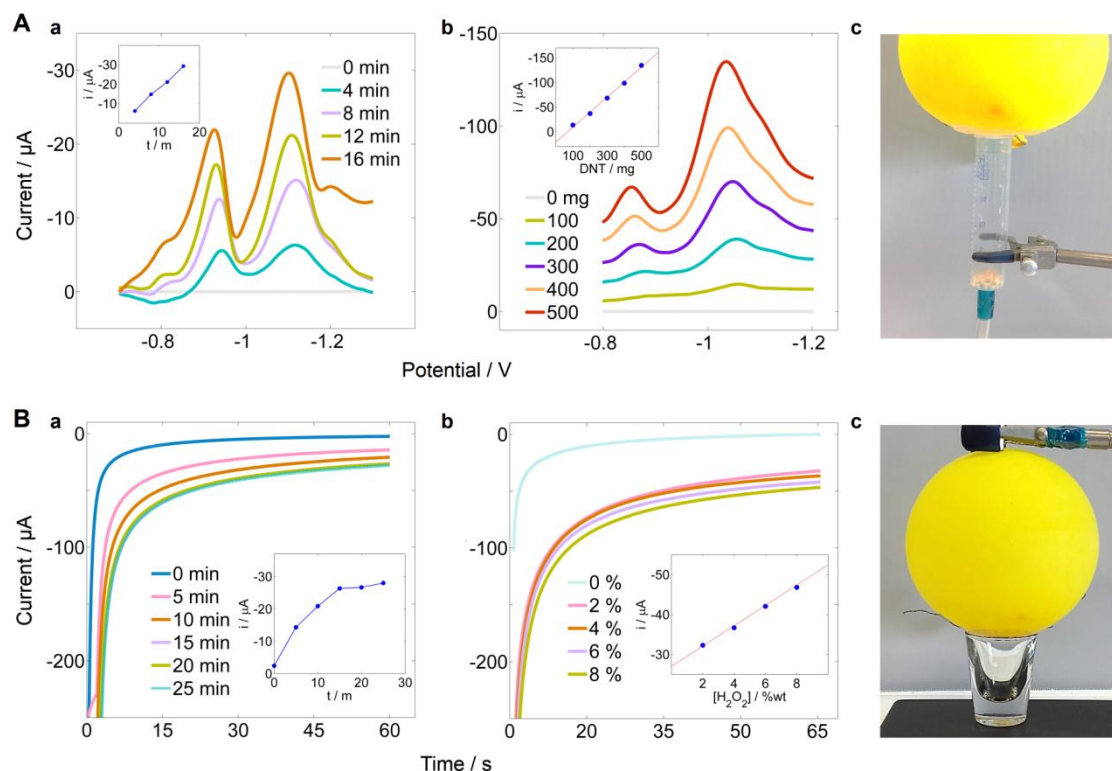


**Figure 5.6.** Explosive vapor detection: gas-phase measurements of DNT and H<sub>2</sub>O<sub>2</sub>. (A) Hydrogel solid-state electrolyte strategy for DNT vapor-phase detection (Aa) equilibration time voltammetric curve for 100 mg DNT, (Ab) voltammetric signal upon increasing the amount of DNT from 100-500 mg and (Ac) the corresponding experimental arrangement. (B) Ionogel solid-state electrolyte strategy for H<sub>2</sub>O<sub>2</sub> vapor-phase detection, (Ba) equilibration time amperometric curve for 1% H<sub>2</sub>O<sub>2</sub>, (Bb) calibration curve for increasing amount of H<sub>2</sub>O<sub>2</sub> and (Bc) corresponding configuration.

## 5.4. CONCLUSIONS

The development of balloon-embedded sensors that withstand a simultaneous extreme multiaxial and global bending mechanical deformation was reported in this chapter. Moreover, their potential for detecting different explosive compounds in gas and liquid phases was demonstrated. Such stress-enduring sensors rely on hybrid nanocomposite printable electrodes, combining the electronic properties of MWCNTs with the mechanical compliance of PU elastomer, on inflated balloon platforms. The electroactive area of the electrochemical device provided by the MWCNTs is maintained during the stretching of the elastomer providing high electronic compliance.

The present study is of considerable significance for two important reasons. First, it examines the role of the nanocomposite upon the sensor performance during extreme multidimensional strains. The nanocomposite provides efficient electron-transport path with the MWCNTs backbone and high degree of energy distribution even when high mechanical stress is applied. Mechanical deformation tests indicate remarkable performance of the hybrid nanocomposite electrochemical device without compromising the performance (even with >400% surface area increase). Such attention to the extreme demands of the inflated spherical dynamic balloon substrate reflects the elastomeric, electrical and electrochemical properties of the new expandable composite inks. Second, it offers great prospects for developing flying expandable sensor systems for in-situ security and environmental monitoring. The present work is thus opening up new possibilities in device engineering, with very important applications in different technological areas. The new balloon sensor holds great promise for field-based screening operations, aimed at assisting security-surveillance and environmental missions. Finally, the integration with wireless electronics could facilitate real-time monitoring and warning capabilities. In addition to security surveillance applications, the new balloon sensing system should benefit other monitoring scenarios, ranging from tracking pollution to surveillance of industrial process controls.

## 5.5. REFERENCES

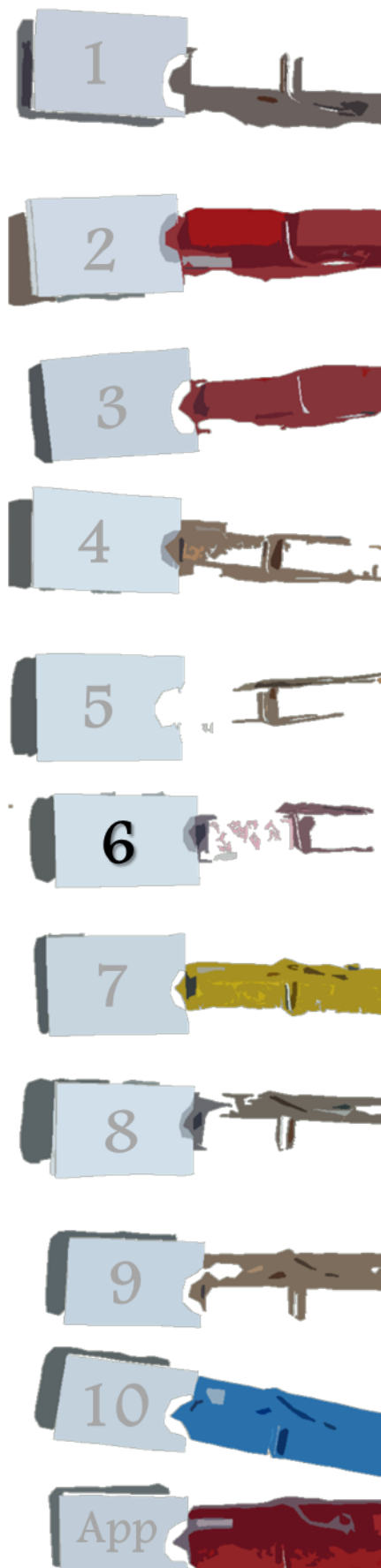
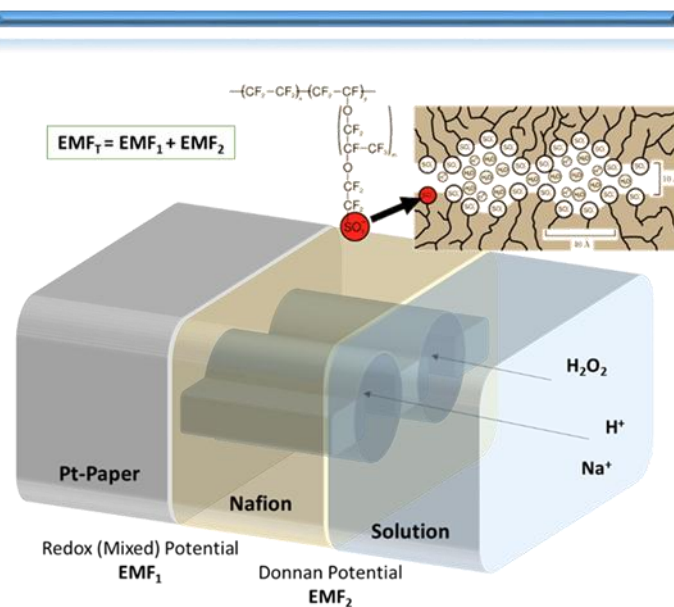
- [1] M. Amjadi, K. U. Kyung, I. Park, M. Sitti, *Adv. Funct. Mater.* **2016**, 26, 1678.
- [2] W. Honda, S. Harada, T. Arie, S. Akita, K. Takei, *Adv. Funct. Mater.* **2014**, 24, 3299.
- [3] X. Liao, Q. Liao, X. Yan, Q. Liang, H. Si, M. Li, H. Wu, S. Cao, Y. Zhang, *Adv. Funct. Mater.* **2015**, 25, 2395.
- [4] T. Q. Trung, S. Ramasundaram, B. U. Hwang, N. E. Lee, *Adv. Mater.* **2015**, 28, 502.
- [5] W. Gao, S. Emaminejad, H. Y. Y. Nyein, S. Challa, K. Chen, A. Peck, H. M. Fahad, H. Ota, H. Shiraki, D. Kiriya, D.-H. Lien, G. A. Brooks, R. W. Davis, A. Javey, *Nature* **2016**, 529, 509.
- [6] D. Son, J. Lee, S. Qiao, R. Ghaffari, J. Kim, J. E. Lee, C. Song, S. J. Kim, D. J. Lee, S. W. Jun, S. Yang, M.

- Park, J. Shin, K. Do, M. Lee, K. Kang, C. S. Hwang, N. Lu, T. Hyeon, D.-H. Kim, *Nat. Nanotechnol.* **2014**, *9*, 397.
- [7] J. A. Rogers, T. Someya, Y. Huang, *Science*. **2010**, *327*, 1603.
- [8] D. Y. Khang, H. Jiang, Y. Huang, J. A. Rogers, *Science*. **2006**, *311*, 208.
- [9] J. Cai, K. Cizek, B. Long, K. McAferty, C. G. Campbell, D. R. Allee, B. D. Vogt, J. La Belle, J. Wang, *Sensors Actuators, B Chem.* **2009**, *137*, 379.
- [10] A. J. Bandodkar, R. Nuñez-Flores, W. Jia, J. Wang, *Adv. Mater.* **2015**, *27*, 3060.
- [11] N. Matsuhisa, M. Kaltenbrunner, T. Yokota, H. Jinno, K. Kuribara, T. Sekitani, T. Someya, *Nat. Commun.* **2015**, *6*, 7461.
- [12] M. Parrilla, R. Cánovas, I. Jeerapan, F. J. Andrade, J. Wang, **2016**, *5* (9), 996.
- [13] A. J. Bandodkar, J. Wang, *Trends Biotechnol.* **2014**, *32*, 363.
- [14] W. Zeng, L. Shu, Q. Li, S. Chen, F. Wang, X. M. Tao, *Adv. Mater.* **2014**, *26*, 5310.
- [15] D. J. Lipomi, Z. Bao, *Energy Environ. Sci.* **2011**, *4*, 3314.
- [16] H. J. Chung, M. S. Sulkin, J. S. Kim, C. Goudeseune, H. Y. Chao, J. W. Song, S. Y. Yang, Y. Y. Hsu, R. Ghaffari, I. R. Efimov, J. A. Rogers, *Adv. Healthc. Mater.* **2014**, *3*, 59.
- [17] D. H. Kim, N. Lu, R. Ghaffari, Y. S. Kim, S. P. Lee, L. Xu, J. Wu, R. H. Kim, J. Song, Z. Liu, J. Viventi, B. de Graff, B. Elolampi, M. Mansour, M. J. Slepian, S. Hwang, J. D. Moss, S.-M. Won, Y. Huang, B. Litt, J. A. Rogers, *Nat. Mater.* **2011**, *10*, 316.
- [18] N. Reuge, F. M. Schmidt, Y. Le Maout, M. Rachik, F. Abbé, *Polym. Eng. Sci.* **2001**, *41*, 522.
- [19] A. Patil, A. Dasgupta, *Eur. J. Mech. A/Solids* **2013**, *41*, 28.
- [20] M. De Beule, P. Mortier, S. G. Carlier, B. Verheghe, R. Van Impe, P. Verdonck, *J. Biomech.* **2008**, *41*, 383.
- [21] H. Takuda, K. Mori, N. Takakura, K. Yamaguchi, *Int. J. Mech. Sci.* **2000**, *42*, 785.
- [22] L. J. Hart-Smith, J. D. C. Crisp, *Int. J. Eng. Sci.* **1967**, *5*, 1.
- [23] J. E. Adkins, R. S. Rivlin, *Philos. Trans. R. Soc. A Math. Phys. Eng. Sci.* **1952**, *244*, 505.
- [24] F. Gervaso, C. Capelli, L. Petrini, S. Lattanzio, L. Di Virgilio, F. Migliavacca, *J. Biomech.* **2008**, *41*, 1206.
- [25] F. Ju, Z. Xia, K. Sasaki, *J. Mech. Behav. Biomed. Mater.* **2008**, *1*, 86.
- [26] J. Yinon, *TrAC - Trends Anal. Chem.* **2002**, *21*, 292.
- [27] J. Wang, F. Lu, D. MacDonald, J. Lu, M. E. S. Ozsoz, K. R. Rogers, *Talanta* **1998**, *46*, 1405.
- [28] J. Wang, *Electroanalysis* **2007**, *19*, 415.
- [29] R. Yan, F. Zhao, J. Li, F. Xiao, S. Fan, B. Zeng, *Electrochim. Acta* **2007**, *52*, 7425.
- [30] M. K. Shin, J. Oh, M. Lima, M. E. Kozlov, S. J. Kim, R. H. Baughman, *Adv. Mater.* **2010**, *22*, 2663.
- [31] A. J. Bandodkar, I. Jeerapan, J.-M. You, R. Nuñez-Flores, J. Wang, *Nano Lett.* **2015**, *16*, 721.
- [32] J. A. Rogers, *Mrs Bull.* **2014**, *39*, 549.



- [33] N. G. Sahoo, Y. C. Jung, H. J. Yoo, J. W. Cho, *Macromol. Chem. Phys.* **2006**, *207*, 1773.
- [34] M. N. Charalambides, L. Wanigasooriya, G. J. Williams, S. Chakrabarti, *Rheol. Acta* **2002**, *41*, 532.
- [35] N. Reuge, F. M. Schmidt, M. Rachik, *Engineering* **2001**, *41*, 532.
- [36] Z. Spitalsky, D. Tasis, K. Papagelis, C. Galiotis, *Prog. Polym. Sci.* **2010**, *35*, 357.
- [37] N. G. Sahoo, S. Rana, J. W. Cho, L. Li, S. H. Chan, *Prog. Polym. Sci.* **2010**, *35*, 837.
- [38] R. Carta, P. Jourand, B. Hermans, J. Thone, D. Brosteaux, T. Vervust, F. Bossuyt, F. Axisa, J. Vanfleteren, R. Puers, *Sensors Actuators, A Phys.* **2009**, *156*, 79.
- [39] K. Cizek, C. Prior, C. Thammakhet, M. Galik, K. Linker, R. Tsui, A. Cagan, J. Wake, J. La Belle, J. Wang, *Anal. Chim. Acta* **2010**, *661*, 117.
- [40] M. C. Chuang, J. R. Windmiller, P. Santhosh, G. V. Ramírez, M. Galik, T. Y. Chou, J. Wang, *Electroanalysis* **2010**, *22*, 2511.
- [41] J. Benedet, D. Lu, K. Cizek, J. La Belle, J. Wang, *Anal. Bioanal. Chem.* **2009**, *395*, 371.
- [42] J. Wang, S. B. Hocevar, B. Ogorevc, *Electrochem. commun.* **2004**, *6*, 176.
- [43] M. Armand, F. Endres, D. R. MacFarlane, H. Ohno, B. Scrosati, *Nat. Mater.* **2009**, *8*, 621.
- [44] J. Le Bideau, L. Viau, A. Vioux, *Chem. Soc. Rev.* **2011**, *40*, 907.

# ENHANCED POTENTIOMETRIC DETECTION OF HYDROGEN PEROXIDE USING A PLATINUM ELECTRODE COATED WITH NAFION



UNIVERSITAT ROVIRA I VIRGILI

TAILOR-MADE CHEMICAL SENSING PLATFORMS FOR DECENTRALIZED HEALTHCARE AND WELLBEING

Rocío Cánovas Martínez

This second section (from chapters 6 to 9), presents the fabrication of enzymatic sensors using potentiometric detection. Therefore, these chapters describe the foundations of the mechanism of response of these sensors as well as the development of affordable platforms to challenge the current paradigm of point of care devices.

This chapter introduces the first level of a complex system developed along this thesis. This chapter together with the following two show a new way to develop potentiometric biosensors with enhanced analytical features. The potentiometric sensor presented here opens up new forms to think about the potentiometric detection mechanism and the way how the different elements that are involved in interact between each other to produce an enhanced potentiometric response.

The potentiometric response to hydrogen peroxide of a platinum electrode coated with a layer of Nafion® is presented. The results show that the Nafion ion-exchange membrane acts as an effective permselective barrier against negative ions, thus significantly reducing the response to some redox active species, such as ascorbate (one of the main interference in electrochemical sensors). Preliminary studies suggest that the coupling between the redox kinetics at the electrode in the form of a mixed potential and the Donnan potential of the membrane play a role on this enhancement. This combination of potentials would further explain the complexity of the system as well as the sensitivity values associated with calibrations. Considering this improved sensitivity, stability and linear ranges, this system is promising as a platform to build enzyme-based potentiometric biosensors.

## 6.1. INTRODUCTION

The working principle of a large number of chemical and biochemical sensors is based on the use of an enzymatic reaction that generates hydrogen peroxide ( $\text{H}_2\text{O}_2$ ), a substance that is then detected using a suitable analytical technique.<sup>[1-5]</sup> Therefore, finding alternative methods for the sensitive and selective detection of  $\text{H}_2\text{O}_2$  may have significant impact in all those fields such as clinical diagnostics,<sup>[6]</sup> food<sup>[7]</sup> and environmental analysis,<sup>[8]</sup> etc. where these biosensors play a central role.

Among the many different alternatives, the detection of  $\text{H}_2\text{O}_2$  using electrochemical techniques is particularly attractive since it allows the integration of the enzyme-electrode system into a simple and compact arrangement. Voltammetric techniques have been traditionally preferred because they provide high sensitivity and low limits of detection. As a result, bioanalytical platforms<sup>[9,10]</sup> using enzyme-based amperometric sensors have become almost the norm, and because of this success the development of alternative solutions has been somehow hindered.<sup>[11,12]</sup> Nevertheless, with the growing interest on devices for point of

care and decentralized measurements, new platforms that can offer additional advantages such as simplicity of operation and cost are increasingly required.<sup>[13,14]</sup> For this reason, potentiometric detection is re-gaining momentum. Potentiometry shows unrivalled simplicity of operation and instrumentation, low power consumption, easy of miniaturization and (with the recent trends, such as paper-based devices<sup>[15]</sup>) ability to produce ultra-low-cost sensors.<sup>[16]</sup> Therefore, in many applications where extremely low limits of detection might not be a main issue, potentiometric tools may offer a simple and affordable alternative.<sup>[17]</sup>

A major limitation for the electrochemical detection of  $\text{H}_2\text{O}_2$  is the interference produced by other redox-active species, such as ascorbic acid,<sup>[18,19]</sup> often present in biological media. To deal with this problem, the use of polyelectrolytes as permselective membranes has been successfully applied.<sup>[20]</sup> A negatively charged sulfonated tetra-fluoroethylene-based polymer called Nafion has been used as an effective barrier against electrode fouling and the interference produced by large negative ions.<sup>[21–23]</sup> Amperometric electrodes that are coated with this polymer have shown an improved stability and selectivity towards negatively charged redox species, such as ascorbate.<sup>[24,25]</sup> In the case of potentiometric methods, the direct detection of  $\text{H}_2\text{O}_2$  can be easily performed using a platinum electrode. However, it is evident that this approach is also heavily interfered by the presence of redox active species.<sup>[26]</sup> Interestingly, to the best of our knowledge, the use of permselective membranes (such as Nafion) to coat platinum (Pt) electrodes for the potentiometric detection of  $\text{H}_2\text{O}_2$  has not been yet reported.

It is worth noticing that the nature of the potentiometric response between  $\text{H}_2\text{O}_2$  and bare Pt electrodes is not yet fully understood and has been the subject of many recent studies.<sup>[27–29]</sup> It has been shown that the  $\text{H}_2\text{O}_2$ -Pt system presents a non-Nernstian response, with the slopes that vary depending on the crystalline structure of the Pt, the surface of the electrode and its interaction with the solution pH and composition, as well as the several reactions involved in the decomposition of  $\text{H}_2\text{O}_2$ . Additionally, the use of polyelectrolytes for coating the electrodes adds complexity to the system. The electrochemical response of electrodes coated with polymer films, and in particular with Nafion, has been reported several decades ago.<sup>[30,31]</sup> As a polyelectrolyte with ion-exchanging capabilities, Nafion membranes generate a Donnan potential at the solution interface. Naegeli *et al.* have demonstrated that magnitude of this potential is coupled to the different equilibriums (acid-base, redox) and the electrolyte composition of the solution.<sup>[32]</sup> All in all, the potentiometric response of a Nafion-coated Pt electrode to the addition of  $\text{H}_2\text{O}_2$  is complex and cannot be easily predicted.

In this chapter, the potentiometric response to the addition of  $\text{H}_2\text{O}_2$  of Pt electrodes coated with Nafion is studied. The results show that the Nafion not only prevents the interfering effect of negatively charged redox anions such as ascorbate, but that it also produces a significant enhancement of the potentiometric response that depends on the ionic strength of the solution. The data suggest that this enhancement could be connected to: (i) an additional effect resulting from the Donnan potential generated by the polyelectrolyte coating of the electrode, and (ii) an additional mixed potential due to the alterations of the (redox) balances in the Pt surface. It is also shown that these enhanced sensitivity and selectivity show promise for the development of enzyme-based potentiometric biosensors.

## 6.2. EXPERIMENTAL

### 6.2.1. Reagents and Solutions

Initial measurements were performed in a 0.1 M phosphate buffer solution (PBS) at pH 7. Acetate, phosphate and borate buffer 0.1 M were used for the experiments involving the change of pH. Fresh solutions of hydrogen peroxide ( $\text{H}_2\text{O}_2$ ) were prepared daily. All measurements carried out with PBS containing 0.135 M of NaCl.

### 6.2.2. Materials

A 99.95 % purity Platinum wire of 1mm diameter, (Goodfellow Cambridge Limited, England) was inserted into a Teflon® (polytetrafluoroethylene, PTFE) body to make a flat-disc electrode. The electrodes were polished with 1  $\mu\text{m}$  and 0.3  $\mu\text{m}$  alumina and then thoroughly rinsed with double-distilled water. After that, three steps of 10 minutes bath sonication with acetone, then ethanol and finally with double-distilled water were performed. Thereafter, an electrochemical cleaning step was performed. The electrodes were immersed for 2 min in 0.5 M  $\text{H}_2\text{SO}_4$  solution at a potential of +1.96 V vs. a single junction Ag/AgCl in 3 M KCl reference electrode (type 6.0733.100, Metrohm AG). This process should eliminate organic residues and also anodically dissolves trace metals.<sup>[33]</sup> Finally, electrodes were rinsed with double-distilled water and dried at room temperature. The coating with Nafion was performed by drop casting 10  $\mu\text{L}$  of Nafion solution on top of the platinum electrode. This electrode was left drying overnight at room temperature.

For the enzyme-based potentiometric electrode, a similar construction was applied. After the first Nafion layer, a 10  $\mu\text{L}$  drop (100 mg  $\text{mL}^{-1}$  glucose oxidase solution - GOx) was cast onto the Pt electrode and let it dry at 4°C 24h. Subsequently, a second 10  $\mu\text{L}$  Nafion layer was again drop cast. The enzymatic electrode was left drying overnight at 4°C and keep at the same temperature when not in use.

### 6.2.3. Electrochemical Measurements

Electromotive force measurements (EMF) were performed at room temperature (25 °C) in well stirred solutions using a high input impedance ( $10^{15} \Omega$ ). The experiments were performed in a 20 mL beaker.

Cyclic voltammetry (CV) and electrochemical impedance spectroscopy (EIS) were performed by using an electrochemical analyzer/workstation. The measurements were taken in a solution of 0.1 M KCl at room temperature (25°C). For cyclic voltammetry (CV) experiments, a potassium hexacyanoferrate (III) and potassium hexacyanoferrate (II) ( $\text{Fe}(\text{CN})_6^{3-/4-}$ ) solution (5 mM  $\text{Fe}(\text{CN})_6^{3-/4-}$  and 100 mM NaCl as a supporting electrolyte) was used as redox couple. The working electrode was cycled from 0.4 V to -0.2 V at  $50 \text{ mV}\cdot\text{s}^{-1}$ . Both experiments were performed at room temperature (25°C).

## 6.3. RESULTS AND DISCUSSION

### 6.3.1. Potentiometric detection enhancement

Figure 6.1A shows the typical potentiometric response obtained for a bare and for a Nafion-coated Pt electrode upon the addition of  $\text{H}_2\text{O}_2$  in 0.1 M PBS at pH 7. For the bare electrodes a decrease of the potential as the concentration of  $\text{H}_2\text{O}_2$  increases is observed. In general, this is in agreement with results already reported.<sup>[34–35]</sup> It is true that some works have reported a positive potentiometric signal for  $\text{H}_2\text{O}_2$ .<sup>[36]</sup> Evidently, the type of response depends on the redox couple involved. Zheng *et al.* study uses  $\text{MnO}_2$  microparticles as sensing agents promoting the reduction of  $\text{H}_2\text{O}_2$ . The Pt electrode is sensing the changes on the redox potential of the solution produced by the addition of peroxide. The expected redox half-reaction of  $\text{H}_2\text{O}_2$  on the Pt surface can be expressed as:



and the half-cell potential ( $E$ ) can be calculated according to the Nernst equation for this reaction (at 298 K):

$$E = E^0 - \frac{0.059}{2} \log \frac{[\text{H}_2\text{O}_2]}{p\text{O}_2[\text{H}^+]^2} \quad (\text{Equation 6.2})$$

where the brackets represent the activities of the species,  $p\text{O}_2$  is the partial pressure of oxygen, and  $E^0$  ( $\text{O}_2/\text{H}_2\text{O}_2$ ) is the standard potential for this reaction (0.695V). This equation predicts a linear decrease of the potential with the increase of the logarithm of the activity of peroxide (at a constant pH), as it is observed in Figure 6.1. The expected slope should be around 0.028V/decade. However, because of the many factors affecting the electrochemical behaviour of peroxide on Pt surfaces,<sup>[27,28]</sup> this equation is of limited use in quantitative terms.

In fact, different values for this slope have been reported depending on the surface of Pt, crystalline structure, etc.

The first experimental evidence that shows the difference between bare and Nafion-coated electrodes is the initial potential (i.e., the potential before the addition of peroxide). Electrodes coated with Nafion show a significantly higher initial potential when compared to the bare Pt electrodes. These differences could be attributed to the accumulation of charges at the Nafion-solution interface. Nafion has significant proton-exchange capabilities<sup>[37,38]</sup> due to the negatively charged sulfonate groups. Thus, a Donnan potential can be generated by the incorporation of cations from the solution.<sup>[32]</sup>

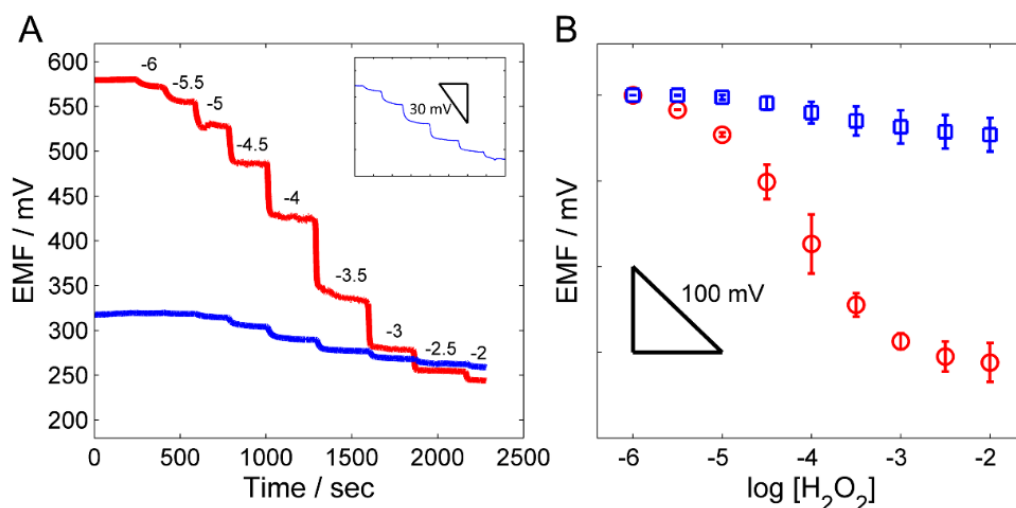


**Figure 6.1.** Potentiometric response curves. (A) Time-trace for bare (blue line) and Nafion-coated (red line) platinum electrode in PBS pH 7 at 25°C (mean  $\pm$  S.D., N=2). Inset shows a magnification of the calibration curve for bare platinum electrode. (B) Corresponding calibration plots for bare (blue,  $\square$ ) and coated (red,  $\circ$ ) electrodes. Initial potentials have been subtracted to better illustrate the differences between the two systems. Error bars correspond to the standard deviation (N=2).

Interestingly, these electrodes coated with Nafion show also a decrease on the potential with the addition of  $\text{H}_2\text{O}_2$ , but the magnitude of the change observed is much more pronounced. First, it has been shown that Nafion forms bi-continuous nanostructures<sup>[39]</sup> that allows the transport of small and neutral molecules. Previous studies have shown the permeability of this material to  $\text{H}_2\text{O}_2$ .<sup>[40]</sup> Therefore, it is not surprising that peroxide reaches the surface of the Pt electrode and produces a redox response. What is more interesting, however, is that this response is somehow modulated by the presence of Nafion. Figure 6.1B compares the response as a function of the logarithm of the concentration of  $\text{H}_2\text{O}_2$  for both electrodes, and regression parameters from these plots are presented in Table 6.1.



**Table 6.1.** Comparison of analytical figures of merit for the determination of  $\text{H}_2\text{O}_2$  with the two types of electrodes in 0.1 M PBS buffer (pH=7).

Parameters	Bare Pt	Nafion-coated Pt
Sensitivity ( $\text{mV decade}^{-1}$ )	$-18.5 \pm 7.9$	$-125.1 \pm 5.9$
Linear Range (M)	$10^{-4.5}$ to $10^{-3}$	$10^{-5}$ to $10^{-3}$
LOD (M)	$10^{-5.1}$	$10^{-5.4}$

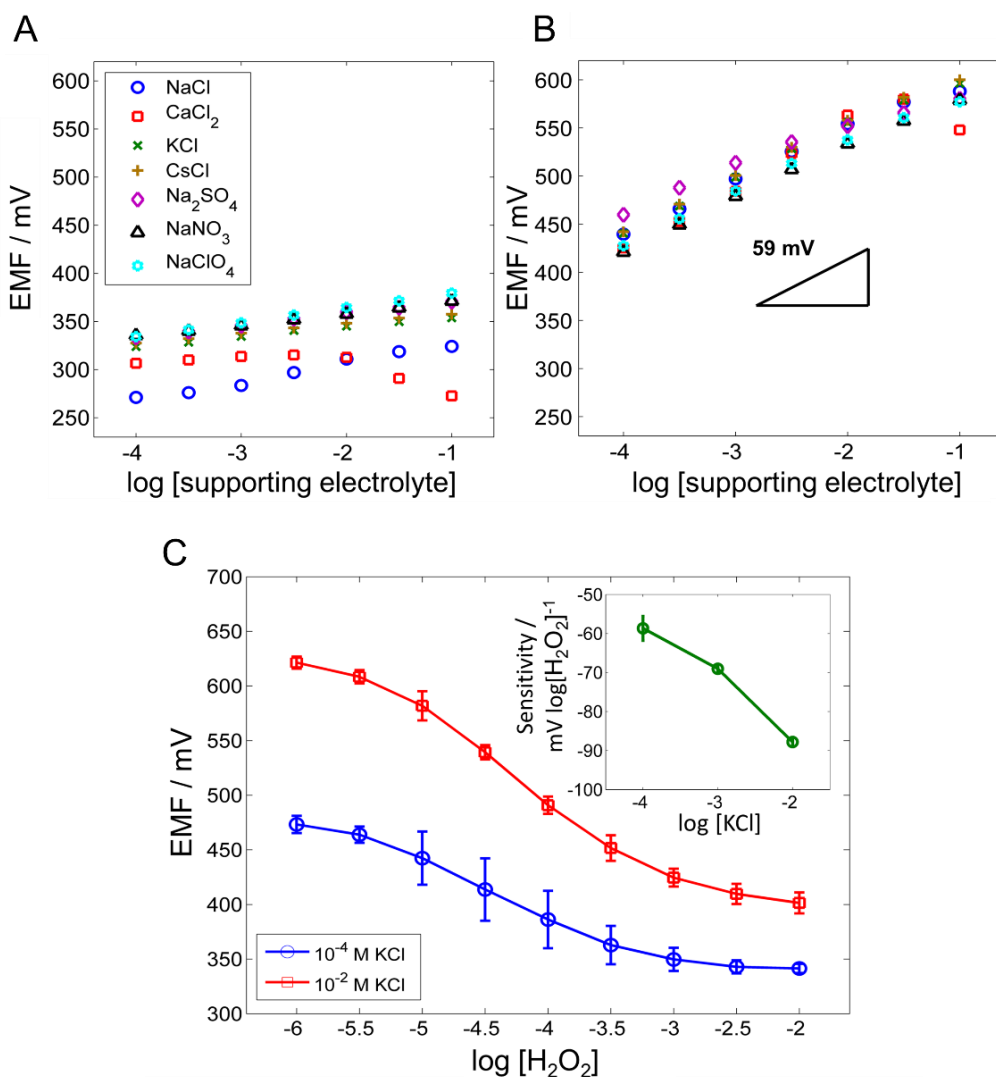


**Figure 6.2.** Comparison of the initial potential as a function of the total electrolyte concentration for (A) bare and (B) Nafion-coated platinum electrodes upon increasing concentration of different supporting electrolytes at 25°C. (C) Comparison of the  $\text{H}_2\text{O}_2$  calibration curves using coated electrodes at different concentrations of supporting electrolyte (KCl):  $10^{-2}$  M ( $\square$ ) and  $10^{-4}$  M ( $\circ$ ) (mean  $\pm$  S.D., N = 2). Inset displays  $\text{H}_2\text{O}_2$  sensitivity versus supporting electrolyte (KCl) concentration.

Since both, coated and uncoated electrodes reach a similar potential at higher concentration of peroxide, the improvement in sensitivity observed can be ascribed to the higher initial potential displayed by the Nafion-coated electrodes, which is in direct relationship with the Donnan potential originated at the Nafion-solution interface as it has been suggested.

To further explore this point, the dependence of this initial potential on the total concentration of the supporting electrolyte for bare (Figure 6.2A) and coated electrodes (Figure 6.2B) was evaluated. The results show a limited response for the bare Pt electrodes, while a marked linear increase with an almost Nernstian dependence is observed when the electrodes are coated with Nafion. This type of response has been already reported for analogous systems and strongly supports the idea of the Donnan contribution in the initial potential of the coated electrodes.<sup>[38]</sup>

For this reason, calibration plots for peroxide at different electrolyte concentrations were also performed and the results are displayed in Figure 6.2C. As the electrolyte concentration in the solution decreases, the slope also decreases and approaches that of bare Pt electrodes. In essence, the sensitivity to peroxide of the electrodes coated with Nafion is dependent on the total concentration of electrolyte. It is also worth noticing that the increase of the concentration of electrolyte improves the reproducibility of the response between electrodes.

The influence of pH on this phenomenon has been also evaluated. Figure 6.3 shows the response of bare (Figure 6.3A) and coated electrodes (Figure 6.3B) to the addition of  $\text{H}_2\text{O}_2$  in a range of pH from 4 to 9. It is worth mentioning that the sensitivity for  $\text{H}_2\text{O}_2$  on bare electrodes increases considerably as the pH increases. It has been suggested that this is in part due to a decrease on the stability of  $\text{H}_2\text{O}_2$  at neutral and basic pH.<sup>[41]</sup> At the higher concentrations, the bare Pt electrodes yield an almost Nernstian dependence with the pH, as predicted by Equation 6.1. The coated electrodes, on the other hand, show also a range with a linear dependence with pH (for a given  $\text{H}_2\text{O}_2$  concentration) but with slopes that are higher than the expected Nernstian value. These results, however, are hard to interpret. First, the changes in pH also imply a change in the total ionic concentration, which modulates the response of the electrode. Second, the changes in the pH of the bulk solution do not imply similar changes on the pH at the interface or at the bulk of the membrane. In other words, the modulation of the pH at the interface induced by the Donnan potential may have a significant effect on the redox response of the electrode. From the plots of Figure 6.3B it is evident that Nafion-coated electrodes display an enhanced sensitivity at all pH values. Nevertheless, the relative enhancement is more pronounced as the pH increases. As the sensitivity increases, the linear

range is shifted towards lower concentrations, which results in an improvement of the limits of detection for H<sub>2</sub>O<sub>2</sub> at higher pH.

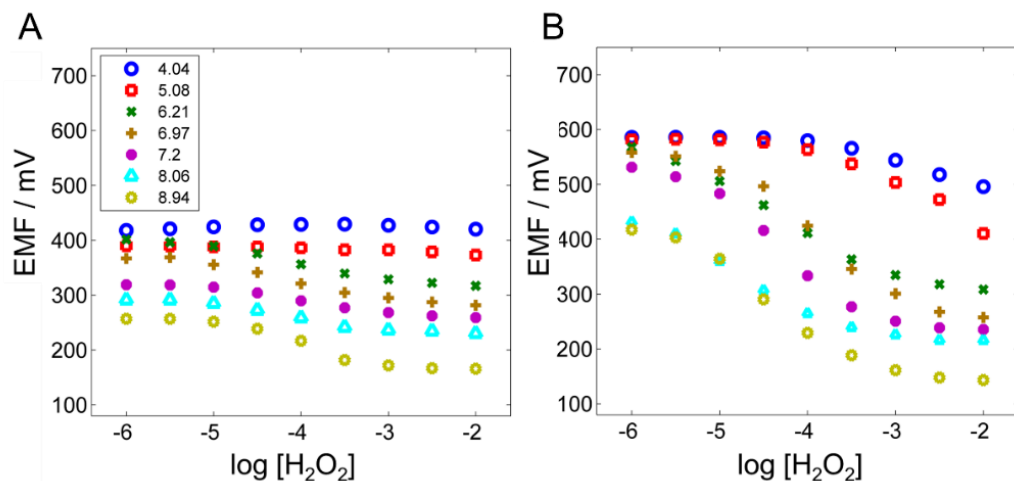


**Figure 6.3.** Calibration plots at several pH for (A) bare and (B) Nafion-coated electrodes in 0.1 M buffers of different pH at 25°C.

As it was mentioned before, there are many factors that make difficult to elaborate an accurate description of the mechanism involved in the phenomena observed. First, the reactivity of H<sub>2</sub>O<sub>2</sub> on Pt is complex and highly dependent on the experimental conditions.<sup>[42,43]</sup> It should be pointed out that the Nernstian description of the response is simplifying the problem, since a mixed potential mechanism must be considered instead.<sup>[44,45]</sup> The reactivity of platinum is determined by its complex electronic structure, which favours the anchoring of species, particularly oxygenated compounds, on its surface. When the oxygen is anchored to the surface of the platinum the surface changes, thus changing the potential and the way in which the hydrogen peroxide can interact with it. Different reactions involving redox processes of hydrogen peroxide or oxygen may occur in parallel on the metal surface (see Equation 6.3 and 6.4). This mixed potential that sets the resting potential of the electrode brings a significant level of complexity to this system:



Under this perspective, the reactions involving the oxidation of hydrogen peroxide and the reduction of water must be considered. These mixed potential systems, deeply studied in

corrosion mechanisms, would produce a non-Nernstian response typically obtained using Pt electrodes.

A second layer of complexity of the system is added when considering the Nafion membrane, which has general affinity for cations with higher selectivity for protons. In fact, the direct interactions of the sulfonate groups of Nafion could be with protons, sodium ion ( $\text{Na}^+$ ) and others cations. That could explain why at the beginning of the calibration some fluctuations in the signal -first decreasing and then increasing- are commonly observed during the calibration curves performed in this thesis. This phenomenon might be produced due to a rehydration of Nafion after the immersion in high concentrated buffered saline solution of the dried Nafion membrane previously deposited by drop casting (in solution). The experimental evidence of this characteristic is exhibited in Figure 6.4. The fluctuations observed suggest a relationship between fluctuations and sodium/proton distribution/equilibration. The decreasing part of the wave could correspond with the negatively charge Nafion membrane at the beginning of the hydration process where protons diffuse to the outside of the membrane (neutral pH). Rapidly, there is a subsequent diffusion of sodium ions into the membrane. Then, the membrane is hydrated -swelling of water- and the presence of positively charges should be equilibrated, therefore the potential becomes more positive. Finally, the membrane is hydrated and the signal stabilizes thus allowing the performance of the calibration.

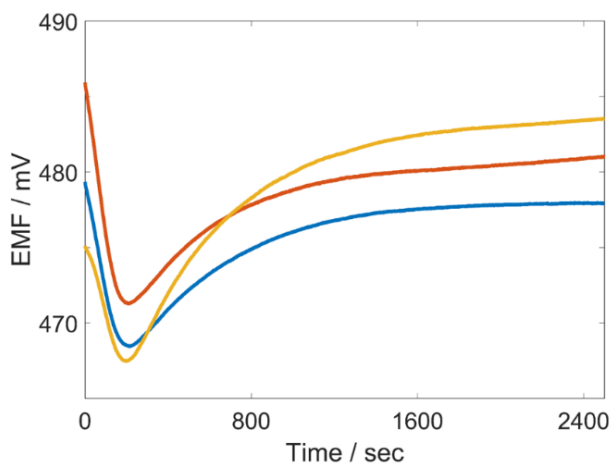


**Figure 6.4.** Time trace showing the initial stabilization of the signal of the Nafion coated electrodes previous to a calibration curve.

Many properties of Nafion are still under study.<sup>[37,46,47]</sup> The Nafion membrane can cause changes at different levels such as: the concentration or diffusion of oxygen, the pH of the system which will be different in the membrane than in the bulk (because of the hydrophobic

and hydrophilic phases of Nafion and the interface), the relationship between electrostatic interactions and the activity of the different components involved in the reactions (i.e., the activity of water will be different inside and outside the membrane). It should be also stressed that when Nafion hydrates, water performs as a membrane plasticizer, modifying the rheological and chemical properties of the system. There are too many considerations at entropic and enthalpic levels that must be taken into account.

Third, the combination of all the systems (i.e., redox-sensitive electrodes coated with polyelectrolytes) adds another level of complexity, since it has been reported that in this type of systems the chemical equilibrium in solution (redox, acid-base) is strongly coupled with the ion-exchange properties of the membrane. Last, but not least, reactions between Nafion and  $\text{H}_2\text{O}_2$  could also occur and they might play a role on these results. This last point, however, is less likely, since the electrodes can be washed and re-used, obtaining reproducible results. All in all, a detailed study of the mechanism of generation of the potential in this system falls well beyond the scope of this work, and only some general observations can be elaborated.

Regarding the role of the Nafion membrane, it is important to remark that the coated electrodes are stabilized in a solution with high ionic strength (in general 0.1 M NaCl, unless stated otherwise) in neutral to slightly basic pH. Under these conditions, the membrane incorporates cations from the solution (exchanging  $\text{H}^+$ ). This ion-exchange capacity of Nafion with singly charged electrolytes is well known.<sup>[32]</sup> The detection of  $\text{H}_2\text{O}_2$  is performed after this stabilization has taken place. Beyond the permselective behaviour, the response obtained with the coated electrodes seems to be an enhanced form of the response obtained with the bare electrodes. Thus, it could be assumed that the same underlying mechanism operates in both cases, (i.e., the reaction between Pt and  $\text{H}_2\text{O}_2$ ), but that some amplification factor operates when Nafion membranes are present. From the previous evidence (see Figure 6.2B), this amplification is related to the Donnan potential as a result of the ionic concentration of the solution.

The Nafion membrane is stabilized between two different interfaces: the Pt-membrane interface, from one side, where the membrane strongly interacts with the metal through the hydrophobic Nafion domains,<sup>[48]</sup> and the membrane-solution interface, from the other, where the ion-exchange process generates the Donnan potential. The gradient of electrochemical potential of the system Pt||membrane||solution is altered when  $\text{H}_2\text{O}_2$  reaches the surface of the Pt. First, at the metal-membrane interface the mixed potential reactions occur. As a result of this change, the difference on selectivity between protons and other cations and a rearrangement of the ionic species in the membrane and at the interface under the new

equilibrium conditions may occur. This may result in the amplification of the electrode response if changes in the internal pH of the membrane occur. Overall, the features of Nafion membrane and the mixed potential occurring at the platinum surface (oxidation and reduction of peroxide species) enable rearrangements on the acid/base equilibrium at the interface fostering an enhanced potentiometric response. The decrease in the protons concentration inside the membrane due to the coupling of redox reactions might produce the experimental enhancement on the system. This is, of course, a hypothesis that requires further testing.

Clearly, this is at this point speculation, and more work needs to be conducted to understand the conditions inside the membrane and the mechanisms involved. Figure 6.5 illustrates the proposed mechanism. Interestingly, there are many works devoted to the study of the interactions between platinum and  $H_2O_2$ , but there is not complete agreement on the mechanisms involved. Similarly, the recent works on the structure and properties of Nafion membranes reveal the lack of models to fully understand the behaviour of this material.

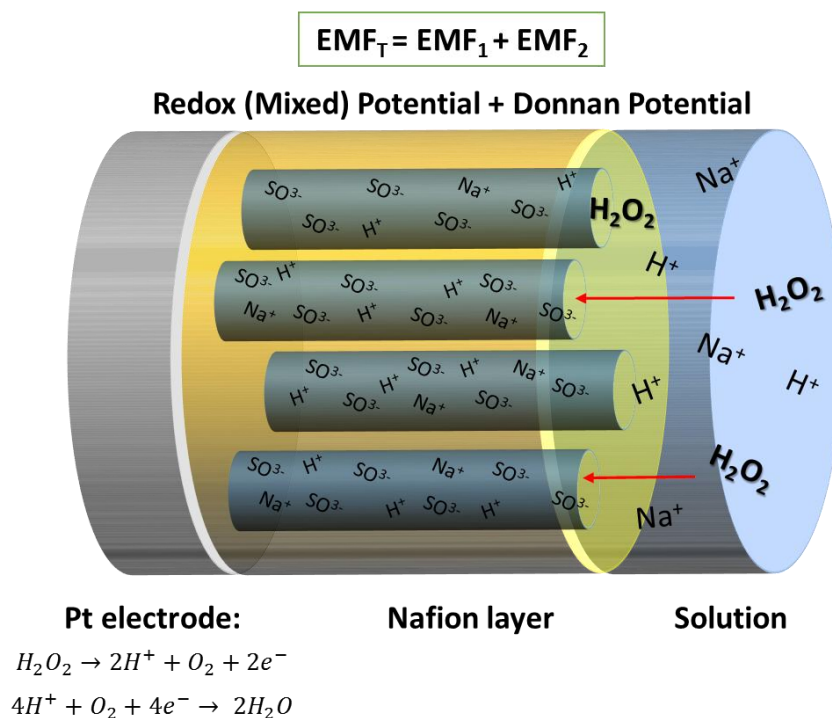


**Figure 6.5.** Schematics of Nafion-coated electrodes mechanism studied during this thesis. The electromotive force (EMF) measured should be the sum of the redox (mixed) and the Donnan potentials.

### 6.3.2. Nafion as a permselective membrane

In order to evaluate the electrochemical properties at the interface, electrochemical impedance experiments were carried out. The comparison of the impedance spectra between bare and Nafion-coated Pt electrodes (Figure 6.6) exhibits a typical capacitive mechanism for the coated electrode, with a single high-frequency semicircle related to the bulk resistance of the Nafion membrane. Nafion membranes exhibit the typical Nyquist plot for a circuit with a resistor and a capacitor in parallel. The Nyquist plot has been zoomed in to stress the differences between the two systems. This resistance is smaller than what is observed in other conventional polymeric membranes electrodes,<sup>[49]</sup> due to the electrical and structural characteristics of Nafion. Furthermore, Nafion membranes exhibit different selectivity coefficients to different counterions and more uniform exchange site environment than conventional sulfonate ion-exchange resins.<sup>[22,50]</sup> The perfluorosulfonate ionomer morphology was suggested to follow an oriented ionic nanochannels embedded within a locally aligned polymer matrix where sulfonate groups ( $-\text{SO}^3$ ) coated channels are invoked to account for intercluster ion hopping of positive charge species but rejection of negative ions.<sup>[40]</sup> However, there are several current models describing the Nafion morphology and membrane behaviour, and the evidence is not yet conclusive.<sup>[37]</sup> Figure 6.7A exhibits the rejection of negatively charge molecules thus performing a decrease in the oxidation and reduction peaks of the cyclic voltammogram. Besides, Figure 6.7B presents redox sensitivity for bare Pt electrode, as expected, and remains insensitive for Nafion-coated electrode.

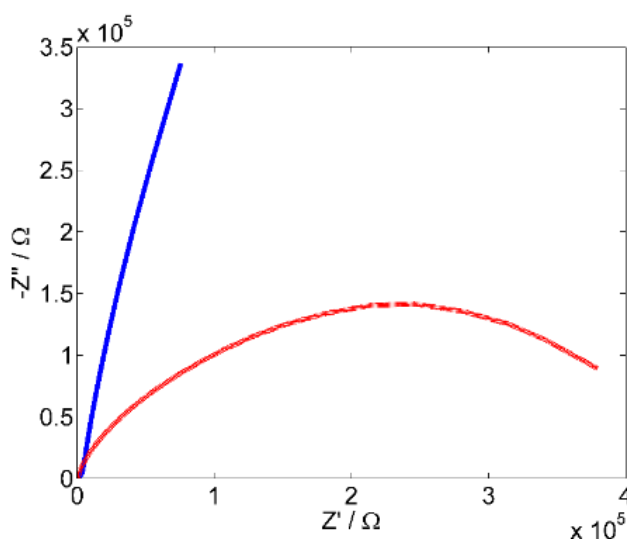


**Figure 6.6.** Electrochemical impedance spectroscopy results of bare (blue line) and Nafion-coated (red line) platinum electrode in 0.1 M KCl as a supporting electrolyte. The impedance spectra were recorded in the frequency range 100 kHz-10 mHz by using a constant direct current potential, (Edc) 0.2 V. The electrodes were studied using excitation amplitude of 10 mV at 25°C.

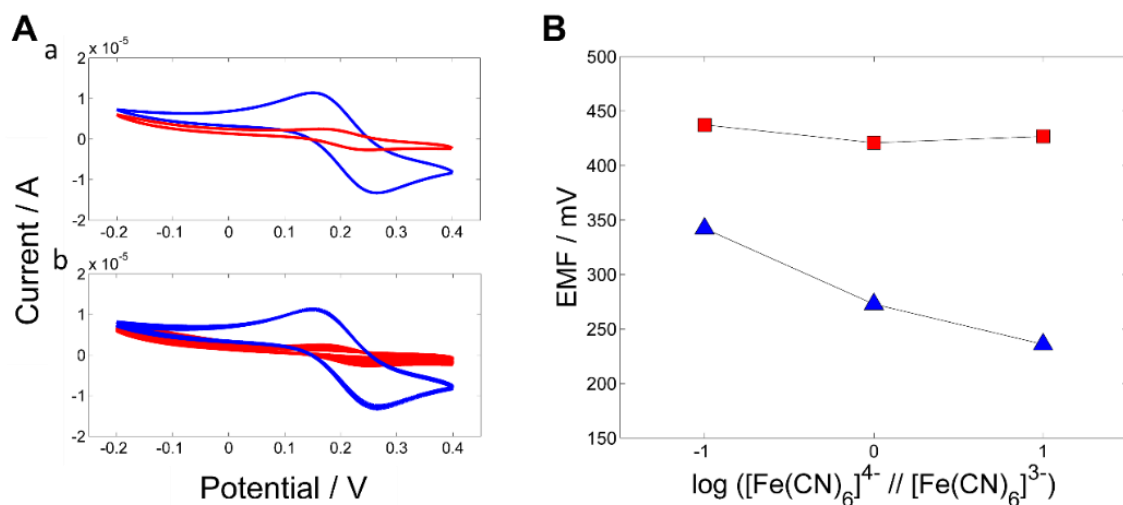


**Figure 6.7.** Cyclic voltammetry results. (Aa) Comparison between bare (blue line) and Nafion-coated (red line) electrodes and (Ab) comparison between bare (blue line) and Nafion-coated (red line) electrodes after 30 minutes in solution in 5 mM  $[\text{Fe}(\text{CN})_6]^{3-/4-}$  and 100 mM NaCl from -0.2 V to 0.4 V at  $50 \text{ mV}\cdot\text{s}^{-1}$ . Redox sensitivity assay. (B) Redox sensitivity of 1 mM  $[\text{Fe}(\text{CN})_6]^{4-} / [\text{Fe}(\text{CN})_6]^{3-}$  at different ratios (0.1, 1 and 10) for bare ( $\blacktriangle$ ) and Nafion-coated ( $\blacksquare$ ) platinum electrodes.

Even though mechanisms are still under debate, Nafion membranes have been extensively used in amperometric sensors as a permselective barrier against negatively charged redox species. Thus, the question remains on whether a similar effect could be used to improved potentiometric sensors. Figure 6.8A shows the results of the addition of ascorbic acid on the calibration plots for peroxide using coated and uncoated electrodes. Ascorbate is a reducing agent that is typically found as interference in biological fluids. Thus, when added to the solution at 100  $\mu\text{M}$  level (normal upper range of the biological fluids) the bare Pt electrode becomes almost insensitive to the addition of peroxide (Figure 6.8A). Indeed, upon the addition of ascorbic the bare Pt electrodes register a drop of the initial potential, which remains almost constant until a higher concentration of peroxide is reached. The coated electrodes, on the other hand, show a significantly different behaviour (Figure 6.8A). Interestingly, all the electrodes reach the same final value of potential, possibly due to the limiting sensitivity of the Pt electrode.

Table 6.2 compares the analytical parameters obtained for the coated electrodes before and after the addition of ascorbate. First, it can be seen that neither the sensitivity nor the limits of detection (LOD) show significant changes. The linear range shows a slight reduction, but it



does not seem to be severely affected. The most significant change that can be observed is a decrease on the initial potential when ascorbate is added (Figure 6.8A). Evidently, an optimization of the Nafion layer could reduce these effects, and the development of suitable working protocols may help to further enhance the applicability of this approach. It has been suggested, for example, that a thickness of the Nafion membrane could be modified to improve the permselectivity towards negatively charged molecules.<sup>[51]</sup> Clearly, further work is needed in order to optimize these aspects. However, as a preliminary conclusion, the results suggest that the interference of the potentiometric detection caused by negatively charged redox species can be overcome when using the Nafion coating.

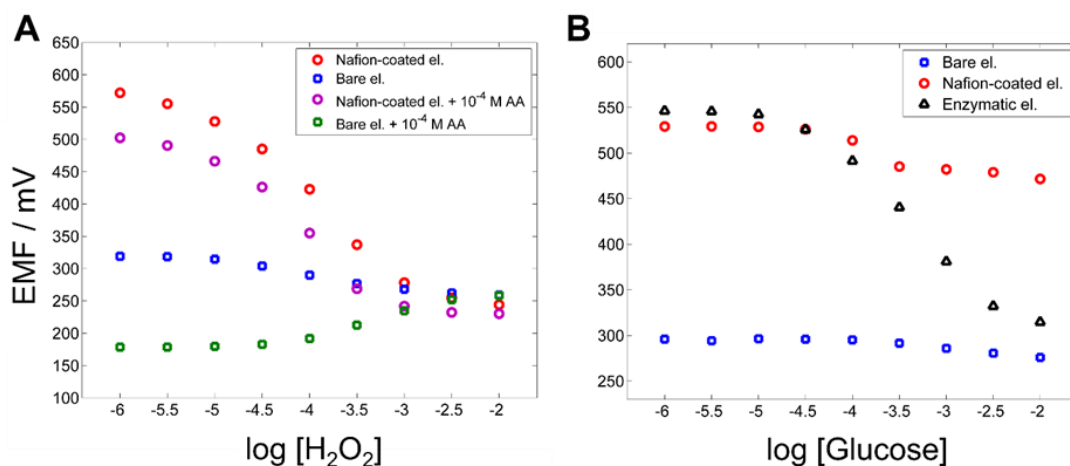


**Figure 6.8.** (A) Evaluation of the addition of ascorbic acid (AA) in the cell for bare and Nafion-coated electrodes in 0.1 M PBS pH 7.2 at 25°C. (B) Calibration curve for increasing glucose concentration over time for bare, Nafion-coated and Nafion-coated enzymatic electrodes in 0.1 M PBS pH 7.4 at 25°C.

**Table 6.2.** Comparison of analytical figures of merit for the determination of H<sub>2</sub>O<sub>2</sub> with Nafion coated electrodes before and after the addition of ascorbic acid in 0.1 M PBS.

Test	No Ascorbate	100 μM Ascorbate
Sensitivity (mV·decade <sup>-1</sup> )	-129.1	-132.3
Linear Range (M)	10 <sup>-5</sup> to 10 <sup>-3</sup>	10 <sup>-5</sup> to 10 <sup>-3.5</sup>
LOD (M)	10 <sup>-5.3</sup>	10 <sup>-5.4</sup>

The results shown so far are extremely relevant, since they present a way to alleviate two of the major limitations of the potentiometric detection of peroxide in biological fluids, namely: limited sensitivity and severe interference caused by redox species. Regarding the sensitivity, the Nafion provides a way to produce an enhancement due to the presence of electrolytes.

While it could be argued that this modulation of the sensitivity by electrolytes might be a problem for some applications, many biological fluids such as blood or serum have a high and constant concentration of ions. Therefore, this should be advantageous for the detection of peroxide. The problem of the interferences, which is also a major issue, can be also successfully overcome as it has been previously shown. The experimental results also show some other practical advantages of the use of Nafion, such as a better reproducibility between sensors and shorter stabilization times of the signal. It is well known that Pt surfaces can be easily contaminated, affecting the electrochemical response. Thus, Nafion might be acting as a barrier that limits this undesired effect.

There are significant implications of these findings in the field of biosensors. The oxidase enzymes, for example, that produce peroxide, could be used for the potentiometric detection of neutral molecules in a simple, sensitive and robust way. As a proof of concept, the enzyme glucose oxidase (GOx) was sandwiched between two layers of Nafion cast on a Pt electrode. The results of the addition of glucose to a bare Pt electrode, an electrode coated with Nafion, and an electrode coated with Nafion containing the GOx enzyme are presented in Figure 6.8B. As the concentration of glucose is increased, peroxide is generated by the enzymatic reaction and potentiometrically detected, as shown previously. The results exhibit a slope of approximately  $110 \text{ mV} \cdot \log[\text{glucose}]^{-1}$ , with a linear range between  $10^{-4} \text{ M}$  to  $10^{-2.5} \text{ M}$ . In the following chapters, further work was performed in this direction in an attempt to develop reliable potentiometric sensors based on enzymatic reactions.

## 6.4. CONCLUSIONS

This chapter demonstrates that permselective membranes such as Nafion can be used as an efficient enhancer for the sensitive and selective potentiometric detection of  $\text{H}_2\text{O}_2$ . The approach presented allows the detection of  $\text{H}_2\text{O}_2$  based on the mixed potential generated in the Pt surface, as well as through the additional contribution of a Donnan potential generated at the membrane-solution interface. Because of this, a modulation of the sensitivity based on the ionic strength and pH of the solution is possible. The maximum sensitivities are thus obtained in high ionic strength, which can be advantageous when dealing with biological fluids.

As a proof of principle, the direct application of this simple  $\text{H}_2\text{O}_2$  detection through the use of an enzymatic reaction is demonstrated. Thus, the proof of principle for the construction of a simple enzymatic electrode with an enhanced potentiometric response using Nafion permselective membranes is demonstrated for the first time. This device should provide significant advantages when facing the challenge of developing simple, low-cost decentralized platforms.

## 6.5. REFERENCES

- [1] J. Wang, *Electroanalysis* **2005**, *17* (2), 7.
- [2] D. T. V Anh, W. Olthuis, P. Bergveld, *Sens. Act. B Chem.* **2003**, *91* (1), 1.
- [3] Y. Xiao, H. X. Ju, H. Y. Chen, *Anal. Chim. Acta* **1999**, *391* (1), 73.
- [4] T. You, O. Niwa, M. Tomita, S. Hirono, *Anal. Chem.* **2003**, *75* (9), 2080.
- [5] S. Hrapovic, Y. Liu, K. B. Male, J. H. T. Luong, *Anal. Chem.* **2004**, *76* (4), 1083.
- [6] J. Wang, *Chem. Rev.* **2008**, *108* (2), 814.
- [7] M. I. Prodromidis, M. I. Karayannis, *Electroanalysis*. **2002**, *14* (4), 241.
- [8] R. Vargas-Bernal, E. Rodríguez-Miranda, G. Herrera-Pérez, *Pestic. Adv. Chem. Bot. Pestic.* **2012**, 329.
- [9] R. Ahmad, N. Tripathy, J. H. Kim, Y. B. Hahn, *Sens. Act. B Chem.* **2012**, *174*, 195.
- [10] T. Kong, Y. Chen, Y. Ye, K. Zhang, Z. Wang, X. Wang, *Sens. Act. B Chem.* **2009**, *138* (1), 344.
- [11] Z. Yang, C. Zhang, J. Zhang, W. Bai, *Biosens. Bioelectron.* **2014**, *51*, 268.
- [12] S. K. Shukla, S. R. Deshpande, S. K. Shukla, A. Tiwari, *Talanta* **2012**, *99*, 283.
- [13] J. Hu, S. Wang, L. Wang, F. Li, B. Pingguan-Murphy, T. J. Lu, F. Xu, *Biosens. Bioelectron.* **2014**, *54*, 585.
- [14] N. P. Pai, C. Vadnais, C. Denkinge, N. Engel, M. Pai, *PLoS Med.* **2012**, *9* (9), e1001306.
- [15] A. K. Yetisen, M. S. Akram, C. R. Lowe, *Lab Chip* **2013**, *13* (12), 2210.
- [16] M. Novell, M. Parrilla, G. A. Crespo, F. X. Rius, F. J. Andrade, *Anal. Chem.* **2012**, *84* (11), 4695.
- [17] M. Novell, T. Guinovart, P. Blondeau, F. X. Rius, F. J. Andrade, *Lab Chip.* **2014**, *14*, 1308.
- [18] F. Martinello, E. Luiz da Silva, *Clin. Chim. Acta* **2006**, *373* (1-2), 108.
- [19] J. Anzai, H. Takeshita, Y. Kobayashi, T. Osa, T. Hoshi, *Anal. Chem.* **1998**, *70* (4), 811.
- [20] A. Wynne, N. Finnerty, *Chemosensors* **2015**, *3* (2), 55.
- [21] R. Vaidya, P. Atanasov, E. Wilkins, *Med. Eng. Phys.* **1995**, *17* (6), 416.
- [22] M. Szentirmay, C. Martin, *Anal. Chem.* **1984**, *1902* (52), 1898.
- [23] Manowitz, P.; Stoecker, P. W.; Yacynych, A. M. *Biosens. Bioelectron.* **1995**, *10*, 359.
- [24] J. Wang, M. Musameh, Y. J. Lin, *Am. Chem. Soc.* **2003**, *125* (9), 2408.
- [25] S. Karra, M. Zhang, W. Gorski, *Anal. Chem.* **2013**, *85* (2), 1208.
- [26] S. B. Adeloju, A. N. Moline, *Biosens. Bioelectron.* **2001**, *16*, 133.
- [27] S. B. Hall, E. A. Khudaish, A. L. Hart, *Electrochim. Acta* **1997**, *43* (5-6), 579.
- [28] I. Katsounaros, W. B. Schneider, J. C. Meier, U. Benedikt, P.U. Biedermann, A. A. Auer, K. J. J. Mayrhofer, *Phys. Chem. Chem. Phys.* **2012**, *14*, 7384.
- [29] L. D. Burke, L. M. Hurley, *Electrochim. Acta* **1999**, *44*, 3451.

- [30] D. Dewulf, A. J. J. Bard, *Macromol. Sci. Part A - Chem.* **1989**, 26 (8), 1205.
- [31] D. R. J. Lawson, *Electrochem. Soc.* **1988**, 135 (9), 2247.
- [32] R. Naegeli, J. Redepenning, F. C. J. Anson, *Phys. Chem.* **1986**, 90, 6227.
- [33] E. L. Goldstein, M. R. Van de Mark, *Electrochim. Acta* **1982**, 27 (8), 1079.
- [34] J. Weiss, *Trans. Faraday Soc.* **1935**, 31, 1547.
- [35] J. F. Castner, L. B. Wingard, *Anal. Chem.* **1984**, 56 (14), 2891.
- [36] X. Zheng, Z. Guo, *Talanta* **2000**, 50, 1157.
- [37] K. A. Mauritz, R. B. Moore, *Chem. Rev.* **2004**, 104, 4535.
- [38] E. Grygolicz-Pawlak, G. A. Crespo, M. G. Afshar, G. Mistlberger, E. Bakker, *Anal. Chem.* **2013**, 85, 6208.
- [39] M. A. Hickner; H. Ghassemi; Y. S. Kim. *Chem. Rev.* **2004**, 104, 4587.
- [40] K. Schmidt-Rohr, Q. Chen, *Nat. Mater.* **2008**, 7 (1), 75.
- [41] R. J. Watts, M. K. Foget, S.-H. Kong, A. L. J. Teel, *Hazard. Mater.* **1999**, 69 (2), 229.
- [42] I. Katsounaros, W. B. Schneider, J. C. Meier, U. Benedikt, P. U. Biedermann, A. A. Auer, K. J. J. Mayrhofer, *Phys. Chem. Chem. Phys.* **2012**, 14, 7384.
- [43] R. J. Urbach, H.B. and Bowen, *Electrochem. Acta* **1969**, 14, 927.
- [44] S. J. Percival, A. J. Bard, *Anal. Chem.* **2017**, 89, 9843.
- [45] A. M. Gómez-marín, K. J. P. Schouten, M. T. M. Koper, J. M. Feliu, *Electrochem. Commun.* **2012**, 22, 153.
- [46] X. Kong, K. Schmidt-Rohr, *Polymer.* **2011**, 52, 1971.
- [47] O. Diat, G. Gebel, *Nat. Mater.* **2008**, 7, 13.
- [48] D. L. Wood, J. Chlistunoff, J. Majewski, R. L. J. Borup, *Am. Chem. Soc.* **2009**, 131, 18096.
- [49] G. A. Crespo, S. Macho, F. X. Rius, *Anal. Chem.* **2008**, 80, 1316.
- [50] H. L. Yeager, A. Steck, *Water Pollut. Control* **1979**, 51 (7), 862.
- [51] B. D. Bath, H. S. White, E. R. Scott, *Anal. Chem.* **2000**, 72 (3), 433.

UNIVERSITAT ROVIRA I VIRGILI

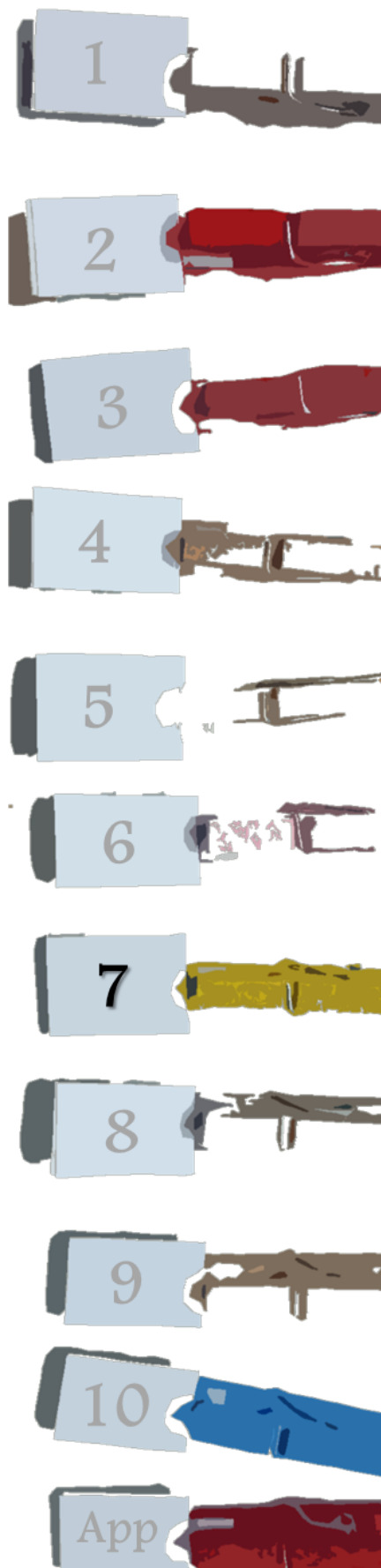
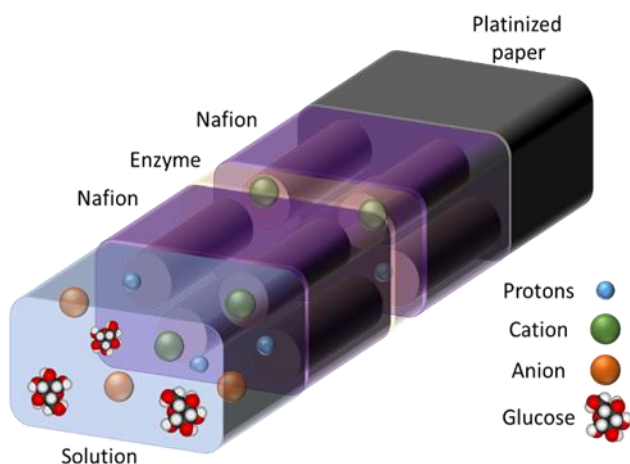
TAILOR-MADE CHEMICAL SENSING PLATFORMS FOR DECENTRALIZED HEALTHCARE AND WELLBEING

Rocío Cánovas Martínez

# PAPER-BASED ENZYMATIC ELECTRODE WITH ENHANCED POTENTIOMETRIC RESPONSE FOR MONITORING GLUCOSE IN BIOLOGICAL FLUIDS

---

---



UNIVERSITAT ROVIRA I VIRGILI

TAILOR-MADE CHEMICAL SENSING PLATFORMS FOR DECENTRALIZED HEALTHCARE AND WELLBEING

Rocío Cánovas Martínez

This chapter introduces the second step in the way to developing a potentiometric biosensor. A novel paper-based potentiometric electrode with an enhanced response for the detection of glucose in biological fluids is described. The system is based on the use of the detection of hydrogen peroxide with Pt electrodes described in the previous chapter. The working electrode is made with a layer of platinum sputtered onto a conventional filter paper and two layers of Nafion to immobilize the enzyme glucose oxidase. The response obtained, which is due to the enzymatic generation of  $\text{H}_2\text{O}_2$ , is proportional to the logarithm of the concentration of glucose. Under optimal conditions a sensitivity of  $-119 \pm 8 \text{ mV}\cdot\text{decade}^{-1}$ , a linear range that spans from  $10^{-4} \text{ M}$  to  $10^{-2.5} \text{ M}$  and a limit of detection of  $10^{-4.5} \text{ M}$  of glucose is obtained. The role of Nafion to increase the sensitivity of the technique as well as to help to minimize the interferences caused by redox-active species, such as ascorbate, is studied. Validation of this system in human serum samples shows an excellent agreement when compared to standard methods. This approach can become an interesting alternative for the development of simple and affordable devices for decentralized settings, such as point of care and home-based diagnostics.

## 7.1. INTRODUCTION

Enzymatic biosensors have traditionally drawn significant attention because of their attractive analytical features. The specificity of the recognition obtained by the use of an enzyme allows the development of devices with exceptional selectivity. Additionally, these sensors display good reproducibility, stability and low limits of detection in complex matrices, such as biological fluids. Last -but not least-, a limited group of enzymes (oxidases, reductases, etc.) allows a wide range of molecules to be detected with a simplified detection approach.<sup>[1,2]</sup> For this reason, enzymatic biosensors are extensively used in different applications, such as clinical, environmental, forensic, food analysis, etc.<sup>[3-7]</sup>

As a general approach, the enzyme is used as a recognition element, catalyzing a specific reaction of the analyte, and then one of the reaction products is detected. Oxidase-type enzymes, for example, are widely used since they generate hydrogen peroxide ( $\text{H}_2\text{O}_2$ ) as a byproduct.<sup>[4,8]</sup> Thus, there is a plethora of sensors for different molecules that are based on the detection of  $\text{H}_2\text{O}_2$  using a suitable technique.<sup>[9-11]</sup> From the many different options, detection of peroxide using electrochemical-based techniques provide significant advantages, since they show outstanding analytical figures and a simple, compact setup.<sup>[12]</sup> Traditionally, electrochemical enzyme-based biosensors have relied on voltammetric techniques. Amperometric detection is by far the most used approach,<sup>[13]</sup> since it shows outstanding sensitivity and robustness. In fact, one of the greatest achievements on the use of this technique for solving social needs was the successful development of devices to monitor



glucose at home (glucometers), most of which are based on the use of glucose oxidase and amperometric detection.<sup>[13,14]</sup> Therefore, for many years, this technique has become almost the norm for many biosensors.

Despite of this undisputable success, emerging social needs are creating a growing demand for alternative detection schemes. As the need for new tools for decentralized chemical analysis -such as those required in point of care- is gaining momentum, new detection schemes that can combine good analytical performance with enhanced robustness, simplicity and lower costs are required. This is the case, for example, of wearable devices,<sup>[15]</sup> where power consumption, robustness and size are paramount, or the recent trend in the development of paper-based analytical platforms.<sup>[16]</sup> It is for this reason that approaches such as potentiometry are attracting a renewed interest, since they can offer an unrivalled simplicity of operation and instrumentation,<sup>[17-19]</sup> robustness and -with recent progress in the field- also ultra-low-cost devices.

Potentiometric biosensors using enzymatic reactions were proposed several decades ago. The first proposals made use of an enzyme immobilized on a glass electrode surface in order to detect the change in protons resulting from the reaction.<sup>[20]</sup> Following this seminal work, different types of devices where the enzymatic reaction generates a positively charge species - such as protons or ammonium ions- to be then detected by a suitable ion-selective electrode. For instance, a pH-based enzyme potentiometric sensor for glucose determination using glucose oxidase (GOx) was investigate.<sup>[21]</sup> In a similar work, some discussions regarding the role of the changes on pH were also addressed.<sup>[22]</sup> Also, a coated-wire potentiometric enzyme sensor was also developed to detect urea and penicillin.<sup>[23]</sup> Nevertheless, most of these approaches never became widely adopted, possibly because they did not offer significant advantages over alternative schemes. Very recently, however, with the introduction of new materials, novel enzymatic biosensors with potentiometric detection have been reported. Willander *et al.* explored the use of ZnO nanostructures to immobilize cholesterol oxidase and glucose oxidase in order to build suitable biosensors.<sup>[24,25]</sup> Similarly, Adeloju *et al.*, developed enzyme-based potentiometric sensors for glucose and phosphate.<sup>[26-28]</sup> The advantages of this type of devices, which have been recently studied present many attractive features for practical applications.<sup>[29,30]</sup> Nevertheless, most of them have not yet been validated with real samples. It is well known that interferences commonly found in biological fluids are major roadblocks for these sensors.

The search for alternative routes for the determination of glucose in biological fluids is still a very relevant topic of research. First, because it can be used as model to compare the performance with other systems. Second, because existing solutions only reach a fraction of the total population in need. It was estimated that 285 million adults were affected by diabetes

in 2010, and it is expected that this number increases to 439 million by 2030. Most of this increment will be registered in developing countries, where conventional glucometers are still unaffordable<sup>[31]</sup> and public healthcare systems are crumbling under the increasing cost-cutting pressure. Hence, new detection approaches that can offer reduced cost and enhanced simplicity are needed. To reduce the cost of the sensors, new approaches to produce electrodes in large scale have been developed during the last years. Screen-printed techniques have partially addressed this problem.<sup>[32]</sup> More recently, breakthroughs in the area of nanomaterials and flexible electronics have helped to further reduce the cost of potentiometric sensors<sup>[33,34]</sup> by applying simple dyeing or direct printing approaches using paper as a substrate.<sup>[35]</sup> Last but not least, potentiometric sensors can be miniaturized (thus reducing even further the manufacturing cost) without affecting the analytical performance. Therefore, the development of a paper-based potentiometric biosensor for glucose may bring significant advantages in order to solve a growing social need.

Low-cost paper-based platforms to make affordable and portable analytical tools for poor and remote regions of the planet have been proposed many years ago.<sup>[36]</sup> Paper has been used in combination with new materials to fabricate sensors in a cost-effective manner.<sup>[37,38]</sup> However, the majority of paper-based enzymatic devices use the paper as a substrate for colorimetric assays, as in the traditional dipsticks, lateral flow systems and bioactive papers.<sup>[39,40]</sup> More recently, paper was proposed as a substrate to build enzymatic electrodes using amperometric detection approach.<sup>[41]</sup> Interestingly, paper sensors are based on a 3D network of cellulose fibers, which increases the active area where enzyme is immobilized and, consequently, improves the analytical performance. To the best of our knowledge, paper-based enzymatic biosensors with potentiometric detection that can be used in real samples have not yet been reported.

This work introduces a novel approach for the construction of a simple, robust and sensitive enzymatic paper-based biosensor for the potentiometric detection of glucose. The method is based on the detection of the hydrogen peroxide generated as a result of the oxidation of glucose catalyzed by glucose oxidase (GOx). A platinum-sputtered paper sensor is used as a redox sensitive substrate and, in order to eliminate interferences and increase the sensitivity of the technique, a recent approach where the enzyme is immobilized using a Nafion layer is proposed. The results show that this device can accurately predict levels of glucose in body fluids such as serum. Furthermore, considering that the generation of peroxide is common to many enzymes, it is expected that this sensor can be applied for wide range of substances. Some limitations and potential future applications of these novel sensors in real life scenarios are discussed. For example, while platinum (Pt) was used in this first proof of principle, it is

expected that the use of a redox-sensitive material may help to further reduce costs. This study opens a new avenue for the development of electrochemical paper-based enzymatic sensors.

## 7.2. EXPERIMENTAL

### 7.2.1. Materials and methods

Sodium urate, sodium ascorbate and D-Fructose were purchased from Sigma-Aldrich. Phosphate buffered saline (PBS) was prepared at 0.1 M with 0.135 M NaCl and used in all the experiments. An adhesive plastic mask (0.3 mm thick) coated with an acrylic adhesive on one side (Arcare 8565, Adhesives Research Inc., Limerick, Ireland) was used to expose a given area of a platinized paper and isolate the rest of the conductive surface.

For morphological analysis, all membranes were covered with a gold layer to improve the transduction and characterized using an environmental scanning electron microscope. For the chemical analysis of the surface, an attenuated total reflectance Fourier transform infrared spectrometer (Agilent 4100 ExoScan FT-IR) was used. A spectrum, collected as the average of 64 scans with a resolution of  $4\text{ cm}^{-1}$ , was recorded from  $4000$  to  $650\text{ cm}^{-1}$ .

### 7.2.2. Electrochemical measurements

Laboratory measurements were made using a 4 mL cell in 0.1M PBS (pH 7.4) at  $25^{\circ}\text{C}$  as it is described in Chapter 3.

### 7.2.3. Fabrication of glucose biosensor

For the fabrication of the electrodes, Pt was sputtered on one side of a conventional filter paper, which was then cut into rectangular pieces (20 mm x 5 mm) sandwiched between two rectangular plastic masks. The top mask (15 mm x 10 mm) had a 3 mm diameter circular window and the bottom mask was slightly larger (20 mm x 10 mm), as shown in Figure 1A. Thus, the conductive paper is exposed only at the top, to connect with the reading instrument, and the circular window that will be used as the electrochemically active surface.

These bare Pt electrodes are then functionalized with the biosensing membrane, which is made using Nafion as polymeric coating and glucose oxidase enzyme as the biological receptor. First, the window of each electrode was rinsed with double-distilled water and air-dried. Thereafter, a first layer of Nafion -responsible of the selectivity of the sensor- was made by drop casting  $4\text{ }\mu\text{L}$  of the Nafion solution air-dried for 60 minutes at room temperature. Thereafter,  $20\text{ }\mu\text{L}$  of a solution containing  $20\text{ mg}\cdot\text{mL}^{-1}$  of glucose oxidase (GOx) in distilled water was drop cast on top of the Nafion membrane and the system was left drying overnight at  $4^{\circ}\text{C}$ . Finally,  $2.5\text{ }\mu\text{L}$  of the same solution of Nafion was applied in order to make a second layer

that entraps the enzymatic layer and let dry overnight at 4°C (See Figure 7.1) This electrode was kept at 4°C when not in use.

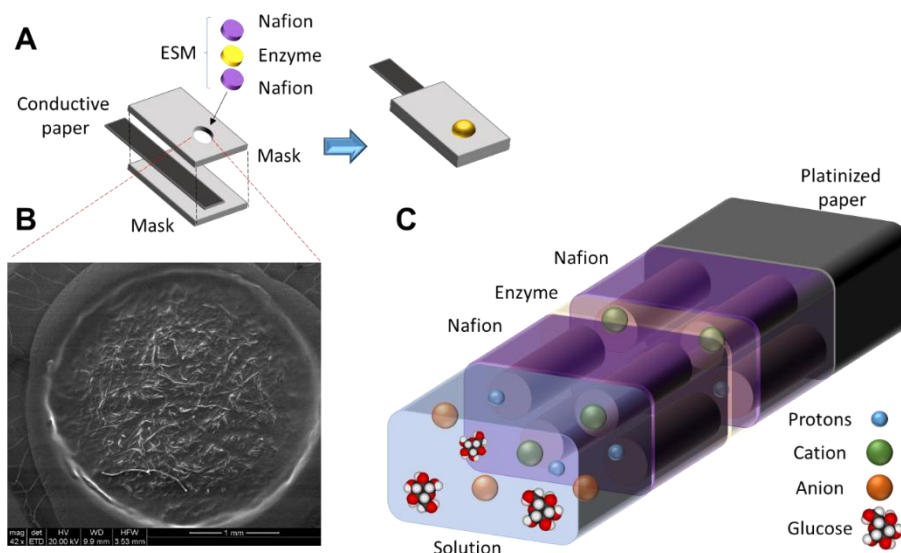


**Figure 7.1.** Illustration of paper-based biosensor. (A) Fabrication of the paper-based electrode, using a strip of platinumized conductive paper sandwiched between two plastic masks with a window of electroactive surface (B) Electron microscope (ESEM) images of a Nafion membrane drop cast on top of an electrode. (C) Scheme of the enzymatic membrane: Pt-Paper Substrate, enzyme (GOx) sandwiched between two layers of Nafion, one at Pt-interface and the other at the solution interface.

#### 7.2.4. Analysis of real samples

Serum samples of patients were obtained by a local hospital (Hospital de Sant Pau i Santa Tecla). Values from serum samples were provided by the hospital using hexokinase/glucose-6-phosphate dehydrogenase colorimetric test as a standard method for further validation of the paper-based potentiometric system.

### 7.3. RESULTS AND DISCUSSION

#### 7.3.1. Characterization of the platinumized paper-based electrodes

Environmental scanning electron microscopy (ESEM) was used to study the surface of the paper-based electrodes. The results reveal the cross-linked cellulose fibers completely covered by a thin layer of sputtered platinum (Figure 7.2A). Preliminary tests were conducted by adding a drop of water on top of the Pt layer to evaluate the wettability of this coated paper. The results show that the water does not percolate through the metallic layer. When the sputtering is performed over a flat surface -such as glass-, a layer of a thickness of approximately 100 nm

is obtained. In the case of paper, because of roughness and 3D nature of the network created by the cellulose fibers, it is difficult to assess the actual thickness of the metal layer. In any case, the Pt-coated surface is waterproof and shows a homogenous and very low electrical resistance that corresponds to a metallic conductor. The tridimensional structure of the cellulose increases the electrochemically active surface of the electrode where the Nafion membrane and the enzyme are cast. When the Nafion is added, the surface of the metalized paper is completely covered by the polymer (Figure 7.2B). The membrane has an irregular morphology, as the Nafion layer follows the uneven cross-linked cellulose fibers. A transversal cut of the electrode reveals a membrane with approximately 40  $\mu\text{m}$  thickness that is evenly spread over the platinized surface (Figure 7.2C).

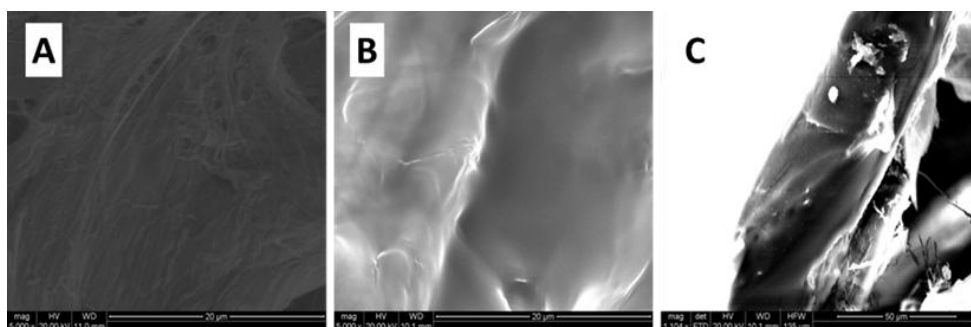
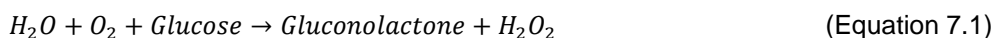


**Figure 7.2.** ESEM images of the paper-based electrode surface: (A) a bare platinized paper electrode, (B) a membrane (double layer of Nafion) on top of a platinized paper electrode and (C) transversal cut of the electrode membrane (ca. 40  $\mu\text{m}$  thickness).

### 7.3.2. Electrode response and principle of detection

Preliminary experiments were conducted in order to verify the response of the enzymatic sensor. The results show that over certain concentration ranges the electrode potential decreases linearly with the logarithm of the concentration of glucose. To explore the nature of this response, “blank” measurements were performed. To do this, experiments where the enzymatic sensor was replaced either by a bare Pt electrode or by a Nafion coated electrode (i.e., without enzyme) were also conducted (Figure 7.3A). The results show that none of these electrodes respond to the addition of glucose (Figure 7.3B). Therefore, it is clear that the enzymatic sensor is responding to some byproduct of the enzymatic reaction. The reaction catalyzed by the GOx can be expressed as:



The gluconolactone quickly turns into gluconic acid. Therefore, for practical purposes, it can be considered that the reaction generates gluconic acid and hydrogen peroxide. To evaluate the influence of these products on the observed signal, the response of the sensor to each one of these substances was studied using a bare and Nafion-coated platinized electrode. The results show that none of the systems respond to the addition of gluconate (Figure 7.3C); however, the addition of peroxide produces a negative response that, in the case of the electrode coated with Nafion, is similar to the response obtained when adding glucose in the enzymatic sensor (Figure 7.3D). This evidence suggests that the response shown in Figure 7.3A is produced by the change on the redox potential due to the generation of hydrogen peroxide resulting from the enzymatic oxidation of glucose. The difference in response between the bare Pt and the coated electrode also suggests that the response to peroxide is modulated by the presence of the Nafion membrane, as it will be discussed later.

Although there are multiple models that have been proposed to describe the structure of Nafion<sup>[42]</sup> and its interactions with substrates such as carbon or platinum interfaces,<sup>[43]</sup> the topic is still a matter of debate. There is an agreement, though, on the presence of hydrophilic structures that allow the aqueous solutions to pass through the membrane. More recently, the Nafion structures have been described as randomly packed water channels surrounded by partially hydrophilic side branches, forming inverted-micelle cylinders.<sup>[44]</sup> These new model explains important features of Nafion, including fast diffusion of water and protons. It is important to stress that Nafion is a polyelectrolyte with negatively charged sulfonate groups ( $-\text{SO}^{-3}$ ), which provide strong ion-exchange capabilities. Because of this, a Donnan potential at the Nafion-solution interface is generated.<sup>[45]</sup>

In the previous chapter we have demonstrated that Pt electrodes coated with a layer of Nafion show an enhanced sensitivity and selectivity for the determination of  $\text{H}_2\text{O}_2$ . Indeed, bare Pt electrodes showed a limited sensitivity for peroxide and an unspecific response to any kind of redox-active species. However, when the Pt is coated with a layer of Nafion, the sensitivity increases significantly, while the effect of negatively charged species -such as ascorbate- can be significantly reduced. The improved selectivity can be explained in terms of the permselective behavior of the Nafion, a characteristic that has been already used in amperometric sensors. The enhanced sensitivity, on the other hand, is more difficult to explain, and has been ascribed to the effects produced by the Donnan potential on the physicochemical properties of the membrane as well as by the mixed potential generated in the Pt surface. It is well known that due to the potential generated and the interface factors such as the pH may show local variations that significantly differ from the bulk properties of the solution.<sup>[46]</sup> As a result, complex coupling between the redox and acid-base equilibria at the bulk of the

membrane show results that are different from what could be expected from the properties of the solution.<sup>[45]</sup> The nature of this coupling is still a matter of study.

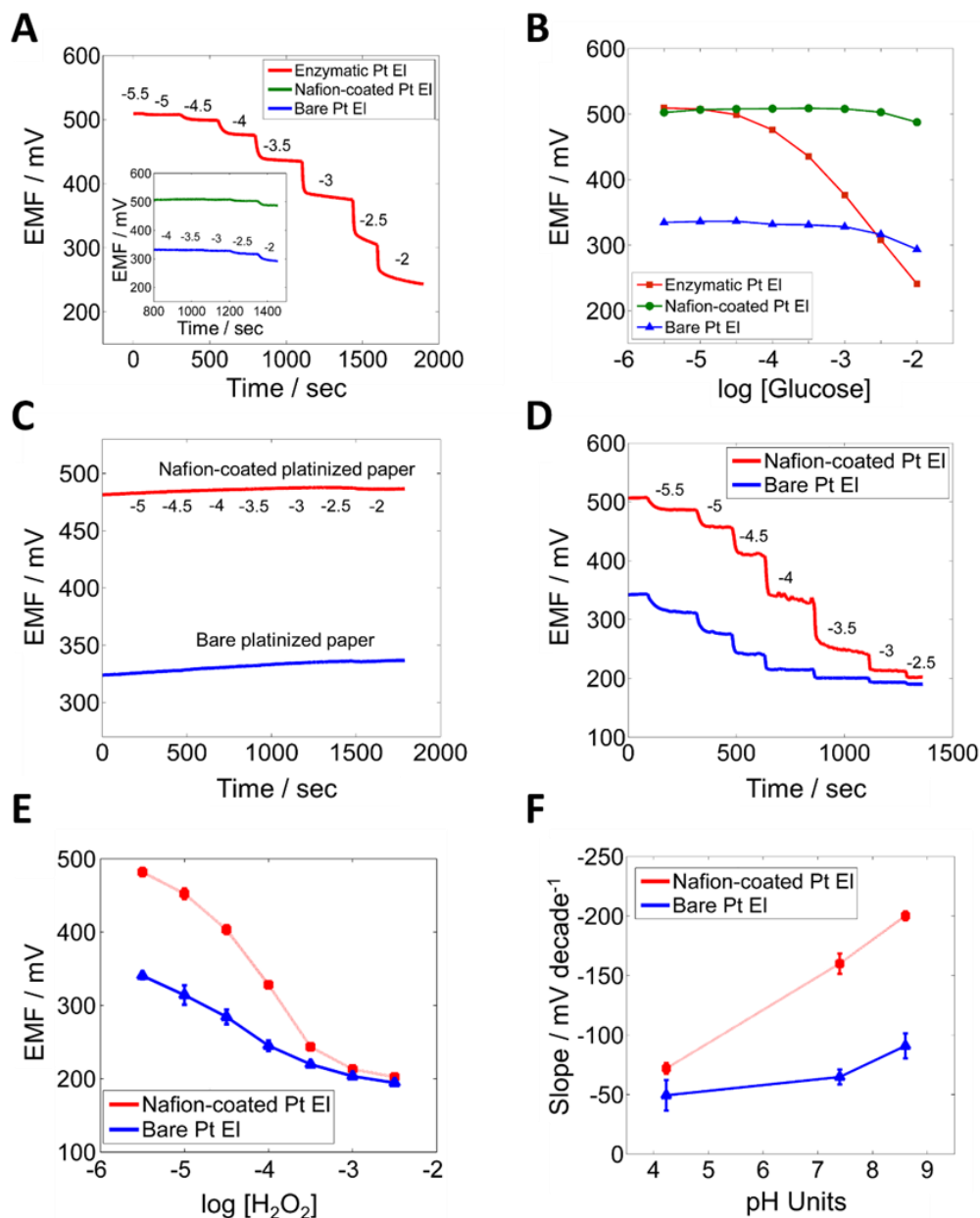


**Figure 7.3.** Response study of enzymatic paper-based electrode: (A) Potentiometric time-trace and (B) corresponding calibration curve of enzymatic, Nafion coated and bare platinumized paper electrode upon additions of glucose; (C) potentiometric time-trace for gluconic acid for bare and Nafion-coated paper electrode; (D) H<sub>2</sub>O<sub>2</sub> potentiometric time-trace and (E) corresponding calibration curve for H<sub>2</sub>O<sub>2</sub> for bare and Nafion-coated platinumized paper electrode (average  $\pm$  S.D., N=2). (F) pH dependence of the sensitivity for H<sub>2</sub>O<sub>2</sub> in the range from 10<sup>-5</sup> M to 10<sup>-3.5</sup> M (average  $\pm$  S.D., N=2). All the measurements were performed in 0.1 M buffers, acetic buffer (pH 4.2), PBS (pH 7.4), borate buffer (pH 8.6) at 25°C.

To illustrate this point, experiments with bare platinized papers and Nafion-coated platinized papers were performed (Figure 7.3D). Figure 7.3E displays the significant increase in the sensitivity that was obtained when electrodes were coated with Nafion ( $-140.4 \pm 7.4$  mV·decade<sup>-1</sup>, N=2) in comparison to bare platinized paper electrode ( $-53.6 \pm 6.2$  mV·decade<sup>-1</sup>, N=2) in a linear range of  $10^{-5}$  M to  $10^{-3.5}$  M after additions of H<sub>2</sub>O<sub>2</sub>. These results are in general agreement with those previously reported. However, it is important to remark that the sensitivity for peroxide is highly dependent on the Pt surface. Indeed, while for a bare flat disk electrode sensitivities have found in the order of 20-30 mV·decade<sup>-1</sup> of H<sub>2</sub>O<sub>2</sub>, these paper electrodes - with clean sputtered Pt- show higher sensitivities (in the order of 50 mV·decade<sup>-1</sup>).

All in all, this enzymatic sensor responds to changes in the mixed potential that are modulated by the Donnan potential created by the polyelectrolyte coating. To the best of our knowledge, this is the first time that this type of detection scheme is reported. Therefore, as it happens with more conventional amperometric sensors, the working principle of this sensor is based on the detection of H<sub>2</sub>O<sub>2</sub>. Thus, it should be different from the potentiometric sensors recently reported by Willander *et al.*, which are claimed to be based on the local changes of pH resulting from the enzymatic reaction.<sup>[47]</sup> Therefore, the optimization of the detection of peroxide was considered as a first step prior the detection of glucose.

Because of the influence of the Donnan potential, the sensitivity for the detection of peroxide of these electrodes coated with Nafion is dependent on the total electrolyte concentration, as it was demonstrated in the previous chapter. Indeed, the initial potential (i.e., before the addition of peroxide) of the coated electrodes is strongly dependent on the Donnan potential at the Nafion-solution interface. High electrolyte concentrations show higher initial potentials, and this improves the sensitivity of the detection. Similarly, the enhancement of the sensitivity for peroxide is increased at higher pHs, as shown in Figure 7.3F. While bare Pt electrodes show a slight dependence of the sensitivity with the pH, the coated electrodes show a marked increase -almost three times- when the pH is changed from 4.2 to 8.9. Unfortunately, it not possible to withdraw conclusions regarding the mechanisms directly from this plot, since the pH of the bulk of the solution does not necessarily matches the pH inside the membrane. In fact, variations of several pH units may take place on the vicinity of the membrane-platinum interface thus producing the enhancement of the signal. In any case, it is promising to observe that optimum conditions for detection of H<sub>2</sub>O<sub>2</sub>, such as high electrolyte concentrations and pHs slightly about 7, match the conditions usually found in many biological fluids.



### 7.3.3. Optimization of the detection of glucose

After the optimization of the detection of peroxide, the optimization of the detection of glucose is performed. In this case, conditions to immobilize the enzyme and to achieve optimum activity are explored. Preliminary experiments show that optimum results are obtained when the biosensor is built by sandwiching the enzyme between two layers of Nafion. The layer of Nafion cast on top of the Pt electrode plays 3 important roles. First, as it happens in other electrochemical sensors, it acts as a permselective barrier that minimizes the interference of negatively charged redox-active substances, such as ascorbic acid.<sup>[48]</sup> Second, as shown in the previous sections, the layer of Nafion produces an enhancement of the potentiometric detection of peroxide, due to the coupling of the redox (mixed) and the Donnan potentials. Third, the Nafion offers a better substrate for the stabilization and preservation of the enzymatic activity. Indeed, preliminary experiments (results not shown) display that when the enzyme is deposited directly onto the metallic surface, lower levels of activity are observed. Thus, a layer of Nafion on top of the Pt is beneficial before the enzyme is immobilized (a similar effect has been already described in the literature).<sup>[49]</sup> This immobilization is performed simply by direct drop casting of the enzyme solution on top of this first layer of Nafion. After the solution of the enzyme has dried, a second layer of Nafion is drop cast on top. This step is aimed to further improve the immobilization -avoiding any leaching of the enzyme on the solution- as well as to isolate the generation of peroxide from the rest of the solution, avoiding the potential interferences.

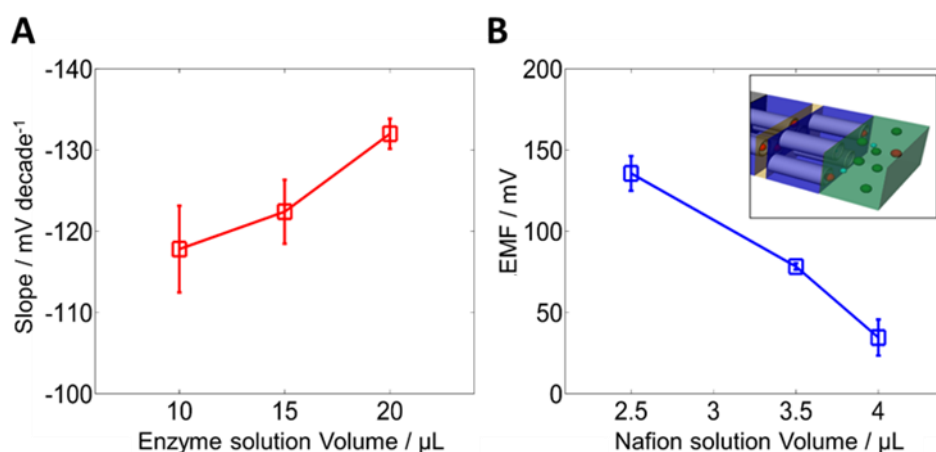


**Figure 7.4.** Optimization of the analytical conditions for the biosensor. (A) Sensitivity for glucose vs. volume of solution of enzyme concentration ( $20 \text{ mg}\cdot\text{mL}^{-1}$ ) cast. (B) Change on the potentiometric signal after the addition of  $10^{-4}$  M ascorbic acid as function of the increasing volume of Nafion membrane cast. In all cases, error bars correspond to the standard deviation of 3 different electrodes.

In order to optimize the analytical performance, the influence of the amount of enzyme was evaluated by adding a fix volume (15  $\mu\text{L}$ ) of solution with different concentrations of enzyme (0.2, 2, 20  $\text{mg}\cdot\text{mL}^{-1}$ ). Experimental evidence shows that none of these concentrations yield a difference on the final sensitivity obtained. Nevertheless, kinetic factors are improved at the highest concentration of enzyme. Under these conditions, faster production of  $\text{H}_2\text{O}_2$  allows reaching steady state signal in less than 90 seconds. Alternatively, the amount of enzyme added was modified by adding different volumes (10, 15 and 20  $\mu\text{L}$ ) of the highest concentration (20  $\text{mg}\cdot\text{mL}^{-1}$ ) of the enzyme solution. Higher volume was not able to be deposited and thus 20  $\mu\text{L}$  was the maximum volume deposited in the area of the electrode. In this case, an improvement in the sensitivity for glucose is observed (Figure 7.4A), suggesting a better distribution of the enzyme on the membrane during the drying process. Thus, optimum conditions for building the sensor were set at 20  $\mu\text{L}$  of 20  $\text{mg}\cdot\text{mL}^{-1}$  of enzyme.

Selectivity of the biosensor was assessed by monitoring the response in presence of redox interferences. Nafion ion-exchange membranes are negatively charge polyelectrolytes due to the sulfonic groups. Hence, Nafion is able to work as a cation exchange membrane, rejecting negatively charged species such as ascorbate and urate that are redox active molecules typically found in biological media. Experiments were carried out to evaluate the permselectivity of the first layer of Nafion, which separates the electrode from the solution. Different volumes of the Nafion solution (2, 3.5 and 4  $\mu\text{L}$ ) were cast on the electroactive area, verifying that in all cases the whole Pt surface was covered. Therefore, the increase of the volume of solution cast produces an increase on the thickness of the membrane. To evaluate the performance of this membrane, the potentiometric response to a 100  $\mu\text{M}$  ascorbate solution (upper concentration level typically found in body fluids) was tested. The difference in potential -before and after the addition of ascorbic acid- was used to characterize the selectivity of the system. The results are shown in Figure 7.4B. Clearly, the degree of interference is significantly reduced as the volume of solution cast (therefore, the membrane thickness) is increased. Therefore, in a compromise between selectivity and sensitivity, a volume of 4  $\mu\text{L}$  of Nafion solution was chosen as optimum drop-cast volume.

#### 7.3.4. Analytical performance

Enzymatic paper-based electrode was studied by monitoring change in electrochemical potential for increasing concentrations of glucose. Figure 7.5A shows the time-response curve of three different electrodes at different potentiometric cells in the concentration range from  $10^{-5.5}$  M up to  $10^{-1.5}$  M. A decrease in the potential was observed after addition of each glucose standard. Figure 7.5B presents the calibration curve on potential and glucose concentration

with a linear response from  $10^{-4}$  M to  $10^{-2.5}$  M of glucose. The corresponding linear regression equation for the three calibration curves was:  $EMF \text{ (mV)} = -118.6 \pm 7.6 \log[\text{Glucose}] - 532.08 \pm 34.8$ ,  $R^2 = 0.99$ ,  $N=3$ . The limit of detection was found to be  $10^{-4.5 \pm 0.08}$  M. This is the first time that such high sensitivity is obtained for a potentiometric paper-based enzymatic electrode.

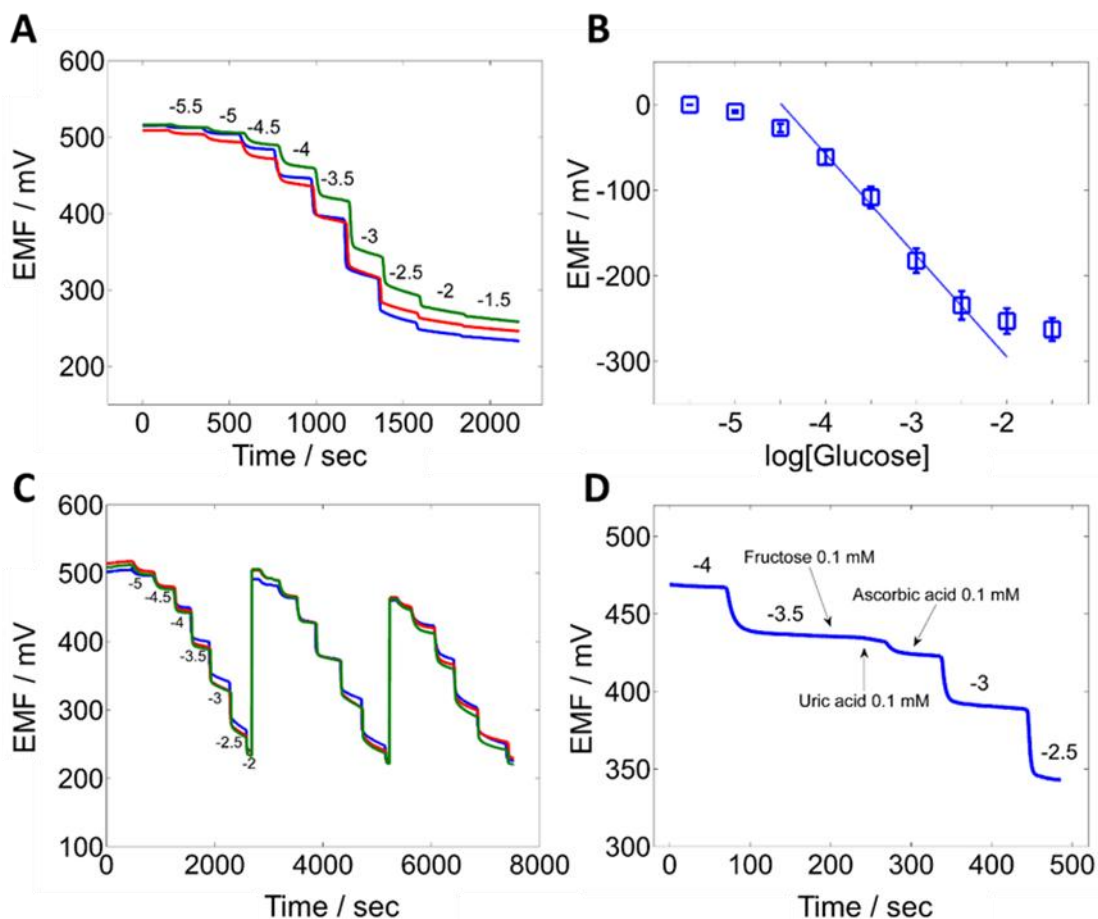


**Figure 7.5.** Analytical performance of the paper-based enzymatic electrode: (A) Time-trace plot of three different electrodes in three separated potentiometric cells, (B) the corresponding calibration curve of enzymatic electrodes showing the linear range (mean  $\pm$  S.D.,  $N=3$ ). (C) Repeatability test for three different electrodes during consecutive calibration curves for glucose. (D) Enzyme-based electrode selectivity assessment to the main redox sensitive molecules (ascorbate and urate) and fructose. All the measurements were performed in 0.1M PBS (pH 7.4) at 25°C.

Repeatability tests were carried out by performing several consecutive calibration curves for three different electrodes from  $10^{-5}$  M to  $10^{-2}$  M (Figure 7.5C). The comparison between calibration curves (Table 7.1) yields an outstanding reproducibility between slopes (3.4% RSD,  $N=3$ ). However, in the third calibration curve the linear range was narrowed on the upper end.

In this last case, a decrease on the initial potential of the system was observed, possibly due to some rearrangement of the Nafion membrane. In any case, very reproducible potentiometric calibration curves between electrodes were obtained.

**Table 7.1.** Repeatability test. Analytical performance for 3 consecutive calibrations.

Sensors (N=3)	1 <sup>st</sup> Curve	2 <sup>nd</sup> Curve	3 <sup>rd</sup> Curve
Sensitivity / mV·decade <sup>-1</sup>	-118.7 ± 1.9	-122.8 ± 3.3	-114.8 ± 1.5
Linear range / M	10 <sup>-4</sup> - 10 <sup>-2.5</sup>	10 <sup>-4</sup> - 10 <sup>-2.5</sup>	10 <sup>-4.5</sup> - 10 <sup>-3</sup>

The selectivity of the enzymatic sensors is associated with the specific enzymatic reaction between the enzyme and the target analyte. However, some redox sensitive interfering molecules found in real samples can induce to an error in the prediction. It is well-known that some molecules interfere in amperometric glucometers measurements such as uric acid and ascorbic acid. In this work, fructose, uric acid and ascorbic acid were tested at the high level of concentration found in blood (Figure 7.5D). For fructose and uric acid addition, the potentiometric response was almost negligible. However, for ascorbic acid addition (10<sup>-4</sup> M) some small drop in potential was observed. Thus, despite of the permselectivity of Nafion, some residual electrochemical effect of the ascorbic was observed, possibly due to a slight diffusion of the ascorbic through the hydrophilic membrane. This effect, however, is observed at the highest concentration usually found in blood. Some further work is being currently performed to eliminate this residual effect. The stability test of the enzymatic electrode did not show any significant decrease in the performance over 2 months' period. The conditions of the storage were at 4°C under dried environment (in a close compartment with silica gel) in order to avoid the loss of activity of the enzyme.

### 7.3.5. Membrane characterization

To gain insights on the changes during the enzymatic reaction, the membrane was characterized by ESEM to see possible electrode surface changes due to the hydration process. Besides, it is important to evaluate whether the surface is damaged by the action of the H<sub>2</sub>O<sub>2</sub>. Hence, Figure 7.6Aa shows the Nafion membrane over the platinized paper after the step of stabilization - hydration on PBS. In this case, a heterogeneous layer, showing some irregularities on the surface was observed. It has been reported that the interfacial area strongly increases with hydration,<sup>[50]</sup> thus producing different shapes along the surface. Figure 7.6Ab reveals similar behavior as the previous image, with some orifices on the surface after a calibration curve for glucose has been performed. Finally, Figure 7.6Ac exhibits the minor

effects on the electrode exposure to glucose ( $10^{-2}$  M), thus to consequently  $H_2O_2$  generation in the membrane. The wrinkles that are observed on the surface could be attributed to the rearrangement of the Nafion polymer structure. First, some small degree of decomposition of the sulfonated tetrafluoroethylene based fluoropolymer-copolymer caused by oxidation with  $H_2O_2$  may occur. Second, the ion-exchange process produced during the enzymatic reaction by-products (protons, gluconate, etc.).

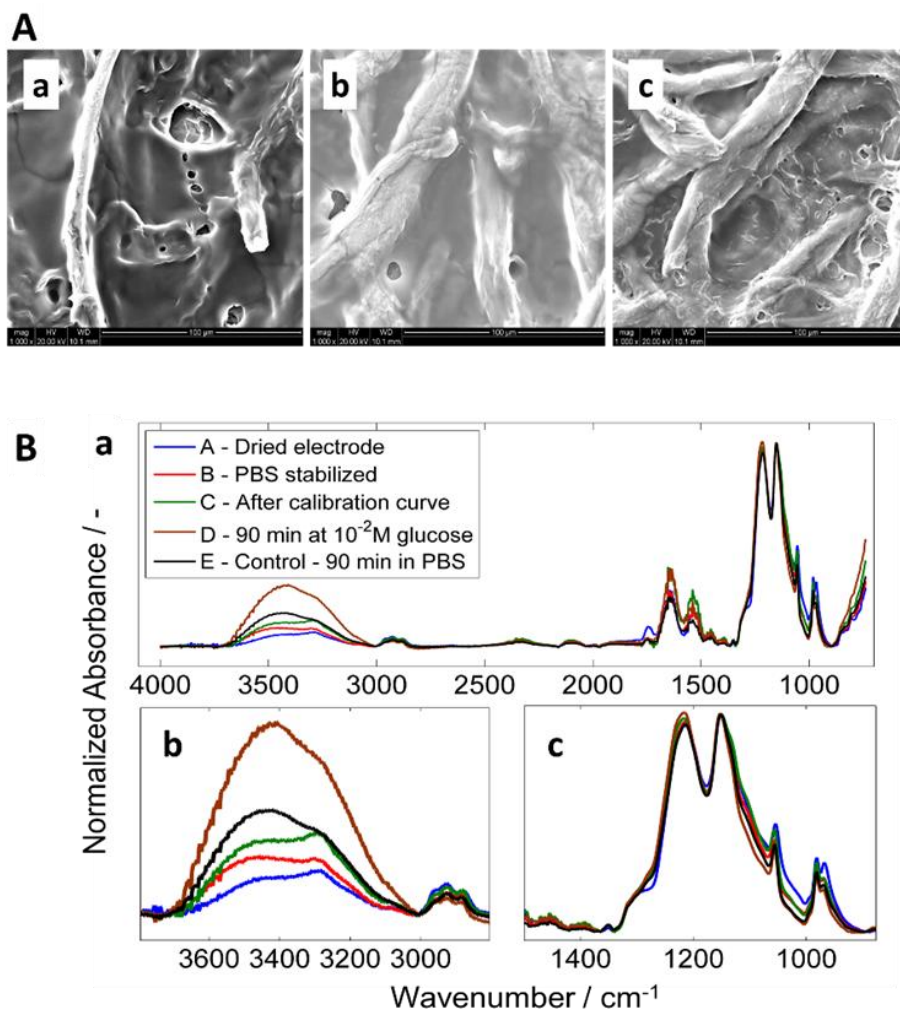


**Figure 7.6.** (A) ESEM images of the surface of the paper-based enzymatic electrode after hydration of the membrane: (Aa) PBS-solution-stabilized electrode, (Ab) after glucose calibration curve and (Ac) after 1.5 h  $10^{-2}$  M glucose solution. Enzymatic reaction was performed in PBS pH 7.4 at 25 °C. (B) FT-IR spectra of the paper-based enzymatic electrode in different conditions: (Ba) Whole overlap spectra, (Bb) magnification of peak at  $3400\text{ cm}^{-1}$  of membrane swelling and (Bc) magnification from  $900\text{ to }1500\text{ cm}^{-1}$  showing Nafion backbone peaks. Potentiometric measurements were performed in PBS pH 7.4 at 25 °C.

An infrared spectrum of the enzymatic electrode surface was performed to study the distribution of the chemical species over the membrane. Figure 7.6B is consistent with the results of the FT-IR studies of Nafion performed by other authors<sup>[51,52]</sup> that reported at 1145 and 1200  $\text{cm}^{-1}$  the C–F peaks and the C–C peak at 1300  $\text{cm}^{-1}$ . These peaks represent the polytetrafluoroethylene (PTFE) backbone (main chain) of a Nafion membrane. Furthermore, the double peaks at 970 and 982  $\text{cm}^{-1}$  assigned to the C–O–C bond, and the vibration at 1059  $\text{cm}^{-1}$  assigned to the S–O bond are characteristic peaks of the pendant side chain and sulfonic groups of Nafion, respectively. A broad band at 3400  $\text{cm}^{-1}$  was identified for water absorption from the membrane (OH stretching). FT-IR spectra of the enzymatic electrode before and after potentiometric measurements are shown in Figure 7.6Ba. Figure 7.6Bb exhibits the water absorption peak. Increasing time of the electrode in aqueous solution allows the membrane swelling through the polymer ionic domains. Interestingly, the peroxide reaction may produce an alteration in the hydrophilic nanostructures causing an increment of the swelling by hydration. Figure 7.6Bc displays the Nafion characteristic peaks for the main and pendant side chains.

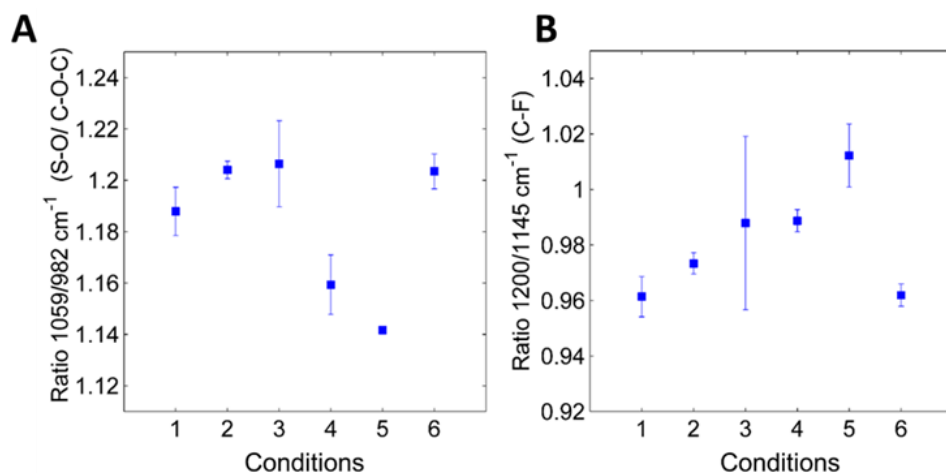


**Figure 7.7.** Ratio from FT-IR spectra between peaks (A) 1059/982 and (B) 1200/1145 in different conditions: (1) dried, (2) PBS stabilized, (3) after calibration curve, (4) 45 min at  $10^{-2}$  M glucose, (5) 90 min at  $10^{-2}$  M glucose and (6) control electrode, 90 min in PBS. Measurements were performed in PBS pH 7.4 at 25 °C.

A comparison of the chemical study of the surface during glucose exposure onto the potentiometric cell was also carried out. The difference between peak ratios indicated that a chemical modification was performed on the Nafion membrane after the determination of glucose and during long-time exposures to glucose (conditions 4 and 5) and thus  $\text{H}_2\text{O}_2$  (Figure 7.7). Figure 7.7A describes the ratio of groups on the side chain. As long time exposures to

glucose, higher change in the ratio was generated. Moreover, Figure 7.7B shows the ratio between the chemical groups in the main chain. Also, a slightly variation was found after long exposure to glucose. In this case, the change in the ratios was lower indicating that the modification of the polymer started from the side chain. This variation may be attributed to a slightly degradation of the polymer by the long exposure to glucose, consequently to the oxidative activity of the  $H_2O_2$ .

All in all, it is suggested that the enzymatic electrodes undergo almost no degradation of the Nafion membrane after a calibration curve and only a hydration process is involved. For long time exposures, membrane experiences slightly degradation that may produce small difference in the formal potential of the system. However, a detailed study of the reactions involved in this system falls well beyond the scope of this work, and only some general observations can be elaborated.

### 7.3.6. Analysis of real samples

The feasibility of the paper-based enzymatic electrodes was evaluated through the determination of glucose concentration in real samples. In this work, serum samples from patients provided from a local hospital were used in order to proof the enzymatic paper-based electrode system (Figure 7.8A). As the physiological range is higher than the current sensor linear range, a dilution (1:10) in PBS (0.1 M) was performed for the analysis of the serum samples. For the prediction of glucose, three different electrodes were used for each sample in order to have a reliable validation. Before the analysis, a calibration curve from  $10^{-5}$  M to  $10^{-2.5}$  M was performed. After that, the diluted serum sample was placed in the potentiometric cell. Potentiometric signal was recorded after a steady-state value of about 150 seconds.

Clarke's error grid plot (Figure 7.8B) is used to assess the clinical significance of differences between the glucose measurement technique under test (the experimental development) and the blood glucose reference measurements (in this approach, a commercial glucometer). The method uses a Cartesian diagram, in which the values predicted by the technique under test are displayed on the y-axis, whereas the values received from the reference method are displayed on the x-axis. The diagonal represents the perfect agreement between the two, whereas the points below and above the line indicate, respectively, overestimation and underestimation of the actual values. Zone A (acceptable) represents the glucose values that deviate from the reference values by 20% or are in the hypoglycemic range (<70 mg/dL), when the reference is also within the hypoglycemic range. The values within this range are clinically exact and are thus characterized by correct clinical treatment. Zone B (benign errors) is located above and below zone A; this zone represents those values that deviate from the reference

values, which are incremented by 20%. The values that fall within zones A and B are clinically acceptable, whereas the values included in areas C-E are potentially dangerous, and there is a possibility of making clinically significant mistakes.<sup>[53-56]</sup>

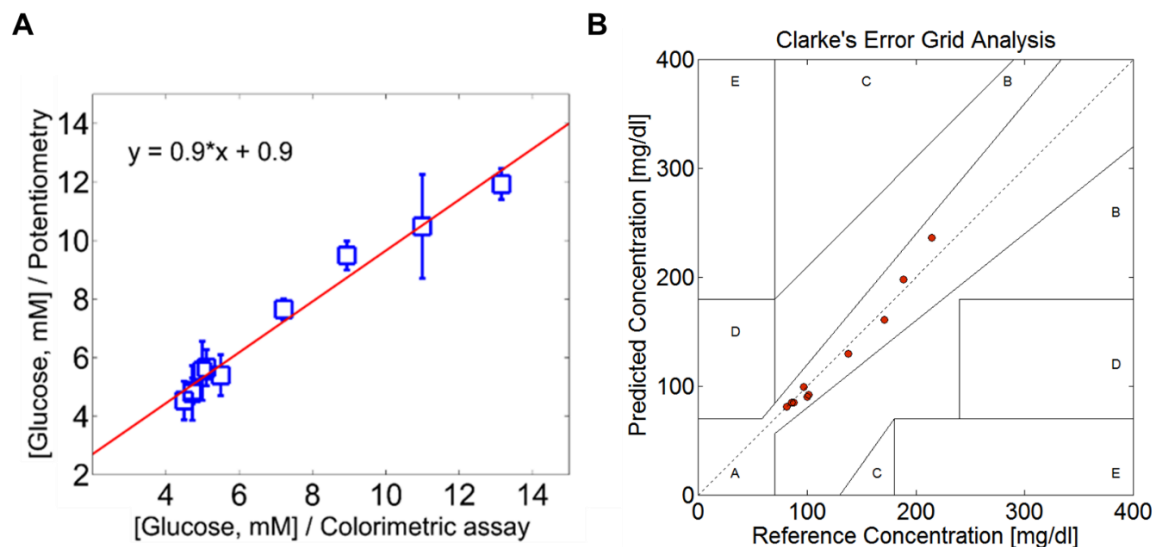


**Figure 7.8.** (A) Comparison of glucose determination (mM) in real samples obtained by the potentiometric paper-based electrode (mean  $\pm$  S.D., N=3) and colorimetric assay (data provided by the local hospital) at 25°C. (B) Clarke plot demonstrates that the values are clinically relevant because all of them are inside the zone A.

**Table 7.2.** The recovery of glucose determination in serum samples (diluted 1:10).

Nº Sample	Potentiometry (mM)	Colorimetric assay (mM)	Recovery (%)
1	11.93 $\pm$ 0.53	13.15	90.66
2	5.65 $\pm$ 0.62	5.11	110.72
3	4.76 $\pm$ 0.93	4.72	101.49
4	7.65 $\pm$ 0.35	7.22	105.99
5	4.53 $\pm$ 0.66	4.50	100.86
6	4.87 $\pm$ 0.44	4.72	103.17
7	9.49 $\pm$ 0.5	8.94	106.18
8	10.48 $\pm$ 1.77	10.99	95.34
9	5.4 $\pm$ 0.7	5.50	98.20
10	5.55 $\pm$ 1.01	5.00	111.12



Results shown in Table 7.2 indicate an excellent recovery in agreement with the reference method results provided by the hospital (hexokinase/glucose-6-phosphate dehydrogenase colorimetric test). Moreover, Figure 7.8 presents a good linear correlation between both methods. The recoveries for the assays from serum samples reached between 90.6-111.1 %, indicating that serum matrix had no significant effect on glucose determination. It should be mentioned that the same electrodes were used repeatedly for at least 6 predictions without losing their performance indicating high resistance to biofouling. Nevertheless, ideally the system is conceived to be used as a disposable sensor to make easy to handle and avoid contamination between biological samples.

**Table 7.3.** Comparison of the analytical performance of potentiometric biosensors for glucose detection.

Sensor <sup>a</sup>	Sensitivity (mV·decade <sup>-1</sup> )	Linear range (M)	Limit of detection (M)	Time of response (seconds)	Analysis in real samples	Reference
GOx/Gy/BSA platinum foil	-52	10 <sup>-3.4</sup> to 10 <sup>-2.4</sup>	---	---	No	Wingard et al., 1984
GOx/ZnONPs/CHIT/PVAL indium tin oxide	---	10 <sup>-5.7</sup> to 10 <sup>-2.9</sup>	10 <sup>-6.7</sup>	---	No	Shukla et al., 2012
GOx/Fe <sub>3</sub> O <sub>4</sub> NPs/CHIT gold coated glass	27.3±0.8	10 <sup>-6</sup> to 10 <sup>-1.5</sup>	---	7	No	Khun et al., 2012
GOx/ZnONWs silver coated glass	35	10 <sup>-6.3</sup> to 10 <sup>-3</sup>	---	4	No	Usman Ali et al., 2010
GOx/Fe <sub>3</sub> O <sub>4</sub> NPs/Ppy MGCE	19.4	10 <sup>-6.3</sup> to 10 <sup>-1.5</sup>	10 <sup>-6.5</sup>	6	Human serum	Yang et al., 2014
GOx/AgNPs over a polymeric membrane Ag-ISE (glass electrode)	---	10 <sup>-4</sup> to 10 <sup>-2.5</sup>	10 <sup>-5</sup>	---	Beverages	Ngeontae et al., 2009
AuNs/PtNPs/GOx Aluminum foil	33,4	10 <sup>-4</sup> to 10 <sup>-2.1</sup>	---	---	No	Xu et al., 2013
GOx Iodide electrode	65.2±0.2	10 <sup>-4</sup> to 10 <sup>-2</sup>	---	60-120	Human serum	Karakus et al., 2013
PPy-GOx film PtE	38.3	10 <sup>-3</sup> to 10 <sup>-2</sup>	---	60-120	No	Trojanowicz et al., 1996
PPy-GOx film Pt disk	76,5	10 <sup>-5.2</sup> to 10 <sup>-1.4</sup>	10 <sup>-5.2</sup>	30	No	Ayenimo et al. 2014
<b>Nafion/GOx/Nafion platinized paper</b>	-119±8	10 <sup>-4</sup> to 10 <sup>-2.5</sup>	10 <sup>-4.5</sup> M	50	Human serum	<b>Current work</b>

<sup>a</sup> GOx – Glucose Oxidase // Gy – Glutaraldehyde // BSA – Bovine serum albumin // ZnONPs – Zinc oxide nanoparticles // CHIT – Chitosan // PVAL – Polyvinyl alcohol // ZnONWs – Zinc oxide nanowires // Ppy – Polypyrrole // PtNPs – Platinum nanoparticles // MGCE - Magnetic glassy carbon electrode // PtE – Platinum electrode

Table 7.3 provides a comparison of the analytical performances of the enzymatic paper-based electrode described in this study with those of other reported glucose potentiometric biosensors. The system described in this work reports the highest potentiometric sensitivity and the cheapest method of fabrication of the electrode for the measurement of glucose in real samples.

## 7.4. CONCLUSIONS

A new paper-based enzymatic electrode that shows high sensitivity for the determination of biomolecules such as glucose has been presented. Under optimal conditions this sensor exhibits excellent enzymatic activity and high reproducibility for the detection of glucose in a linear range from  $10^{-4}$  M to  $10^{-2.5}$  M with a limit of detection of  $10^{-4.5}$  M. The use of the hydrophilic negatively charged Nafion membrane avoids minimizing interferences from negative redox active molecules such as ascorbate as well as the biofouling effect. The analytical parameters shown by the paper-based enzymatic electrode can be attributed to the elevated enzyme loading capacity and high stability provided by the Nafion membrane, which yield a favourable environment for glucose molecules oxidation. Furthermore, properties from thin Nafion membrane allowed this enhancement of the potentiometric response as a result from a coupling of redox (mixed) and Donnan potential. This principle opens a new strategy to develop highly sensitive paper-based enzymatic sensors for diseases monitoring. Other biomolecules determination could also be applied by only changing the biological receptor, the enzyme. Future prospects involve a study of the storage properties and an integration with a reference electrode and wireless device to develop a full potentiometric cell for the completely decentralization of the biochemical analysis.

## 7.5. REFERENCES

- [1] G. A. Evtugyn, H. C. Budnikov, E. B. Nikolskaya, *Talanta* **1998**, *46*, 465.
- [2] J. Anzai, H. Takeshita, Y. Kobayashi, T. Osa, T. Hoshi, *Anal. Chem.* **1998**, *70*, 811.
- [3] I. Karube, Y. Nomura, *J. Mol. Catal. B Enzym.* **2000**, *10*, 177.
- [4] G. S. Wilson, Y. Hu, *Chem. Rev.* **2000**, *100*, 2693.
- [5] L. Wang, W. Chen, D. Xu, B. S. Shim, Y. Zhu, F. Sun, L. Liu, C. Peng, Z. Jin, C. Xu, N. A. Kotov, *Nano Lett.* **2009**, *9*, 4147.
- [6] R. Khan, A. Kaushik, P. R. Solanki, A. Ansari, M. K. Pandey, B. D. Malhotra, *Anal. Chim. Acta* **2008**, *616*, 207.
- [7] J. Wang, *Biosens. Bioelectron.* **2006**, *21*, 1887.
- [8] S. A. Ansari, Q. Husain, *Biotechnol. Adv.* **2012**, *30*, 512.
- [9] J. M. You, Y. N. Jeong, M. S. Ahmed, S. K. Kim, H. C. Choi, S. Jeon, *Biosens. Bioelectron.* **2011**, *26*, 2287.

- [10] D. T. V Anh, W. Olthuis, P. Bergveld, *Sens. Act. B Chem.* **2003**, *91*, 1.
- [11] Y. Xiao, H. X. Ju, H. Y. Chen, *Anal. Chim. Acta* **1999**, *391*, 73.
- [12] L. Li, Y. Wang, L. Pan, Y. Shi, W. Cheng, Y. Shi, G. Yu, *Nano Lett.* **2015**, *15*, 1146.
- [13] J. Wang, *Chem. Rev.* **2008**, *108*, 814.
- [14] M. A. Invernale, B. A. Tang, R. L. York, L. Le, D. Y. Hou, D. G. Anderson, *Adv. Healthc. Mater.* **2014**, *3*, 338.
- [15] A. J. Bandoekar, I. Jeerapan, J. Wang, *ACS Sensors* **2016**, *1*, 464.
- [16] E. J. Maxwell, A. D. Mazzeo, G. M. Whitesides, *MRS Bull.* **2013**, *38*, 309.
- [17] Z. Yang, C. Zhang, J. Zhang, W. Bai, *Biosens. Bioelectron.* **2014**, *51*, 268.
- [18] V. N. Psychoyios, G.-P. Nikoleli, N. Tzamtzis, D. P. Nikolelis, N. Psaroudakis, B. Danielsson, M. Q. Israr, M. Willander, *Electroanalysis* **2013**, *25*, 367.
- [19] F. Ismail, S. B. Adeloju, *Electroanalysis* **2014**, *26*, 2701.
- [20] D. J. Pasto, R. Meyer, S.-Z. Kang, *J. Am. Chem. Soc.* **1969**, *91*, 2164.
- [21] S. D. Caras, J. Janata, *Anal. Chem.* **1985**, *57*, 1917.
- [22] B. H. van der Schoot, P. Bergveld, *Biosensors* **1988**, *3*, 161.
- [23] J. Anzai, T. Osa, *Chem. Pharm. Bull.* **1986**, *34*, 3522.
- [24] S. M. Usman Ali, O. Nur, M. Willander, B. Danielsson, *Sens. Act. B Chem.* **2010**, *145*, 869.
- [25] M. Q. Israr, J. R. Sadaf, M. H. Asif, O. Nur, M. Willander, B. Danielsson, *Thin Solid Films* **2010**, *519*, 1106.
- [26] S. B. Adeloju, A. N. Moline, *Biosens. Bioelectron.* **2001**, *16*, 133.
- [27] J. G. Ayenimo, S. B. Adeloju, *Anal. Methods* **2014**, *6*, 8996.
- [28] A. T. Lawal, S. B. Adeloju, *Biosens. Bioelectron.* **2013**, *40*, 377.
- [29] M. H. Asif, S. M. U. Ali, O. Nur, M. Willander, C. Brännmark, P. Strålfors, U. H. Englund, F. Elinder, B. Danielsson, *Biosens. Bioelectron.* **2010**, *25*, 2205.
- [30] S. K. Shukla, S. R. Deshpande, S. K. Shukla, A. Tiwari, *Microchim. Acta* **2012**, *99*, 283.
- [31] J. E. Shaw, R. a. Sicree, P. Z. Zimmet, *Diabetes Res. Clin. Pract.* **2010**, *87*, 4.
- [32] O. D. Renedo, M. a. Alonso-Lomillo, M. J. A. Martínez, *Talanta* **2007**, *73*, 202.
- [33] T. Guinovart, M. Parrilla, G. A. Crespo, F. X. Rius, F. J. Andrade, *Analyst* **2013**, *138*, 5208.
- [34] M. Novell, M. Parrilla, G. A. Crespo, F. X. Rius, F. J. Andrade, *Anal. Chem.* **2012**, *84*, 4695.
- [35] M. Novell, T. Guinovart, P. Blondeau, F. X. Rius, F. J. Andrade, *Lab Chip* **2014**, *14*, 1308.
- [36] D. Mabey, R. W. Peeling, A. Ustianowski, M. D. Perkins, *Nat. Rev. Microbiol.* **2004**, *2*, 231.
- [37] D. D. Liana, B. Raguse, J. Justin Gooding, E. Chow, *Sensors* **2012**, *12*, 11505.
- [38] J. H. Kim, S. Mun, H. U. Ko, G. Y. Yun, J. Kim, *Nanotechnology* **2014**, *25*, 092001.

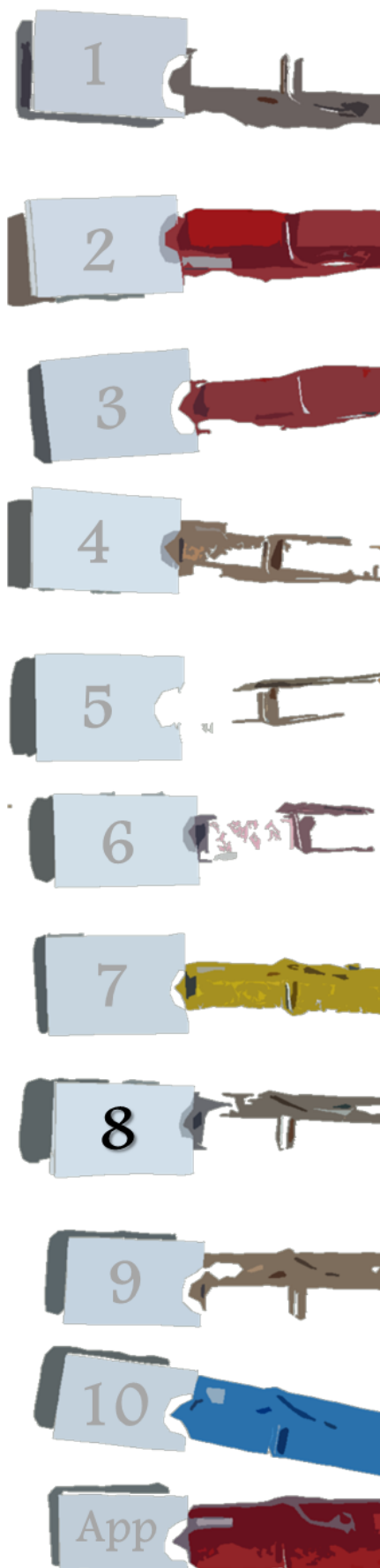
- [39] V. F. Curto, N. Lopez-Ruiz, L. F. Capitan-Vallvey, A. J. Palma, F. Benito-Lopez, D. Diamond, *RSC Adv.* **2013**, 3, 18811.
- [40] A. K. Yetisen, M. S. Akram, C. R. Lowe, *Lab Chip* **2013**, 13, 2210.
- [41] Z. Nie, C. a Nijhuis, J. Gong, X. Chen, A. Kumachev, A. W. Martinez, M. Narovlyansky, G. M. Whitesides, *Lab Chip* **2010**, 10, 477.
- [42] K. A. Mauritz, R. B. Moore, *Chem. Rev.* **2004**, 104, 4535.
- [43] D. L. Wood, J. Chlistunoff, J. Majewski, R. L. Borup, *J. Am. Chem. Soc.* **2009**, 131, 18096.
- [44] K. Schmidt-Rohr, Q. Chen, *Nat. Mater.* **2008**, 7, 75.
- [45] R. Naegeli, J. Redepenning, F. C. Anson, *J. Phys. Chem.* **1986**, 90, 6227.
- [46] R. B. M. Schasfoort, P. Bergveld, R. P. H. Kooyman, J. Greve, *Anal. Chim. Acta* **1990**, 238, 323.
- [47] S. M. Usman Ali, N. H. Alvi, Z. Ibupoto, O. Nur, M. Willander, B. Danielsson, *Sens. Act. B Chem.* **2011**, 152, 241.
- [48] A. Wynne, N. Finnerty, *Chemosensors* **2015**, 3, 55.
- [49] T. Klotzbach, M. Watt, Y. Ansari, S. D. Minteer, *J. Memb. Sci.* **2006**, 282, 276.
- [50] X. Kong, K. Schmidt-Rohr, *Polymer.* **2011**, 52, 1971.
- [51] M. Ludvigsson, J. Lindgren, J. Tegenfeldt, *Electrochim. Acta* **2000**, 45, 2267.
- [52] Z. Liang, W. Chen, J. Liu, S. Wang, Z. Zhou, W. Li, G. Sun, Q. Xin, *J. Memb. Sci.* **2004**, 233, 39.
- [53] A. Maran *et al.* *Diabetes Care.* **2002**, 25, 2.
- [54] B.P. Kovatchev, L. A. Gonder-Frederick, D. J. Cox, W. L. Clarke, *Diabetes Care.* **2004**, 27, 8.
- [55] E. Guevara and F. J. Gonzalez, *Medical Physics: Tenth Mexican Symposium on Medical Physics.* **2008**, 1032, 259261.
- [56] E. Guevara and F. J. Gonzalez, *Journal of Mexican Chemistry.* **2010**, 56, (5), 430434.

UNIVERSITAT ROVIRA I VIRGILI

TAILOR-MADE CHEMICAL SENSING PLATFORMS FOR DECENTRALIZED HEALTHCARE AND WELLBEING

Rocío Cánovas Martínez

# A NOVEL WIRELESS PAPER-BASED POTENTIOMETRIC PLATFORM FOR MONITORING GLUCOSE IN BLOOD



UNIVERSITAT ROVIRA I VIRGILI

TAILOR-MADE CHEMICAL SENSING PLATFORMS FOR DECENTRALIZED HEALTHCARE AND WELLBEING

Rocío Cánovas Martínez

This chapter presents the final achievement of the goals pursued during the two previous chapters, presenting a novel, low-cost, compact and sensitive paper-based platform for the accurate monitoring of glucose in biological fluids. Paper-based working and reference electrodes are combined to build a whole potentiometric cell, which also fits a sampling module for the simple and fast determination of glucose in a single drop of blood. The working electrode is built using a platinized filter paper coated with Nafion membrane that entraps the enzyme glucose oxidase; the reference electrode is made by casting a polyvinylbutyral-based membrane onto a conductive paper. The system works by detecting the hydrogen peroxide generated as a result of the enzymatic reaction. Selectivity is achieved due to the permselective behaviour of Nafion, while a significant enhancement of the sensitivity is reached by exploiting the Donnan-coupled formal potential. Under optimum conditions, a sensitivity of  $-95.9 \pm 4.8 \text{ mV}\cdot\text{decade}^{-1}$  in the 0.3 - 3 mM range is obtained. Validation of the measurements has been performed against standard methods in human serum and blood. Final integration with a wireless reader allows for truly in situ measurements with less than 2-minute procedure including a two-point calibration, washing and measurement. This low-cost analytical device opens up new prospects for rapid diagnostic results in non-laboratory settings.

## 8.1. INTRODUCTION

The sharp rise on the number of people affected by chronic diseases is creating a growing problem that largely exceeds the capacities of current healthcare models and infrastructures. For this reason, there is a general agreement that approaches where patients can be more involved in the self-management of their conditions are the best way to face this challenge. During the 21<sup>st</sup> century, the use of home-based devices for monitoring clinical parameters will become a common way to enhance the quality of life of the patients and improving the healthcare systems,<sup>[1,2]</sup> providing also access to those who cannot be easily reached by the traditional solutions. Nevertheless, developing home-based instruments at the mass-market level is a paradigm-shifting challenge for the analytical science, since factors such as the simplicity of operation and affordability become as relevant as the robustness of the information generated.<sup>[3,4]</sup> Only by addressing these three factors simultaneously, namely: analytical performance, decentralized usability and cost, these future devices can be successfully adopted at a massive scale.<sup>[5,6]</sup>

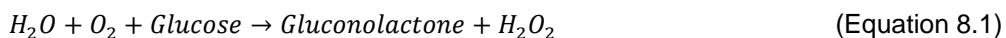
The monitoring of blood glucose levels is a good example of the challenges still unsolved.<sup>[7,8]</sup> The significant improvements brought by the home glucometer<sup>[9]</sup> cannot still be accessed by a large number of patients,<sup>[10]</sup> and this problem is expected to worsen in the near future. Estimations show that by 2030 more than 430 million people -most of them from



developing countries- will be affected by diabetes.<sup>[11,12]</sup> Thus, significant efforts towards the development of highly affordable approaches,<sup>[13,14]</sup> ranging from new sensors to alternative detection schemes, are increasingly needed.

The use of paper as a substrate to build analytical tools has emerged during the last decades as one of the most promising solutions to produce simple, powerful and low-cost analytical platforms.<sup>[15-17]</sup> The group of Whitesides pioneered the development of microfluidic devices exploiting the capillarity of the cellulose fibres to perform complex analytical operations<sup>[18,19]</sup> using both, colorimetric and electrochemical detection.<sup>[20-22]</sup> Paper-based amperometric sensors for the determination of metals in water<sup>[23]</sup> and for the evaluation of the levels of glucose, lactate and uric acid in serum<sup>[24]</sup> have been also recently reported. Alternative detection schemes, such as potentiometry, have shown some key advantages. Indeed, potentiometry has traditionally shown an unrivalled combination of robustness, simplicity of operation and low-cost of instrumentation. During the last few years, our group has pioneered the development of paper-based potentiometric sensors for the determination of ions in water and blood.<sup>[25-27]</sup> Willander *et al.* expanded the development of low-cost potentiometric sensors for the determination of biomolecules such as glucose, cholesterol or uric acid.<sup>[28,29]</sup> Despite of the promising results of these devices, their validation against real samples has been scarce.

In a similar line and during this thesis, a novel approach to produce enzyme-based potentiometric sensors has been developed. Using a platinized paper as a substrate and a Nafion membrane to entrap the enzyme glucose-oxidase (GOx), a highly sensitive and selective sensor for glucose was developed (Chapter 7).<sup>[30]</sup> The system is based on the reaction of oxidation of glucose (Equation 8.1) with the oxygen dissolved in the solution according to the following reaction:



The platinum surface monitors the changes in the redox potential as a result of the generation of hydrogen peroxide:



In previous works<sup>[30]</sup> and chapters it has been demonstrated that the Nafion membrane has 3 different roles: first, it entraps the enzyme; second, it enhances the sensitivity to peroxide;

third, it acts as a permselective barrier to minimize the effect of common interferences. The use of these sensors for the determination of glucose in biological fluids has been recently demonstrated.<sup>[31]</sup> Furthermore, although illustrated for the case of glucose, this system is attractive because it can work as a generic detection approach for oxidase-type enzyme catalysed reactions. Nevertheless, to prove the real usefulness of this paper-based enzymatic platform, system that can provide solutions to the whole analytical challenge -from sample introduction to data generation- is required.

This chapter introduces for the first time a fully integrated, compact, portable and disposable wireless paper-based potentiometric system for detection of glucose in biological fluids such as serum and whole blood. Optimization of the sensitivity and selectivity of the working electrode is achieved by tuning the thickness of the Nafion layer and the cell design. After the development of the paper-based solid-state reference electrode, a complete potentiometric cell is presented (potentiometric cell A, PCA, Figure 8.1). Thereafter, a suitable sampling module is designed to adapt to the potentiometric cell in order to reduce the sample volume to a single 25  $\mu\text{L}$  drop (potentiometric cell B, PCB, Figure 8.1). The system is first validated in the lab and then, through the integration with a portable miniaturized wireless potentiometer, is tested in real settings. The results show that this device displays a performance that is comparable to commercial glucometers, with the additional advantages of the low cost, simplified detection scheme and low power consumption. Extensions of this platform to the determination of other targets are briefly introduced.

## 8.2. EXPERIMENTAL

### 8.2.1. Instrumentation and measurements

Electromotive force (EMF) measurements were performed at room temperature (25°C) with a high input impedance ( $10^{15} \Omega$ ) potentiometer (as described in Chapter 3). First optimization and laboratory trials were made using a 4 mL cell in 0.1 M PBS (pH 7.4) and artificial serum<sup>[32]</sup> (pH 7.4) at 25°C. Fresh solutions of hydrogen peroxide and glucose were prepared daily.

Wireless measurements of the sampling cell were obtained using a Vernier Go Wireless® potentiometer with *Go Wireless* mobile application in a smartphone. Three different sensors (N=3) were evaluated in each experiment. A commercial amperometric glucose sensor (Bayer® Contour glucometer) was used to compare glucose blood values determined by our paper-based potentiometric sensor and also to check values from the local hospital obtained by colorimetric methods (hexokinase/glucose-6-phosphate dehydrogenase assay).

## 8.2.2. Analysis of real samples

Serum samples of patients were obtained in a local hospital (Hospital Sant Joan de Deu, Barcelona). Values from serum samples were provided by the hospital using hexokinase/glucose-6-phosphate dehydrogenase colorimetric test as a standard method for validation of the paper-based potentiometric system. Blood samples were obtained by the finger stick test from different volunteers. For the measurement of glucose levels in serum and blood samples a dilution of 1:10 in PBS (0.1 M, pH 7.4) was required. N=3, three different sensors monitored each sample in this case.

## 8.2.3. Fabrication of the enzymatic paper-based potentiometric cell

As a first step the preparation of the paper used as substrate was performed. For the working electrodes a 100 nm layer of platinum (Pt) was sputtered on one side of the filter paper to create a conductive, redox-sensitive surface. For the reference electrode, a filter paper was first painted with a conductive Ag/AgCl ink and cured for 10 minutes at 90°C. These treated papers were then cut into 10 x 5 mm strips. To build the electrodes, the conductive paper strips were sandwiched within two plastic masks. The top mask has a circular window of 3 mm of diameter to expose the electroactive surface, where the corresponding membrane (either for working or for reference) was drop cast (Figure 8.1A). Further details of the electrode preparation have been described in the previous chapter.<sup>[31]</sup>

**Table 8.1.** Optimization of Nafion layers in paper-based electrodes.

3 mm Electrodes	Nafion + Enzyme + Nafion(μL)	2 mm Electrodes	Nafion + Enzyme + Nafion(μL)
Condition A	2 + 7.5 + 2	Condition a	1 + 5 + 1
Condition B	4.5 + 7.5 + 4.5	Condition b	2 + 5 + 2
Condition C	7 + 10 + 7	Condition c	3 + 5 + 3
Condition D	9 + 10 + 9	Condition d	4.5 + 5 + 4.5

The working electrode was built in three steps: first, a volume of the Nafion solution was drop cast and dried at room temperature for one hour; second, 10 μL of a 20 mg·mL<sup>-1</sup> solution of glucose oxidase (GOx) were cast on top of the Nafion membrane and let it dry overnight at 4°C; third, a volume of the Nafion solution was cast on top of enzyme and let it dry overnight at 4°C. Volumes of 2, 4.5, 7 and 9 μL of the Nafion solution were selected for the optimization. Two different sizes of electrodes with diameters of 3 mm (larger) and 2 mm (smallest) were evaluated. In each case, for the two additions, the volume was kept the same, i.e. 2 μL for the

first and the second layer of Nafion for instance (see Table 8.1). The experiments were performed with three sensors (SD, N=3).

For the reference electrode,<sup>[26]</sup> a total of 9  $\mu\text{L}$  of a reference membrane consisting of 78 mg PVB and 50 mg NaCl in 1 mL of methanol was drop-cast (3 aliquots of 3  $\mu\text{L}$  each, with 10 min drying at room temperature in between) and kept drying overnight. Thereafter, a first (and only) conditioning step of 8 h in 3 M KCl left the reference electrode ready for use.

To build the miniaturised cell (Figure 8.1B), the enzymatic sensor was placed in between the sampling cell and connected to the measuring device through the conductive ends. This cell was kept at 4°C when not in use. The sampling cell was designed and optimised for a sample volume of 25  $\mu\text{L}$ . This sampling module is made first with a plastic mask to accommodate working and reference electrodes (Figure 8.1Ba). Two strips made of hydrophilic plastic material were placed at the end of the sensor to facilitate sample flow (Figure 8.1Bb). Then, two plastic masks were placed around the electrodes to develop the sampling channel (Figure 8.1Bc). Finally, a strip of hydrophilic plastic was placed on top of the sampling cell closing the microfluidic system (Figure 8.1Bd). The last hydrophilic plastic was stacked with the plastic mask. The potentiometric cell integrated into sampling cell had a size of 20 x 25 mm. Solution samples were placed in one entry and let it flow inside the channel driven by capillary forces. It is worth to mention that the hydrophilic plastic improved the transport of the fluid through the sampling cell as well as the easy washing of the cell.

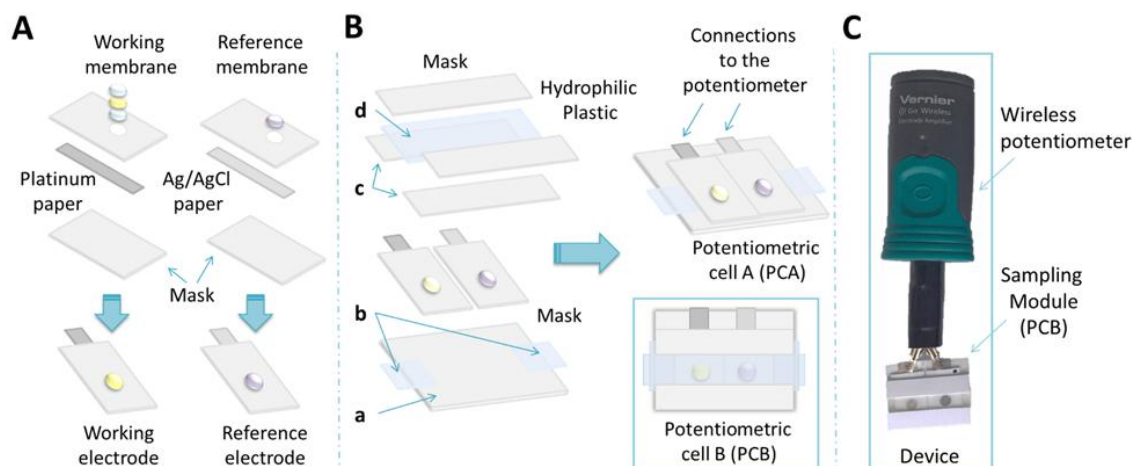


**Figure 8.1.** (A) Scheme for the construction of the working and the reference electrodes. (B) Integration of both electrode into a sensor (potentiometric cell A, PCA) and with the sampling module (PCB). (C) Picture of the device containing the sensor as sampling cell and the wireless potentiometer.

## 8.3. RESULTS AND DISCUSSION

### 8.3.1. Optimization of the potentiometric sensor

The detection of glucose is based on monitoring the change of the mixed potential produced by the enzymatic reaction. Traditionally, Pt electrodes have been used to monitor the change on the redox potential of a solution, which can be produced by any redox-active substance (hydrogen peroxide among them). Thus, if a bare Pt electrode is used, the detection of the peroxide ( $H_2O_2$ ) generated by the enzymatic reaction would be interfered by any other redox substance in the sample. In a previous work, however, it was demonstrated that when Pt electrodes are coated with a layer of Nafion, the selectivity towards peroxide is significantly enhanced, while a considerable increment on the sensitivity is observed.<sup>[30]</sup> The platinised paper acts as a redox-sensitive surface, while the layer Nafion has a double role: it enhances the sensitivity of the detection and it increases the selectivity by restricting the effect of redox-active anions.<sup>[31]</sup> This enhanced selectivity is due to the negatively charged nature of Nafion, which acts as a permselective barrier against interference of anions such as ascorbate and urate, i.e., typical redox-active species found in biological media. It has been shown that the improvement in sensitivity is linked to the Donnan potential, which is generated because of the ion-exchange capacity of Nafion.<sup>[33,34]</sup> This phenomena, however, is rather complex and several works have been devoted to characterize and understand the coupling between the redox (mixed) and Donnan potentials of this system.<sup>[35,36]</sup> In any case, this approach provides a very simple, sensitive and selective way to detect peroxide. In this case, a single enzyme and no additional reagents are required. Clearly all the advantages mentioned are due to the coating of Nafion. Therefore, in order to gain further insights and optimize the response of the system, the influence of the thickness and casting of the Nafion layer on both, the sensitivity and selectivity of the sensor, was assessed.

Figure 8.2 shows that all the curves follow the same pattern, with a growing offset in potential at higher concentrations. In general, it can be concluded that there is a difference in the shape of the calibration plot when peroxide is generated via enzymatic reaction or when is added externally, an also when peroxide is added externally to an enzyme-free electrode. Evidently, more work needs to be done to assess the degree of conversion of the glucose, the transport of the reaction byproduct (peroxide) through the Nafion and the response of Pt under these conditions. It is true that the linear range is limited, and -in the case of the current application- it should (ideally) be shifted towards higher concentrations to avoid dilutions. Regarding the reasons for this narrow limit, a first explanation from a redox point of view could be that at high concentrations of one of the redox species the system will buffer itself, setting

an upper limit to the change observed. But of course, more considerations need to be taken into account, this is just an approach. Elucidating the actual mechanism behind the signal enhancement will be fundamental to understand the factors that control the analytical parameters.

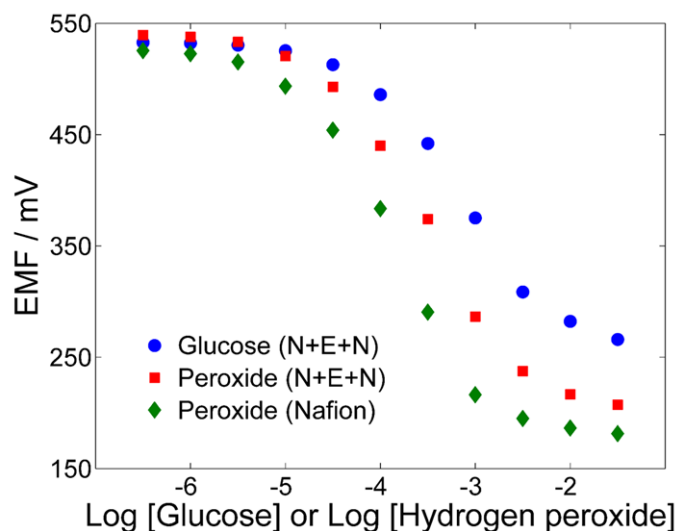


**Figure 8.2.** Comparison of the potentiometric response under different conditions. Blue dots: enzymatic sensor (Nafion || Enzyme || Nafion || Pt) with addition of glucose; Red squares: same enzymatic sensor, but no glucose and direct addition of hydrogen peroxide; Green diamonds: response of a Nafion-coated platinum electrode (i.e. no enzyme) with addition of hydrogen peroxide.

The construction of the electrode is based on the entrapment of the GOx, which is performed by drop-casting the Nafion in two consecutive steps. Thus, experiments were performed where an increasing volume of Nafion -from 2 to 9  $\mu\text{L}$ - was drop cast on the electrodes and the resulting sensitivity and interference from ascorbate were monitored (see Table 8.1). In all cases, a linear range from 0.3 – 3 mM of glucose (Figure 8.3A and Figure 8.4A) was obtained. The selectivity was measured by recording the change of electrode potential produced by the addition of ascorbic acid at 0.1 mM, which is usually considered the upper limit of the physiological levels in blood. The results are shown in Figure 8.3B. This approach is analogous to one of the most used methods to determine the selectivity coefficient of ion-selective electrodes, i.e. the fix interference method (FIM).<sup>[37,38]</sup>

Interestingly, the results displayed in Figure 8.3A show that increasing the amount of Nafion reduces the enhancement of the sensitivity. For example, the sensitivity (in  $\text{mV}\cdot\text{decade}^{-1}$ ) was reduced from -128.2 down to -76.7 when the volume of Nafion cast was increased from 2 to 9  $\mu\text{L}$  respectively. Since the electroactive area is constant, these results seem to suggest that the

thinner the layer of Nafion, the greater the increment on sensitivity. However, a clear explanation of these observations is still under study, since many interdependent factors have to be considered. First, the way in which the Nafion dries may have an effect on the structure of the membrane. Second, the response of this system results from a complex coupling between mixed potential of  $\text{H}_2\text{O}_2$  on the platinum electrode and the Donnan potential of the Nafion membrane. Thus, factors such as the local changes in pH, surface charges, etc., must be considered.

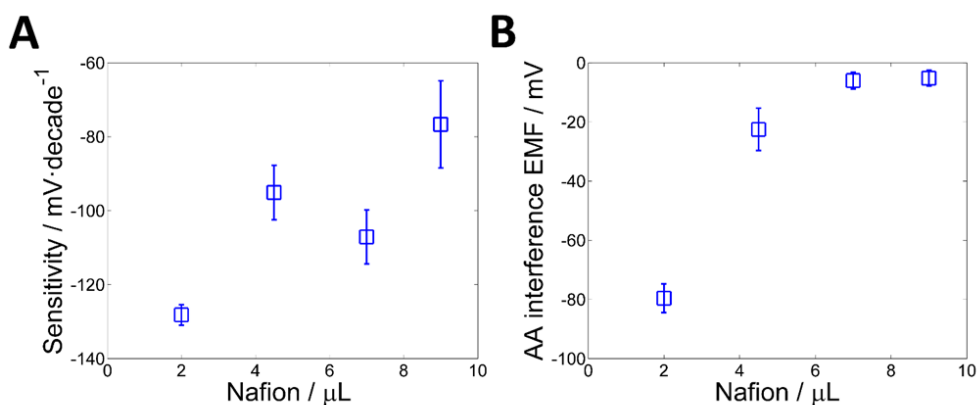


**Figure 8.3.** (A) Sensitivity of the working electrode versus the Nafion layer amount and (B) refers to the response to the main interferent (Ascorbic Acid: AA) vs. the amount of the Nafion layer (2, 4.5, 7 and 9 μL). N=3, three different sensors for each amount.

The effect of the amount of Nafion on the selectivity is shown in Figure 8.3B (and Figure 8.4B in the miniaturized cell). Unlike the sensitivity, the selectivity tends to increase as the amount of Nafion is increased. Although properties and structure of the Nafion are still a matter of study, it is well known that Nafion creates structures with negatively charged sulfonate groups in the sidechain forming nanopores, so that anionic molecules are unlikely to reach the electrode surface.<sup>[39,40]</sup> This permselective behaviour is further enhanced as the thickness of the Nafion layer is increased.<sup>[41-43]</sup> A maximum seems to be reached for a volume of membrane cast of approximately 7 μL, a point where a change of less than 5 mV is observed when the 0.1 mM ascorbate solution is added.

It is worth mentioning that the reproducibility between sensors is also affected by the amount of Nafion. In general, the greater the volume of Nafion, the larger the variation between sensors. This is probably due to the higher level of irreproducibility of the manual work.

Because of the compromise between sensitivity and selectivity, the optimal amount of Nafion cast was set in 7  $\mu\text{L}$ . Under these conditions, the working electrode exhibited a good sensitivity ( $-107.1 \pm 7.2 \text{ mV} \cdot \log[\text{Glucose}]^{-1}$ ,  $N=3$ ) in the linear range (0.3 – 3 mM) and reduced level of interference. The most relevant analytical parameters are summarised in Table 8.2.

It is well known that one of the key advantages of potentiometry is the possibility of miniaturization without affecting the analytical performance of the system. For this reason, experiments where the sensing area of the electrode was reduced in size were conducted. The results (Figure 8.4) are encouraging, since they show that the analytical parameters remain constant. However, a reduced window size (from 3 mm diameter to 2 mm diameter) increases the variability between electrodes, something that is most likely due to the error introduced by the manual deposition of the membranes.

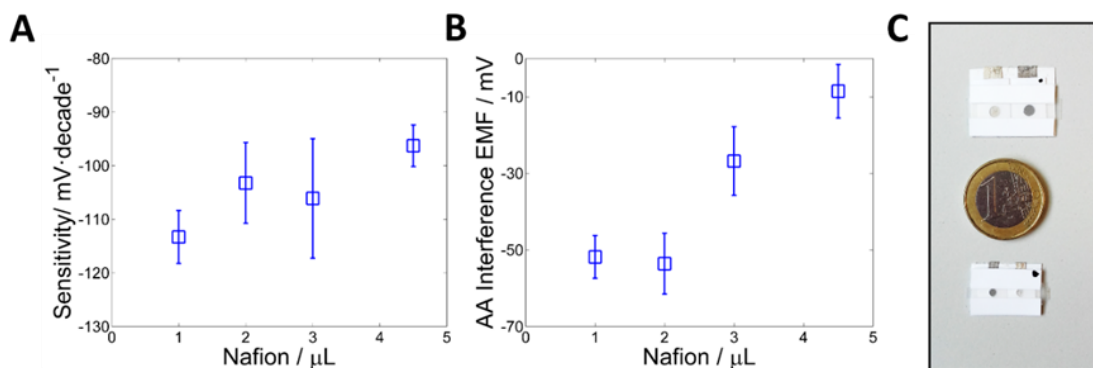


**Figure 8.4.** (A) Sensitivity of the working electrode vs. the amount of Nafion layer and (B) response to the main interferent ascorbic acid (AA) versus amount of the Nafion layer (1, 2, 3 and 4.5  $\mu\text{L}$ ). (C) Picture of the comparison in size of the devices with 3 mm (top) and 2 mm (bottom) diameter.

All in all, the results show that these electrodes provide a sensitive and selective method for the direct potentiometric determination of glucose, with an unrivalled simplicity of construction and operation. While the sensitivity is fairly reproducible, the electrodes show a shifted potential response, a limitation that requires a calibration step. This is likely to be due to the manual method used to cast the membrane, problem that can be minimized by using automated methods. A quick calculation of the cost of fabrication of the electrodes in the lab yields roughly 0.81 €/ working electrode, 0.09 €/ reference electrode and 1.05 €/sampling cell. This is, of course, a rough calculation that should be considered only as an upper limit to the cost, due to the off-the-shelf components and manual work. In terms of materials, the highest cost (so far) is due to the 100 nm Pt layer (a few micrograms) and the enzyme. Further optimization of the



redox-sensitive surface will certainly improve this factor. Therefore, what is more important than the actual costs is that the techniques employed are scalable at the mass manufacturing level, which means that cost could be reduced by several orders of magnitude.

**Table 8.2.** Total cost of making these electrodes in the lab based on platinized paper, GOx and Nafion.

Working electrode - Material (including service)	Price in euros (€)
3 Platinum paper (technician+process+room)→ 76 electrodes +(15€/100 filters)	$(145€/3+0.15)/76 = 0.64$
Glucose Oxidase ((0.3 gr/0.002 gr) x 10)=1500 electrodes)	$169€/1500 = 0.11$
Nafion® solution (25 mL/0.014 mL=1785.7 electrodes)	$115€/1785.7 = 0.06$
SubTotal	0.81 €/electrode
Reference electrode - Material (including service)	Price in euros (€)
Ag/AgCl paper ((200€ Ag/AgCl ink)/30 filter paper)+(15€/100 filters)	$(6.6*+0.15)/76 = 0.09$
*(price depends on the market price of silver)	
PVB membrane (39€/100g)→(0.078g/10 electrodes)	$0.39x0.0078 = 0.003$
SubTotal	0.093 €/electrode
Sampling cell - Material	Price in euros (€)
Plastic mask (roll of 10x0.15m)	$500€/5000 = 0.1$
Hydrophilic plastic	$350€/ 6000 = 0.05$
SubTotal	0.15 €/ cell
<b>Total</b>	<b>1.05 €/ device</b>

A brief optimization of the reference electrode (RE) was also carried out. The most important step here is the conditioning step due to the presence of salts in the polymeric membrane.<sup>[26]</sup> Figure 8.5A displays the time-trace curve of three different electrodes in different conditioning times in 3 M KCl: 0 h, 3 h and at least 24 hours. The analytical performance of this paper RE was assessed by adding increasing concentrations of salts and monitoring the potential against a commercial RE. Hence, a calibration curve from 0.1 mM to 100 mM in double-distilled water was performed. An ideal behavior was obtained after a one time conditioning in 3 M KCl solution for 24 hours. Under these experimental conditions, the RE exhibited less than  $0.14 \text{ mV}\cdot\text{decade}^{-1}$  and a long term stability of  $0.014 \text{ mV}\cdot\text{h}^{-1}$  were obtained for a period of about 14 hours (Figure 8.5C). This paper-based reference electrode showed an outstanding performance with almost no potentiometric response and high stability and was used in the following section. Noteworthy, the conditioning was only mandatory for the first time after fabrication, i.e. the electrodes could be dry stored and be ready for use afterwards.

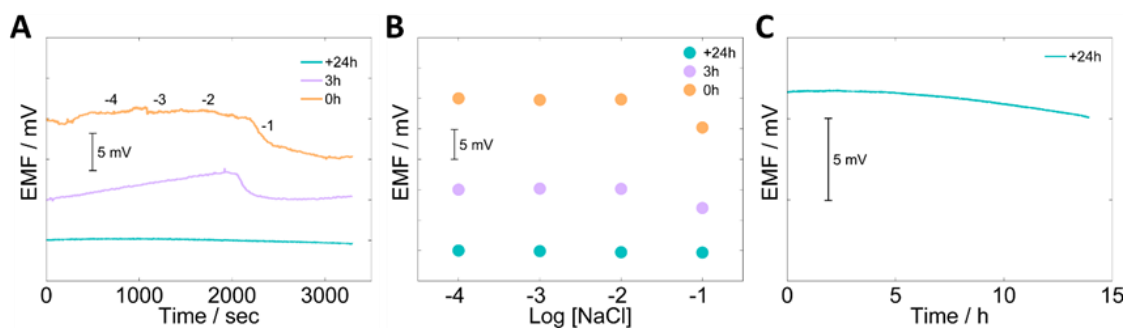


**Figure 8.5.** Comparison between three different conditioning steps of reference electrodes. (A) Time trace, (B) calibration plot -under three different conditions of conditioning: more than 24 hours (blue), only 3 hours (purple) and no conditioning (orange)- and (C) long term stability study for used references electrodes.

Finally, in order to assess the influence of the matrix, calibrations performed in artificial serum were compared with those made in PBS. A slight reduction in sensitivity (from  $-107.1 \pm 7.2$  to  $-90.4 \pm 4.9$  mV·decade<sup>-1</sup>) but similar linear ranges and LODs were found (Table 8.3, Figure 8.6). The time of response was also increased to approximately 60s, but this is acceptable for real scenarios. This difference in sensitivity could be related to the change in the background solution (from PBS to artificial serum) since it has been already shown that the response of these systems is influenced by the total concentration of ions. Fortunately, biological fluids such as serum or blood have a relatively constant ion concentration, which allows performing the determination of glucose with major problems.

**Table 8.3.** Analytical parameters of the working electrode and the potentiometric cells A and B.

Parameters	WE (PBS)	WE (Artificial Serum)	Potentiometric cell PCA (Artificial Serum)	Potentiometric cell PCB (Artificial Serum)
Sensitivity (mV·decade <sup>-1</sup> )	$-107.1 \pm 7.2$	$-90.4 \pm 4.9$	$-95.8 \pm 2.9$	$-95.9 \pm 4.8$
Linear Range (mM)	0.3 – 3	0.3 – 3	0.3 – 3	0.3 – 3
LOD (mM)	0.2	0.1	0.1	0.1
Response time (sec)	50	60	60	80

### 8.3.2. Analytical performance of the integrated devices (ID)

After their independent optimization, both working and reference electrodes were combined to build two potentiometric cells (PCA and PCB). In the first case (PCA) the electrodes were simply assembled together. In the second case (PCB), the electrodes were fitted with the

“sampling module”, an arrangement where a hydrophilic plastic mask is placed over the electrodes in order to create a channel that reduces the required measuring volume down to 25  $\mu\text{L}$  (Figure 8.1B). Figure 8.6 shows both, time-trace and calibration curves for glucose in artificial serum for all these system. In Figure 8.6A the individual time trace for the WE and RE separately, then for the PCA (in a 4 mL cell) and finally for the PCB (using only 25  $\mu\text{L}$  of solution) are shown. Figure 8.6B shows the corresponding calibration plots from 0.003 – 10 mM of glucose. The results are shown in Table 8.3. Hence, similar parameters were obtained after integration of the WE and RE compared to the commercial reference electrode.

These results show that the integration of the electrodes does not affect the performance of the sensors. Indeed, all the arrangements show a similar analytical performance. The most remarkable difference between the systems is the initial potential that makes the curves to be shifted by a constant value. Changes on the value of the reference electrode, as well as changes on the electrical characteristics of the cell will lead to this offset of the response, which is certainly not a problem if calibration is going to be performed. Also, a difference in the time-trace is observed for the PCB, i.e., when the electrodes are integrated in the miniaturized potentiometric cell. Likely, the incorporation of the sampling system might be altering the mass transport pattern and some electrical characteristics of the whole cell. For this reason, the response of PCB seems to be first dropping, and then taking slightly longer to stabilize. This time, however, it is not highly relevant from a practical point of view. Consequently, the system was validated using real sample.

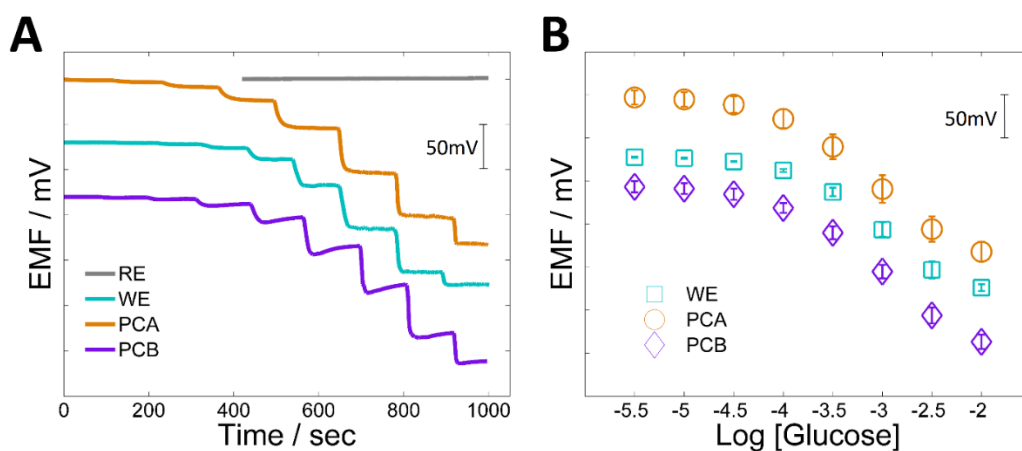


**Figure 8.6.** Potentiometric response of paper-based electrodes in artificial serum: (A) time trace and (B) corresponding calibration curves of paper-based reference electrodes, paper-based working electrodes (WE), and potentiometric cells A, PCA (in a 4 mL cell) and PCB (using only 25  $\mu\text{L}$  of solution).

### 8.3.3. Prediction of glucose in real samples

The validation of the PCB was carried out using 10 (real) serum samples provided by a local hospital from different patients (diabetic and non-diabetic). To begin, the device was calibrated with two standards of glucose of 0.3 – 3 mM in PBS with a 1:10 dilution of artificial serum, in order to simulate the conditions of real sample analysis. These two standards were chosen as they are the limits of the linear range of the sensor. Therefore, to monitor glucose in the physiological range of interest, a ten-fold dilution of the sample was required. After calibration, the cell was rinsed and then the dilution of the sample was added with a pipette until the whole sampling channel was filled (approximately 25  $\mu\text{L}$ ). After approximately 100s a steady-state signal was obtained. Thereafter, the sampling cell was rinsed thoroughly to remove any trace of the sample. The cleaning of the cell can be evaluated by checking that the open circuit potential returns to the initial value. This indicates that the system is ready to receive a new sample. This procedure, which was repeated using three different paper-based devices (Figure 8.7), allows measuring 5 samples in about 6 minutes, including the calibration curve, washing, etc. For each sample, the protocol would be reduced to a couple of minutes.

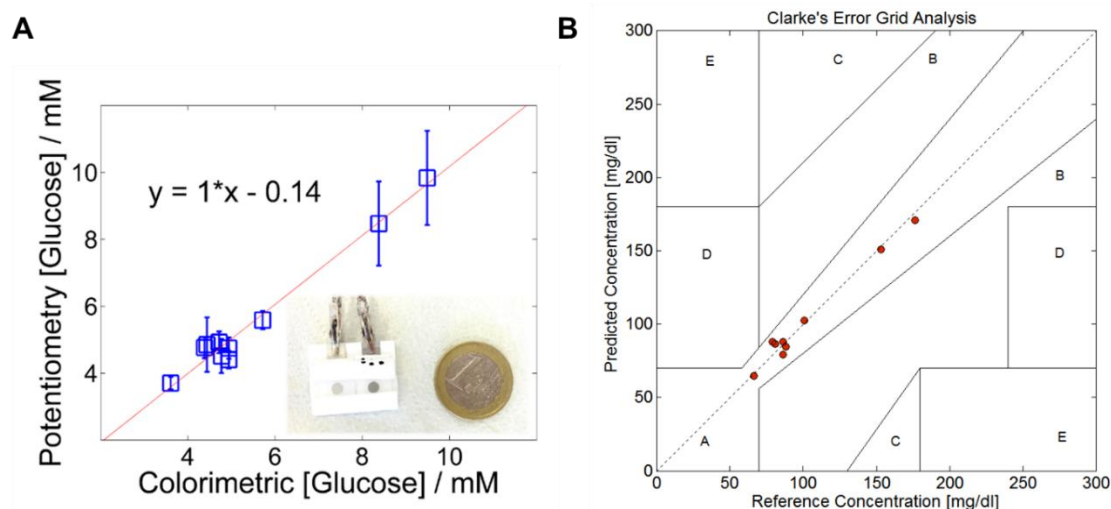


**Figure 8.7.** (A) Prediction of glucose concentrations (mM) in real serum samples determined by the enzymatic paper-based sensor -assembled in the sampling cell- (N=3) compared with conventional colorimetric technique (Standard lab-based technique). Inset illustrates the size comparison of the sensor. (B) Clarke plot proofs the reliability of the sensor.

Figure 8.7A shows the validation plot of the measurements using the PCB vs. the values of glucose measured in the clinical lab of the hospital using the standard method

hexokinase/glucose-6-phosphate dehydrogenase assay. These results show an encouraging correlation between the two methods (Table 8.4). An average recovery of 100.7% (RSD 6.3, N= 10) was obtained, confirming the ability of the PCB to accurately monitor glucose in serum. Nevertheless, at high concentrations the precision is reduced and we are currently exploring this point. Figure 8.7B displays the values obtained in the validation in a standard Clarke error grid. This plot shows that all values are within zone A showing that the methodology is accurate enough to measure in blood samples for diabetes management.<sup>[44-47]</sup>

**Table 8.4.** Comparison between concentrations: Potentiometry method vs. Hospital provided values of glucose in 10 real serum samples.

Potentiometry [Glucose] / mM	H-6-G-PD Hospital	Recovery / %
9.8 ± 1.4	9.5	103.6
4.8 ± 0.8	4.4	109.2
3.7 ± 0.2	3.6	102.5
5.6 ± 0.3	5.7	97.7
4.9 ± 0.3	4.7	104.3
4.5 ± 0.5	4.8	94.5
4.4 ± 0.3	4.9	89.1
4.8 ± 0.3	4.9	96.1
8.5 ± 1.3	8.4	101.1
4.8 ± 0.3	4.4	108.6

### 8.3.4. Instrumental advantages and future prospects

A simple and low cost sensor for glucose is only the first part. Instrumental aspects are also crucial when aiming to provide real solutions in decentralized settings with scarcity of resources. In this situation, potentiometry also offers significant advantages. From an electronic perspective, potentiometry requires extremely simple components, which makes the system cheap and less prone to noise and interferences. This is particularly relevant when dealing with systems that -following current trends in decentralized devices- have to be wirelessly connected to a central system where data can be uploaded. Furthermore, the overwhelming simplicity of operation makes the system easy to use with minimal training or expertise. To prove this point, a complete integration and miniaturization of the system was accomplished by using a high input impedance voltmeter with a Bluetooth data transmission system connected to a conventional smartphone. In this way, this kind of devices should facilitate the remote management of chronic conditions, such as diabetes.

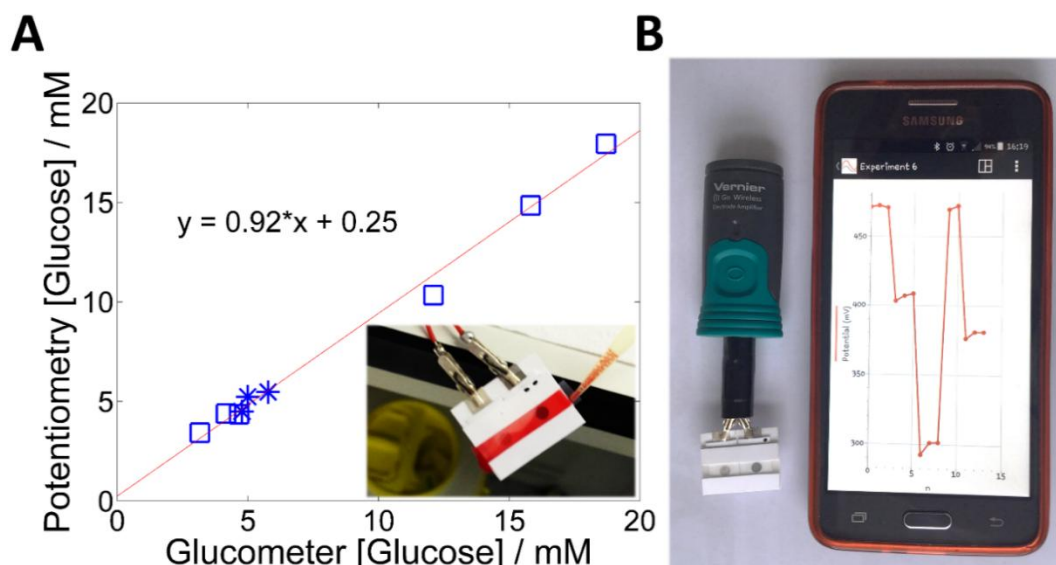


**Figure 8.8.** (A) Prediction of glucose concentrations (mM) for six (■)serum samples and three (✱) whole blood samples determined by the wireless potentiometric device vs. a commercial (amperometric) glucometer. (B) Picture showing the wireless device connected to PCB and the screen showing the results of the two-point calibration, washing and sample measurement.

Figure 8.8 demonstrates the proof of concept of a PCB connected to a portable wireless data transmission device. The cell phone illustrates the time-trace plot performed by the whole sensor system for one complete measurement including a two-points calibration, washing and sample measurement (Figure 8.8B). Data was recorded wirelessly by Bluetooth® with the corresponding cell phone application and real-time plot it in the screen. Calibration curve yielded a linear relationship with a slope of  $-118 \text{ mV} \cdot \log[\text{glucose}]^{-1}$  over the 0.3 – 3 mM range.

The wireless system was also validated with whole blood and serum samples from diabetic patients, using the same protocol described above for PCB, i.e., using a ten-fold dilution of the samples in PBS. Figure 8.8A shows the comparison between the wireless potentiometric system and a well-extended point-of-care (POC) method, a commercially available glucometer. Potentiometry and amperometry techniques were indeed compared. Here, the glucometer did not require calibration nor dilution. An encouraging result was obtained using the potentiometric system and the standard POC device. Moreover, Table 8.5 indicates the recovery of each sample giving an average of 97.3 (RSD 7.3, N= 9). Hence, validation using blood and serum samples demonstrated the proof of principle of the low-cost diagnostics device.

**Table 8.5.** Comparison of glucose levels: Potentiometry vs. commercial glucometer for six serum and three blood samples.

Potentiometry [Glucose] / mM	Glucometer	Recovery / %
Blood: 4.5	4.8	94.2
Blood: 5.2	5.0	104.8
Blood: 5.5	5.8	94.9
Serum: 3.4	3.2	108.4
Serum: 4.4	4.2	105.4
Serum: 4.4	4.7	93.3
Serum: 14.9	15.8	93.9
Serum: 10.3	12.1	85.4
Serum: 17.9	18.7	95.9

## 8.4. CONCLUSIONS

A simple, robust, low-cost and fully integrated potentiometric device for the determination of glucose in human serum and whole blood has been presented in this chapter. The use of paper as substrate for building the potentiometric cell combined with the Pt/Nafion interface provides a highly convenient way to detect the peroxide generated by the enzymatic reaction. Furthermore, the incorporation of a sample introduction channel facilitates the miniaturization of the system in order to reduce the volume of sample required. Finally, with the use of a simple electronic instrumentation, the wireless collection of data is possible. This portable system was validated against the standard lab-based methodologies as well as the standard point-of-care glucometer, confirming that this new platform could become a valuable tool in the growing fields of telemedicine and point-of-care.

There are still many technological issues to be faced. From one side, current work is being focused on the control of the sensitivity and linear ranges of the system, in order to avoid dilutions or any other manipulation of the sample. Additionally, the work on the reproducibility of the sensor manufacturing should allow the minimization (or even elimination) of the calibration steps.<sup>[48,49]</sup> Finally, the extension of this approach to other oxidase-type enzymes open a new and exciting avenue for the development of low-cost, simple and robust platforms for decentralized biochemical analysis.<sup>[50,51]</sup>

## 8.5. REFERENCES

- [1] E. Nolte, C. Knai, M. McKee, Managing chronic conditions. Experience in eight countries, Obs. Stud. Ser. N°15, **2008**, ISBN 978 92 890 4294 9.
- [2] S. Nayak, N. R. Blumenfeld, T. Laksanasopin, S. K. Sia, *Anal. Chem.*, **2016**, *89*, 102.
- [3] A. J. Bandonkar, I. Jeerapan, J. Wang, *ACS Sensors*, **2016**, *1*, 464.
- [4] J. L. Monteagudo, C. H. Salvador, L. Kun, *Health Technol. (Berl.)*, **2014**, *4*, 79.

- [5] N. P. Pai, C. Vadnais, C. Denkinge, N. Engel, M. Pai, *PLOS Med.*, **2012**, 9, 1.
- [6] A. Nemiroski, D. C. Christodouleas, J. W. Hennek, A. A. Kumar, E. J. Maxwell, M. T. Fernández-Abedul, G. M. Whitesides, *Proc. Natl. Acad. Sci.*, **2014**, 111, 1.
- [7] D. E. Goldstein, R. R. Little, R. a. Lorenz, J. I. Malone, D. Nathan, C. M. Peterson, D. B. Sacks, *Diabetes Care*, **2004**, 27, 1761.
- [8] J. C. N. Chan, R. Y. M. Wong, C. K. Cheung, P. Lam, C. C. Chow, V. T. F. Yeung, E. C. Y. Kan, K. M. Loo, M. Y. L. Mong, C. S. Cockram, *Diabetes Res. Clin. Pract.*, **1997**, 36, 91.
- [9] B. Solnica, J. W. Naskalski, J. Sieradzki, *Clin. Chim. Acta*, **2003**, 331, 29.
- [10] E. J. Maxwell, A. D. Mazzeo, G. M. Whitesides, *MRS Bull.*, **2013**, 38, 309.
- [11] J. E. Shaw, R. A. Sicree, P. Z. Zimmet, *Diabetes Res. Clin. Pract.*, **2010**, 87, 4.
- [12] H. King, R. E. Aubert, W. H. Herman, *Diabetes Care*, **1998**, 21, 1414–1431.
- [13] S. K. Vashist, *Anal. Chim. Acta*, **2012**, 750, 16.
- [14] C. McCormick, D. Heath, P. Connolly, *Sensors Actuators, B Chem.*, **2012**, 166, 593.
- [15] A. W. Martinez, S. T. Phillips, M. J. Butte, G. M. Whitesides, *Angew. Chem. Int. Ed. Engl.*, **2007**, 46, 1318.
- [16] J. L. Delaney, C. F. Hogan, J. Tian, W. Shen, *Anal. Chem.*, **2011**, 83, 1300.
- [17] S. Chen, Q. Wan, A. K. Badu-Tawiah, *J. Am. Chem. Soc.*, **2016**, 138, 6356.
- [18] Z. Nie, C. A. Nijhuis, J. Gong, X. Chen, A. Kumachev, A. W. Martinez, M. Narovlyansky, G. M. Whitesides, *Lab Chip*, **2010**, 10, 477.
- [19] V. F. Curto, N. Lopez-Ruiz, L. F. Capitan-Vallvey, A. J. Palma, F. Benito-Lopez, D. Diamond, *RSC Adv.*, **2013**, 3, 18811.
- [20] S. N. Tan, L. Ge, H. Y. Tan, W. K. Loke, J. Gao, W. Wang, *Anal. Chem.*, **2012**, 84, 10071.
- [21] C. Desmet, C. A. Marquette, L. J. Blum, B. Doumèche, *Biosens. Bioelectron.*, **2016**, 76, 145.
- [22] D. M. Cate, J. A. Adkins, J. Mettakoonpitak, C. S. Henry, *Anal. Chem.*, **2015**, 87, 19.
- [23] J. Mettakoonpitak, K. Boehle, S. Nantaphol, P. Teengam, J. A. Adkins, M. Srisa-Art, C. S. Henry, *Electroanalysis*, **2016**, 28, 1420.
- [24] W. Dungchai, O. Chailapakul, C. S. Henry, *Anal. Chem.*, **2009**, 81, 5821.
- [25] M. Novell, M. Parrilla, G. a. Crespo, F. X. Rius, F. J. Andrade, *Anal. Chem.*, **2012**, 84, 4695.
- [26] T. Guinovart, G. A. Crespo, F. X. Rius, F. J. Andrade, *Anal. Chim. Acta*, **2014**, 821, 72.
- [27] M. Novell, T. Guinovart, P. Blondeau, F. X. Rius, F. J. Andrade, *Lab Chip*, **2014**, 14, 1308.
- [28] M. Willander, K. Khun, Z. H. Iupoto, *Sensors (Switzerland)*, **2014**, 14, 8605.
- [29] M. H. Asif, B. Danielsson, M. Willander, *Sensors*, **2015**, 15, 11787.
- [30] M. Parrilla, R. Cánovas, F. J. Andrade, *Electroanalysis*, **2017**, 29 (1), 223.
- [31] M. Parrilla, R. Cánovas, F. J. Andrade, *Biosens. Bioelectron.*, **2017**, 90, 110.



- [32] K. Kimura, H. Oishi, T. Miura and T. Shono, *Anal. Chem.*, **1987**, *59*, 2331.
- [33] R. Das, G. H. Pollack, *Am. Chem. Soc.*, **2013**, *29*, 2651.
- [34] K. Kanamura, H. Morikawa, T. Umegaki, *J. Electrochem. Soc.*, **2003**, *150*, 193.
- [35] R. Naegeli, J. Redepenning, F. C. Anson, *J. Phys. Chem.*, **1986**, *90*, 6227.
- [36] E. J. Calvo, A. Wolosiuk, *J. Am. Chem. Soc.*, **2002**, *124*, 8490.
- [37] E. Bakker, E. Pretsch, P. Bühlmann, *Anal. Chem.*, **2000**, *72*, 1127.
- [38] E. Bakker, *Electroanalysis*, **1997**, *9*, 7.
- [39] K. A. Mauritz, R. B. Moore, *Chem. Rev.*, **2004**, *104*, 4535.
- [40] K. Schmidt-Rohr, Q. Chen, *Nat. Mater.*, **2008**, *7*, 75.
- [41] B. D. Bath, H. S. White, E. R. Scott, *Anal. Chem.*, **2000**, *72*, 433.
- [42] E. J. Calvo, A. Wolosiuk, *J. Am. Chem. Soc.*, **2002**, *124*, 8490.
- [43] M. A. Izquierdo-Gil, V. M. Barragán, J. P. G. Villaluenga, M. P. Godino, *Chem. Eng. Sci.*, **2012**, *72*, 1.
- [44] A. Maran *et al.*, *Diabetes Care*. **2002**, *25*, 2.
- [45] B.P. Kovatchev *et al.* *Diabetes Care*. **2004**, *27*, 8.
- [46] E. Guevara, F. J. Gonzalez, Medical Physics: Tenth Mexican Symposium on Medical Physics. **2008**, *1032*, 259261.
- [47] E. Guevara, F. J. Gonzalez, *Journal of Mexican Chemistry*. **2010**, *56*, (5), 430434.
- [48] X. U. Zou, X. V Zhen, J. H. Cheong, P. Bühlmann, *Anal. Chem.*, **2014**, *86*, 8687.
- [49] U. Vanamo, J. Bobacka, *Anal. Chem.*, **2014**, *86*, 10540.
- [50] E. Witkowska Nery, M. Kundys, P. S. Jeleń, M. Jönsson-Niedziółka, *Anal. Chem.*, **2016**, *88*, 11271.
- [51] H. Lee, T. K. Choi, Y. B. Lee, H. R. Cho, R. Ghaffari, L. Wang, H. J. Choi, T. D. Chung, N. Lu, T. Hyeon, S. H. Choi, D. H. Kim, *Nat. Nanotechnol.*, **2016**, *11*, 566.

# NEW ADVANCEMENTS IN THE DEVELOPMENT OF POTENTIOMETRIC BIOSENSORS

---

---



UNIVERSITAT ROVIRA I VIRGILI

TAILOR-MADE CHEMICAL SENSING PLATFORMS FOR DECENTRALIZED HEALTHCARE AND WELLBEING

Rocío Cánovas Martínez

Despite the number of advantages and achievements presented in the previous chapters, the enzyme-based potentiometric sensors show also some limitations. Thus, in order to continue the search for improvements and adaptations of this technology to better address social needs, this chapter describes some experimental approaches that improve the response of these biosensors. In the first part, a novel procedure to create an alternative redox-sensitive substrate is presented in order to decrease the cost of the platform, thus making the device more affordable. Hence, as a proof of concept, sensors with ability to detect hydrogen peroxide ( $H_2O_2$ ) were built using platinum nanoparticles (PtNPs) deposited on a commercial carbon ink in paper substrate. Second, a novel strategy to develop a potentiometric biosensor for the direct detection of glucose in blood without any pretreatment (such as dilution) is presented. This approach is based in a similar mechanism previously reported,<sup>[1-3]</sup> although using a different polyelectrolyte coating that confers interesting features to the biosensor. Thereafter, general conclusions regarding the benefits, limitations and horizons of these biosensors as analytical platforms are presented.

## 9.1. INTRODUCTION

The growing demand for tools to generate chemical information in decentralized settings is creating a vast range of opportunities for potentiometric sensors, since their combination of robustness, simplicity of operation and cost can hardly be rivalled by any other technique.<sup>[4]</sup> In this chapter, approaches to improve the detection scheme and future applications for the development of ultra-low-cost biosensors have being studied. Factors affecting the generation of the signal and the principle of detection are also discussed.

Biosensing technologies have grown from a small niche activity back in the 1980s into a major worldwide industry. Nowadays, biological sensing is a fundamental tool for understanding living systems, performing diagnostics, etc. For this reason, it has useful applications in different fields such as medicine, drug discovery, food safety, environmental monitoring, defense and personal security, among many others.<sup>[5]</sup> Biosensors based on nanomaterials have widespread potential in applications for medical diagnostics and environmental monitoring due to their sensitivity, specificity, speed of response, simplicity and cost-effectiveness.<sup>[6]</sup> The applicability of the biosensors is rich and versatile, nanostructures for the construction of biosensors are widely used.<sup>[7]</sup> Besides, the construction of these biosensors on platforms such as paper will result in simple, portable and low-cost devices.<sup>[8-10]</sup> making possible their extension to diagnostics in poor regions of the planet, remote locations, refugees camps, etc.<sup>[11,12]</sup>

However, to make this possible, biosensors have still many technological challenges to be faced, with affordability and user-friendliness on the top of this list. In an attempt to solve these issues two different approaches were followed. First, as an attempt to decrease the cost of the sensors, an alternative substrate was evaluated. Second, the use of a different polymeric matrix was employed as a way to tune the sensor's response. As a result, the need for an initial dilution step was eliminated, thus simplifying the sensor manipulation by the end user. As it has been explained previously (Chapters 6, 7 and 8)  $\text{H}_2\text{O}_2$  is one of the most important byproducts generated by the oxidase enzymes. For this reason, finding alternative substrates that are redox sensitive is crucial for the development of new, simpler, more affordable and efficient biosensors.<sup>[13,14]</sup> How can this problem be addressed? A part of the sensor with significant contribution to the overall cost is the substrate, which is composed of paper with a platinum coating. Reductions on the cost of the substrate may help to expand the reach to new users.<sup>[15-17]</sup> The main limitation at this point would be the price of the platinum sputtering, even considering that in a macroscale production the final cost of the manufacturing is limited. Nevertheless, as a scientist that strives solving society issues, it is important to open avenues for continuously improving the affordability of these devices.<sup>[18,19]</sup> In this way, the generalized use of these tools may lead to a truly democratization of the technology. From a technological point of view, the use of alternative substrates that can avoid the sputtering process might affect the performance of the sensors. Hence, a careful exploration of the effect of the new substrates on the analytical performance of the system must be performed. Thus, the final evaluation of the usefulness of the change can not be considered only based on the analytical figures of merit, but also on all the practical implications of the change, including some advantages, such as an improved manufacturing process and increased versatility of the platform.

In order to find substrates with enhanced properties, some researchers have used nanostructures based on ZnO (a growing field of research due to their attractive chemical properties).<sup>[20]</sup> Other studies have compared three kinds of metal nanostructures: gold, copper, and platinum as catalysts for electrochemical oxidation of  $\text{H}_2\text{O}_2$  showing that platinum nanoflakes decorated electrode promoted a better sensitivity and detection limit for the target by providing favorable microenvironment to retain the bioactivity of the enzyme.<sup>[21]</sup> For these reasons and due to its relationship with  $\text{H}_2\text{O}_2$ ,<sup>[22-24]</sup> the generation of PtNPs over a carbon surface was chosen for this work, since it offers significantly lower fabrication costs when compared to other nanotechnology-based approaches.

On the other hand, improving the simplicity of the sensor can also expand the use of this tool. On-site detection of the analyte of interest in a rapid and sensitive way without a need for sophisticated equipment or skilled personnel is extremely important in clinical settings as well

as in resource-limited settings.<sup>[25]</sup> By simplifying the detection approach, a larger number of users can be reached. Despite the importance of diabetes, the development of glucose sensors<sup>[26]</sup> is often related to the low cost of the enzyme as well as its non-toxicity and easy handling. In this way, glucose serves as a model analyte to present novel electrode modification methods.<sup>[27]</sup> As in our previous biosensors, a dilution was needed for the potentiometric detection of glucose; an exploration of different polymers (e.g. polyelectrolytes) were performed in order to find the suitable polymer that fits the analytical requirements of glucose detection.

Overall, this chapter is divided in two sections that will present two lines of development. First, in part 1, the goal of finding alternative and redox-sensitive substrates for the development of potentiometric biosensors is followed. Second, in part 2, in an attempt to simplify the sampling procedure, a new approach for the development of an enzyme-based potentiometric paper sensor with ability to measure glucose in whole blood is also described. The detection of glucose is presented as a proof-of-principle for the extension of such sensors to other analytes. Ideally, the final step would be the integration of different enzymes in this new alternatives substrates and matrices.

## **9.2. PART 1: Exploring alternatives redox-sensitive substrates**

### **9.2.1. Experimental**

#### **9.2.1.1. Reagens and materials**

Chloroplatinic acid ( $\text{H}_2\text{PtCl}_6 \cdot 6\text{H}_2\text{O}$ ) as well as sulfuric acid ( $\text{H}_2\text{SO}_4$ ) were obtained from Sigma-Aldrich. Phosphate buffered saline (PBS) was prepared at 0.1 M with 0.138 M NaCl and used in all the experiments. The sensor components and assembly are similar to what has been already described.

#### **9.2.1.2. Preparation of the redox-sensitive substrates**

There are several methods to create redox-sensitive substrates. Platinum is a very good catalyst and redox-sensitive metal, and for this reason was used along this thesis, since it provides good sensitivity to  $\text{H}_2\text{O}_2$ . Thus, following current trends in nanotechnology, the decoration of different types of substrates with Platinum nanoparticles (PtNPs) was carried out. The synthetic route followed in this case is the electrodeposition of PtNPs, which is described elsewhere.<sup>[28–31]</sup>

To do this, a  $\text{H}_2\text{PtCl}_6$  stock solution using chloroplatinic acid ( $\text{H}_2\text{PtCl}_6 \cdot 6\text{H}_2\text{O}$ ) was prepared in order to perform PtNP electrodeposition experiments. Electrodeposition of platinum on different

electrode materials was carried out in an electroplating bath. The composition of the bath consisted of 1.3 mM  $\text{H}_2\text{PtCl}_6$  and 0.5 M  $\text{H}_2\text{SO}_4$ , making a total volume of 10 mL. The electrode was immersed in the plating bath and a constant potential of -0.25 V was applied for 5 min under gentle stirring condition.<sup>[32]</sup>

Figure 9.1 shows the general scheme of the electrodeposition method, which consists in a chronoamperometric approach. The metal media dissolved in the electrolytic solution are reduced at the interface between the solution and the cathode.

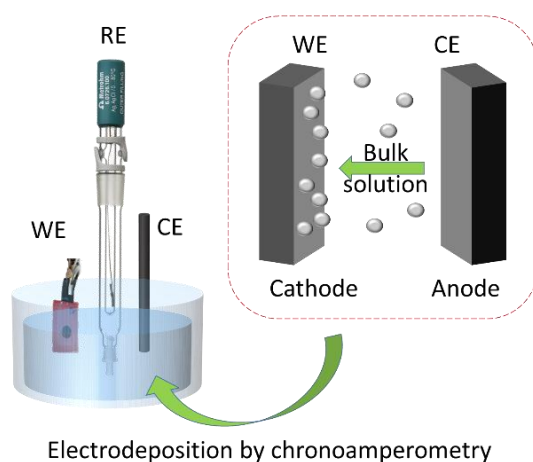


**Figure 9.1.** Scheme of the electrodeposition process where the platinum salt that is present in the bulk solution is reduced on the working electrode (WE) surface.

### 9.2.1.3. Electrochemical measurements

Cyclic voltagrams were recorded in the -0.1 V to 0.5 V potential range with a scan rate of  $0.1 \text{ V}\cdot\text{s}^{-1}$ . The electrode area is  $6.16 \text{ mm}^2$ . The electrolyte redox probe consisted of ferro/ferricyanide 10 mM. Electromotive force (EMF) measurements were performed at room temperature ( $25^\circ\text{C}$ ) with a high input impedance ( $10^{15} \Omega$ ) potentiometer, as described in Chapter 3. Laboratory measurements were made using a 4 mL cell in 0.1 M PBS with a physiological pH of 7.4, at  $25^\circ\text{C}$ .

## **9.2.2. Results and Discussion**

### 9.2.2.1. Characterization of the Pt-NPs

After the electrodeposition the characterization and verification of the material deposited on the surface of the electrodes was performed using different techniques.

Electrodeposition experiments were carried out in four different type of substrates: (i) CNT paper-based electrodes; (ii) glassy carbon (GC) electrodes; (iii) carbon ink rubber-based electrodes and (iv) carbon ink paper-based electrodes.

Cyclic voltammetry was used to verify the electrodeposition by evaluating the peak current of species that are oxidized or reduced. When the PtNPs are deposited, an increment in the redox peaks is observed due to the catalytic enhancement produced by the Pt. Figure 9.2 displays the cyclic voltagrams (CVs) before and after electrodeposition, showing bigger areas after deposition. The electrochemical behavior depends on the nature of the substrate as it can be appreciated in CVs. Overall, the electrodeposition step allows to increase the redox feature of all types of electrodes.

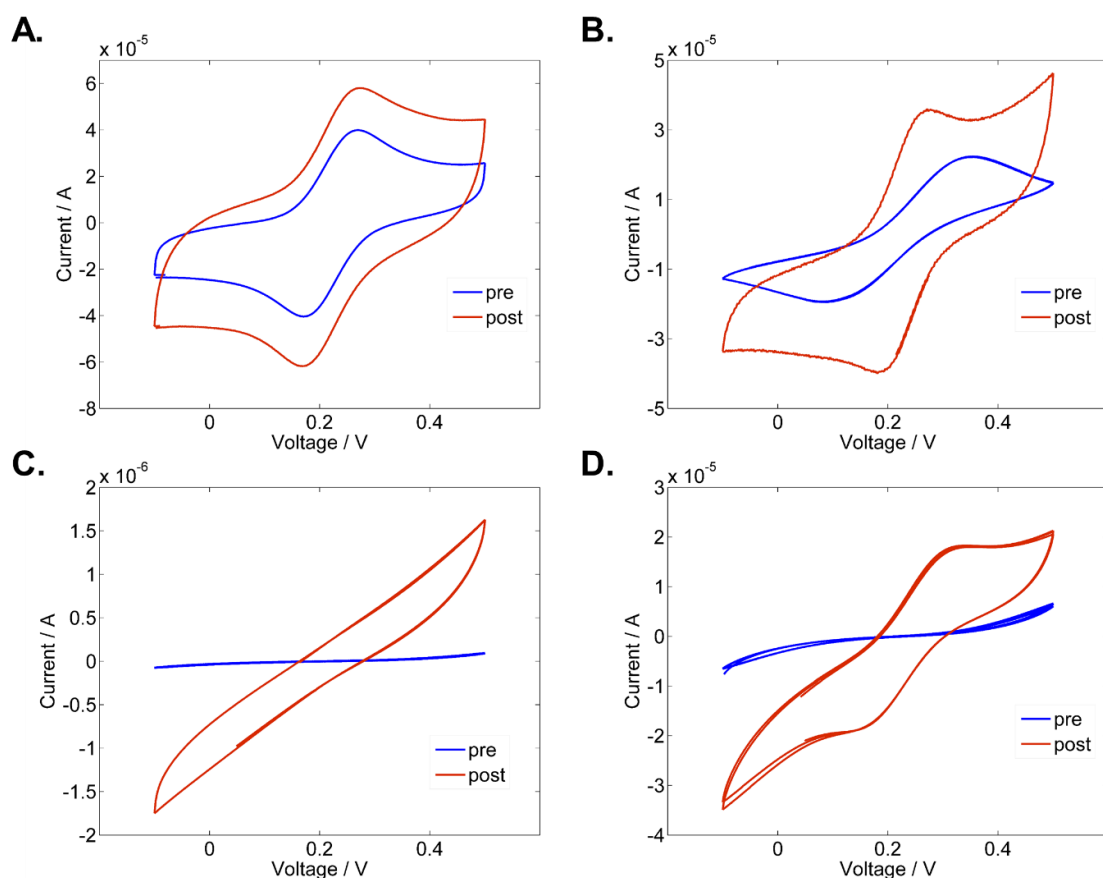


**Figure 9.2.** Cyclic voltagrams obtained before (in blue) and after (in red) of Pt-NPs electrodeposition in four different substrates: (A) CNT paper-based electrodes; (B) glassy carbon -GC- electrodes; (C) carbon ink rubber-based electrodes and (D) carbon ink paper-based electrodes.



Environmental scanning electron microscope (ESEM) was used to check if the electrodeposition was effective. Figure 9.3 exhibits different types of particles with different morphologies and sizes depending on the material and substrate. Some formations and clusters were obtained on top of CNT-paper substrate whereas a very low density of Pt-NPs were observed on the carbon ink-rubber electrodes.

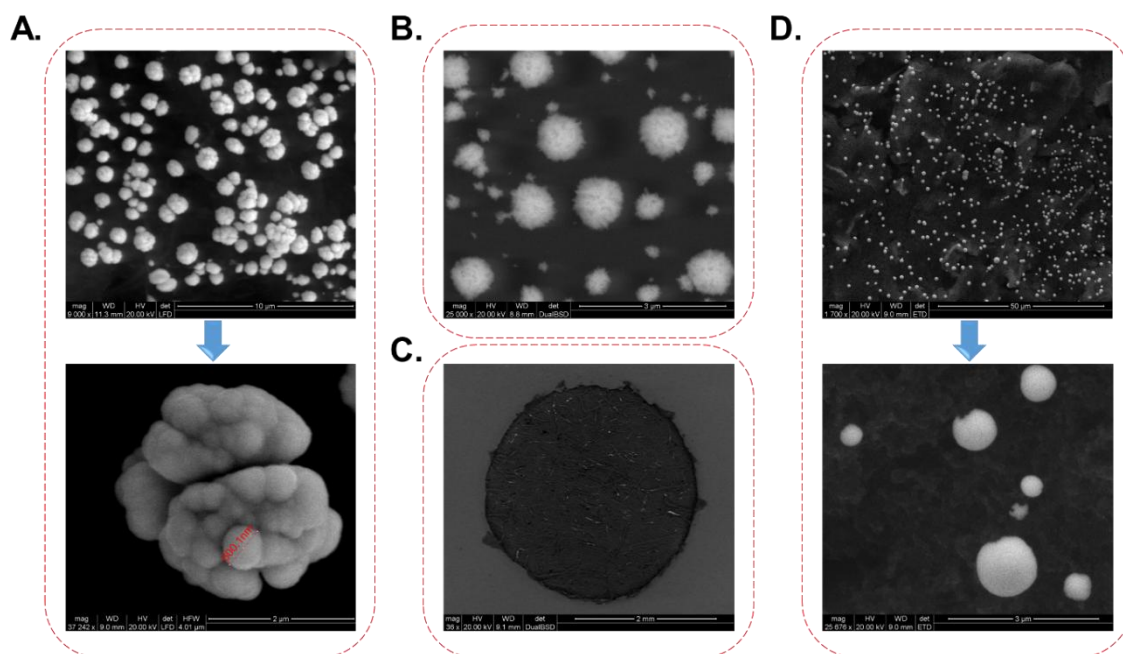


**Figure 9.3.** ESEM images of the shape and size of Pt particles created in four different substrates (A) CNT paper-based electrodes; (B) glassy carbon -GC- electrodes; (C) carbon ink rubber-based electrodes and (D) carbon ink paper-based electrodes.

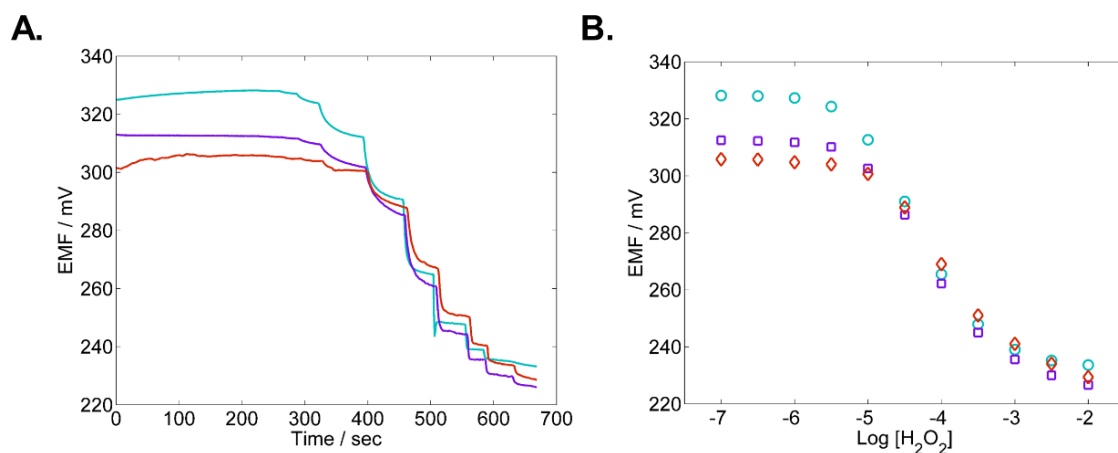
The electrodeposition procedure was then carefully studied and optimized. For example, other studies have reported the use of nitrogen bubbling, but in this case it was found that it produced a negligible effect to obtain the particles. Initial time of 5 min was the fixed timing in the original protocol but a direct correlation between time and clusters was observed. Hence, a final optimized time of 2 min was found. Figure 9.2 and Figure 9.3 show that in the rubber-based material the electrodeposition was not effective. The voltage applied, concentration of platinum salt or stirring speed were also checked and optimized maintaining the voltage as -0.25 volts, the salt concentration as 1.3 mM and the stirring in 300 rpm (no stirring promotes a poor distribution of the platinum particles on the surface).

Figure 9.3 shows clusters and agglomerations (“Cauliflowers”) of Pt particles on top of CNT ink in a paper-based substrate (Figure 9.3A). Similar particles are also shown on top of GC electrodes (Figure 9.3B) but once again the effects of the electrodeposition are negligible in all the surface of the carbon ink rubber-based material (Figure 9.3C). “Snowball” shape particles with an homogeneous deposition along the entire surface of the electrode can be observed in the case of carbon ink paper-based electrodes (Figure 9.3D).

### 9.2.2.2. Analytical performance of the PtNPs carbon ink paper-based electrodes

After the characterization and optimization of the electrodeposition protocol, carbon ink paper-based substrate was chosen as the best candidate because: (i) the inherent simplicity for manufacture these electrodes; (ii) its non-toxicity in comparison with the CNTs; (iii) the reproducibility in terms of the shape and size of particles obtained (“cauliflowers vs. snowballs”); and (iv) it is sensitive to redox potential changes (although the cyclic voltogram does not exhibit well defined peaks, the deposition of PtNPs is clearly demonstrated in comparison to the bare carbon ink paper-based).

Considering this choice, the optimized electrodeposition protocol was applied and a batch of paper-based carbon-ink electrodes were used. Figure 9.4 shows the results obtained during an assay using PtNPs decorated carbon ink paper-based electrodes. It should be stressed that carbon-ink electrodes (without Pt) do not show any significant redox response. The calibration was carried out adding increasing concentrations of hydrogen peroxide in a 4 mL cell using PBS 0.1 M at pH 7.4.



**Figure 9.4.** (A) Time trace and (B) calibration curve of three different carbon ink paper-based electrodes responding to increasing concentration of H<sub>2</sub>O<sub>2</sub> in PBS 0.1 M (pH 7.4) at 25°C.

After checking the redox-sensitive substrate upon the addition of peroxide, the incorporation of Nafion on top of the electrode was carried out. When the Nafion is introduced into the system, the enhancement produced by the Donnan potential associated can be observed. Figure 9.5 displays the comparison with time trace and calibrations curves for a set of three electrodes without Nafion and with Nafion on top of the carbon ink paper-based decorated with Pt particles.

Several factors such as the temperature of curing for the layers of the membrane were evaluated. Nevertheless, the drying process is strongly dependent on the environmental conditions (humidity and temperature change according to the season). For that reason, the drying at RT was compared with drying in the oven at different times and temperatures. The optimal conditions for curing of the first layer of Nafion were at 36°C during 40 min, since it stabilize the response and improves the reproducibility among the electrodes.

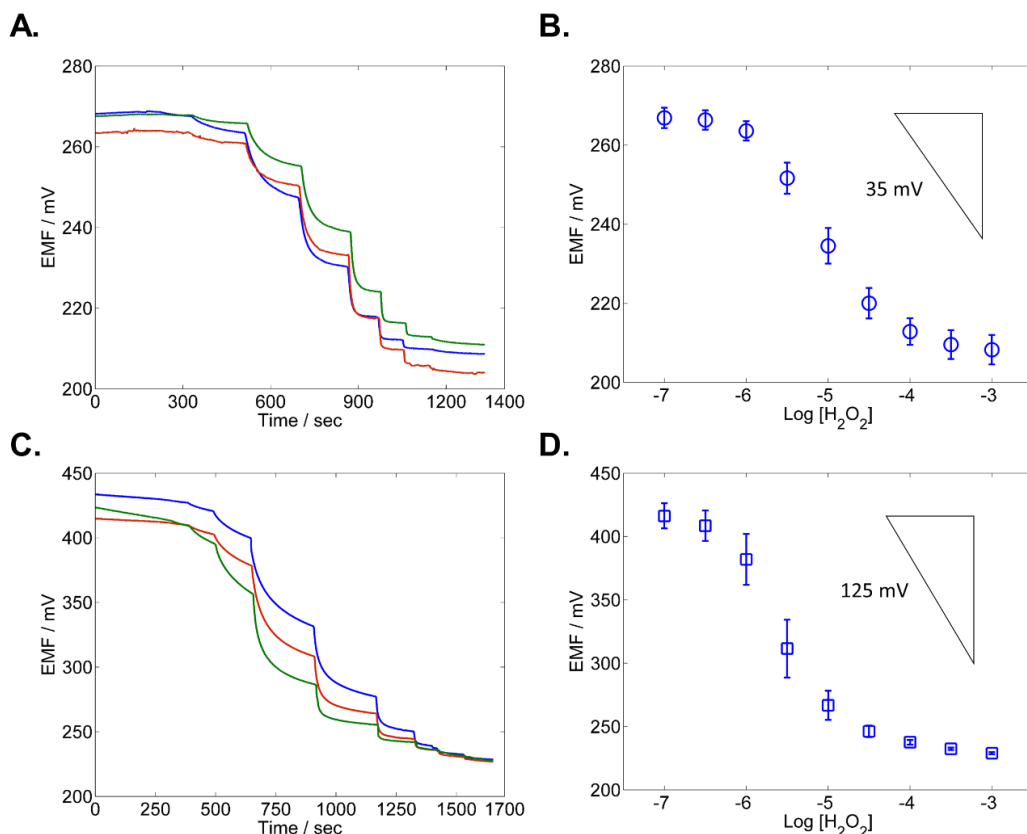


**Figure 9.5.** Comparison of the potentiometric response to H<sub>2</sub>O<sub>2</sub> using paper-based sensors with PtNPs-carbon ink with or without Nafion layer on top. (A) Time trace and (B) calibration curve of three different PtNPs-carbon ink paper-based electrodes responding to increasing concentration of H<sub>2</sub>O<sub>2</sub>. (C) Time trace and (D) calibration curve of three different PtNPs-carbon ink paper-based electrodes with a layer of Nafion on top responding to increasing concentration of hydrogen peroxide.

The comparison between calibration curves (Table 9.1) yields an acceptable reproducibility on the slopes.

**Table 9.1.** Analytical performance compare between electrodes with and without Nafion layer on top of carbon ink paper-based electrode decorated with Pt particles.

Parameters	PtNPs without Nafion	PtNPs with Nafion
Sensitivity ( $\text{mV}\cdot\text{decade}^{-1}$ )	$-31.65 \pm 1.53$	$-115.26 \pm 8.73$
Linear range (M)	$10^{-5.5} - 10^{-4.5}$	$10^{-6} - 10^{-5}$
Limit of detection (M)	$10^{-5.97 \pm 0.16}$	$10^{-6.24 \pm 0.13}$

After this exploration, a calibration curve with blank electrodes (i.e., no PtNPs) was performed in order to check the selective response obtained in the previous experiments. Figure 9.6 shows the response to  $\text{H}_2\text{O}_2$  of four different types of blank electrodes. As the substrate is carbon ink cured on top of paper, the first blank called C has this basic component. The second blank (C-N) has on top of the carbon ink-paper a layer of Nafion. The third type (C-ED) is a carbon ink paper-based electrode that has been carried out an electrodeposition protocol but without using the Pt salt component in the solution. And the last blank (C-ED-N) is composed by a carbon ink paper that has been applied the electrodeposition protocol (without Pt salt) and then a layer of Nafion has been drop cast. No response of  $\text{H}_2\text{O}_2$  was detected, demonstrating how the Pt particles are involved in the generation of the output signal.

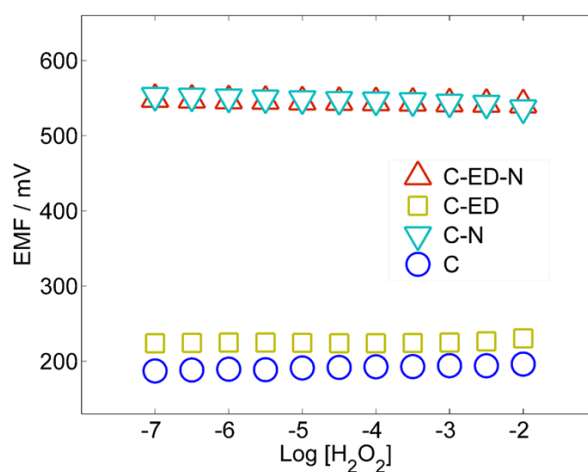


**Figure 9.6.** Calibration curve showing the response of different blanks electrodes to  $\text{H}_2\text{O}_2$ . C = carbon ink substrate, C-N = carbon ink with a layer of Nafion, C-ED = carbon ink after an electrodeposition without the Pt salt and C-ED-N = carbon ink paper after an electrodeposition process without particles and a layer of Nafion.

Once the blanks and the effect of the Nafion have been confirmed, the next step is the incorporation of the enzymatic layer. The integration of the enzyme glucose oxidase (GOx) entrapped between two layers of Nafion was carried out. In order to find the best option, an optimization regarding the thickness of the different Nafion and enzymatic layers were performed (see Table 9.2). Unfortunately, several problems related to reproducibility between electrodes were found. The stabilization of the EMF signal was quite poor, showing a high response time in comparison with the previous results. There are several factors to consider. First, the kinetic response of the surface is significantly altered when comparing with the previous, Pt-coated paper. The resting potential of the electrode established by a mixed potential mechanism is highly dependent on the nature of the surface. Additionally, the enzyme kinetics might be also affected by the nature of the surface. All in all, further studies need to be carried out in order to understand this phenomena and evaluate ways to fix it.

**Table 9.2.** Conditions used for the optimization of the thickness of the different Nafion and enzymatic layers.

<i>Condition</i>	<i>Nafion    Enzyme    Nafion</i>
<i>A</i>	4    20    2.5
<i>B</i>	4    20    4
<i>C</i>	7    20    7
<i>D</i>	10    20    10

### 9.3. PART 2: Searching an alternative polyelectrolyte matrix

#### 9.3.1. Experimental

##### 9.3.1.1. Reagents and materials

Aquivion® D98-25BS consisting in a liquid dispersion, 25% in water, PFSA eq. wt. 980 g/mole SO<sub>3</sub>H with CF<sub>3</sub> polymer and chain ends as stabilizer was obtained in Sigma-Aldrich. All the rest of reagent and materials were prepared as described in Chapter 3 and in previous chapters.

##### 9.3.1.2. Electrochemical measurements

Electromotive force (EMF) measurements were performed at room temperature (25°C) with a high input impedance (10<sup>15</sup> Ω) potentiometer. Laboratory measurements were made using a 4 mL cell in 0.1 M PBS (pH 7.4 145 mM NaCl) and artificial serum<sup>[33]</sup> (pH 7.4) at 25°C. Fresh solutions of hydrogen peroxide and glucose were prepared daily.

Blood samples were measured directly using a potentiometric sampling cell similar to the one used in the Chapter 8. N=3, three different sensors in each experiment. A commercial amperometric glucose sensor (Bayer® Contour glucometer) was used to compare glucose blood values determined by our paper-based potentiometric sensor.

### 9.3.1.3. Fabrication of glucose biosensor

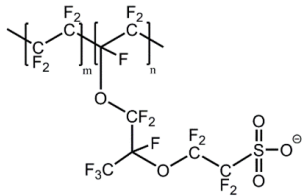
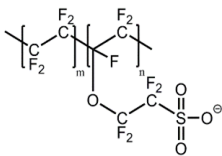
Enzymatic paper-based electrodes were built using a platinum sputtering approach as was described previously. Glucose oxidase entrapped between two layers of a polymeric matrix (as described in Chapter 7 and 8) was used as a model.<sup>[27]</sup> Two different polymers (Nafion and Aquivion)<sup>[34]</sup> were tested to evaluate the influence on the polymeric matrix on the analytical parameters. The deposition of the polymeric matrices (either Nafion or Aquivion) was carried out by drop casting. Dilutions of Aquivion were performed with methanol ≥99.8% in a ratio 1:1 and 1:4. To build the miniaturized cell, the enzymatic sensor was placed in between the sampling cell and connected to the measuring device through the conductive ends. This cell was kept at 4°C when not in use. The sampling cell was designed and optimised for a sample volume of 25 µL (for details of this cell see Figure 8.1 in Chapter 8). Further details of the electrode preparation have been described elsewhere.<sup>[3]</sup>

## 9.3.1. Results and Discussion

### 9.3.1.1. Optimization and analytical performance of the potentiometric biosensor

Analytical performance of the enzymatic sensor built with Nafion as a matrix was extensively described in the previous chapters. In this case, Aquivion was used as a matrix in order to improve the characteristics of the potentiometric biosensor.

**Table 9.3.** Nafion vs. Aquivion comparing the chain and density of charges of these polymers.

	Nafion	Aquivion
<b>Polymer Chain</b>		
<b>EW<sup>a</sup></b>	1100	980
<b>Polymer Composition</b>	5 wt. % in mixture of lower aliphatic alcohols and water	25 wt. % in water
<b>Membrane Composition</b>	5 wt. % in mixture of lower aliphatic alcohols and water	12,5 wt. % in water and methanol (1:1)

EW<sup>a</sup> Equivalent Weight = grams of dry polymer / mol of ion exchange sites

Aquivion is a polymer of the same family as Nafion.<sup>[35–37]</sup> Thus, is a proton-exchange membrane with the same characteristics sulfonate groups. In the case of Aquivion, however, the carbon chains are shorter (Table 9.3). As a result, the Aquivion can be considered as a type of Nafion polymer both with an increased volumetric density of negatively charged groups.

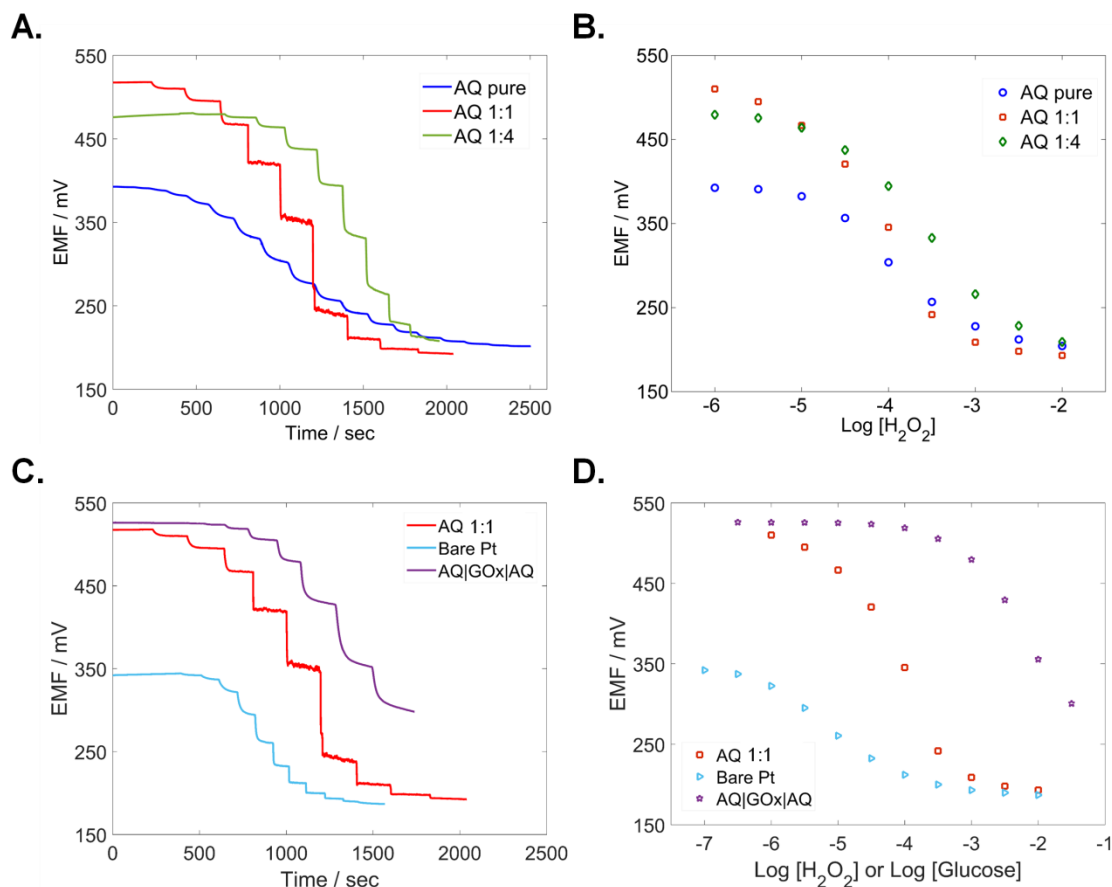


**Figure 9.7.** Comparison of the potentiometric response under different conditions. (A) Time trace and (B) calibration curve comparing the response to  $\text{H}_2\text{O}_2$  of electrodes built with pure Aquivion (blue circles), diluted Aquivion in a mixture 1:1 (red squares) and 1:4 (green diamonds). In a parallel study, (C) time trace and (D) calibration curve showing the response of platinum bare electrodes (blue triangles) and 1:1 diluted Aquivion electrodes (red squares) towards hydrogen peroxide and enzymatic sensor composed by AQ || GOx || AQ to additions of glucose (purple stars).

In order to test the analytical performance of this new polyelectrolyte coating, an optimization of different parameters was carried out. Figure 9.7 shows an optimization regarding the density of the polyelectrolyte. Figure 9.7A and Figure 9.7B (calibration curve) compare the response to hydrogen peroxide given by electrodes built with pure Aquivion (without any dilution), Aquivion diluted with methanol (1:1) and (1:4). Best results are those

obtained with the 1:1 dilution, since it improves the sensitivity as well as the reproducibility between electrodes. Besides, better results were obtained with ratio 1:1 when the enzymatic approach was tested comparing both dilutions (1:1 and 1:4). Interestingly, the poor reproducibility as well as the lower initial potential that pure Aquivion showed probably is due to the major cracks that are formed in the surface of the polymeric membrane (visible to the naked eye after drying at room temperature).

Figure 9.7C and 9.7D exhibit the comparison with a time trace and a calibration curve, respectively, of the potentiometric response to  $H_2O_2$  given by a bare platinum electrode Aquivion-coated electrodes (dilution 1:1) and an enzymatic electrode composed by two layers of Aquivion (diluted 1:1) entrapping the GOx (using, in this case glucose as analyte). Figure 9.7 shows that all the curves follow the same pattern, with an increasing offset in potential at higher amount of polyelectrolyte matrix deposited on top of the platinized paper. It could be concluded that there is a difference in the shape of the calibration plot when peroxide is generated via enzymatic reaction or when is added externally, and even when peroxide is added externally to an enzyme-free electrode (data not shown). Although more work needs to be done to assess the degree of conversion of glucose by the immobilized enzyme, the transport and diffusion of the byproduct ( $H_2O_2$ ) of the enzymatic reaction through the polyelectrolyte matrix might be affected by the configuration of the electrode. Overall, the most important result from an application point of view is that the linear range has been shifted towards higher concentrations, while the sensitivity remains unaffected.

Table 9.4 compares the analytical performance of each electrode, responding to  $H_2O_2$  in the case of bare Pt, pure AQ and two mixtures of AQ with methanol in 1:4 and 1:1 dilutions whereas the complete electrode formed by AQ || GOx || AQ is responding to glucose.

**Table 9.4.** Comparison of analytical parameters using different configurations of the electrodes in 0.1 M PBS buffer (pH = 7.4).

Parameters	Bare Pt	Pure AQ	Aquivion 1:4	Aquivion 1:1	AQ GOx AQ
<b>Sensitivity (mV·decade<sup>-1</sup>)</b>	-56.8 ± 4.3	-94.2 ± 1.4	-124.1 ± 6.5	-180.6 ± 2.2	-133.2 ± 9.9
<b>Linear range (M)</b>	0.001 - 0.1	0.018 – 0.012	0.1 - 1	0.03 – 0.3	1 - 30
<b>Limit of detection (M)</b>	0.0006	0.012 ±0.0004	0.023 ±0.004	0.009 ± 0.001	0.30 ± 0.1

Figure 9.8 displays the images of the electrodes with the different dilutions of Aquivion used. Figure 9.8D shows that the pure Aquivion presents several cracks (highlighted with red dots),



while the other Figures 9.8A, B and C show no apparent damages of the membrane. The result observed in Figure 9.8D could be due to the high viscosity of the pure solution that when it is dried produces these cracks.

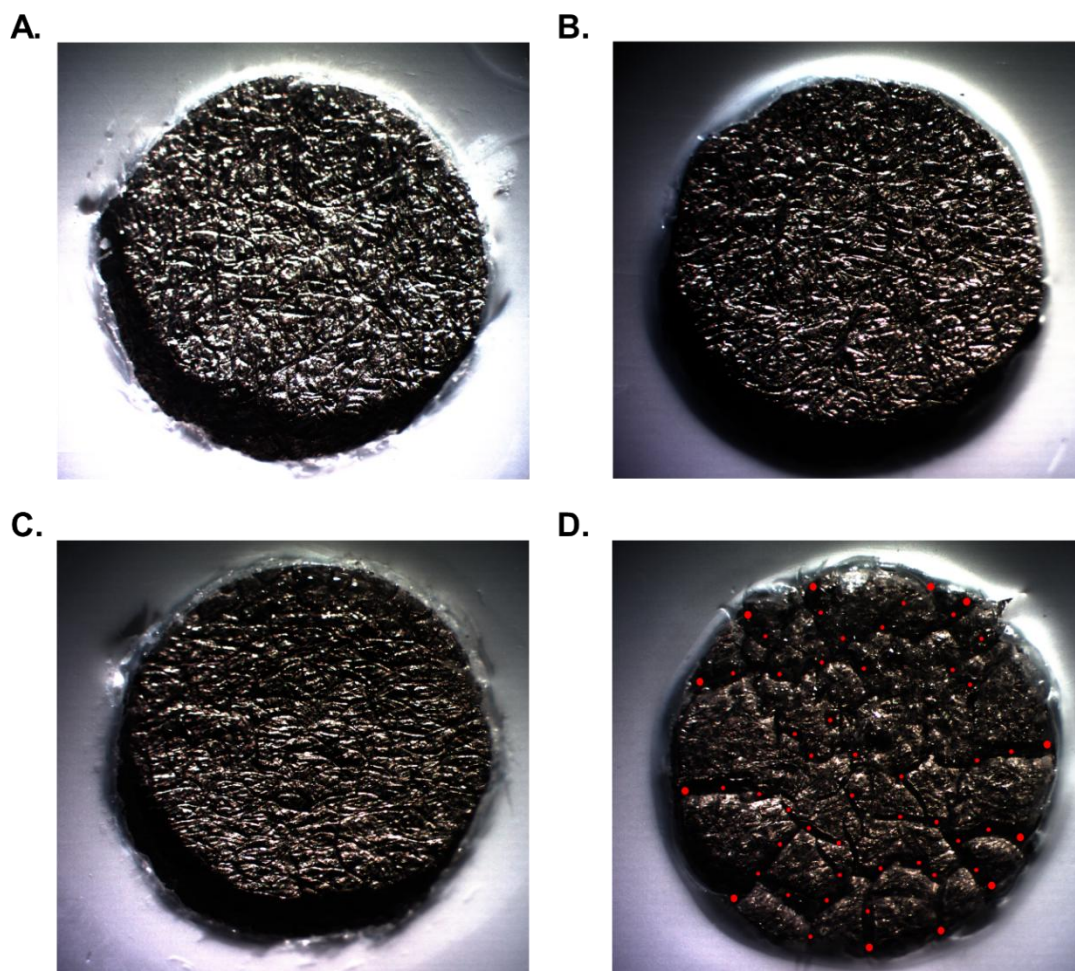


**Figure 9.8.** Images corresponding to paper-based electrodes (A) bare platinum electrode (B) with a layer of 4  $\mu\text{L}$  of Aquivion -dilution 1:4 with methanol-, (C) with a layer of 4  $\mu\text{L}$  of Aquivion -dilution 1:1 with methanol- and, (D) with a layer of 4  $\mu\text{L}$  of pure Aquivion (without any dilution).

Figure 9.9A displays the results of the optimization of the thickness of the polymeric layer, testing the sensitivity of the biosensor to glucose with different amounts of Aquivion drop cast (2, 4, 6 and 8  $\mu\text{L}$ ). After this optimization, the best candidate was chosen as 4  $\mu\text{L}$  because the sensitivity shows the highest values. In another approach (Figure 9.9B), using the configuration of 4  $\mu\text{L}$  for the Aquivion layers, an optimization of the concentration of the enzyme glucose

oxidase (GOx) was performed comparing 1, 10, 20 and 50 mg·mL<sup>-1</sup>. In this optimization, the concentration of 20 mg·mL<sup>-1</sup> was chosen as the best option in order to maximize the sensitivity.

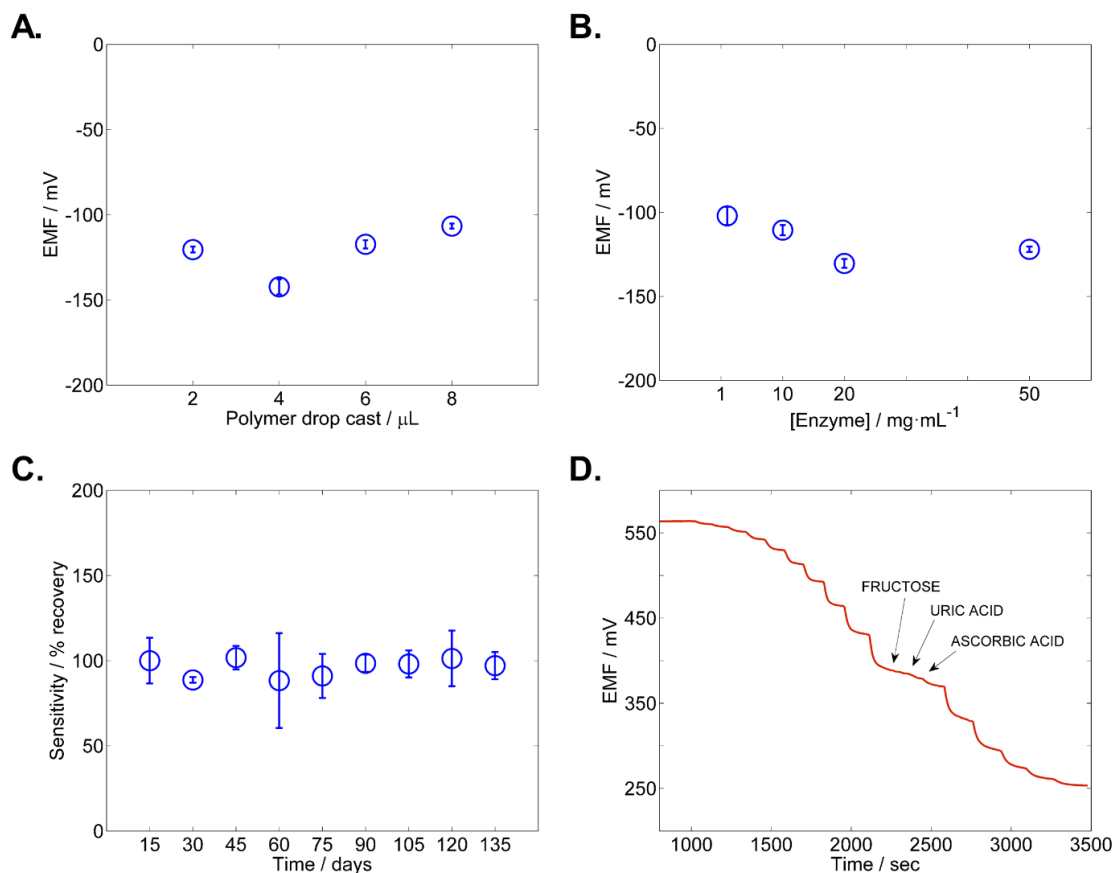


**Figure 9.9.** Optimization of the analytical conditions of the biosensor. (A) Sensitivity for glucose vs. the volume of solution of polymer cast. (B) Sensitivity for glucose vs. the concentration of enzyme cast (fixed volume of 10  $\mu\text{L}$  for enzymatic layer). (C) Stability study exhibits values for the recovery of the sensitivity along a period of more than 4 months. (D) Assessment of the selectivity of the enzyme-based electrode to the main redox sensitive molecules (ascorbate and urate) and fructose. All the measurements (N = 3) were performed in 0.1 M PBS (pH 7.4) at 25°C.

Figure 9.9C exhibits the recovery of the sensitivity (percentage of sensitivity at each time vs. initial sensitivity) during a study of stability performed with the paper-based enzymatic sensors during more than 4 months. In this study, the electrodes (manufactured with 4  $\mu\text{L}$  of Aquivion and a concentration of 20 mg·mL<sup>-1</sup> of enzyme) are tested in a calibration curve of increasing concentrations of glucose in a 4 mL cell using PBS 0.1 M at 25 °C. The reproducibility between electrodes is kept during all this time. Only some increments on the standard deviation were observed in some particular days, probably due to manual errors during the manufacturing of the electrodes.

As the selectivity is also crucial in the characterization of the analytical performance of the electrodes, additions of the main interferences commonly found in blood were evaluated. Figure 9.9D displays the calibration curve performed in PBS 0.1 M with increasing concentrations of glucose with the addition of fructose, uric acid and ascorbic acid in a maximum concentration of 0.1 mM. During the studies of selectivity, it was appreciated that Aquivion eliminates the redox interferences better than Nafion. Considering that Aquivion has higher density of negatively charge species, this could be explained in terms of an enhanced permselective effect.

Figure 9.10 shows a comparison of the potentiometric response obtained by enzymatic electrodes using either Nafion or Aquivion in PBS 0.1 M with a pH of 7.4 the first observation is that both electrodes show a similar standard (initial) potential. However, the potentiometric response seems to be shifted in terms of the linear range. In the case of Nafion, a linear range between 0.3 mM and 3 mM is found, which is similar to what was previously described (because of this, a dilution of blood samples is required to do monitor glucose levels). In contrast, the linear range obtained with the new polymer is shifted towards higher concentrations allowing a direct measurement of glucose in serum or blood. Consequently, a simplification during the analytical process of glucose detection within the clinical range might be carried out. Besides, new applications for these enzymatic sensors might be approached. The elimination of a dilution step or any type of treatment of the sample is crucial in order to simplify and make easy to manipulate the sample thus fostering the development of truly decentralized platforms able to act in a fast, user-friendly and robust way.

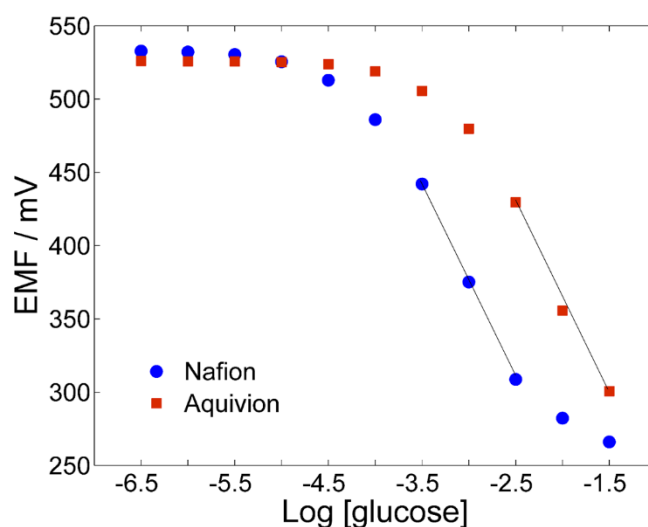


**Figure 9.10.** Comparison of the potentiometric response of glucose using different polyelectrolytes to built the enzymatic electrodes. Blue dots: electrodes built with Nafion and red squares: electrodes built with Aquivion.

### 9.3.1.2. Measurement and validation of glucose in real samples

All the previous experiments were performed in a 4 mL cell using a commercial double junction reference electrode. Hereinafter, the results show in Figure 9.12 were carried out using the WE composed by the scheme Pt || AQ || GOx || AQ and a paper-based RE (see Figure 9.11) optimized and developed in Chapter 8 of this thesis, mimicking the same device and methodology shown in the previous chapter.<sup>[3]</sup> The main advantage, however, is that -due to the modified linear range- the Aquivion-based device does not require a prior dilution of the sample.

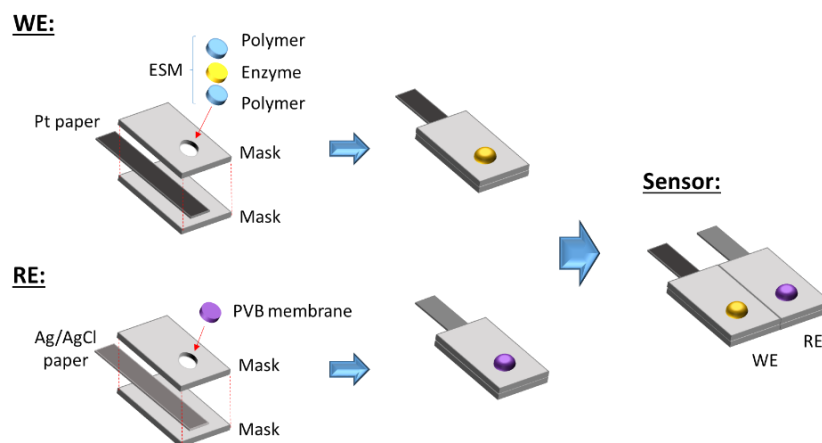


Figure 9.11. Schematic representation of the WE and RE used during the measurements with real samples.

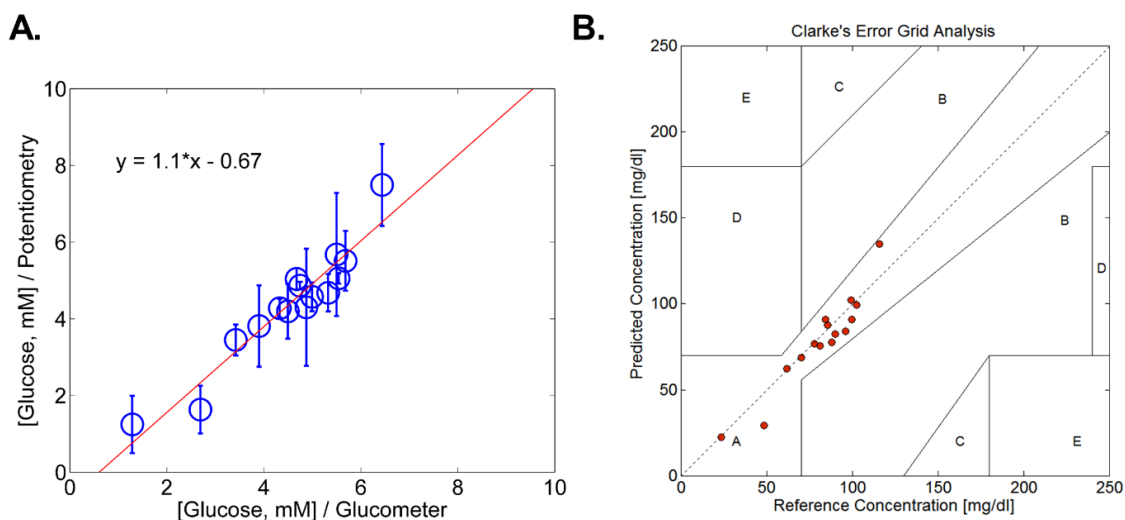


Figure 9.12. (A) Comparison of glucose determination (mM) in real blood samples obtained by the potentiometric biosensor (paper-based WE and paper-based RE) and glucometer device at 25°C. (B) Representation of the well-established Clarke error grid.

The validation of the potentiometric cell was carried out using 15 (real) blood samples provided by different volunteers from our labs. The device was calibrated with three standards of glucose 1, 3.16 and 10 mM in PBS chosen as they are in the linear range of the sensor. The cleaning of the cell (after the measurement of a blood sample) can be evaluated by checking that the open circuit potential returns to the initial value. This indicates that the system is ready to receive a new sample. This procedure, which was repeated using three different paper-based devices, allows measuring several samples in few minutes, including the calibration curve, washing, etc.

Figure 9.12A displays the validation between values of glucose obtained using a commercial glucometer *versus* our potentiometric biosensor. This results represent a good linear correlation between both methods. The recoveries for the assays from blood samples were  $95.6 \pm 12.2\%$  (N=15). This indicates that the blood matrix had no significant effect on glucose determination. It should be mentioned that the same sensor (WE and RE) was used repeatedly for several predictions without changing the performance. This characteristic also indicates the high resilience of the sensors to biofouling. However, as it was discussed in previous chapters, this type of sensors is thought to be disposable making them easier to handle and to avoid contamination between different biological samples. Figure 9.12B displays the values obtained in the validation in a standard Clarke error grid. This plot shows that all values are within zone A showing that the methodology is accurate enough to measure in blood samples for diabetes management.<sup>[38,39]</sup>

**Table 9.5.** The recovery of glucose determination in blood samples without dilution.

Nº of sample	Potentiometry (mM)	Glucometer (mM)	Recovery (%)
1	4.30 ± 1.53	4.88	88.18
2	3.45 ± 0.40	3.42	100.83
3	5.68 ± 1.60	5.50	103.23
4	7.49 ± 1.07	6.44	116.40
5	3.81 ± 1.06	3.90	97.71
6	4.57 ± 0.38	5.00	91.58
7	4.68 ± 0.49	5.33	87.82
8	5.06 ± 0.14	5.54	91.22
9	4.20 ± 0.71	4.50	93.32
10	4.28 ± 0.24	4.33	98.81
11	5.51 ± 0.78	5.69	96.97
12	4.87 ± 0.10	4.75	102.49
13	1.64 ± 0.62	2.69	60.75
14	1.25 ± 0.75	1.29	96.81
15	5.04 ± 0.29	4.68	107.78

Table 9.5 displays the recovery in agreement with the conventional glucometer results.

## 9.4. CONCLUSIONS

In this chapter, novel approaches for the improvement on the development of ultra-low-cost potentiometric biosensors have been presented. First, a novel approach that allows for the highly sensitive and selective detection of  $\text{H}_2\text{O}_2$  using an affordable substrate (paper) as well as low-cost materials (commercial carbon ink with PtNPs) has been successfully described. Particularly, a study of PtNPs over different carbon substrates has been performed. Accordingly, paper-based sensors coated with carbon ink have been proved as potential candidates for an affordable detection of  $\text{H}_2\text{O}_2$ . Further optimization needs to be explored before the integration of enzymes in the new redox substrate. Second, a platinized paper coated with a new polyelectrolyte matrix (Aquivion) has been used to monitor the changes in the redox potential produced by the generation of  $\text{H}_2\text{O}_2$  during an enzymatic reaction. In this approach, the direct measurement of glucose in blood within the clinical range has been accomplished. Besides, an outstanding correlation with the commercial standard method was obtained and it was in perfect agreement with well-known Clarke error grid used in the clinical validation of methodologies for glucose detection.

This chapter has demonstrated that some of the most basic limitations of the biosensors presented previously (such as cost or simplicity) can be reduced by means of new methods and materials that bring new features and benefits. The characterization and validation of the procedures have been carried out through the use of electrochemical techniques such as cyclic voltammetry and instrumental such as ESEM, among others. In addition, meticulous optimizations have been performed to ensure the best operation of the sensors. The analysis of the blank electrodes as well as the complete integration with the enzymatic component has been discussed.

Although the work performed during the first part of this chapter did not reach the final goal, (successful integration of the enzymatic detection), it is important to note that the main objective of finding an alternative redox-sensitive platform has been achieved. On the other hand, in the second part of the chapter, the development of a sensor for the direct measurement of glucose levels in whole blood has been successfully achieved by using a polyelectrolyte material. This process does not require any type of sample treatment or dilution, avoiding excessive manipulation, increasing the simplicity of the system, and thus, making it more user-friendly.

All in all, two main disadvantages were highlighted along these last chapters: i) the dilution and ii) calibration step. Here, the first drawback has been solved by changing the proton

exchange membrane of the sensor. The second one still needs to be solved. Hence, future efforts will be invested in this direction. For example, one possibility is to improve the reproducibility of the sensor by performing a more accurate manufacturing process, among other reported attempts to address calibration-free sensors.<sup>[40,41]</sup>

Moreover, next steps will be the extension of this approach to other oxidase-type enzymes opening a new avenue for the development of affordable, simple and robust platforms for decentralized biochemical analysis.<sup>[42]</sup> All in all, enzymatic sensors are included as a promising technology for highly efficient and economically competent biotechnological processes in the field of environmental monitoring, biotransformation, diagnosis, pharmaceutical and food industries.<sup>[43]</sup>

## 9.5. REFERENCES

- [1] M. Parrilla, R. Cánovas, F. J. Andrade, *Electroanalysis*. **2017**, *29* (1), 223.
- [2] M. Parrilla, R. Cánovas, F. J. Andrade, *Biosens. Bioelectron.* **2017**, *90*, 110.
- [3] R. Cánovas, M. Parrilla, P. Blondeau, F. J. Andrade, *Lab Chip* **2017**, *17*, 2500.
- [4] J. Hu, S. Wang, L. Wang, F. Li, B. Pingguan-Murphy, T. J. Lu, F. Xu, *Biosens. Bioelectron.* **2014**, *54*, 585.
- [5] J. H. T. Luong, K. B. Male, J. D. Glennon, *Biotechnol. Adv.* **2008**, *26*, 492.
- [6] M. Sardar, A. Mishra, R. Ahmad, Eds.: A. Tiwari, A.P.F. Turner, Ed. Scrivener Publishing, *Biosensors Nanotechnology*, **2014**, ISBN 978-1-118-77351-2.
- [7] K. Tian, M. Prestgard, A. Tiwari, *Mater. Sci. Eng. C. Mater. Biol. Appl.* **2014**, *41C*, 100.
- [8] D. D. Liana, B. Raguse, J. Justin Gooding, E. Chow, *Sensors (Switzerland)* **2012**, *12*, 11505.
- [9] A. M. López-Marzo, A. Merkoçi, *Lab Chip* **2016**, *16*, 3150.
- [10] A. Romeo, T. S. Leung, S. Sánchez, *Lab Chip* **2016**, *1377*, 13.
- [11] A. A. Kumar, J. W. Hennek, B. S. Smith, S. Kumar, P. Beattie, S. Jain, J. P. Rolland, T. P. Stossel, C. Chunda-Liyoka, G. M. Whitesides, *Angew. Chemie Int. Ed.* **2015**, *54*, 5836.
- [12] R. W. Peeling, D. Mabey, *Clin. Microbiol. Infect.* **2010**, *16*, 1062.
- [13] J. Su, F. Gao, Z. Gu, M. Pien, H. Sun, *Sensors Actuators B Chem.* **2013**, *181*, 57.
- [14] T. V. A. Dam, D. Pijanowska, W. Olthuis, P. Bergveld, *Analyst* **2003**, *128*, 1062.
- [15] A. Harvey, A. Brand, S. T. Holgate, L. V. Kristiansen, H. Lehrach, A. Palotie, B. Prainsack, *N. Biotechnol.* **2012**, *29*, 625.
- [16] P. Yager, T. Edwards, E. Fu, K. Helton, K. Nelson, M. R. Tam, B. H. Weigl, *Nature* **2006**, *442*, 412.
- [17] E. Bakker, J. Gooding, *ACS Sensors* **2016**, *1*, 834.
- [18] E. J. Maxwell, A. D. Mazzeo, G. M. Whitesides, *MRS Bull.* **2013**, *38*, 309.

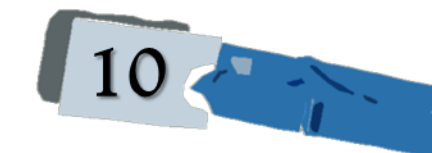
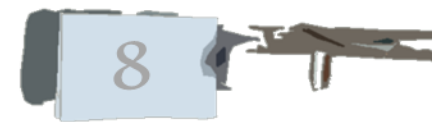
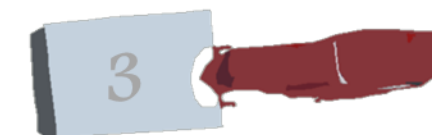
- [19] K. Mahato, A. Srivastava, P. Chandra, *Biosens. Bioelectron.* **2017**, 96, 246.
- [20] J. L. Gomez, O. Tigli, *J. Mater. Sci.* **2013**, 48, 612.
- [21] E. C. S. Transactions, T. E. Society, *Electrochem. Soc.* **2015**, 69, 7.
- [22] A. M. Gómez-marín, K. J. P. Schouten, M. T. M. Koper, J. M. Feliu, *Electrochem. commun.* **2012**, 22, 153.
- [23] I. Katsounaros, W. B. Schneider, J. C. Meier, U. Benedikt, P. U. Biedermann, A. A. Auer, K. J. J. Mayrhofer, *Phys. Chem. Chem. Phys.* **2012**, 14, 7384.
- [24] X. Li, D. Heryadi, A. A. Gewirth, *Langmuir* **2005**, 21, 9251.
- [25] S. M. Z. Hossain, C. Ozimok, C. Sicard, S. D. Aguirre, M. M. Ali, Y. Li, J. D. Brennan, *Anal. Bioanal. Chem.* **2012**, 403, 1567.
- [26] J. Wang, *Electroanalysis* **2001**, 13, 983.
- [27] E. Witkowska Nery, M. Kundys, P. S. Jeleń, M. Jönsson-Niedziółka, *Anal. Chem.* **2016**, 88, 11271.
- [28] Y. Zou, C. Xiang, L. X. Sun, F. Xu, *Biosens. Bioelectron.* **2008**, 23, 1010.
- [29] X. Kang, Z. Mai, X. Zou, P. Cai, J. Mo, *Talanta* **2008**, 74, 879.
- [30] H. Tang, J. Chen, S. Yao, L. Nie, G. Deng, Y. Kuang, *Anal. Biochem.* **2004**, 331, 89.
- [31] F. Qu, M. Yang, G. Shen, R. Yu, *Biosens. Bioelectron.* **2007**, 22, 1749.
- [32] X. Chu, D. Duan, G. Shen, R. Yu, *Talanta* **2007**, 71, 2040.
- [33] K. Kimura, H. Oishi, T. Miura, T. Shono, *Anal. Chem.* **1987**, 59, 2331.
- [34] G. Alberti, M. L. Di Vona, R. Narducci, *Int. J. Hydrogen Energy* **2012**, 37, 6302.
- [35] S. Siracusano, V. Baglio, A. Stassi, L. Merlo, E. Moukheiber, A. S. Arico', *J. Memb. Sci.* **2014**, 466, 1.
- [36] A. Stassi, I. Gatto, E. Passalacqua, V. Antonucci, A. S. Arico, L. Merlo, C. Oldani, E. Pagano, *J. Power Sources* **2011**, 196, 8925.
- [37] A. Skulimowska, M. Dupont, M. Zaton, S. Sunde, L. Merlo, D. J. Jones, J. Rozière, *Int. J. Hydrogen Energy* **2014**, 39, 6307.
- [38] B. P. Kovatchev, L. A. Gonder-Frederick, D. J. Cox, W. L. Clarke, *Diabetes Care* **2004**, 27, 1922.
- [39] A. Maran, C. Crepaldi, A. Tiengo, *et al.*, *Diabetes Care* **2002**, 25, 347.
- [40] X. U. Zou, X. V Zhen, J. H. Cheong, P. Bühlmann, *Anal. Chem.* **2014**, 86, 8687.
- [41] U. Vanamo, J. Bobacka, *Anal. Chem.* **2014**, 86, 10540.
- [42] S. Lee, A. Reuveny, J. Reeder, S. Lee, H. Jin, Q. Liu, T. Yokota, T. Sekitani, T. Isoyama, Y. Abe, Z. Suo, T. Someya, *Nat. Nanotechnol.* **2016**, 1.
- [43] S. Datta, L. R. Christena, Y. R. S. Rajaram, *Biotech* **2012**, 3, 1.



UNIVERSITAT ROVIRA I VIRGILI

TAILOR-MADE CHEMICAL SENSING PLATFORMS FOR DECENTRALIZED HEALTHCARE AND WELLBEING

Rocío Cánovas Martínez



## CONCLUSIONS

---

---

UNIVERSITAT ROVIRA I VIRGILI

TAILOR-MADE CHEMICAL SENSING PLATFORMS FOR DECENTRALIZED HEALTHCARE AND WELLBEING

Rocío Cánovas Martínez

## 10. CONCLUSIONS

In this thesis, the successful development of tailor-made and low cost sensors for their use in decentralized chemical analysis has been achieved. Moreover, the manufacturing of affordable, simple and robust devices has been exemplified. In the first part of this thesis, wearable and embedded electrochemical sensors based on resilient materials have been developed and characterized. In the second part, a new detection strategy for the fabrication of potentiometric enzymatic sensors has been presented.

The ability of these approaches to build sensors using commodity materials as a substrate, as well as their simplicity in construction and operation make them an optimal tool for the use in decentralized scenarios. In this way, the electrochemical sensors developed throughout this thesis may play an important role in improving the healthcare system in the future. For instance, an early detection and diagnosis can be used to greatly reduce the cost of patient care associated with the advanced stages of many diseases.<sup>[1]</sup> The real challenge here is the true implementation of these tools by users (at the individual or entity level). Hence, in the near future the use and application of these chemical sensors could suppose a clear evolution of the system currently implemented.

This thesis has introduced some progress in terms of the vision and real applicability of affordable tools in a decentralized way. The study of durable and versatile materials such as filter paper, textiles or expandable plastics and their subsequent use as substrates to embed sensors, have been demonstrated in this thesis. For example, a complete potentiometric cell capable of monitoring electrolytes in sweat has been successfully developed (Chapter 4). In addition, this multi-ion sensor has been printed over conventional textiles that have allowed the deep study of different types of mechanical stress such as stretching, wrinkling, bending, etc., without compromising the analytical performance of the system. Likewise, the printing of the sensor was made in a wristband to prove that any adaptation of the sensing system is possible towards a user-friendly approach. This integration of the sensors in or with commodity materials allows to decrease the fabrication cost thus enabling the development of ultra-low-cost sensors.

Another type of sensor embedded in a conventional material, commercial rubber balloons, has been developed. The printed sensor is capable to overcome common mechanical deformation, even the expansion of itself as well as provide a suitable platform for the development of an electrochemical cell. This balloon embedded sensor, which has been created for environmental and security purposes, has shown ability to detect and monitor explosive compounds in air. Thanks to this work (Chapter 5), it has been possible to bring to

the extreme the study of expandability, a concept that includes spatial stretching as well as global bending of the surface in which the sensor is placed. The use of stress-enduring inks over an expandable platform is crucial to overcome daily potential mechanical deformations without losing the electrochemical performance of the printed device. In this way, the great versatility that printing techniques with durable inks can offer has been demonstrated.

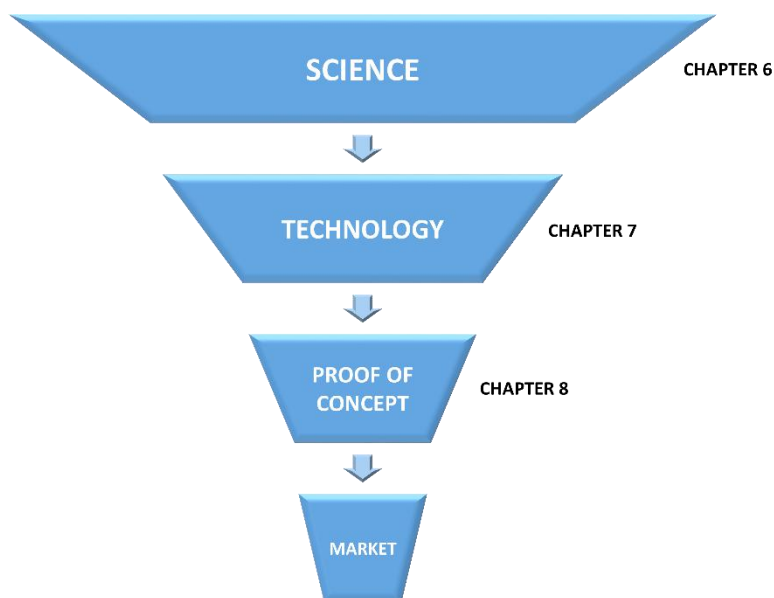


**Figure 10.1.** Technology development of the potentiometric enzyme-based sensors.

A good part of this thesis has been geared towards the study and development of potentiometric enzymatic sensors. Different enzymes and targets have been tested in order to develop enzyme-based sensors to detect different biomolecules in biological samples. Due to its characteristics (mainly stability, cost, availability), glucose oxidase (GOx) has been widely used as a model in enzymatic systems.<sup>[2]</sup> The chemistry between platinum and hydrogen peroxide (byproduct of the enzymatic reaction involved by oxidases and detected in this work) has made the study more complex and interesting. Besides, the incorporation of polyelectrolytes such as Nafion or Aquivion adds greater complexity to the detection mechanism. First, the outstanding potential sensitivity and increased selectivity have been demonstrated by the use of Nafion proton-exchange membrane in addition to the redox sensitive ability of platinum electrodes for hydrogen peroxide detection (Chapter 6). Second, the sensing mechanism has been conceptualized and applied with the development of an enzymatic paper-based sensor. In this case, GOx is sandwiched between two layers of Nafion

in order to determine glucose concentration in biological fluids (Chapter 7). In a third step (Chapter 8), the complete integration of the working and reference electrode in a paper-based potentiometric cell has been accomplished. Moreover, this complete paper-based sensor has been integrated with a wireless device able to collect and transmit the signal obtained in real time in a smartphone or a tablet. This prototype has been a clear example of the reduction to practice of a sensor that can have significant impact on the mHealth ecosystem mentioned along this thesis.

Eventually, different approaches related to the substrate and to the polymeric membrane have been studied (Chapter 9). First, more affordable platforms such as the use of carbon ink instead of platinum sputtering over the paper substrate have been used for the creation of an alternative redox sensitive platform. The detection of hydrogen peroxide has been achieved using the electrodeposition of platinum particles over the carbon ink substrate as the main electrode. Besides, the enhancement of sensitivity has been also accomplished by adding a layer of Nafion. Secondly, the use of another polyelectrolyte of the family of Nafion (Aquion), has been successfully applied to the enzymatic sensors. The characteristics of this new membrane provide a crucial improvement in the system since the dilution of the real sample (blood or serum) can be avoided. At the end of Chapter 8 two clear limitations of our system were explained: i) the inconvenience of the dilution step of the sample, and ii) the requirement of a previous calibration. As it can be seen in Chapter 9, the first inconvenience has been solved. By avoiding dilution of the sample, the direct measurement (faster and simpler) of a drop of blood can be carried out in a more user-friendly manner. Regarding the need of a calibration, this factor can be non-limiting since with a meticulously controlled manufacturing process (not made by hand which produces many more errors) the reproducibility between electrodes could improve considerably.

It is also important to mention, that not all the work developed during this thesis have been included. Some approaches related to the development of potentiometric enzymatic sensors capable of measuring the level of cholesterol, galactose or uric acid have been performed. Moreover, further studies need to be carried out in order to study the mechanism involved in the polyelectrolyte-coated platinum systems and to improve the analytical performance of these enzymatic sensors.

In general terms, it can be then concluded that the main goal of this thesis, i.e., the exploration and development of novel, intuitive and affordable sensors, has been successfully accomplished. Along the work, it has been demonstrated that the content of the thesis can pave the way to the construction of robust, simple and cost-effective platforms for decentralized

chemical and biochemical analysis. Furthermore, the sensors have been successfully implemented into commodity substrates to address social needs in different scenarios such as healthcare and wellbeing, environmental monitoring or threat assessment.

The work performed in this thesis for mobile Health, such as the wireless glucose monitoring showed in Chapter 8, represents a good advance in this area, although some challenges must still be faced. The accuracy of the sensors, stability (enzymatic and signal readout) and biocompatibility should be improved.<sup>[3]</sup> Moreover, the exploration of the scalability at the industrial level should be addressed in order to advance the technology to the market.<sup>[4]</sup> The development of a full analytical system is still an issue to improve and work on. Moreover, sampling, data collection and data treatment need to be deeply improved. The handling and securing of the big data generated by these POC devices will be a crucial issue to investigate.<sup>[5]</sup> This include data security and user privacy to fulfil the demands of the decentralization of the whole sensing network.<sup>[6]</sup>

Future work aimed at the successful adoption of these tailor-made platforms needs to be focused on the miniaturization of the wireless components and data mining system need to be integrated into a whole device.<sup>[7]</sup> Besides, research efforts in the extension of the concept to other analytes such as critical biomolecules for clinical diagnostics should be addressed. Moreover, further explorations are needed in order to use non-invasive biological fluids like urine, saliva, tears, etc.<sup>[8]</sup> Hence, a future step will be the integration of this novel platforms as a non-invasive and multianalyte sensor in a wearable and embedded devices.<sup>[9]</sup>

All in all, the basis of the novel electrochemical sensors has been applied in this doctoral thesis with promising results for its implementation in the market in a near future. Hopefully, many of these results represent one more step towards the improvement of social systems such as healthcare, environmental monitoring of homeland security, thus turning part of the scientific research into concrete social benefits.

## 10.1. REFERENCES

- [1] V. Perumal, U. Hashim, *J. Appl. Biomed.* **2014**, *12*, 1.
- [2] E. Witkowska Nery, M. Kundys, P. S. Jeleń, M. Jönsson-Niedziółka, *Anal. Chem.* **2016**, *88*, 11271.
- [3] J. H. Kim, S. Mun, H.-U. Ko, G.-Y. Yun, J. Kim, *Nanotechnology* **2014**, *25*, 92001.
- [4] J. H. T. Luong, K. B. Male, J. D. Glennon, *Biotechnol. Adv.* **2008**, *26*, 492.
- [5] S. Nayak, N. R. Blumenfeld, T. Laksanasopin, S. K. Sia, *Anal. Chem.* **2016**, *89*, 102.
- [6] MIT Technology Review, **2014**, *117*, 1.
- [7] E. B. Bahadir, M. K. Sezginürk, *Anal. Biochem.* **2015**, *478*, 107.

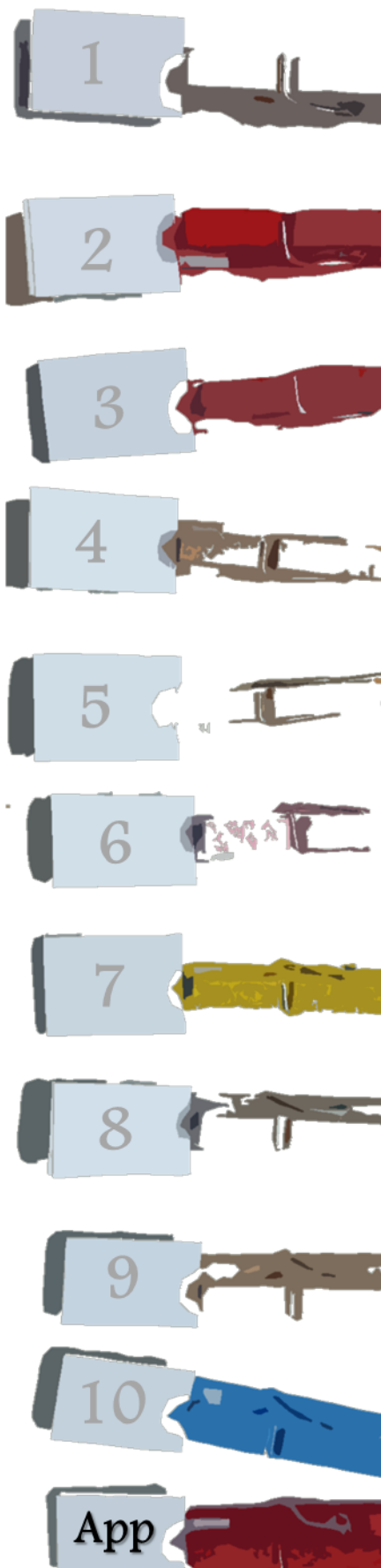
- [8] L. Florea, D. Diamond, *Sensors Actuators B Chem.* **2015**, 211, 403.
- [9] W. Gao, S. Emaminejad, H. Y. Y. Nyein, S. Challa, K. Chen, A. Peck, H. M. Fahad, H. Ota, H. Shiraki, D. Kiriya, D. H. Lien, G. A. Brooks, R. W. Davis, A. Javey, *Nature* **2016**, 529, 509.



UNIVERSITAT ROVIRA I VIRGILI

TAILOR-MADE CHEMICAL SENSING PLATFORMS FOR DECENTRALIZED HEALTHCARE AND WELLBEING

Rocío Cánovas Martínez



## APPENDICES

---

---

UNIVERSITAT ROVIRA I VIRGILI

TAILOR-MADE CHEMICAL SENSING PLATFORMS FOR DECENTRALIZED HEALTHCARE AND WELLBEING

Rocío Cánovas Martínez

## APPENDIX 1. ABBREVIATIONS

$\mu_{i(\text{aq})}^0$  – Chemical standard potentials of the ion in the aqueous phase

$\mu_{i(\text{org})}^0$  – Chemical standard potentials of the ion in the organic phase

$\mu\text{PAD}$  – microfluidic paper-based analytical device

$\Delta E$  – Peak separation

$\sigma$  – Stress

$\varepsilon$  – Planar strain

$\gamma$  – Activity coefficient

$\gamma$  – Potential scan rate

$\lambda$  – Ratio of extension

A - Electrode area

a – original radius

$a_{i(\text{aq})}$  – Activity of the primary ion in the aqueous sample

$a_i$  (DL) – Activity of the primary ion in the limit of detection

$a_{i(\text{org})}$  – Activity of the primary analyte in contact with the organic phase boundary

$a_j$  (BG) – Activity of the interfering ion in the background solution

Ag – Silver

AgCl – Silver chloride

C – Capacitance

c – Concentration of analyte in solution

CAGR – Compound annual growth rate

CCF – Commercial carbon fibers

CD – Bulk capacitance

CE – Counter electrode

CHI – Chitosan

ChOx – Cholesterol oxidase

CNT – Carbon nanotube

CP – Conductive polymer

CV – Cyclic voltammetry

D – Diffusion coefficient

DIW – Deionized (purified) water

DNT – Dinitrotoluene

DOS – Bis(2-ethylhexyl)sebacate

$e^-$  – Electron

E – Enzyme

- $E_i^0$  – Potential of the primary ion at 1 M concentration, also known as standard potential
- $E_j^0$  – Potential of the interfering ion at 1 M concentration
- $E^0$  – Standard potential
- EConst – Constant potential generated at the internal interfaces
- ED – Diffusion potential inside the membrane
- EIS – Electrochemical impedance spectroscopy
- EMF – Electromotive force
- ELISA – Enzyme-linked immuno-sorbent assay
- EP – Complex enzyme-product
- $E_{pa}$  – Anodic peak potential
- EPB – Phase boundary potential between the sample-membrane interfaces
- $E_{pc}$  – Cathodic peak potential
- ES – Complex enzyme-substrate
- ESEM – Environmental scanning electron microscopy
- $E_t$  – Potential at time t
- F – Faraday constant (96485 C/mol)
- FIM – Fixed interference method
- FT-IR – Fourier transform infrared spectroscopy
- G – Gibbs free energy
- GalOx – Galactose oxidase
- GC – Glassy carbon
- GDP – Gross Domestic Product
- GOx – Glucose oxidase
- h – height
- $H^+$  – Proton
- HF – High frequency
- Hz – Hertz (frequency unit)
- $H_2O_2$  – Hydrogen peroxide
- $H_2SO_4$  – Sulfuric acid
- $H_2PtCl_6$  – Chloroplatinic acid hexahydrate
- I – Ionic strength
- i – Current (amperes)
- $I^+$  – Primary ion
- $I_0$  – Amplitude
- ICT – Information and Communication Technology
- IoT – Internet of things

Appendices: Abbreviations

- I<sub>p</sub> – Peak current
- i<sub>pa</sub> – Anodic peak current
- i<sub>pc</sub> – Cathodic peak current
- IS – Internal solution
- ISE – Ion-selective electrode
- ISM – Ion-selective membrane
- IT – Information technology
- I<sub>t</sub> – Current at time t
- J – Interfering ion
- K<sub>ij</sub><sup>pot</sup> – Selectivity coefficient of the I-ISE towards the ion J
- k<sub>r</sub> – Constant function of the relative free energies of solvation in both the sample and the membrane phase
- KCl – Potassium chloride
- K<sub>ps</sub> – Constant of solubility
- K<sub>s</sub> – Dissociation constant
- KTCIPB – Potassium tetrakis (4-chlorophenyl) borate
- LiAc – Litium acetate
- LOD – Limit of detection
- M<sup>0</sup> – Metal
- M<sup>+</sup> – Metal ion
- M<sup>-</sup> – Cation exchanger
- MEMS – Micro-electromechanical systems
- mHealth – Mobile health
- MO – Mineral oil
- MWCNT – Multi-walled carbon nanotube
- n – Number of electrons transferred per molecule diffusing to the electrode surface
- n<sub>i</sub> – Charge of the primary ion
- n<sub>j</sub> – Charge of the interfering ion
- N – Number of replicates
- NPs – Nanoparticles
- NaTFPB – Sodium tetrakis[3,5-bis(trifluoromethyl)phenyl]borate
- O<sub>2</sub> – Oxygen
- OCP – Open circuit potential
- o-NPOE – 2-nitrophenyl octyl ether
- P – Product
- PBS – Phosphate-buffered saline

Appendices: Abbreviations

PEAA – Poly(ethylene-co-acrylic acid)  
PEDOT – Poly(3,4-Ethylenedioxythiophene)  
POC – Point-of-care  
POCT – Point-of-care tests  
Pt – Platinum  
PU – Polyurethane  
PVAL – Polyvinyl alcohol  
PVB – Polyvinyl butyral - Butvar B-98  
PVC – Polyvinyl chloride  
PwC – PricewaterhouseCoopers  
Q – Charge  
R – Resistance  
R – Universal gas constant (8.314 J/K·mol)  
 $R_0$  – Initial resistance  
 $R_f$  – Final resistance  
RE – Reference electrode  
Redox – Reduccion-oxidation  
RS – Solution resistance  
RSD – Relative standard deviation  
 $R_x$  – Extension radius  
s – Surface area  
S – Substrate  
SC – Solid contact  
SDBS – Sodium dodecylbenzenesulfonate  
SEM – Scanning electron microscopy  
SPE – Screen printed electrodes  
SSM – Separate solution method  
SWCNT – Single-walled carbon nanotube  
T – Absolute temperature (K)  
t – Time  
 $t_t$  – Thickness at the top  
 $t_0$  – Initial thickness  
THF – Tetrahydrofuran  
TNT - Trinitrotoluene  
 $v$  - Scan rate  
V – Voltage (volts)

**Appendices: Abbreviations**

- $v_0$  – Michaelis-Menten velocity
- $V_{\max}$  – Maximum velocity of an enzymatic reaction
- $W$  – Warburg impedance
- $W_{\text{Chem}}$  – Chemical work
- $WE$  – Working electrode
- $W_{\text{El}}$  – Electrical work
- wt % – Weight percentage
- $Z_0$  – Impedance magnitude
- $z_i$  – Charge (of analytes in solution)
- $X^-$  – Counterion



## APPENDIX 2. FIGURE INDEX

**Figure 1.1.** Left: diagram summarizing how the concepts inside modern health are interwoven with each other. Right: definitions for eHealth, telehealth and mHealth.

**Figure 1.2.** Interconnectivity of components in a digital health ecosystem.

**Figure 1.3.** The new model of the sanitary ecosystem in which the different sources where the information is obtained converge towards the three main pillars where this information is used.

**Figure 1.4.** Subgroups involved and problems in the existing ecosystem of healthcare and the possible solutions arising with the implementation of mHealth.

**Figure 1.5.** Schematic representation of the integration of different fields required for POC devices.

**Figure 1.6.** Summary of the three main characteristics included in the *Holy Trinity* concept.

**Figure 1.7.** Examples of the diversity of target product profiles, users, and settings within the spectrum of POC testing.

**Figure 1.8.** Basic scheme of the main topics addressed -classified into different chapters- within this thesis.

**Figure 1.9.** Diagram of the different parts of the research performed during this thesis.

**Figure 2.1.** Classification of the electrochemical techniques according to the parameters that can be controlled and measured.

**Figure 2.2.** Schematic representation of a potentiometric cell with the reference (RE) and working electrodes (WE) plus the device needed to transduce the analytical signal, a potentiometer.

**Figure 2.3.** Illustration of an electrochemical cell where three electrodes working, counter and reference (WE, CE and RE) are measuring current by using a potentiostat.

**Figure 2.4.** General overview of the measuring process in an electrochemical sensor.

**Figure 2.5.** Schematic representation of a solid-state ion-selective electrode (SC-ISE). The magnification shows the elements of an ion-selective membrane (ISM).

**Figure 2.6.** Diagram of the mechanism of the phase boundary potential. (A) SC-ISE in an aqueous solution without ions (B) membrane placed in contact with an aqueous solution that contains the primary ion and counterion ( $I^+$  and  $X^-$ ) reaching the electrochemical equilibrium.

**Figure 2.7.** Schematic representation of a paper-based enzymatic electrode and the elements needed to its manufacturing. The enzymatic selective membrane (ESM) is also outlined in three main components.

**Figure 2.8.** Layers (plus substrate) involved in the ESM of a paper-based enzymatic electrode and the detection of the analyte of interest due to the enzymatic reaction that happens in between of these layers.

**Figure 2.9.** Schematic representation of all the elements involved in the development of different types of voltammetric electrodes depending on the voltammetric technique applied (such as stripping voltammetry, amperometry or cyclic voltammetry).

**Figure 2.10.** Typical CV spectra of a redox couple species.  $E_{pa}$  and  $E_{pc}$  are the potential corresponding to the anodic and cathodic peaks respectively.

**Figure 2.11.** Typical chronoamperogram spectra by chronoamperometric technique from increasing concentrations of glucose.

**Figure 2.12.** Typical reduction peaks obtained by adsorptive stripping voltammetry from increasing concentrations of organic molecules such as 2, 4, 6-trinitrotoluene (TNT).

**Figure 2.13.** Schematic representation of the three different types of RE explained in this section: single junction, double junction and solid contact paper-based reference electrodes.

**Figure 2.14.** Graphical representation of some analytical parameters.

**Figure 3.1.** Image showing the platinized paper.

**Figure 4.1.** (A) Schematic representation of the tailor-made stretchable materials and manufacturing process. (B) Image depicting the wearable sensor based on textile and ion-selective membranes (ISM) composition. (C) Image of the stretchable printed sensors on different common textiles and typical time trace plots for potassium and sodium.

**Figure 4.2.** Images illustrating resilience studies involving exposing the printable textile potentiometric sensor to increasing levels of strain (left) along with the corresponding time trace calibration plots (right). (A) Linear stretchability test up to a total of 100% strain, 10 repetitions in each strain step. (B) Stretchability test, using a 75% linear strain for a total of 60 min (time trace recorded after every 15 min). (C) Bending assessment, up to a total of 180°, 10 repetitions in each angle. (D) Crumpling evaluation, up to 30 times wrinklings. (E) Washing step simulations (without soap) using short and long (10 and 40 minutes) periods.

**Figure 4.3.** (A) Carry-over test of a textile-based sensor before, during (50% strain) and after such mechanical deformation. (B) Carry-over testing using artificial sweat test within the physiological range. (C) Correlation of calibration experiments carried out using a compact wireless high-input voltmeter and a conventional potentiostat. (D) Images depicting the versatility of the printable and stretchable sensor array on different common wearable substrates. The tablet displays a real-time trace of increasing potassium levels obtained wirelessly by the underwear printed sensor.

**Figure 5.1.** Expandable electrochemical device. (A) Schematic representation of the layers composition for the expandable balloon device and the representation of its adaptability to curvilinear surfaces. Multiple layers consist of Ecoflex layer (inner), polyurethane (intermediate), printable sensor (Ag/AgCl with Ecoflex composite), the CNT hybrid nanocomposite layer (PU, MO and MWCNTs) and flexible insulator layer (upper). (B) Inflation and deflation status for both designs ((a) linear serpentine and (b) clover designs). (C) Integration of a flexible electronic/wireless circuitry with the expandable balloon device. (D) Different inflation levels (IL) used during the mechanical deformation study and the explosives monitoring.

**Figure 5.2.** (A) Multiaxial stretching with bending motion schematics and (B) schematic representation related with the parameters in the equations.

**Figure 5.3.** Mechanical deformation study and modelling of the expandable device. (A) Static resistance study during increasing inflation levels with the linear serpentine pattern for working, reference and counter electrodes. (B) Schematic representation of the expandable hybrid nanocomposite model of the carbon nanotubes (CNTs) and elastomeric stretchable polyurethane from deflation until inflation status. (C) Dynamic resistance study and comparison between different designs. (D) Cyclic voltammetry study for mechanical compliance assessment (Da) over all the inflation levels and (Db) during inflation and deflation cycles. (E) Schematics of the models between device patterns during the balloon inflation levels.

**Figure 5.4.** Dynamic resistance study and comparison between different designs: (A) linear serpentine pattern and (B) clover pattern, shown in (a). Figure (b) and (c) displays the change of resistance upon different mechanical expansion tests: increasing the inflation levels and inflation-deflation cycles, respectively, for working electrodes.

**Figure 5.5.** Explosive detection liquid-phase TNT, DNT and H<sub>2</sub>O<sub>2</sub> using the balloon-embedded sensor. (A) TNT calibration curve in (Aa) the 1<sup>st</sup>, (Ab) the 4<sup>th</sup> level of inflation for the expandable device and (Ac) voltammetric signals during increasing inflation levels. (B) DNT calibration curve in (Ba) the 1<sup>st</sup>, (Bb) the 4<sup>th</sup> level of inflation for the expandable device and (Bc) voltammetric signals during increasing inflation levels. (C) H<sub>2</sub>O<sub>2</sub> calibration curve in (Ca) the 1<sup>st</sup>, (Cb) the 4<sup>th</sup> level of inflation for the expandable device and (Cc) amperometric signals during increasing inflation levels.

**Figure 5.6.** Explosive vapor detection: gas-phase measurements of DNT and H<sub>2</sub>O<sub>2</sub>. (A) Hydrogel solid-state electrolyte strategy for DNT vapor-phase detection (Aa) equilibration time voltammetric curve for 100 mg DNT, (Ab) voltammetric signal upon increasing the amount of DNT from 100-500 mg and (Ac) the corresponding experimental arrangement. (B) Ionogel solid-state electrolyte strategy for H<sub>2</sub>O<sub>2</sub> vapor-phase detection, (Ba) equilibration time amperometric curve for 1% H<sub>2</sub>O<sub>2</sub>, (Bb) calibration curve for increasing amount of H<sub>2</sub>O<sub>2</sub> and (Bc) corresponding configuration.

**Figure 6.1.** Potentiometric response curves. (A) Time-trace for bare (blue line) and Nafion-coated (red line) platinum electrode in PBS pH 7 at 25°C (mean ± S.D., N=2). Inset shows a magnification of the calibration curve for bare platinum electrode. (B) Corresponding calibration plots for bare (blue, □) and coated (red, ○) electrodes. Initial potentials have been subtracted to better illustrate the differences between the two systems. Error bars correspond to the standard deviation (N=2).

**Figure 6.2.** Comparison of the initial potential as a function of the total electrolyte concentration for (A) bare and (B) Nafion-coated platinum electrodes upon increasing concentration of different supporting electrolytes at 25°C. (C) Comparison of the H<sub>2</sub>O<sub>2</sub> calibration curves using coated electrodes at different concentrations of supporting electrolyte (KCl): 10<sup>-2</sup> M (□) and 10<sup>-4</sup> M (○) (mean ± S.D., N = 2). Inset displays H<sub>2</sub>O<sub>2</sub> sensitivity versus supporting electrolyte (KCl) concentration.

**Figure 6.3.** Calibration plots at several pH for (A) bare and (B) Nafion-coated electrodes in 0.1 M buffers of different pH at 25°C.

**Figure 6.4.** Time trace showing the stabilization of the signal of the Nafion coated electrodes previous to a calibration curve.

**Figure 6.5.** Schematic diagram of Nafion-coated electrodes mechanism studied during this thesis. The exchange capability and the redox reactions performed the suggested mechanism.

**Figure 6.6.** Electrochemical impedance spectroscopy results of bare (blue line) and Nafion-coated (red line) platinum electrode in 0.1 M KCl as a supporting electrolyte. The impedance spectra were recorded in the frequency range 100 kHz-10 mHz by using a constant direct current potential, (Edc) 0.2 V. The electrodes were studied using excitation amplitude of 10 mV at 25°C.

**Figure 6.7.** Cyclic voltammetry results. (Aa) Comparison between bare (blue line) and Nafion-coated (red line) electrodes and (Ab) comparison between bare (blue line) and Nafion-coated (red line) electrodes after 30 minutes in solution in 5 mM  $\text{Fe}(\text{CN})_6^{3-/4-}$  and 100 mM NaCl from -0.2 V to 0.4 V at  $50 \text{ mV}\cdot\text{s}^{-1}$ . Redox sensitivity assay. (B) Redox sensitivity of 1 mM  $[\text{Fe}(\text{CN})_6]^{4-} / [\text{Fe}(\text{CN})_6]^{3-}$  at different ratios (0.1, 1 and 10) for bare ( $\blacktriangle$ ) and Nafion-coated ( $\blacktriangle$ ) platinum electrodes.

**Figure 6.8.** (A) Evaluation of the addition of ascorbic acid (AA) in the cell for bare and Nafion-coated electrodes in 0.1 M PBS pH 7.2 at 25°C. (B) Calibration curve for increasing glucose concentration over time for bare, Nafion-coated and Nafion-coated enzymatic electrodes in 0.1 M PBS pH 7.4 at 25°C.

**Figure 7.1.** Illustration of paper-based biosensor. (A) Fabrication of the paper-based electrode, using a strip of platinized conductive paper sandwiched between two plastic masks with a window of electroactive surface (B) Electron microscope (ESEM) images of a Nafion membrane drop cast on top of an electrode. (C) Scheme of the enzymatic membrane: Pt-Paper Substrate, enzyme (GOx) sandwiched between two layers of Nafion, one at Pt-interface and the other at the solution interface.

**Figure 7.2.** ESEM images of the paper-based electrode surface: (A) a bare platinized paper electrode, (B) a membrane (double layer of Nafion) on top of a platinized paper electrode and (C) transversal cut of the electrode membrane (ca. 40  $\mu\text{m}$  thickness).

**Figure 7.3.** Response study of enzymatic paper-based electrode: (A) Potentiometric time-trace and (B) corresponding calibration curve of enzymatic, Nafion coated and bare platinized paper electrode upon additions of glucose; (C) potentiometric time-trace for gluconic acid for bare and Nafion-coated paper electrode; (D)  $\text{H}_2\text{O}_2$  potentiometric time-trace and (E) corresponding calibration curve for  $\text{H}_2\text{O}_2$  for bare and Nafion-coated platinized paper electrode (average  $\pm$  S.D., N=2). (F) pH dependence of the sensitivity for  $\text{H}_2\text{O}_2$  in the range from  $10^{-5}$  M to  $10^{-3.5}$  M (average  $\pm$  S.D., N=2). All the measurements were performed in 0.1 M buffers, acetic buffer (pH 4.2), PBS (pH 7.4), borate buffer (pH 8.6) at 25°C.

**Figure 7.4.** Optimization of the analytical conditions for the biosensor. (A) Sensitivity for glucose vs. volume of solution of enzyme concentration ( $20 \text{ mg}\cdot\text{mL}^{-1}$ ) cast. (B) Change on the potentiometric signal after the addition of  $10^{-4}$  M ascorbic acid as function of the increasing volume of Nafion membrane cast. In all cases, error bars correspond to the standard deviation of 3 different electrodes.

**Figure 7.5.** Analytical performance of the paper-based enzymatic electrode: (A) Time-trace plot of three different electrodes in three separated potentiometric cells, (B) the corresponding calibration curve of enzymatic electrodes showing the linear range (mean  $\pm$  S.D., N=3). (C) Repeatability test for three different electrodes during consecutive calibration curves for glucose. (D) Enzyme-based electrode selectivity assessment to the main redox sensitive molecules (ascorbate and urate) and fructose. All the measurements were performed in 0.1M PBS (pH 7.4) at 25°C.

**Figure 7.6.** (A) ESEM images of the surface of the paper-based enzymatic electrode after hydration of the membrane: (Aa) PBS-solution-stabilized electrode, (Ab) after glucose calibration curve and (Ac) after 1.5 h  $10^{-2}$  M glucose solution. Enzymatic reaction was performed in PBS pH 7.4 at 25 °C. (B) FT-IR spectra of the paper-based enzymatic electrode in different conditions: (Ba) Whole overlap spectra, (Bb) magnification of peak at  $3400 \text{ cm}^{-1}$  of

membrane swelling and (Bc) magnification from 900 to 1500  $\text{cm}^{-1}$  showing Nafion backbone peaks. Potentiometric measurements were performed in PBS pH 7.4 at 25 °C.

**Figure 7.7.** Ratio from FT-IR spectra between peaks (A) 1059/982 and (B) 1200/1145 in different conditions: (1) dried, (2) PBS stabilized, (3) after calibration curve, (4) 45 min at  $10^{-2}$  M glucose, (5) 90 min at  $10^{-2}$  M glucose and (6) control electrode, 90 min in PBS. Measurements were performed in PBS pH 7.4 at 25 °C.

**Figure 7.8.** (A) Comparison of glucose determination (mM) in real samples obtained by the potentiometric paper-based electrode (mean  $\pm$  S.D., N=3) and colorimetric assay (data provided by the local hospital) at 25°C. (B) Clarke plot demonstrates that the values are clinically relevant because all of them are inside the zone A.

**Figure 8.1.** (A) Scheme for the construction of the working and the reference electrodes. (B) Integration of both electrode into a sensor (potentiometric cell A, PCA) and with the sampling module (PCB). (C) Picture of the device containing the sensor as sampling cell and the wireless potentiometer.

**Figure 8.2.** Comparison of the potentiometric response under different conditions. Blue dots: enzymatic sensor (Nafion || Enzyme || Nafion || Pt) with addition of glucose; Red squares: same enzymatic sensor, but no glucose and direct addition of hydrogen peroxide; Green diamonds: response of a Nafion-coated platinum electrode (i.e., no enzyme) with addition of hydrogen peroxide.

**Figure 8.3.** (A) Sensitivity of the working electrode versus the Nafion layer amount and (B) refers to the response to the main interferent (Ascorbic Acid: AA) vs. the amount of the Nafion layer (2, 4.5, 7 and 9  $\mu\text{L}$ ). N=3, three different sensors for each amount.

**Figure 8.4.** (A) Sensitivity of the working electrode versus the amount of Nafion layer and (B) response to the main interferent ascorbic acid (AA) versus amount of the Nafion layer (1, 2, 3 and 4.5  $\mu\text{L}$ ). (C) Picture of the comparison in size of the devices with 3 mm (top) and 2 mm (bottom) diameter.

**Figure 8.5.** Comparison between three different conditioning steps of reference electrodes. (A) Time trace, (B) calibration plot -under three different conditions of conditioning: more than 24 hours, only 3 hours and no conditioning- and (C) long term stability study for used reference electrodes.

**Figure 8.6.** Potentiometric response of paper-based electrodes in artificial serum: (A) time trace and (B) corresponding calibration curves of paper-based reference electrodes, paper-based working electrodes (WE), and potentiometric cells A, PCA (in a 4 mL cell) and PCB (using only 25  $\mu\text{L}$  of solution).

**Figure 8.7.** (A) Prediction of glucose concentrations (mM) in real serum samples determined by the enzymatic paper-based sensor -assembled in the sampling cell- (N=3) compared with conventional colorimetric technique (Standard lab-based technique). Inset illustrates the size comparison of the sensor. (B) Clarke plot proves the reliability of the sensor.

**Figure 8.8.** (A) Prediction of glucose concentrations (mM) for six (■) serum samples and three (✱) whole blood samples determined by the wireless potentiometric device vs. a commercial (amperometric) glucometer. (B) Picture showing the wireless device connected to PCB and the screen showing the results of the two-point calibration, washing and sample measurement.

**Figure 9.1.** Scheme of the electrodeposition process where the platinum salt that is present in the bulk solution is reduced on the working electrode (WE) surface.

**Figure 9.2.** Cyclic voltagrams obtained before (in blue) and after (in red) of Pt-NPs electrodeposition in four different substrates: (A) CNT paper-based electrodes; (B) glassy carbon -GC- electrodes; (C) carbon ink rubber-based electrodes and (D) carbon ink paper-based electrodes.

**Figure 9.3.** ESEM images of the shape and size of Pt particles created in four different substrates (A) CNT paper-based electrodes; (B) glassy carbon -GC- electrodes; (C) carbon ink rubber-based electrodes and (D) carbon ink paper-based electrodes.

**Figure 9.4.** (A) Time trace and (B) calibration curve of three different carbon ink paper-based electrodes responding to increasing concentration of  $H_2O_2$  in PBS 0.1 M (pH 7.4) at 25°C.

**Figure 9.5.** Comparison of the potentiometric response to  $H_2O_2$  using paper-based sensors with PtNPs-carbon ink with or without Nafion layer on top. (A) Time trace and (B) calibration curve of three different PtNPs-carbon ink paper-based electrodes responding to increasing concentration of  $H_2O_2$ . (C) Time trace and (D) calibration curve of three different PtNPs-carbon ink paper-based electrodes with a layer of Nafion on top responding to increasing concentration of hydrogen peroxide.

**Figure 9.6.** Calibration curve showing the response of different blanks electrodes to  $H_2O_2$ . C = carbon ink substrate, C-N = carbon ink with a layer of Nafion, C-ED = carbon ink after an electrodeposition without the Pt salt and C-ED-N = carbon ink paper after an electrodeposition process without particles and a layer of Nafion.

**Figure 9.7.** Comparison of the potentiometric response under different conditions. (A) Time trace and (B) calibration curve comparing the response to  $H_2O_2$  of electrodes built with pure Aquivion (blue circles), diluted Aquivion in a mixture 1:1 (red squares) and 1:4 (green diamonds). In a parallel study, (C) time trace and (D) calibration curve showing the response of platinum bare electrodes (blue triangles) and 1:1 diluted Aquivion electrodes (red squares) towards hydrogen peroxide and enzymatic sensor composed by AQ || GOx || AQ to additions of glucose (purple stars).

**Figure 9.8.** Images corresponding to paper-based electrodes (A) bare platinum electrode (B) with a layer of 4  $\mu$ L of Aquivion -dilution 1:4 with methanol-, (C) with a layer of 4  $\mu$ L of Aquivion -dilution 1:1 with methanol- and, (D) with a layer of 4  $\mu$ L of pure Aquivion (without any dilution).

**Figure 9.9.** Optimization of the analytical conditions of the biosensor. (A) Sensitivity for glucose vs the volume of solution of polymer cast. (B) Sensitivity for glucose vs the concentration of enzyme cast (fixed volume of 10  $\mu$ L for enzymatic layer). (C) Stability study exhibits values for the recovery of the sensitivity along a period of more than 4 months. (D) Assessment of the selectivity of the enzyme-based electrode to the main redox sensitive molecules (ascorbate and urate) and fructose. All the measurements (N = 3) were performed in 0.1 M PBS (pH 7.4) at 25°C.

**Figure 9.10.** Comparison of the potentiometric response of glucose using different polyelectrolytes to built the enzymatic electrodes. Blue dots: electrodes built with Nafion and red squares: electrodes built with Aquivion.

**Figure 9.11.** Schematic representation of the WE and RE used during the measurements with real samples.

**Figure. 9.12.** (A) Comparison of glucose determination (mM) in real blood samples obtained by the potentiometric biosensor (paper-based WE and paper-based RE) and glucometer device at 25°C. (B) Representation of the well-established Clarke error grid.

**Figure 10.1.** Technology development of the potentiometric enzyme-based sensors.

## APPENDIX 3. TABLE INDEX

**Table 4.1.** Average sensitivity values and intercept values obtained during several mechanical deformations of the textile ISE system.

**Table 4.2.** Selectivity values obtained experimentally and in literature for the sodium and potassium-based polymeric membrane.

**Table 6.1.** Comparison of analytical figures of merit for the determination of  $H_2O_2$  with the two types of electrodes in 0.1 M PBS buffer (pH=7).

**Table 6.2.** Comparison of analytical figures of merit for the determination of  $H_2O_2$  with Nafion coated electrodes before and after the addition of ascorbic acid in 0.1M PBS.

**Table 7.1.** Repeatability test. Analytical performance for 3 consecutive calibrations.

**Table 7.2.** The recovery of glucose determination in serum samples (diluted 1:10).

**Table 7.3.** Comparison of analytical performances of potentiometric biosensors for glucose detection.

**Table 8.1.** Optimization of Nafion layers in paper-based electrodes.

**Table 8.2.** Total cost of making these electrodes in the lab based on platinized paper, GOx and Nafion.

**Table 8.3.** Analytical parameters of the working electrode and the potentiometric cells A and B

**Table 8.4.** Comparison between concentrations: Potentiometry method vs. Hospital provided values of glucose in 10 real serum samples.

**Table 8.5.** Comparison of glucose levels: Potentiometry vs. commercial glucometer for six serum and three blood samples.

**Table 9.1.** Analytical performance compare between electrodes with and without Nafion layer on top of carbon ink paper-based electrode decorated with Pt particles.

**Table 9.2.** Conditions used for the optimization of the thickness of the different Nafion and enzymatic layers.

**Table 9.3.** Nafion vs. Aquivion comparing the chain and density of charges of these polymers.

**Table 9.4.** Comparison of analytical parameters using different configurations of the electrodes in 0.1 M PBS buffer (pH = 7.4).

**Table 9.5.** The recovery of glucose determination in blood samples without dilution.

## APPENDIX 4. LIST OF PUBLICATIONS

### Journal Publications:

1. Parrilla, M.\*, Cánovas, R.\*, Jeerapan, I., Andrade, F.J., Wang, J., 2016. *A Textile-Based Stretchable Multi-Ion Potentiometric Sensor*. *Advanced Healthcare Materials*. 5, 996–1001. Doi:10.1002/adhm.201600092 (\*Shared first author)
2. Cánovas, R.\*, Parrilla, M.\*, Mercier, P., Andrade, F.J., Wang, J., 2016. *Balloon-Embedded Sensors Withstanding Extreme Multiaxial Stretching and Global Bending Mechanical Stress: Towards Environmental and Security Monitoring*. *Advanced Materials Technologies* 1-11. Doi:10.1002/admt201600061 (\*Shared first author)
3. Parrilla, M., Cánovas, R., Andrade, F.J., 2016. *Enhanced Potentiometric Detection of Hydrogen Peroxide Using a Nafion-coated Platinum Electrode*. *Electroanalysis*. 29, 223-230. Doi:10.002/elan.201600403.
4. Parrilla, M., Cánovas, R., Andrade, F.J., 2017. *Paper-based enzymatic electrode with enhanced potentiometric response for glucose determination in biological fluids*. *Biosensors and Bioelectronics*. 90, 110-116. Doi: 10.1016/j.bios.2016.11.034.
5. Cánovas, R., Parrilla, M., Blondeau, P., Andrade, F.J., 2017. *A novel wireless paper-based potentiometric platform for monitoring glucose in blood*. *Lab on a Chip*. 17, 2500-2507. Doi: 10.1039/C7LC00339K.
6. Cánovas, R., Blondeau, P., Andrade, F.J., 2018. *Direct glucose potentiometric measurement in whole blood*. In preparation.

### Poster Presentations:

1. Biosensors 2016 Conference, Gothenburg, Sweden. An enzymatic paper-based potentiometric cell for monitoring glucose in decentralized settings.
2. Matrafüred 2017, Budapest, Hungary. Novel approaches to build potentiometric biosensors for decentralized chemical analysis.
3. VIII International Congress on Analytical Nanoscience and Nanotechnology 2017, Barcelona, Spain. Novel approaches to build potentiometric biosensors for decentralized chemical analysis.



UNIVERSITAT ROVIRA I VIRGILI

TAILOR-MADE CHEMICAL SENSING PLATFORMS FOR DECENTRALIZED HEALTHCARE AND WELLBEING

Rocío Cánovas Martínez

UNIVERSITAT ROVIRA I VIRGILI

TAILOR-MADE CHEMICAL SENSING PLATFORMS FOR DECENTRALIZED HEALTHCARE AND WELLBEING

Rocío Cánovas Martínez

